THE UNIVERSITY
of EDINBURGH

Bimetallic actinide complexes for small molecule activation

JORDANN A. L. WELLS

UNIVERSITY OF EDINBURGH

Thesis submitted for the degree of Doctor of Philosophy

February 2018

Declaration

I declare that this thesis is an original report of my research, has been written by me and has not been submitted for any previous degree. The experimental work is almost entirely my own; the collaborative contributions have been indicated clearly and acknowledged. Due references have been provided on all supporting literatures and resources.

Abstract

The work described in this thesis concerns the synthesis of actinide complexes and their reactivity towards small unsaturated molecules. Complexes bearing tetraphenoxide, borohydride and boroxide ligands have been evaluated. Additionally, work towards the synthesis of heterobimetallic uranium transition metal complexes and their applications in catalysis is discussed.

Chapter one reviews important organoactinide complexes reported in the literature which effect chemical transformations on small unsaturated substrates. Actinide complexes supported by aryloxide or borohydride ligands are reviewed, along with actinide complexes in which metal π-arene interactions are present.

Chapter two reports the synthesis and characterisation of a set of tetraphenol ligands, in addition to a number of attempted synthetic routes to tetraphenol ligands with alternate substitution. The chemistry of those tetradentate aryloxide ligands is introduced with bimetallic uranium(IV) and thorium(IV) complexes using different An(IV) and U(III) precursors.

Chapter three reports the synthesis and characterisation of monometallic uranium and thorium complexes using a tetraphenol ligand. The varying chemistry between the two similar An(IV) ions, where the uranium complexes exist as a mixture of oligomers and the thorium complexes remain as well defined mononuclear complexes, is discussed within. A range of base adducts of mononuclear actinide complexes are reported, including a thorium trimethylsilylazide complex, a rare example of a metal organoazide.

Chapter four describes the synthesis of homoleptic boroxide and heteroleptic borohydride complexes of uranium(III). The reactivities of these complexes with small unsaturated molecules are assessed, including the reaction of a low coordinate uranium(III) boroxide complex towards CO_2 to provide a dinuclear uranium carbonate bridged complex.

Chapter five introduces work towards heterobimetallic uranium transition metal complexes carried out in the Arnold group. The application of these complexes towards ring opening polymerisation chemistry is discussed in addition to investigations into the incorporation of transition metals into uranium(IV) complexes.

Chapter Six presents the detailed experimental methods used to carry out this research.

Lay Summary

This thesis presents research carried out towards the aim of transforming abundant and simple molecules to more complex and useful products. The work herein focusses mostly on the chemistry of specific uranium complexes and equivalent thorium complexes in achieving these transformations.

The introductory chapter details selected literature examples of relevant uranium chemistry. Related complexes to those explored during this project are discussed, concentrating particularly on complexes that have previously been shown to achieve transformations similar to those targeted within this thesis. A strategy to form uranium and thorium complexes capable of those transformations was proposed from this literature analysis.

Chapter Two presents the synthesis of a range of uranium and thorium complexes that contain two identical metal centres, and the attempted synthesis of uranium products that may enable the targeted transformations. Decomposition products obtained from these attempts are presented and strategies to avoid their formation are discussed.

Chapter Three details the synthesis of uranium and thorium complexes that contain a single metal centre and their interaction with a range of molecules. The differences between the uranium and thorium complexes is discussed, as well as their potential application for the desired chemical transformations.

Chapter Four reports the synthesis of two different types of uranium complexes and their ability to achieve transformations previously seen within the literature.

Chapter Five reports the synthesis of complexes which contain a uranium-rhodium bond. The nature and strength of the bond is discussed. Also presented in this chapter are the synthesis of uranium and cerium complexes and their use in the catalytic production of polymers. These catalysts were found to be quite active and highly selective under certain conditions.

Chapter Six provides experimental details for this work.

Acknowledgements

I would firstly like to thank my supervisor Prof. Polly Arnold FRS for the enthusiasm and guidance she has supplied throughout my PhD. Thanks also go to the EPSRC for funding my project.

I am very grateful for the help and crystallography wisdom imparted by Dr Gary Nichol, and the NMR spectroscopy assistance provided by Dr Lorna Murray and Mr Juraj Bella.

Thank you to the fantastic Arnold/Love group postdocs who have been generous with their advice, and even more so with their time. In particular, I would like to thank Johann and Brad who have been on the receiving end of a few hundred questions (sometimes all at once). Thank you to my Arnold group PhD comrades, past and present, especially to all in office 34D. My time in Edinburgh has been all the better for knowing you.

Most of all, thank you to my friends and family, who I have seen so little of over the last three or so years. Solenne and Marcus, I am indebted to you for providing me a stepping stone to get to where I am today. The thesis support team, Ros & Chris and Brad, thank you so much for your time and input. And finally, Abby. Thank you for all your support and long nights during my time as a reclusive thesis-writing crazy cat man. I cannot wait for our next adventures.

List of abbreviations

Ad Adamantyl

An Actinide

Ar Aryl

BBN 9-Borabicyclo(3.3.1)nonane

bdpmp 2,6-bis(diphenylmethane)-4-methylphenoxide

Bn Benzyl

btfmp Bis(trifluromethyl)phenyl

cod Cyclooctadiene

coe Cyclooctene

COSY Homonuclear correlation spectroscopy

COT Cyclooctatetraenyl

Cp Cyclopentadienyl

Ct Centroid

CV Cyclic voltammetry

DCE Dichloroethane

DFT Density functional theory

dipp Diisopropylphenyl

DME Dimethoxyethane

dmp Dimethylphenyl

DMPE Bis(dimethylphosphino)ethane

dtbp Di-*tertiary*-butylphenyl

EPR Electron paramagnetic resonance

eq. Equivalents

EXSY Exchange spectroscopy

GPC Gel permeation chromatography

HMBC Heteronuclear multiple bond correlation

HOMO Highest occupied molecular orbital

HSAB Hard soft acid base

HSQC Heteronuclear single quantum coherence

IM Imidazole

Ind Indenyl

IR Infra-red

ITI Inverse trans influence

L Neutral 2-electron donor

Ln Lanthanide

LUMO Lowest unoccupied molecular orbital

MALDI Matrix assisted laser desorption/ionisation

Me Methyl

MeCN Acetonitrile

Mes Mesityl

MVS Metal vapour synthesis

N″ $N(SiMe_3)_2$

Neop textitneo-pentyl

NIR Near infra-red

NMR Nuclear magnetic resonance

^{n}Pr "Normal"-propyl

^{i}Pr isopropyl

OAr^P 2,4-di-*tertiary*-butyl-6-diphenylphosphinoaryloxide

PLA Poly(lactic acid)

P_r Probability of racemic linkages

pTP *para*-tetraphenoxide

***p*-TSA** *para*-toluenesulfonic acid

ROP Ring opening polymerisation

SQUID Superconducting quantum interference device

tacn Triazacyclononane

tBu *tertiary*-butyl

TEMPO Tetramethylpiperidine oxide

Ter^{Mes} 2,6-dimesitylphenyl

THF Tetrahydrofuran

TIPS Triisopropylsilyl

TMANO Trimethylamine-N oxide

TMP Tetramethylphospholyl

TMS Trimethylsilyl

Tp† Hydrotris(2,5-diisopropylpyrazolyl)borate

trip Triisopropylphenyl

ttbp Tri-*tertiary*-butylphenyl

UV-vis Ultraviolet-visible

XRD X-ray diffraction

xs Excess

Xyl Xylyl

δ chemical shift

ppm parts per million

s Singlet

d Doublet

t Triplet

q Quintet

m Multiplet

J coupling constant

Contents

Chapter 1

Introduction

Uranium is the heaviest naturally occurring element and is the 51st most abundant in the Earth's crust. The ground-state electronic configuration of uranium is $[Rn]5f^36d^17s^2$. Uranium has two main isotopes: 99.3% is the ^{238}U isotope which is a weak α emitter, while ^{235}U is a fissile isotope and constitutes less than 1% of naturally occurring uranium.[1] The ores of uranium are extensively mined globally for the nuclear industry where the fissile isotope is used as an initiator in fuel for nuclear reactors. For use as a fuel in nuclear power stations, the ^{235}U content is increased to *circa* 5% by the enrichment process. Enrichment takes naturally occurring uranium and separates the isotopes by centrifugation of volatile uranium compounds leading to an increased ^{235}U content and is termed enriched uranium. The by-product of enrichment is depleted uranium, in which the fissile isotope content has been considerably reduced ($0.2-0.4\%$), making ^{238}U the largest component of nuclear waste. The global stocks of depleted uranium are estimated to be 1.6 million tonnes and increasing every year. The low ^{235}U content in depleted uranium, weak α emitting properties and its long half-life render it safe to handle under laboratory conditions as long as care is taken not to ingest or inhale any material. The moderate toxicity, global abundance and unusual chemical properties of depleted uranium render it an attractive alternative to expensive transition metals generally used in catalysis.

The chemical behaviour of actinides differs from that of the lanthanides (Ln) and transition metals. The atomic and ionic radii of the actinides (An) are larger than that of the lanthanides (Ln). This is due to the radial node in the $5f$ electronic wavefunction, which shields the electrons from the nucleus, decreasing the ionisation potential for $5f$ electrons. Therefore, the early actinides (uranium to curium) have quasi-degenerate $5f$, $6d$ and $7s$ electrons enabling interactions with ligand-based orbitals and multiple accessible oxidation states. The presence of actinide valence electrons at the ligand-field results in a greater degree of covalency in bonding when compared with the lanthanides, cirumventing disallowed electronic transitions resulting in

intensely coloured organometallic complexes. The cyclopentadienyl (Cp) chemistry of dark red [U(η^5-$C_5H_5)_3$Cl] exemplifies this difference in bonding character when compared with lightly coloured [Ln(η^5-$C_5H_5)_3$], as shown in Scheme 1.1. Whereas [U(η^5-$C_5H_5)_3$Cl] is unreactive towards iron(II) chloride, [Ln(η^5-$C_5H_5)_3$] reacts to yield ferrocene, suggesting ionic character in the Ln−Cp bond. The weakness of the Ln−Cp bond results in a salt metathesis reaction for the lanthanides driven by the formation of higher bond strength in ferrocene. Conversely, the lack of reactivity in the case of uranium suggests greater covalency in the U−Cp bond, preventing ligand rearrangement.[2] Calculations to predict the behaviour of actinides is computationally demanding due to multiple unpaired electrons and non-trivial electronic wavefunctions, often rendering chemical reactivity patterns the most practical and cost-effective way of developing existing knowledge. The large ionic radii of the actinides results in higher coordination numbers than in transition metal and lanthanide complexes. The record for the highest coordination number observed is held by the fifteen-coordinate thorium complex [Th($H_3BNMe_2BH_3)_4$].[3]

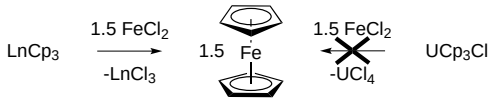

Scheme 1.1 – Contrasting reactivity between uranium and lanthanide tris(cyclopentadienyl) complexes.[2]

Uranium is chemically versatile with oxidation states ranging from uranium(II) ([Rn] $5f^4$) to uranium(VI) ([Rn]); +6 is the most stable in aqueous conditions while +2 has been reported only twice in the literature to date.[4,5] The organometallic chemistry of uranium was initially developed during World War II when investigations into volatile uranium complexes for isotopic separation were carried out during the Manhattan project. Low oxidation-state uranium became prominent in the literature with the development of its anaerobic chemistry and is dominated by hard anionic ligands such as alkoxides, aryloxides, amides and carbocycles (cyclopentadienyl or cyclooctatetraenyl ligands).[6–11] While the +4 oxidation state plays a major role in anaerobic organouranium chemistry, the +3 oxidation state is also of chemical significance. With a redox couple estimated to be between −1.7 and −2.8 V *versus* ferrocene, the uranium(III) oxidation state is strongly reducing.[12] Recent developments in the accessibility of uranium(III) precursors have led to the isolation of a large number of organouranium(III) complexes, which are featured in small molecule reduction chemistry.[13–15] One electron oxidation of the uranium centre is the main pathway of reductive chemistry, often leading to dimeric structures bridged

by a doubly reduced substrate.

A notable example of small molecule reduction chemistry at a uranium(III) centre was reported by Cloke *et al.* in 2006 in a mixed sandwich complex, incorporating a C_5Me_5 ligand and a bis(tri-*iso*-propylsilyl)cyclooctatetraenyl ring (COT^{TIPS}), [U(C_5Me_5)(COT^{TIPS})] (**A**).[16] Exposing pentane solutions of **A** to one bar of carbon monoxide at −78 °C provided a dimeric product, bridged by a cyclic deltate dianion, $C_3O_3^{2-}$. In subsequent reports, Cloke *et al.* found that changing the steric bulk on the Cp ligand altered the outcome of carbon monoxide reduction. Relieving steric hindrance by removing a methyl group led to the formation of a squarate dianion, $C_4O_4^{2-}$, which is the product of reductive tetramerisation of CO.[17] Increasing steric pressure by introducing an ethyl group led to the reductive dimerisation of CO to the ynediolate dianion, $C_2O_2^{2-}$ (Scheme 1.2).[18]

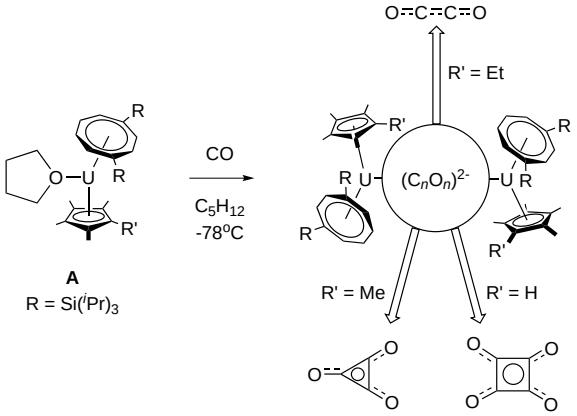

Scheme 1.2 – The impact of varying the steric properties of **A** on the reductive oligomerisation of carbon monoxide.[16–18]

Actinide carbonyl chemistry differs significantly from that of transition metals, where the carbonyl ligand is ubiquitous and acts as an innocent ancillary ligand. Organometallic mediated reductive cyclisation of carbon monoxide is unprecedented, and the reactivity outlined above demonstrates the unique reactivity of organouranium complexes with small molecules, to yield compounds of potential commercial interest.[19]

Exposing solutions of **A** to a stoichiometric amount of syngas led to the isolation of a uranium methoxide complex, obtained from the reduction of carbon monoxide with H_2.[20] By reacting the uranium methoxide with trimethylsilyl triflate, trimethylsilyl methyl ether was eliminated to yield a uranium triflate from which the parent complex could be synthesised by reduction with K/Hg. These represent all the steps of a catalytic cycle (Scheme 1.3).[20]

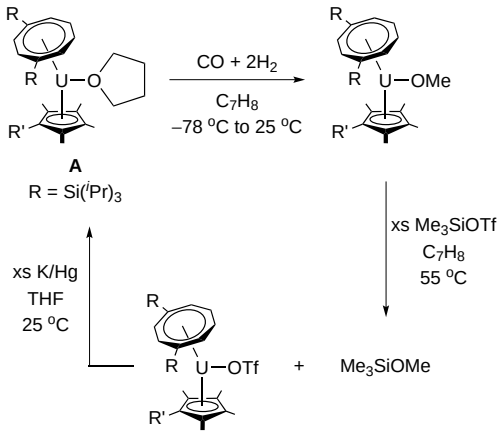

Scheme 1.3 – Synthesis of a uranium methoxide complex by reaction of **A** with a mixture of carbon monoxide gas and dihydrogen gas. The reactive complex **A** could be regenerated by treating the methoxide complex with Me_3SiOTf at elevated temperatures and reducing the resulting uranium(IV) triflate with K(Hg).[20]

The reduction of CO_2 has also been reported with mixed sandwich uranium(III) complexes to yield carbonate products issued from the reductive disproportionation of CO_2 (Equation (1.1)) and oxalate-bridged complexes from the reductive coupling of CO_2 (Equation (1.2)) depending on steric environment.[21]

$$2\,CO_2 + 2\,e^- \longrightarrow {CO_3}^{2-} + CO \tag{1.1}$$

$$2\,CO_2 + 2\,e^- \longrightarrow {C_2O_4}^{2-} \tag{1.2}$$

Recently, our group has shown that such transformations can be accomplished with simple uranium(III) aryloxide complexes, as detailed in the following section.[22,23]

1.1 Actinide aryloxide complexes

1.1.1 Monodentate aryloxides

Uranium alkoxides were initially targeted for the synthesis of volatile complexes for isotopic separation during the Manhattan project during the second World War and were among the first organometallic uranium complexes reported. Extending this chemistry to aryloxides has had a profound effect on the field of uranium organometallic chemistry.[24–26] Early investigations utilised unsubstituted phenol, but it was the use of 2,6-di-*tert*-butylphenol (HOdtbp) pioneered by Lappert *et al.* in 1983 which allowed the isolation of first monomeric uranium complexes.[27–30]

Using sterically bulky aryloxides was key in the isolation of the first uranium tris(aryloxide) complexes. The reaction of uranium(III) tris(silylamide), $[U\{N(SiMe_3)_2\}_3]$ or UN''_3, with three equivalents of HOdtbp or 2,6-di-*iso*-propylphenol (HOdipp) in hexanes led to the isolation of the uranium tris(aryloxide) complexes $[U(Odtbp)_3]$ (**B**, Scheme 1.4) and $[U(Odipp)_3]$ (**C**), respectively.[31] Complexes **B** and **C** constitute some of the earliest reported well-defined mononuclear uranium(III) complexes. The solid-state structure of **C** shows a dimeric complex in which one aryloxide bridges two metals through a metal-π arene interaction, which will be discussed in further detail in Section 1.2.1.

The reducing nature of **B** was investigated early on by Burns and co-workers. The oxo- and sulfido-bridged complexes $[\{U(Odtbp)_3\}_2(\mu\text{-O})]$ (**D**) and $[\{U(Odtbp)_3\}_2(\mu\text{-S})]$ (**E**) were synthesised from the reaction of **B** with oxidants (*ie*: N_2O, NO, Me_3NO or PyNO) and sulfur-containing reagents (*ie*: COS or Ph_3PS), respectively (Scheme 1.4).[32] The authors commented that a reaction occurred between **B** and CO_2, but they were unable to characterise the reaction products and also remarked that, under certain conditions, the homoleptic uranium(IV) aryloxide $[U(Odtbp)_4]$ (**F**) forms as a by-product of oxidation.

The reactions of **B** with small unsaturated substrates were not investigated further until a report by our group.[23] It was found that synthesising **B** under a nitrogen atmosphere led to the isolation of the dimeric U(IV) dinitrogen complex $[\{U(Odtbp)_3\}_2(\mu\text{-}N_2)]$ (**G**, Scheme 1.4) as a minor product. Increasing the electron-donating properties of the ligand by employing the 2,4,6-tri-*tert*-butylphenoxide (HOttbp) ligand resulted in near quantitative yields of the dinitrogen complex $[\{U(Ottbp)_3\}_2(\mu\text{-}N_2)]$ (**H**). Dinitrogen is spontaneously captured from the inert atmopshere under which the reaction is carried out. Structural elucidation reveals an elongation of the dinitrogen ligand N−N bond in **H**, which is consistent with a doubly reduced dinitrogen molecule with a reduction in bond order.[23] The base-free complex, $[U(Ottbp)_3]$ (**I**), could be obtained by reacting UN''_3 with HOttbp in hexanes under an argon atmosphere.

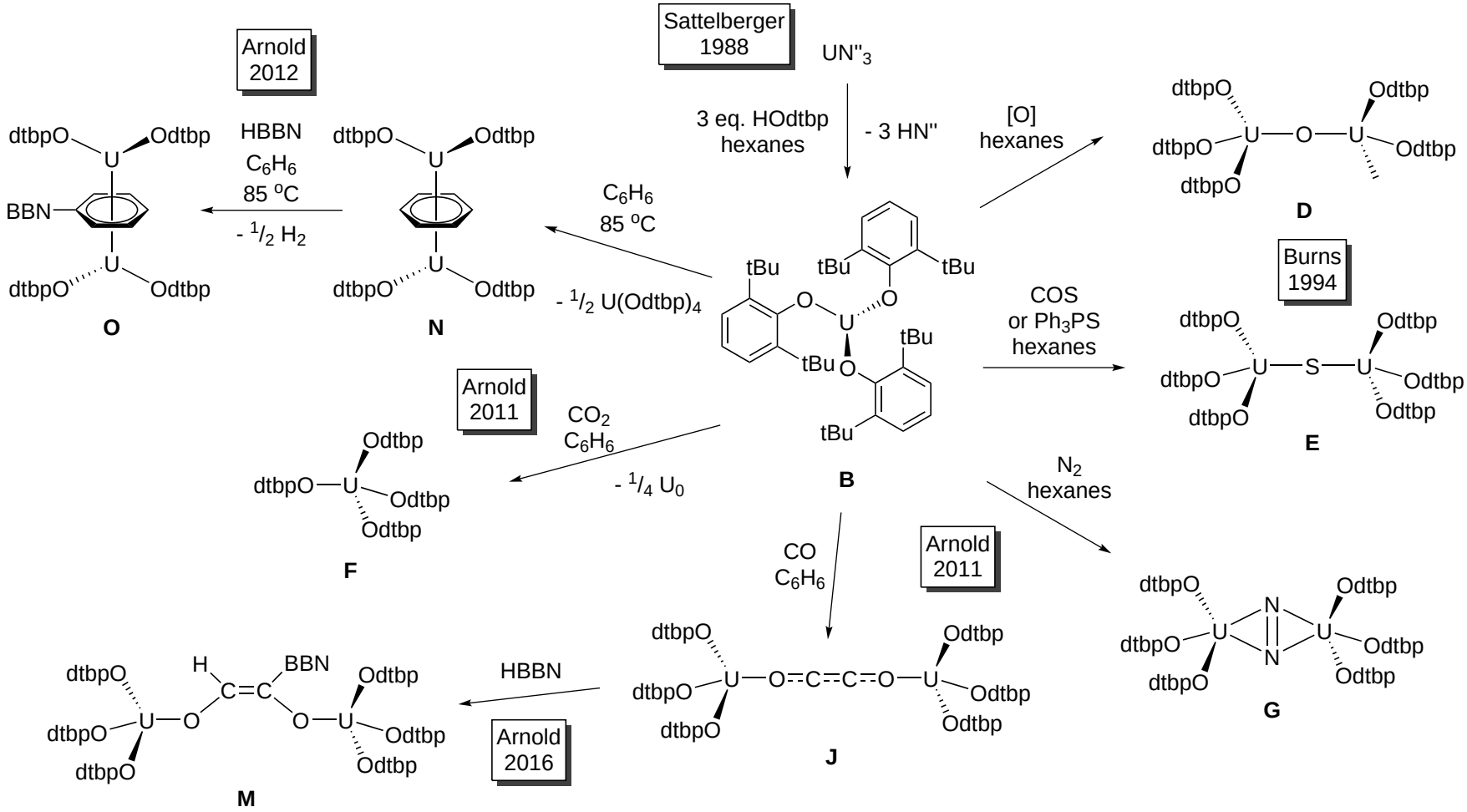

Scheme 1.4 – Synthesis and reactivity of **B** with various small molecules, as reported by the Sattelberger, Burns and Arnold groups.[23,31–34]

The dinitrogen complex **H** and the uranium tris(aryloxide) **B** were both found to react with 1 bar pressures of CO to effect the reductive coupling of carbon monoxide to yield the dimeric ynediolate-bridged products [{U(OAr$_3$)}$_2$(μ-C$_2$O$_2$)] (Ar = dtbp, **J**, Scheme 1.4; Ar = ttbp, **K**). This demonstrates the strong reducing ability of uranium(III) aryloxides and the efficient steric protection of the reactive metal centres. Additionally, the reaction of **H** with CO, despite the uranium centres being formally in the +4 oxidation state, suggests the dinitrogen ligand can be displaced by a suitable substrate if a thermodynamically strong bond is created. The metal centres in **H** can be considered as uranium(III) synthons, with electrons stored in the bridging N_2 ligand. Furthermore, the dinitrogen ligand may result in more controlled reactivity: where reacting **B** with CO_2 led to oxidative formation of **F**, the dinitrogen complex **H** was found to react with CO_2 to produce an oxo-bridged dimer with double insertion of CO_2 into a U−Ottbp bond and elimination of the dinitrogen ligand, providing [{U(Ottbp)$_2$}$_2$(μ-O)(μ-O$_2$COttbp)$_2$] (**L**). The bridging oxo ligand was suggested to originate from the reductive disporpotionation of CO_2, eliminating CO as a by-product.

A considerable challenge in organouranium small molecule activation chemistry is the removal or functionalisation of a substrate once the reductive transformation has occurred. In a recent private communication, our group reported that the reaction of 9-borabicyclo(3.1.1)nonane (HBBN) and **J** results in the hydroboration of the ynediolate bridge to furnish the borylated enediolate complex [{U(Odtbp)}$_2${μ-OCHC(BBN)O}] (**M**, Scheme 1.4).[34]

A further report from our group demonstrated that benzene solutions of **B** heated under reflux yield the uranium inverse sandwich complex [{UOdtbp$_2$}$_2$(μ-η^6-C$_6$H$_6$)] (**N**), forming two equivalents of homoleptic uranium(IV) aryloxide **F** as a by-product of the disproportionation reaction.[33] This methodology could be extended to a range of aromatic compounds, including substituted benzenes (*i.e.*: toluene, phenylsilane, biphenyl), but is also extended to aromatic systems (naphthalene or anthracene). Furthermore, carrying out the synthesis of **N** in the presence of HBBN (HBBN = 9-borabicyclo[3.1.1]nonane) or treating solutions of **N** with HBBN in refluxing solvent results in C−H borylation of the arene bridge, yielding the diuranium inverse sandwich complex [{UOdtbp$_2$}$_2$(μ-η^6-C$_6$H$_5$BBN)] (**O**, Scheme 1.4). Computational calculations suggest that decreasing the electron density on the bridging arene by borylation strengthens the uranium-arene interaction.[33]

The use of simple monodentate aryloxides in low oxidation state uranium chemistry has brought to light new uranium-based reactivity and advanced our knowledge. Multidentate aryloxides have also been prominent in the field, particularly tris(aryloxide) ligand platforms

reported by Meyer *et al*. The chemistry of these complexes will be discussed in the following section.

1.1.2 Tris(aryloxide) ligand platforms

Meyer has pioneered the use of tris(aryloxide) ligand platforms in uranium(III) chemistry. The ligands are composed of three aryloxides tethered to an organic linker such as triazacyclononane (tacn, [(^{R}ArO)$_3$tacn]), amine ([(^{Ad}ArO)$_3$N]) or mesitylene ([(^{R}ArO)$_3$Me])) (Figure 1.1). Each of these ligand environments can accommodate a uranium(III) centre, and the uranium(III) complexes [U{(^{R}ArO)$_3$tacn}] (**P^{R}**), [U{(^{Ad}ArO)$_3$N}] (**Q**) and [U{(^{R}ArO)$_3$Mes}] (**R^{R}**) are conveniently accessed by protonolysis of the pro-ligands with the uranium(III) silylamide UN″$_3$ (Figure 1.1).[35–37] The contrasting reactivity of the complexes **P, Q, R** denotes the importance of the coordination environment and steric and eletronic factors in organouranium chemistry, as discussed in the following sections.

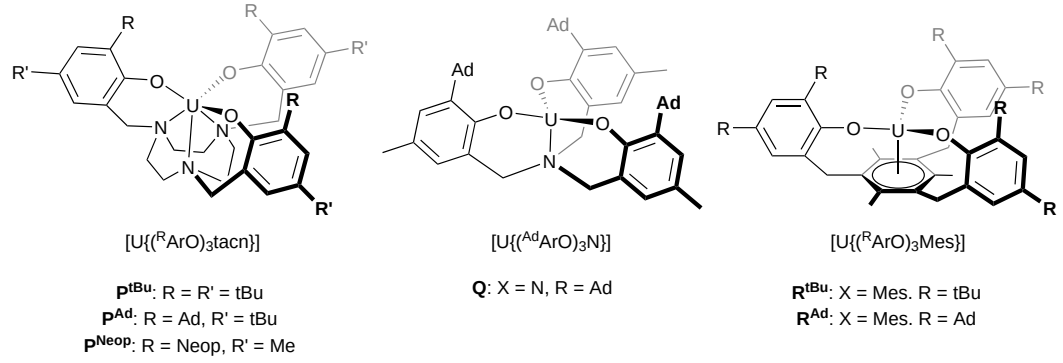

Figure 1.1 – Synthesis of uranium(III) complexes of tris(aryloxide) platform ligands as reported by Meyer and co-workers.[35–37]

All three complexes were crystallographically characterised, and the solid-state structure of **P^{tBu}** is particularly noteworthy. The seven-coordinate uranium centre is bound to the three *N* atoms of the tacn unit and the three aryloxide *O* atoms; the seventh coordination site *trans* to the tacn unit is occupied by a cyclic alkane molecule (C_5H_9Me or $C_6H_{11}Me$).[38] The authors suggested this to be a rare example of a metal alkane interaction, with short U−C distances of 3.8 Å that compare well to the sum of the van der Waals radii of 3.9 Å.[38]

Using the same ligand platform, Meyer and co-workers reported the diversity of uranium coordination chemistry with the synthesis of the first uranium(III) *N*-heterocyclic carbene adduct [U{(^{Ad}ArO)$_3$tacn}(:CIMMe$_4$)] (**S**), in which the carbene occupies the coordination site *trans* to

the tacn anchor.[39] DFT calculations on **S** suggest that carbene coordination is supported by π backbonding from the electron-rich metal centre to the ligand utilising metal f electrons.[39]

With these three ligand platforms in hand, the Meyer group have been able to probe and expand the reductive chemistry of uranium(III).

Oxocarbon reactivity

Exposing $\mathbf{P^{Neop}}$, **Q** or $\mathbf{R^{tBu}}$ solutions to CO_2 atmospheres produces the bimetallic carbonate-bridged complexes $[(U\{(^{Neop}ArO)_3tacn\})_2(\mu\text{-}CO_3)]$ (**T**), $[(U\{(^{Ad}ArO)_3N\})_2(\mu\text{-}CO_3)]$ (**U**) and $[(U\{(^{tBu}ArO)_3Mes\})_2(\mu\text{-}CO_3)]$ (**V**), respectively.[37,40,41] Each of these complexes can be synthesised by reacting the parent complex with N_2O, forming the oxo-bridged complexes $[\{U(ArO)_3L\}_2(\mu\text{-}O)]$ (L = tacn, $\mathbf{W^{Neop}}$; L = N, **X**;L = Mes, **Y**), which then react with CO_2 (Scheme 1.5). This provides insight into the mechanism of the reaction with CO_2, which must proceed *via* reductive cleavage of CO_2 to produce the oxo-bridged complexes ($\mathbf{W^{Neop}}$, **X** and **Y**), which then react with the remaining CO_2 (Scheme 1.5).[37,40,41]

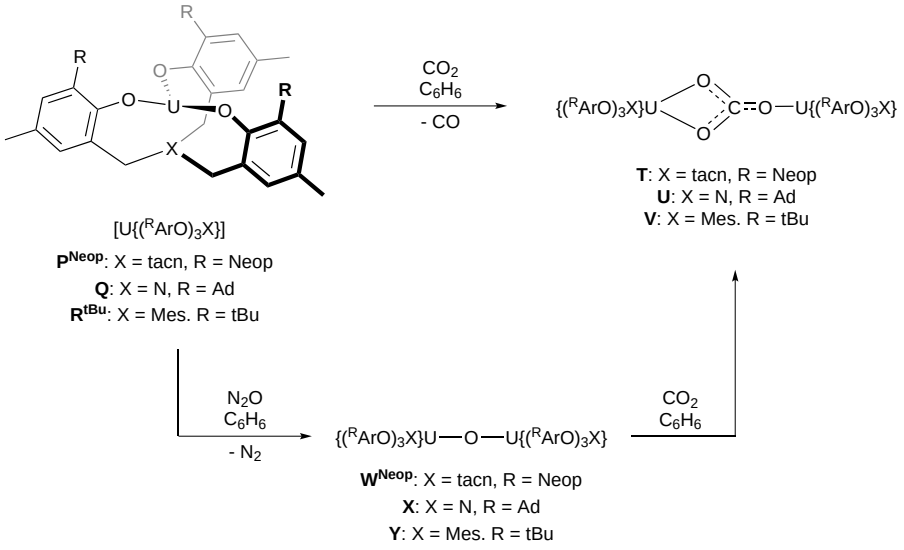

Scheme 1.5 – Reactivity of uranium(III) tris(aryloxide) platform ligand complexes with CO_2 to form bis-uranium(IV) carbonate-bridged complexes as reported by Meyer and co-workers.[37,40,41]

Contrasting reactivity is observed when the steric bulk of the ligand is modified in the tacn complexes. Placing solutions of the more sterically demanding $\mathbf{P^{Ad}}$ under a CO_2 atmosphere furnished the linear *O*-coordinated CO_2 adduct $[U(\eta^1\text{-}OCO)\{(^{Ad}ArO)_3tacn\}]$ (**Z**).[42] The CO_2 ligand in **Z** is likely to be a radical anion, as suggested by the U−O distance of 2.351(3) Å,

and a redshift in the vibrational frequency to 2188 cm^{-1}. Using the less sterically demanding $\mathbf{P^{tBu}}$ only yields the bridging oxo complex [(U{(^{tBu}ArO)$_3$tacn})$_2$(μ-O)] ($\mathbf{W^{tBu}}$) when exposed to CO_2, and is formed by reductive cleavage of CO_2 (Scheme 1.6).[43]

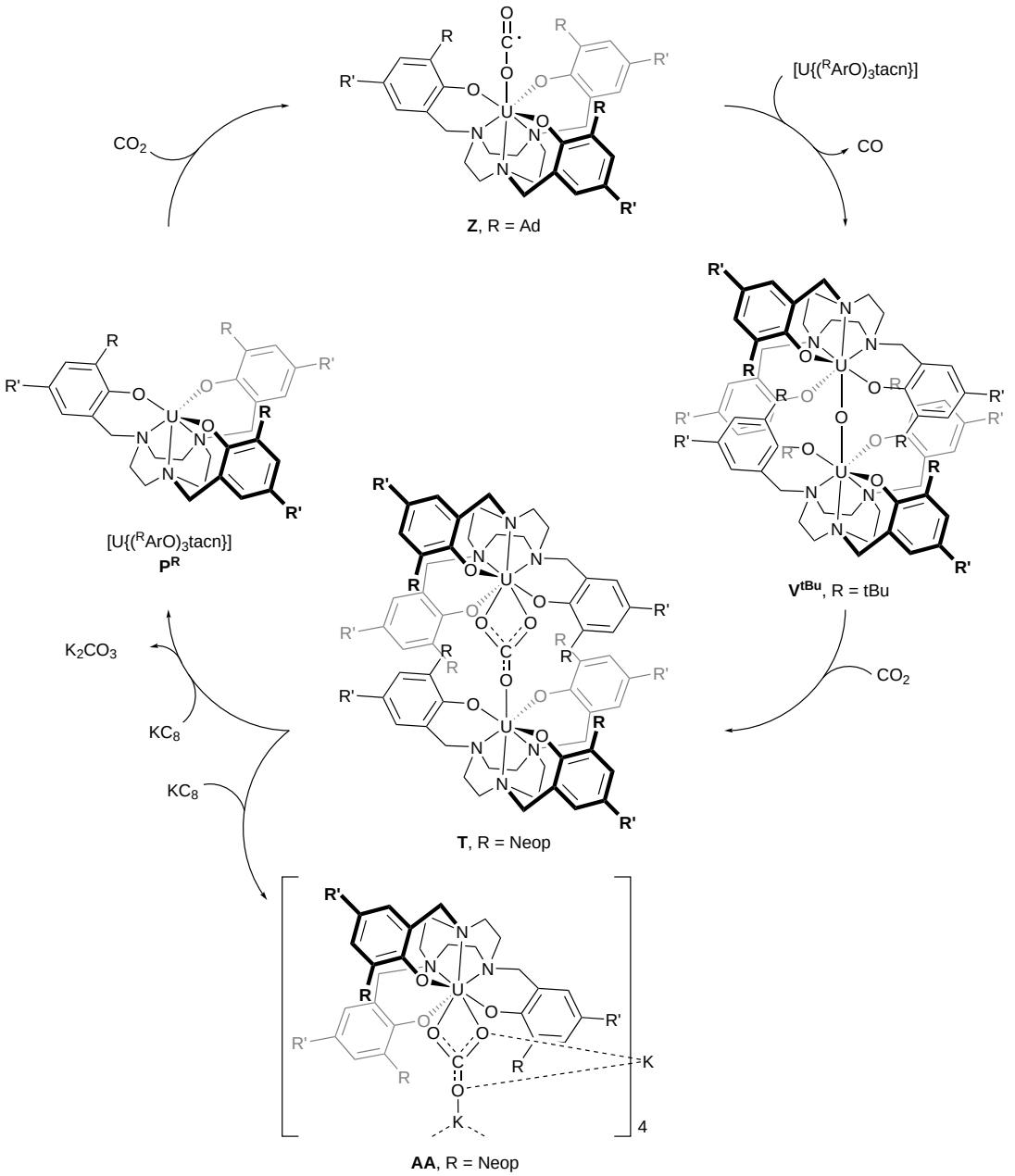

Scheme 1.6 – Impact of variating the steric parameters of uranium(III) tris(aryloxide) triazacyclononane complexes on their reactivity with carbon dioxide.[40]

The difference in reactivity of the three triazacyclononane complexes was ascribed by the authors to the shape of the reactive cavity imposed by the ligand frame at the metal centre. The narrow and linear cavity in $\mathbf{P^{Ad}}$ allows the coordination and one-electron reduction of

the substrate, but not the approach of another metal centre to effect the second one-electron reduction.[42] The second one-electron reduction is possible in complex $\mathbf{P^{tBu}}$, but the resulting oxo-bridged complex $\mathbf{W^{tBu}}$ is too well shielded by the *tert*-butyl groups to allow the approach of another CO_2 molecule.[43] In $\mathbf{P^{Neop}}$, the additional flexibility of the neopentyl group allows both the formation of the oxo complex $\mathbf{W^{Neop}}$ and the approach of another CO_2 molecule close to the oxo bridge to form the carbonate complex **T** (Scheme 1.6).[40]

The neopentyl-substituted ligand has allowed another notable reaction. Unlike **Q** and $\mathbf{R^{tBu}}$, the carbonate complex **T** can be reduced with excessive amounts of KC_8 to regenerate $\mathbf{P^{Neop}}$, forming K_2CO_3 and C as side products. Several catalytic cycles were obtained using excessive amounts of CO_2 and KC_8, until the tetranuclear uranium(IV) complex **AA** is formed and terminates the cycle (Scheme 1.6).[40]

The oxalate complex [U({(^{Neop}ArO)$_3$tacn})$_2$(μ-C_2O_4)] (**AB**) could also be obtained when the reaction of $\mathbf{P^{Neop}}$ with CO_2 was carried out in the presence of KC_8 (Scheme 1.7).[41] In this case, the two uranium centres, aided by the reducing power of potassium metal, effect a reductive coupling of two CO_2 molecules to form a new C−C bond.[41]

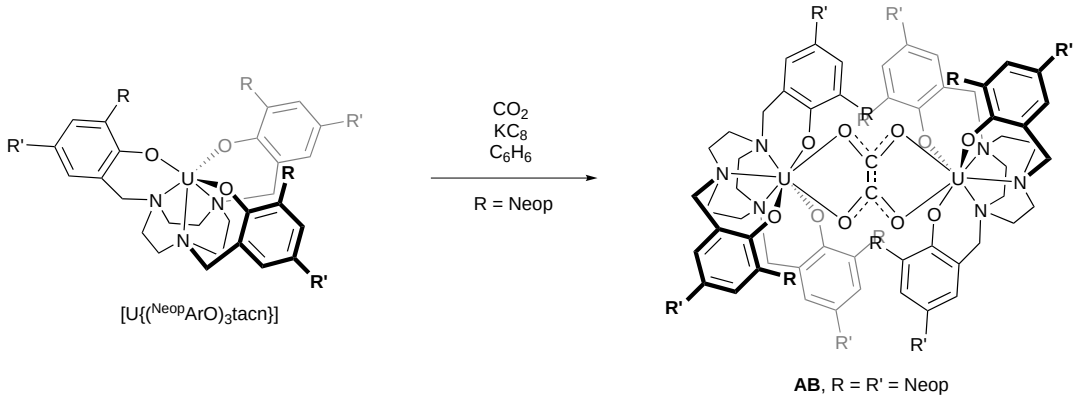

Scheme 1.7 – Formation of the oxalate-bridged complex **AB** by reaction of $\mathbf{P^{Neop}}$ with CO_2 in the presence of KC_8.[41]

The reduction chemistry of carbon monoxide with these systems is relatively unexplored, however Meyer and co-workers have reported the synthesis of the only end-on carbonyl-bridged diuranium complex [(U{(^{tBu}ArO)$_3$tacn})$_2$(μ-CO)] (**AC**, Scheme 1.8). Similarly to the oxo-bridged complex $\mathbf{W^{tBu}}$, the efficient steric shielding of the bridging carbonyl ligand in **AC** prevents the approach of another carbon monoxide molecule to furnish an unusual compound where the two uranium centres are of different oxidation state.[43]

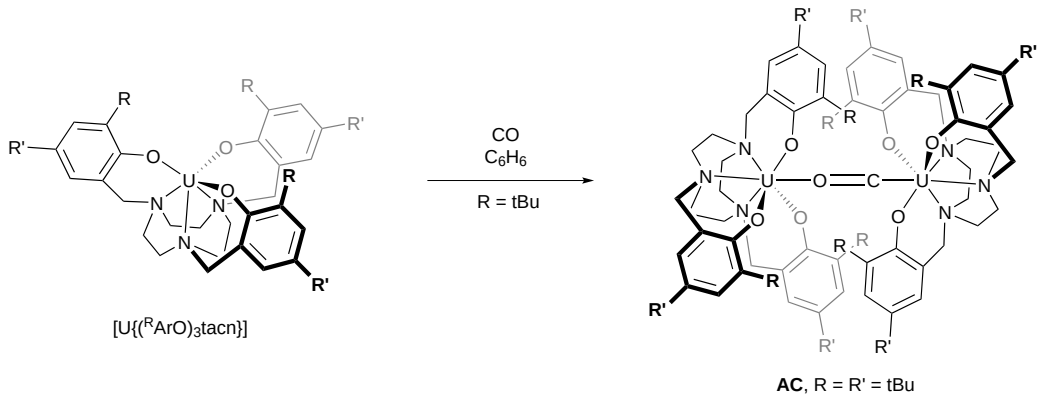

Scheme 1.8 – Formation of the carbon monoxide-bridged complex **AC** by reaction of $\mathbf{P^{tBu}}$ with CO.[43]

The oxocarbon reactivity of the triazacyclononane complexes $\mathbf{P^{R}}$ was extended to organic molecules containing unsaturated C−O bonds. Reaction of $\mathbf{P^{tBu}}$ with di-*tert*-butylbenzophenone lead to the isolation of the uranium coordinated ketyl radical $[U(OCAr_2)\{(^{tBu}ArO)_3tacn\}]$ which, upon hydride abstraction of 1,4-cyclohexadiene, gave the corresponding diphenylmethoxide complex $[U(OCHAr_2)\{(^{tBu}ArO)_3tacn\}]$ (**AD**, Scheme 1.9).[44] When benzophenone was used, a bimetallic uranium complex was isolated in poor yields in which the two uranium centres were bridged by two coupled benzophenone molecules (**AE**, Scheme 1.9).[44]

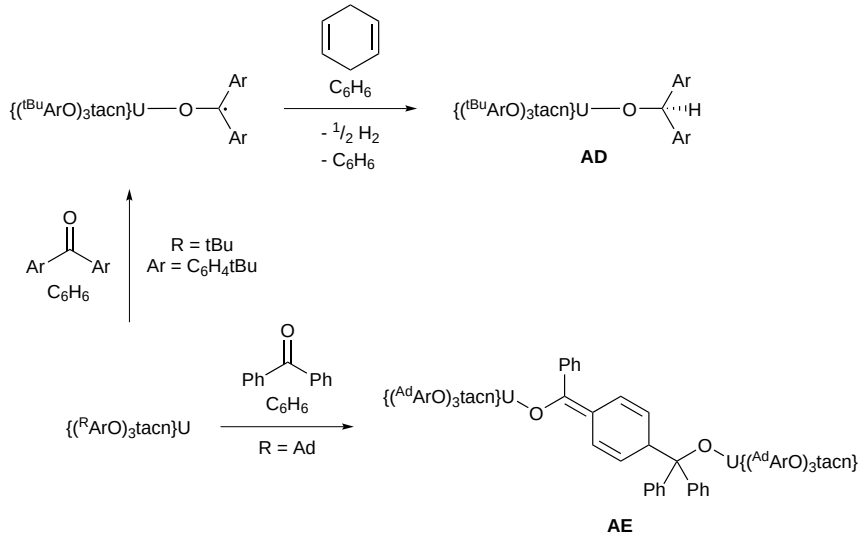

Scheme 1.9 – Reactivity of $\mathbf{P^{R}}$ with ketones, forming uranium ketyl complexes.[44]

The investigations into organic ligands containing carbon heteroatom multiple bonds were extended to diphenyldiazomethane, which was shown to react with $\mathbf{P^{tBu}}$ to yield the bent

η^2-bound complex [U(η^2-N_2CPh_2){(^{tBu}ArO)$_3$tacn}] (**AF**, Scheme 1.10).[45] In contrast, the linear η^1-bound complex [U(N_2CPh_2){(^{Ad}ArO)$_3$tacn}] was obtained with the more sterically bulky $\mathbf{P^{Ad}}$. The diazomethane ligand rearranges upon heating to provide the 3-phenylindazole coordinated complex [U{3-Ph(Ind)}{(^{Ad}ArO)$_3$tacn}] (**AG**, Scheme 1.10).[45]

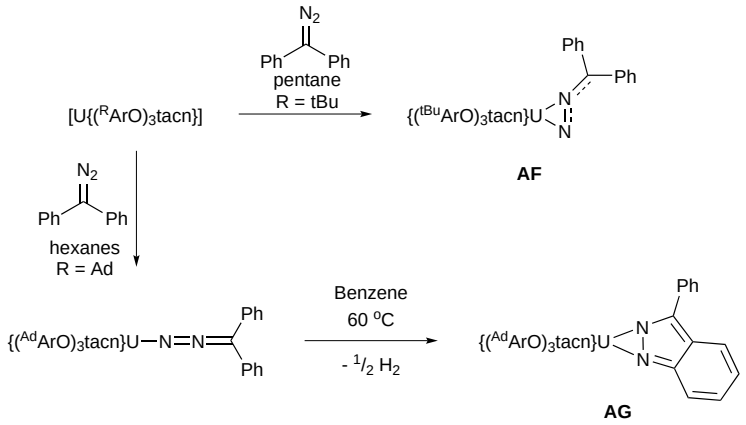

Scheme 1.10 – Reactivity of $\mathbf{P^{tBu}}$ with diphenyldiazomethane.[45]

Meyer showed $\mathbf{P^{tBu}}$ can react with organic molecules containing several carbon heteroatom multiple bonds, as exemplified by the reactivity with 1,2-diketones.[46] Reaction of $\mathbf{P^{tBu}}$ with equimolar dibenzoyl provided [U{κ^2-$(OCPh)_2$}{(^{tBu}ArO)$_3$tacn}] (**AH**, Scheme 1.11), with a *cis*-bound diketone. Reaction of substoichiometric dibenzoyl with $\mathbf{P^{tBu}}$ results in the formation of the diketone-bridged bimetallic complex [(U{(^{tBu}ArO)$_3$tacn})$_2${μ-$(OCPh)_2$}] (**AI**). While the monometallic adduct **AH** is unreactive towards CO_2, it was found that the *trans*-diketone-bridged compound **AI** reacts with CO_2 forming a new C−C bond and yielding the carboxylatodiketone-bridged complex [(U{(^{tBu}ArO)$_3$tacn})$_2${μ-$(OCPhOCPh_2CO_2)$}] (**AJ**, Scheme 1.11).[46]

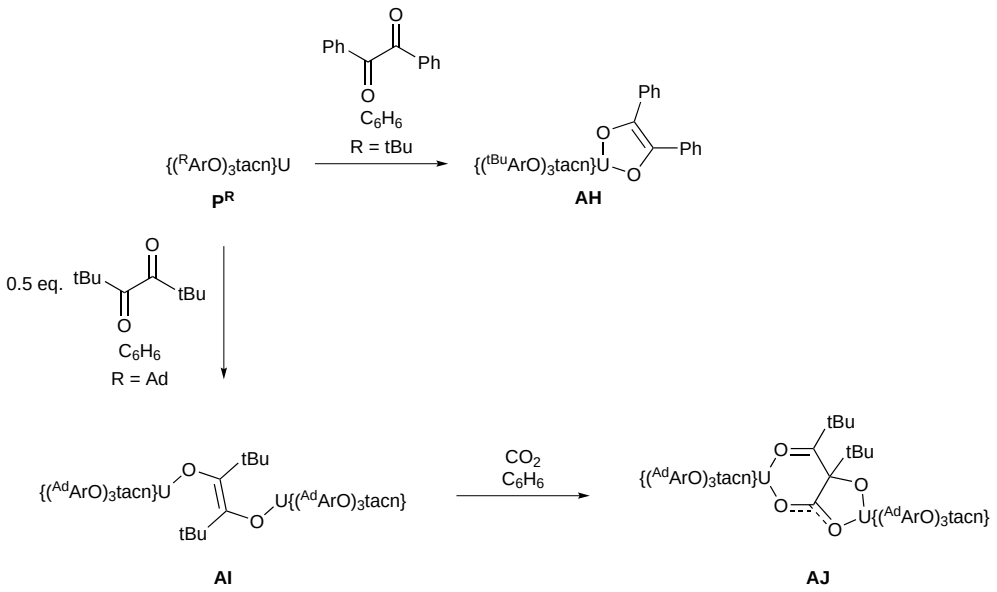

Scheme 1.11 – Reactivity of $\mathbf{P^{tBu}}$ with 1,2-diketones.[46]

Chalcogenide reactivity

In addition to CO_2 reactivity, Meyer extended the reactivity of uranium(III) to a range of heavier chalcogen substrates. Reaction of **Q** with CS_2 yields the tetrathiooxalate-bridged bimetallic U(IV)/U(IV) complex $[(U\{(^{Ad}ArO)_3N\})_2(\mu\text{-}C_2S_4)]$ (**AK**, Scheme 1.12) as the major product (*circa* 80%). The C_2S_4 bridge in **AK** can be reduced by reaction with Na(Hg) to afford the ethylene tetrathiolate complex $Na_2[(U\{(^{Ad}ArO)_3N\})_2(\mu\text{-}C_2S_4)]$ (**AL**, Scheme 1.12).[47] The minor product in the reaction of **Q** with CS_2 was identified as the trithiocarbonate-bridged complex $[(U\{(^{Ad}ArO)_3N\})_2(\mu\text{-}CS_3)]$ (**AM**). Unlike the CO_2 reactivity of **Q**, the thermodynamic product of CS_2 activation is not the trithiocarbonate-bridged complex but the tetrathiooxalate-bridged complex.[48]

Complex $\mathbf{P^{Neop}}$ was shown to react cleanly with SO_2 to provide the dithionite-bridged bimetallic complex $[(U\{(^{Neop}ArO)_3tacn\})_2(\mu\text{-}O_2SSO_2)]$ (**AN**). This contrasts with the reactivity of $\mathbf{P^{Neop}}$ with CO_2, which requires an external reducing agent to yield the oxalate-bridged complex **AB**.[41] Analogously to the CO_2 reactivity of $\mathbf{P^{Neop}}$, reaction of the oxo-bridged complex $\mathbf{W^{Neop}}$ with SO_2 leads to the formation of the uranium(IV) sulfite-bridged complex $[(U\{(^{Neop}ArO)_3tacn\})_2(\mu\text{-}SO_3)]$ (**AO**) by SO_2 insertion into a U−O bond of the bridging oxo ligand.[41]

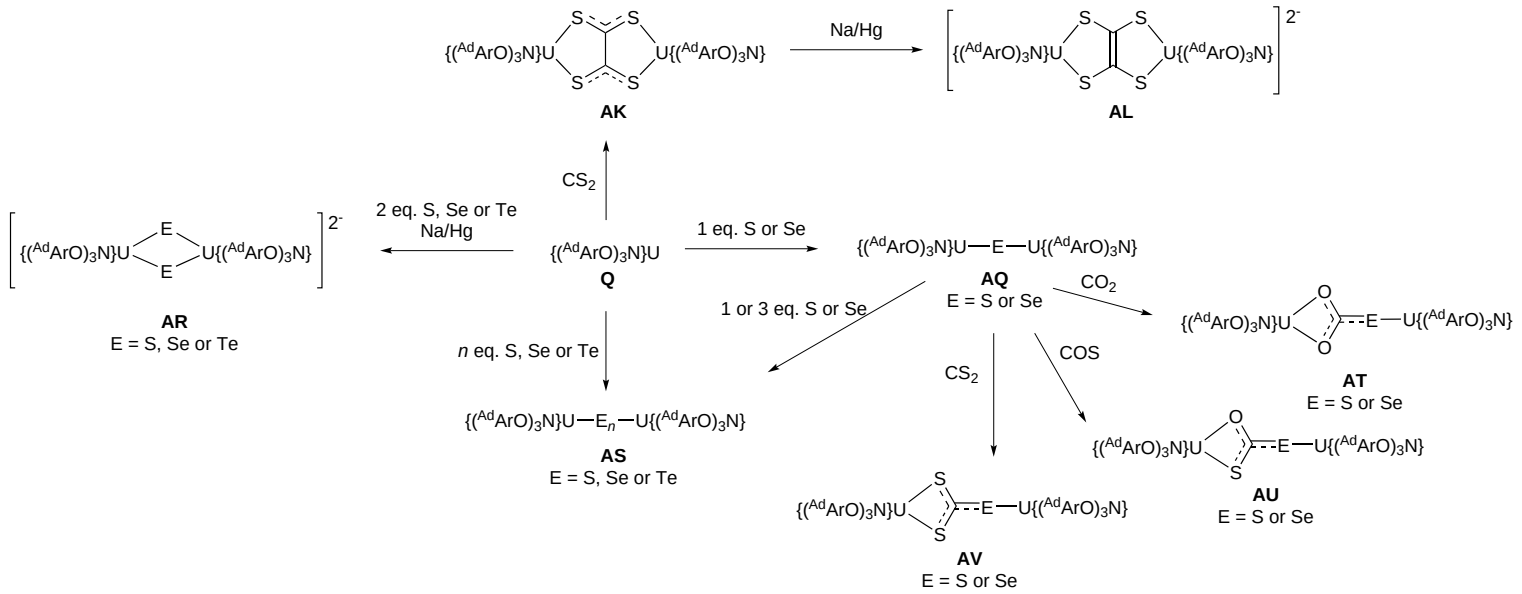

Scheme 1.12 – Reactivity of **Q** with chalcogenides and chalcogen-containing reagents.[41,47–50]

Reactivity was also observed with elemental chalcogens. Complexes $\mathbf{P^{tBu}}$ and **Q** were both found to react with elemental sulfur or selenium to yield chalcogenide-bridged complexes $[(U\{(^{tBu}ArO)_3tacn\})_2(\mu\text{-}E)]$ (**AP**, E = S or Se) and $[(U\{(^{Ad}ArO)_3N\})_2(\mu\text{-}E)]$ (**AQ**, E = S or Se, Scheme 1.12).[47] However, unlike with $\mathbf{P^{tBu}}$, the reaction of **Q** with elemental chalcogenides S, Se or Te in the presence of the strong reducing agent Na(Hg) provided the bis-chalcogenide-bridged complexes $Na_2[(U\{(^{Ad}ArO)_3N\})_2(\mu\text{-}E)_2]$ (**AR**, Scheme 1.12).[47] Complex **Q** was subsequently found to react with varying quantities of elemental chalcogenides to yield mono-, bis- or tetra-chalogenide-bridged complexes, in which the chalcogen-chalcogen bonds are retained (**AS**, Scheme 1.12).[49]

Additionally, it was found that the chalcogenide-bridged complexes could react further with small unsaturated molecules.[50] Exposing the bridging chalcogenido complexes **AQ** to an atmosphere of CO_2 yields the thio or seleno carbonate complexes $[(U\{(^{Ad}ArO)_3N\})_2(\mu\text{-}O_2CE)]$ (**AT**, E = S, Se), by insertion of CO_2 into a uranium chalcogenide bond. As the uranium centres are in the +4 oxidation state, the reactivity is likely to be centred on the bridging chalcogenide ligand. Reactions with COS or CS_2 also provided insertion products with chalcogenothiocarbonate ($ECOS^{2-}$, **AU**, Scheme 1.12) and chalcogenodithiocarbonate ($ECS_2{}^{2-}$, **AV**, Scheme 1.12) bridged complexes.[50]

Imido and terminal oxo chemistry

The triazacyclononane supported complexes $\mathbf{P^{tBu}}$ and $\mathbf{P^{Ad}}$ react with trimethylsilylazide to give the uranium(V) imido complexes $[U(NSiMe_3)\{(^{R}ArO)_3tacn\}]$ (R = tBu, $\mathbf{AW^{tBu}}$; R = Ad, $\mathbf{AW^{Ad}}$, Scheme 1.13).[51] No further reaction was observed with $\mathbf{AW^{tBu}}$, however the complex of the more sterically demanding ligand $\mathbf{AW^{Ad}}$ could react with methylisocyanide to eliminate hexamethyldisilane and provide the cyanamide complex $[U(CNCMe)\{(^{Ad}ArO)_3tacn\}]$ (**AX**).[52] The cyanamide complex **AX** was found to be reactive towards electrophiles such as CH_2Cl_2 or CH_3I to eliminate the carbodiimides MeNCNR (R = CH_2Cl or Me) and yield the corresponding uranium(IV) halide $[UX\{(^{Ad}ArO)_3tacn\}]$ (**AY**; X = Cl or I) which can be reduced back to the uranium(III) precursor $\mathbf{P^{Ad}}$ with Na(Hg). These reactions represent the individual steps of a catalytic cycle (Scheme 1.13).[52] The U(V) imido complex $\mathbf{AW^{Ad}}$, was shown to react with the strong π acid carbon monoxide to yield the uranium(IV) isocyanate complex $[U(NCO)\{(^{Ad}ArO)_3tacn\}]$ by elimination of Si_2Me_6.[52]

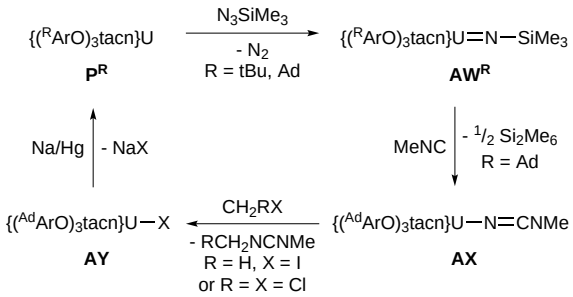

Scheme 1.13 – Reactivity of $\mathbf{P^{tBu}}$ and $\mathbf{P^{Ad}}$ with trimethylsilylazide to form the corresponding uranium(V) imido complexes. The more sterically demanding imido complex $\mathbf{AW^{Ad}}$ was found to be reactive with strong π acids.[51,52]

Contrasting reactivity is also observed between the *tert*-butyl and *neo*-pentyl substituted complexes. Complex $\mathbf{P^{tBu}}$ effects a one-electron reduction of Ph_3CN_3 to form the uranium(IV) azido complex $[UN_3\{(^{tBu}ArO)_3tacn\}]$ (**AZ**, Scheme 1.14) by elimination of Gomberg's dimer, the coupling product of two trityl radicals. In comparison, the reaction of Ph_3CN_3 with $\mathbf{P^{Neop}}$ results in the elimination of N_2 to furnish the uranium(V) tritylimido complex $[U(NCPh_3)\{(^{Neop}ArO)_3tacn\}]$ (**BA**).[51,53] The redox chemistry of **BA** is surprisingly rich; oxidation with $AgSbF_6$ yields the uranium(VI) tritylimido complex $[U(NCPh_3)\{(^{Neop}ArO)_3tacn\}][SbF_6]$ (**BB**, Scheme 1.14) while reduction with KC_8 provides the uranium(IV) tritylimido -ate complex $K[U(NCPh_3)\{(^{Neop}ArO)_3tacn\}]$ (**BC**, Scheme 1.14). The potassium-ate complex **BC** is reactive towards CO_2, yielding the uranium(IV) oxo potassium-ate complex $K[UO\{(^{Neop}ArO)_3tacn\}]$ (**BD**, Scheme 1.14) by elimination of tritylisocyanate.[53]

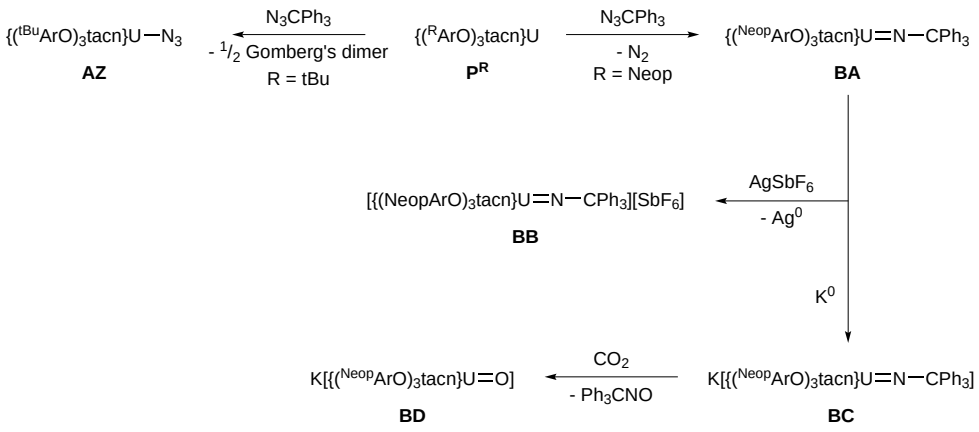

Scheme 1.14 – Differing reactivity of $\mathbf{P^{tBu}}$ and $\mathbf{P^{Neop}}$ with trityl azide. The uranium(V) tritylimido complex **BA** can be oxidised to the uranium(VI) terminal azide complex **BB** or reduced to the terminal uranium(IV) azide **BC**, which exhibits CO_2 reactivity.[51,53]

The imido complexes were found to be a convenient entry into terminal uranium(V) oxo chemistry. Reaction of $\mathbf{P^{tBu}}$, $\mathbf{P^{Ad}}$ or $\mathbf{P^{Neop}}$ with mesitylazide resulted in the formation of the uranium(V) mesitylimide complexes [UNMes{(^{R}ArO)$_3$tacn}] (R = *t*-Bu, $\mathbf{BE^{tBu}}$; R = Ad, $\mathbf{BE^{Ad}}$; R = Neop, $\mathbf{BE^{Neop}}$). Upon reaction with CO_2, $\mathbf{BE^{tBu}}$ and $\mathbf{BE^{Ad}}$ eliminate mesitylisocyanate to provide the uranium(V) terminal oxo complexes [UO{(^{R}ArO)$_3$tacn}] (R = *t*-Bu, $\mathbf{BF^{tBu}}$; R = Ad, $\mathbf{BF^{Ad}}$).[54] The same reaction with $\mathbf{BE^{Neop}}$, however, results in the formation of the dioxo-bridged complex [(U{(^{R}ArO)$_3$tacn})$_2$(μ−O)$_2$ (**BG**).[55] Oxidation of the three complexes $\mathbf{BF^{tBu}}$, $\mathbf{BF^{Ad}}$ and **BG** with SbF_6 resulted in the formation of the uranium(VI) terminal oxo complexes [UO{(^{R}ArO)$_3$tacn}][SbF_6] (R = *t*-Bu, $\mathbf{BH^{tBu}}$; R = Ad, $\mathbf{BH^{Ad}}$; R = Neop, $\mathbf{BH^{Neop}}$).[55,56]

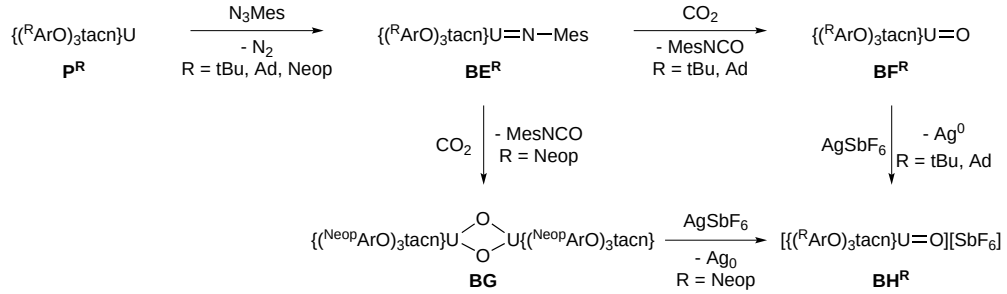

Scheme 1.15 – Synthesis of uranium(V) terminal mesitylimido complexes from $\mathbf{P^R}$ and their reactivity with CO_2 to form uranium(V) oxo complexes. The oxidation of the oxo complexes provided the uranium(IV) terminal oxo complexes $\mathbf{BH^R}$.

Reduction chemistry

Having explored the oxidation chemistry of uranium(III) of **R**, Meyer also reported its reduction chemistry.[5,57] Reaction of $\mathbf{R^{Ad}}$ with potassium sand in the presence of 2,2,2−cryptand at −30 °C in THF resulted in the formation of the red brown uranium(II) complex **BI**. A shortening of the U−arene$_{Ct}$ (*Ct* = centroid) distance in the solid-state from 2.352(2) Å in $\mathbf{R^{Ad}}$ to 2.188(2) Å in **BI** suggests higher bonding character in the δ interaction, rationalised by an additional electron in the HOMO. **BI** was shown to be EPR inactive, suggesting an integer spin consistent with a $5f^4$ ground state. This was further confirmed by DFT and SQUID magnetic measurements. In addition, it was found that intramolecular C-H activation of the benzylic position occurs upon warming, affording the functionalised arene complex **BJ** previously characterised as an oxidation product of $\mathbf{R^{Ad}}$ (Scheme 1.16).[57] The reaction has been shown to occur *via* the formation of a uranium hydride in the absence of cryptand or a crown ether.[57]

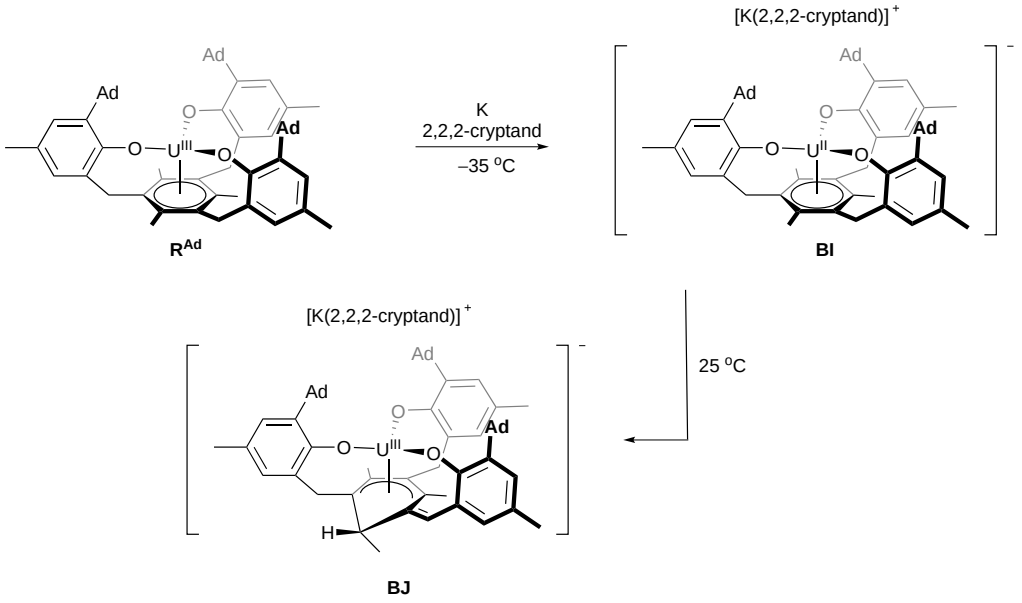

Scheme 1.16 – Synthesis of uranium(II) anion from the mesityl-bridged uranium(III) tris(aryloxide) platform complex $\mathbf{R^{Ad}}$.

1.2 Actinide arene complexes

The seminal discovery of bis(arene) lanthanide(0) complexes by co-condensation of metal atoms and ligand vapours was reported by Cloke and co-workers in 1987, 32 years after the synthesis of bis(benzene)chromium by Fischer.[58] Employing the bulky tri-*tert*-butylbenzene ligand, Cloke was able to isolate the yttrium complex $[Y(C_6H_3{}^tBu_3)_2]$ and the gadolinium complex $[Gd(C_6H_3{}^tBu_3)_2]$ (**BK** and **BL**, respectively; Scheme 1.17). Whilst extremely specialised and harsh conditions are required for the synthesis of these complexes (and the analogues of other electropositive metals), they are remarkably robust once synthesised. Lanthanide(III) ions have extremely contracted electronic shells due to the lack of radial nodes in the $4f$ electronic wavefunction. For lanthanide(0) complexes, the $4f$ and $5d$ orbitals have been calculated to be close in energy, allowing the $5d$ orbitals a degree of ligand-field interaction in excited states $4f^{n-x}5d^{0+x}$. The metal centres in these complexes are suggested to be in the $+0$ oxidation state. This is supported by paramagnetic ^{1}H NMR spectra for both **BK** and **BL**. Furthermore, while paramagnetic EPR measurements on **BK** gave rise to an EPR silent spectrum at room temperature, a doublet with g value of 2 was observed when the sample was cooled to 77 K, consistent with an yttrium centred unpaired electron. Structural elucidation of **BL** revealed the Gd−C distances are comparable to isostructural complexes of early transition metals and

displayed no arene ring distortion. This demonstrated for first time that a lanthanide complex in which the formal oxidation state is +0 could be formed and that the bis(arene) motif could be extended beyond the *d*-block metals. This approach was extended by Cloke and co-workers to the tri-*tert*-butylphosphorin ligand to isolate a Ho(0) complex (**BM**, Scheme 1.17) for the third and final crystallographically characterised f element bis(arene) complex.[59]

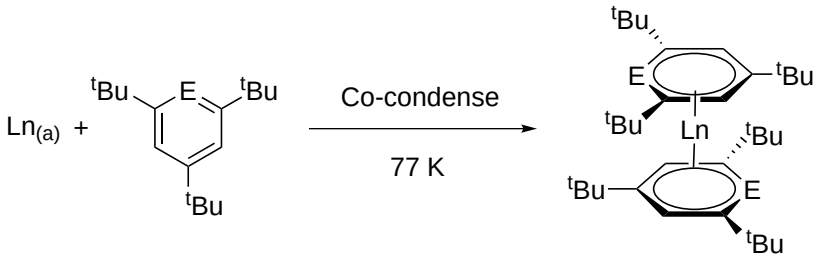

E = CH, Ln = Y (**BK**), Gd (**BL**)
E = P, Ln = Ho (**BM**)

Scheme 1.17 – Metal vapour synthesis of compounds **BK, BL** and **BM**, as reported by Cloke and co-workers.

This methodology was extended by Arnold and Cloke to other lanthanides (Sm, Eu, Tm and Yb) using both tri-*tert*-butylbenzene and tri-*tert*-butylphosphorin ligands, as well as introducing the tri-*tert*-butylpyridine ligand, but the complexes were not crystallographically characterised and some proved to be unstable at temperatures above 77 K and could only be observed in an inert matrix.[60] Computational calculations on $4f$ and $5f$ analogues suggest a bent geometry may be favoured for less sterically hindering ligands such as benzene which is induced by better d and f orbital overlap with the ligands.[61]

The closest structural motif to homoleptic bis(arene) metal complexes obtained with the actinides is the bis(cyclooctatetraene) actinide motif, $An(COT)_2$ (COT = cyclooctatetraene), with the isolation of uranocene and thorocene.[26]

1.2.1 Uranium arene complexes

Efforts to obtain uranium complexes with the bis(arene) motif by conventional synthetic methods applied to transition metals have invariably failed and afforded unexpected products. The first of such examples was reported by Cesari and co-workers in 1971 who obtained the first uranium complex containing a neutral bound arene, $[U(\eta^6\text{-}C_6H_6)(AlCl_4)_3]$ (**BN**), using the Fisher-Hafner method.[62] UCl_4, $AlCl_3$ and aluminium powder were refluxed in benzene for seven hours, which yielded black crystals upon standing at room temperature after filtration. In the

solid-state structure, the seven-coordinate *pseudo* trigonal bipyramidal uranium(III) centre is bound to five chlorine atoms that belong to $AlCl_4$ ligands in the equatorial plane, and the axial plane is occupied by a chloro ligand and a coordinated benzene molecule. The uranium-arene ring centroid (arene$_{Ct}$) distance is 2.56(1) Å, however the authors commented that the X-ray data was not reliable beyond connectivity.

Cotton *et al*. reported in 1985 an attempt to use the same methodology with hexamethylbenzene but were unable to isolate an arene complex.[63] They modified the procedure by separating the electrophilic addition and the reduction steps; UCl_4, $AlCl_3$ and hexamethylbenzene were refluxed in hexane for 12 hours prior to extraction with dichloromethane, yielding a yellow solution which was subsequently reduced with zinc granules to give a red solution. Yellow crystals which were determined to be $[\{U(\eta^6\text{-}C_6Me_6)Cl_2\}(\mu\text{-}Cl)_3][AlCl_4]$ (**BO**, Figure 1.2), were obtained by slow diffusion of hexanes in a solution of **BO** in CH_2Cl_2, followed by precipitation of a red powder. The crystal structure of **BO** revealed a dimeric complex in which each uranium centre was η^6 coordinated to hexamethylbenzene and possessed two terminal chloro ligands and three bridging chloro ligands. Additionally, a non-coordinated $AlCl_4$ ligand confirmed **BO** to be a bimetallic U(IV)/U(IV) complex. The average uranium-arene$_{Ct}$ distance in **BO** is 2.55(1) Å, which is remarkably similar to that of **BN**. As the oxidation state differs between **BN** and **BO**, the authors suggest the similarity in U−arene$_{Ct}$ is indicative of a very weak interaction. The authors proposed that **BO** may be obtained directly from the yellow CH_2Cl_2 solution prior to reduction based on the colour and oxidation state of the compound in a subsequent paper.[64]Therein, they reported the trimeric complex $[\{U(\eta^6\text{-}C_6Me_6)Cl_2\}_2(\mu\text{-}Cl)_6\{UCl_2\}]$ (**BP**, Figure 1.2) which is obtained by a similar procedure to **BO**. The $AlCl_3$ equivalents were reduced to near stoichiometric quantities and the reduction step was removed altogether. The authors commented that **BP** can be obtained reproducibly and in good yields, unlike **BO**. The compound was structually characterised, and the U−arene$_{Ct}$ distance was found to be slightly longer than that of the previous two examples at 2.58(1) Å. All three uranium centres in **BP** were in the +4 oxidation state.[64]

After a further modification, Cotton *et al*. reported the synthesis of the trimeric uranium(III) complex $[\{U(\eta^6\text{-}C_6Me_6)(\mu\text{-}Cl)(\mu\text{-}Cl_2AlCl_2)\}_3(\mu^3\text{-}Cl)][AlCl_4]$ (**BQ**, Figure 1.2).[65] This was achieved by carrying out the reaction in refluxing toluene as opposed to hexane and by substituting zinc with aluminium as the reducing agent in the preparation of **BO**. The reaction yields a red brown solution from which dark red-brown crystals of **BQ** can be isolated from slow cooling of the reaction mixture after filtration. Compound **BQ** is probably a related material to the red

powder obtained after reduction of **BO** with zinc.

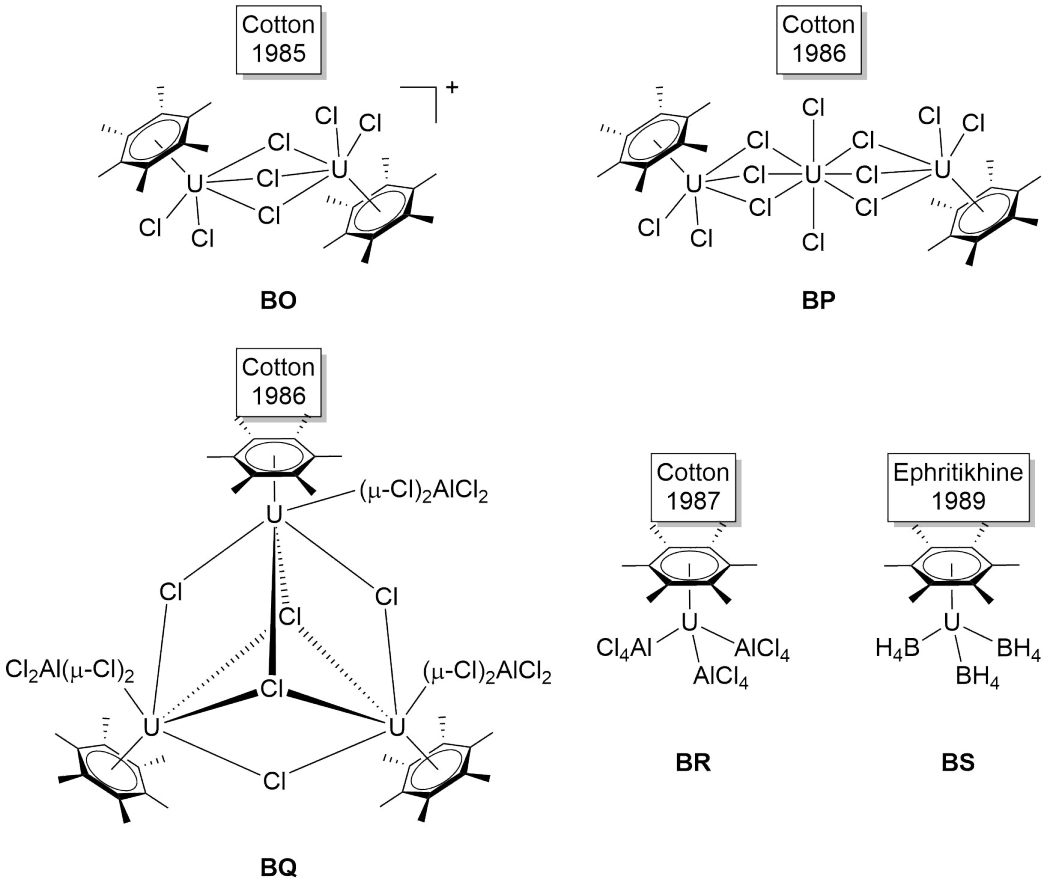

Figure 1.2 – Uranium hexamethylbenzene complexes as reported by Cotton and Ephritikhine and co-workers.[63–67]

In 1987, Cotton *et al.* reported the synthesis of $U(\eta^6\text{-}C_6Me_6)(AlCl_4)_3$ (**BR**, Figure 1.2), the hexamethylated analogue of **BN**, by carrying out a two-step reaction in toluene with excessive amounts of $AlCl_3$ and using aluminium powder as the reducing agent. Dark brown crystals of **BR** were obtained by cooling refluxing toluene solutions of **BR** to room temperature. **BR** is isostructural to **BN**, with the hexamethylbenzene occupying one of the axial positions of the pentagonal bipyramidal uranium centre.[66]

Cotton *et al.* initially proposed that carrying out the reaction in an arene solvent would cause competition issues between the more electron-deficient arene solvent which is in excess and electron-rich C_6Me_6, which is present in stoichiometric quantities. However, they found that uranium, which is highly Lewis acidic, preferred the electron-rich arene, precluding the need to avoid arene solvents. Using stoichiometric amounts of $AlCl_3$ proved useful to give non-Al containing compounds, but the poor solubility and oligomeric nature of the resulting

complexes limited their usefulness as reagents in organometallic chemistry. An excess of $AlCl_3$ led to monometallic complexes bearing $AlCl_4$ ligands with appreciable solubility in non-coordinating solvents. Invariably, the compounds were unstable in donor solvents (*i.e.*: THF, MeCN), which provided the UCl_4 solvates. The uranium−arene distances are comparable in all examples reported by Cotton and co-workers regardless of oxidation state, ranging from 2.55(1) to 2.58(1) Å.[63–66]

In 1989, Ephritikhine and co-workers reported the thermal decomposition of $U(BH_4)_4$ in mesitylene, which unexpectedly yielded the U(III) arene complex [U(η^6-Mes)$(BH_4)_3$] (**BS**). The affinity of the uranium centre for more electron-rich arenes was demonstrated by the displacement of the mesitylene ligand with a hexamethylbenzene ligand at room temperature in a toluene solution, from which they obtained single crystals of [U(η^6-C_6Me_6)$(BH_4)_3$] (**BT**, Figure 1.2)). The average U−arene$_{Ct}$ distance is 2.581(8) Å in **BT**, which is comparable to the examples reported by Cotton and co-workers. In contrast to Cotton's examples, these complexes were appreciably soluble in aromatic solvents and thermally robust. However, they were still unstable in donor solvents, decomposing to [$U(BH_4)_3(THF)_3$] in THF. The lability of the coordinated arene was also exemplified by reactions with CpH, NaCp and KCp, the products of which are discussed in Section 1.3.[67]

In 2000, diuranium inverse arene interactions emerged as a new motif in actinide chemistry.[68] The first diuranium inverse sandwich complex, [{U(N(Ad)Ar)$_2$}$_2$(μ−C_6H_6)] (**BU**, Scheme 1.18), was obtained from the reduction of an iodo tris(amido)uranium(IV) complex in benzene. As outlined in the report by Cummins and co-workers, the oxidation state at the metal centre can be rationalised in three ways from the bonding motif: i) two uranium(II) centres and a neutral arene, ii) two uranium(III) centres and an anti-aromatic arene dianion, or iii) two uranium(IV) centres and an aromatic arene tetraanion.[69]

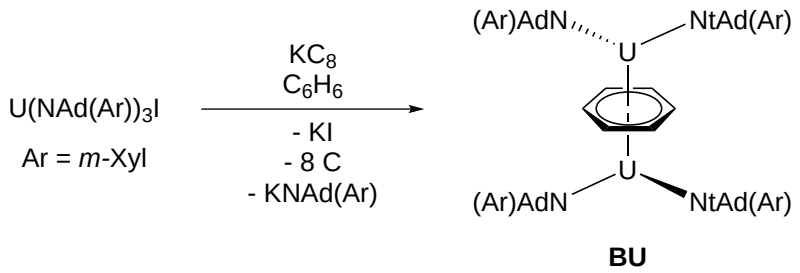

Scheme 1.18 – Synthesis of the inverse sandwich complex **BU** as reported by Cummins and co-workers.[68]

Since the discovery of uranium inverse sandwich complexes, many contributions have been made from various groups displaying a range of oxidation states at the uranium centre. These complexes are supported by various ligand frames and give rise to varying degrees of arene bridge reduction.[69] To date, however, no examples of intramolecular arene-bridged complexes have been reported.

An early report of a charge-separated cycloheptatrienyl-bridged diuranium borohydride complex, $[U(BH_4)_2(thf)_5][U_2(BH_4)_7(\mu\text{-}C_7H_7)]$ (**BV**), by Ephritikhine and co-workers in 1994 hinted at uranium's ability to stabilise the diuranium inverse sandwich motif.[70] Complex **BV** is the first example of an organouranium compound exhibiting the inverse sandwich motif. The use of the trianionic cycloheptatriene ligand means that the interaction between the uranium metal centre and ligand is somewhat unsurprising, and could be attributed to an ionic interaction rather than uranium-based orbital participation in a covalent interaction.

Evans and co-workers reported the interesting intermolecular arene complex of a tetraphenylborate anion, $[U(C_5Me_4H)_2(\mu\text{-}Ph_2BPh_2)]$ (**BW**) using the tetramethylcyclopentadienyl ligand.[71] The uranium(III) borate complex **BW** was synthesised from the uranium(IV) dimethylmetallocene, $[(C_5Me_4H)_2UMe_2]$, by reduction with potassium and subsequent protonolysis with two equivalents of $[Et_3NH][BPh_4]$ (Scheme 1.19). In the solid-state structure of **BW**, the uranium metallocene fragment is $(\mu\text{-}\eta^6{:}\eta^1\text{-}Ph)(\mu\text{-}\eta^1{:}\eta^1\text{-}Ph)BPh_2$-bound to the tetraphenylborate anion, with a U$-$arene$_{Ct}$ distance of 2.618(2) Å. Interestingly, the analogous reaction with $[(C_5Me_5)_2UMe_2]$ results in the $(\mu\text{-}\eta^2{:}\eta^1\text{-}Ph)_2BPh_2$ coordination of the BPh_4 ligand, which could be ascribed to the relief in the steric environment in **BW** compared to its permethylated analogue.[71]

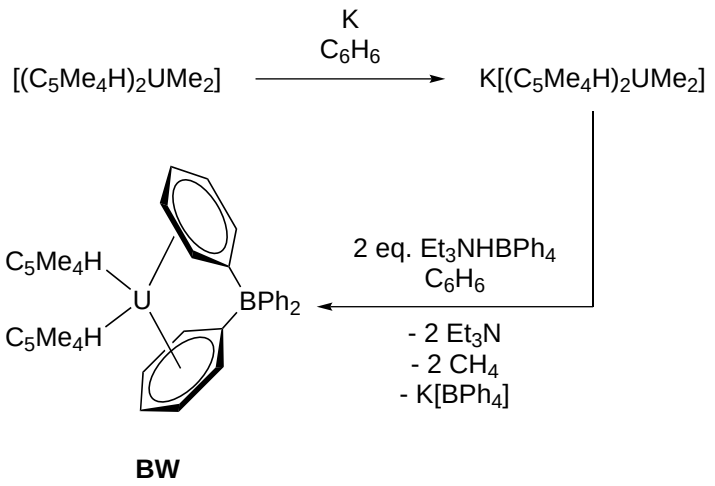

BW

Scheme 1.19 – Synthesis of the metallocene tetraphenyl borate complex **BW** as described by Evans and co-workers.[71]

As discussed in Section 1.1.1, the crystal structure of the first homoleptic uranium(III) aryloxide, $U(Odipp)_3$ (**C**) was reported by Sattelberger in 1988 .[31] The uranium(III) tris(aryloxide) **C** was obtained by treating UN''_3 with three equivalents of HOdipp in hexane. The structure shows a dimeric complex in which one phenoxide bridges two metal centres by a metal η^6-arene interaction (Figure 1.3). Due to their scarcity, the uranium-arene interaction in **C** was not anticipated. As discussed in Section 1.1.1, the congener with the more sterically demanding aryloxide $U(Odtbp)_3$ (**B**) was shown to be monometallic, suggesting that the arene interaction in dimeric **C** is caused by a decrease in steric demand. The U−$arene_{Ct}$ distance is 2.563(6) Å.

In 2013, a joint report by the Mindiola and Meyer groups introduced the aryl-substituted ligand, 2,6-bis(diphenylmethyl)-4-methylphenol (HObdpmp), which exhibits coordination of the pendant arene to a uranium(III) centre upon complexation.[72] Interestingly, this arene interaction was formed by both a salt metathesis reaction with UI_3 in THF to yield the THF adduct $[U(thf)(Obdpmp)_3]$ (**BX**) or protonolysis using UN''_3 in hexanes to give the unsolvated complex $U(Obdpmp)_3$ (**BY**, Figure 1.3). The U−$arene_{Ct}$ distances are 2.964(3) and 2.853(3) Å in **BX** and **BY**, respectively. Unfortunately, due to paramagnetic broadening in the ^{1}H NMR spectra and lack of variable temperature measurements, the authors were not able to comment on whether the arene interaction was retained in solution. The soft U−arene binding was demonstrated by reaction of either **BX** or **BY** with N_2O to give the terminal oxo complex **BZ**.[72] It is noteworthy that the resulting U(V) complex does not have an arene interaction, suggesting that either the lower oxidation state is required for uranium arene binding, or that the

larger uranium(III) ion has better overlap with the arene than the smaller uranium(V) ion.

Our group has previously investigated the use of boroxide ligands in organoactinide chemistry (unpublished results). Treating UN''_3 with dimesitylborinic acid ($HOBMes_2$) in toluene yields purple $U(OBMes_2)_3$ (**CA**). The crystal structure revealed a dimeric complex in which one diarylboroxide ligand bridges two uranium centres *via* a uranium-arene interaction similar to that found in **C** (Figure 1.3). The uranium-arene interaction is retained in solution, as evidenced by a desymmetrised ligand environment in the ^{1}H NMR spectrum.

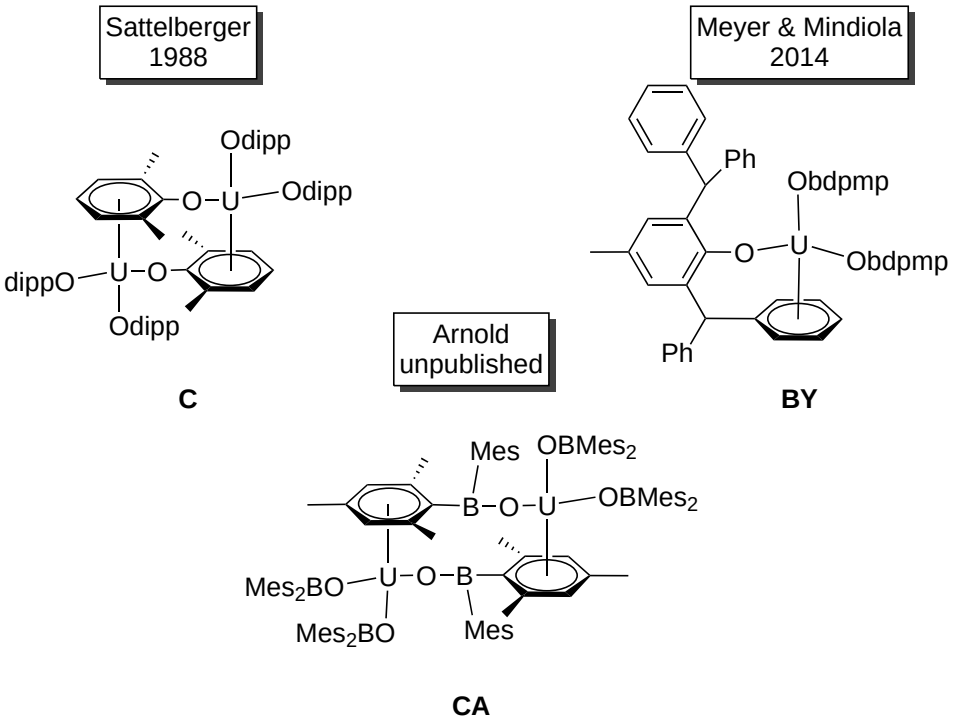

Figure 1.3 – Homoleptic inter- and intra-molecular uranium(III) arenes as reported by the Sattelberger, Meyer and Mindiola, and Arnold groups.[31,72]

With mounting evidence suggesting that arene coordination to low oxidation state uranium complexes is possible, several groups investigated the use of arene-containing ligands, with U−arene interactions in mind. In collaboration with the Love group, our group has reported the use of the polypyrrolic macrocyclic ligand, H_2L, which can exhibit a range of binding modes. Most relevant here is the bis(arene) binding to uranium(III) centres of which there are now a few examples. Reduction of the bis(iodo)uranium(IV) complex $[UI_2L]$ with KC_8 provided the bis-arene iodo uranium(III) complex [UIL] (**CB**). In the crystal structure of **CB**, the uranium centre resides in the centre of the ligand cavity with a near linear $arene_{Ct}$-U−$arene_{Ct}$ angle of $174.4(1)^\circ$ and a U−$arene_{Ct}$ distance of $2.614(2)$ Å.

Uranium(III) complexes of L^{2-} could be obtained reproducibly and in high yield directly by reacting the ligand potassium salt K_2L with $[U(BH_4)_3(THF)_2]$ to provide the corresponding borohydrido uranium(III) complex $[U(BH_4)L]$ (**CC**). Similarly to the iodo uranium(III) complex **CB**, the solid-state structure of **CC** has a near linear arene$_{Ct}$-U−arene$_{Ct}$ angle (174.73(6)°) and a slightly shorter U−arene$_{Ct}$ distance of 2.590(1) Å. Furthermore, **CC** was found to be a useful precursor for further derivatisation, as exemplified by reactions with KOdtbp or KN″ to yield complexes **CD** and **CE**, respectively (Scheme 1.20). While the bis(arene) coordination motif was retained in the solid-state structures of **CD** and **CE** with near linear angles of 174.21(3)° and 176.04(8)°, respectively, the uranium centre is not centred in the ligand cavity, with U−arene$_{Ct}$ distances of 2.62(1) and 2.745(1) Å for **CD** and 2.642(3) and 2.814(3) Å for **CE**. The U−X bonds of the ancillary ligands are elongated when compared to their homoleptic uranium(III) analogues, which suggests that the considerable steric requirements of the aryloxide and silylamide ligands may be responsible for the off-centre placement of the uranium centre.

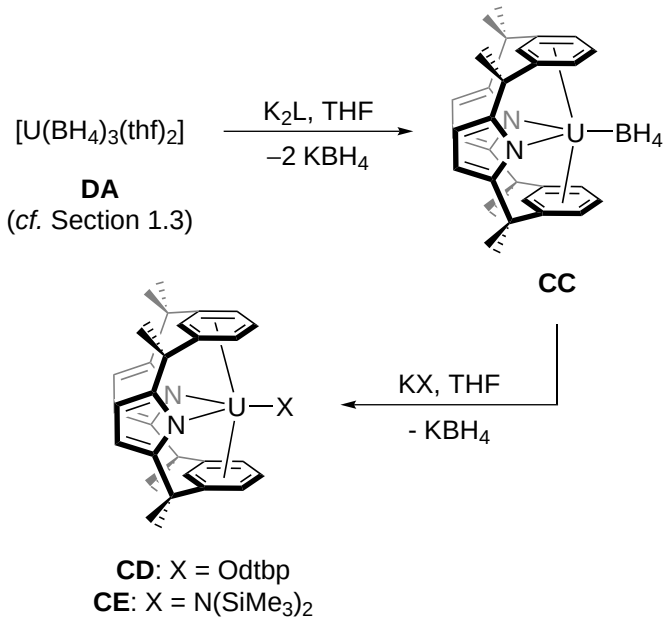

Scheme 1.20 – Polypyrrolic Schiff base macrocycle uranium(III) complexes which contain uranium-arene coordination.[15,73]

It is worth noting that the macrocyclic ligand L^{2-} has also been used in organoneptunium chemistry. Reaction of the potassium salt K_2L with $NpCl_4$ results in a spontaneous reduction to the neptunium(III) complex **CF** which adopts the bis(arene) coordination mode. Complex **CF** reacts with reductants in DME to yield the methoxy-bridged dimeric complex **CG**, a product of solvent activation thought to be the result of a transient Np(II) complex.[74]

1.2.2 Thorium arene complexes

In contrast to the examples of uranium arene complexes discussed in Section 1.2.1, thorium arene complexes are extremely sparse in the literature.

Intermolecular thorium arene complexes are particularly rare, within only five examples reported thus far by Emslie and co-workers using NNN or NON pincer ligands.[75,76]

Alkyl abstraction from [Th(NON)R_2] (R = CH_2Ph, CH_2SiMe_3) with [Ph_3C][$B(C_6F_5)_4$] in aromatic solvents resulted in the isolation of [Th(η^6-arene)(NON)R][$B(C_6F_5)_4$] (**CH**: R = CH_2Ph, arene = PhMe; **CI**: R = CH_2SiMe_3, arene = PhH; Scheme 1.21), which are cationic thorium arene complexes. Exchange was observed with excessive amounts of arene solvent by EXSY NMR spectroscopy on **CH** over long periods of time suggesting the coordinated toluene ligand to be weakly bound. The Th-arene$_{Ct}$ distances in the solid-state structures of these cationic complexes are 2.935(3) and 2.950(3) Å for **CH** and **CI**, respectively.[75]

Abstraction of the benzyl group of [Th(NON)$(CH_2Ph)_2$] with the Lewis acid $B(C_6F_5)_3$ results in the formation of two complexes: [Th(NON)$(CH_2Ph)\{(\mu$-$PhCH_2)B(C_3F_5)_3]\}$ and [Th(NON)$\{(\mu$-$PhCH_2)B(C_3F_5)_3\}_2$] (**CJ** and **CK**, respectively; Scheme 1.21). The complexes **CJ** and **CK** are best described as benzylborate complexes, where the Lewis pair formed by the benzyl ligand and $B(C_6F_5)_3$ acts as a charged ligand, similar to complex **BW**, which was reported by Evans and discussed in Section 1.2.1 (*vide supra*). The monoborate complex **CJ** was identified by ^{1}H and ^{11}B NMR spectroscopy but was not structurally characterised, whereas the poor solubility of **CK** in inert solvents precluded NMR spectroscopic characterisation while facilitating crystallisation. The solid-state structure reveals Th-arene$_{Ct}$ distances of 2.738(4) and 2.728(3) Å, which are considerably shorter than those in **CH** and **CI**. The preference of the borate arene over the abundant arene solvent is likely due to the electrostatic interaction between the electropositive thorium centre and the partial negative charge of the borate ligand arene.[76]

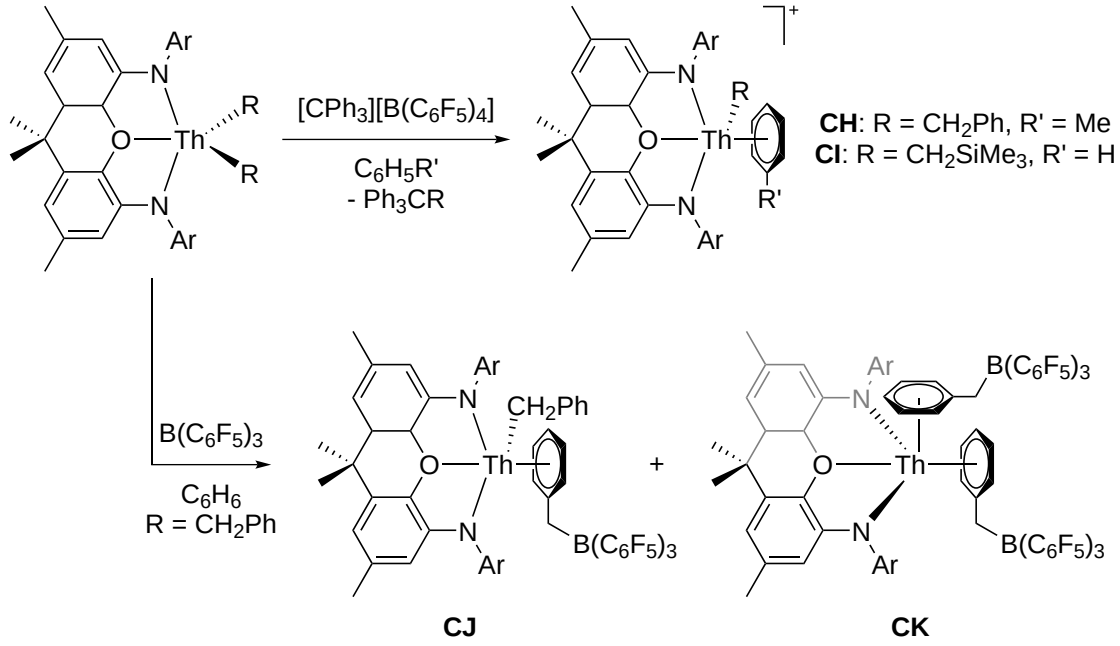

Scheme 1.21 – Synthesis of compounds **CH, CI, CJ, CK** by alkyl abstraction with trityl cations and Lewis acidic boranes as reported by Emslie and co-workers.[75,76]

In contrast, abstracting a benzyl ligand from the NNN pincer complex $[Th(NNN)(CH_2Ph)_2]$ with $[Ph_3C][B(C_6F_5)_4]$ in benzene provided a dimeric complex in which a bridging benzyl ligand is μ-η^6:η^1-bound to two thorium centres, $[\{Th(NNN)(CH_2Ph)\}_2(\mu\text{-}PhCH_2)]^+$ (**CL**, Scheme 1.22). Due to the high electropositivity of thorium, thorium alkyls have a high bond polarity with a partial negative charge residing on the carbon atom. The slight negative charge localised across the benzyl ligand could explain the preference of the thorium benzyl arene over the arene solvent, similarly to the borate ligand in **CK**. The solid-state structure of **CL** reveals that the Th-arene$_{Ct}$ distance is $2.798(5)$ Å, comparable to those exhibited by **CK**.[75]

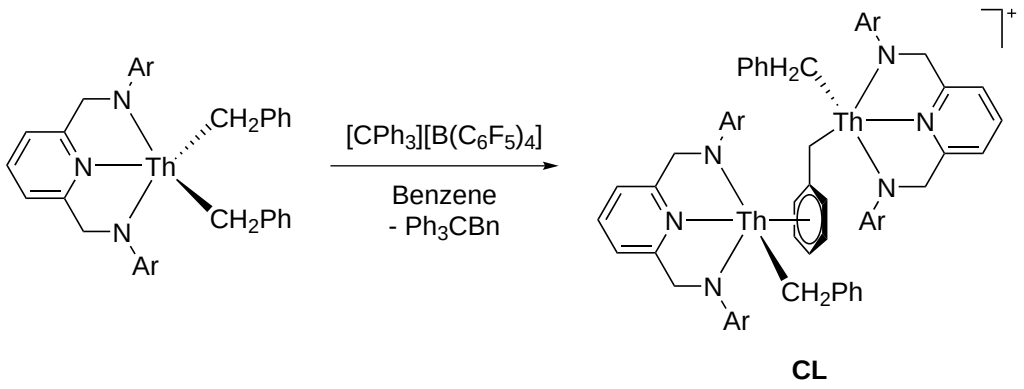

Scheme 1.22 – Synthesis of compound **CL** as reported by Emslie and co-workers.[75]

Gambarotta reported two intramolecular anionic thorium arenes supported by a *meta*-arene-bridged bispyrrollide ligand.[77] The thorium arene complexes are obtained by reaction of the ligand dilithium salt with $[ThCl_4(dme)_2]$ (DME = dimethoxyethane), giving the lithium chloride ate complex **CM**. Reaction of **CM** with $AlMe_3$ or potassium disrupts the thorium arene interaction: the Brønsted basic $AlMe_3$ deprotonates the arene bridge causing a switch in the coordination mode to bis(κ^5)pyrrolide, and reduction with potassium generates a bridging arene-based radical and an η^5-pentadienyl binding mode. In contrast, reduction of **CM** with lithium followed by quenching with azobenzene led to a retention of the Th−arene interaction in the resulting azobenzene dianion adduct **CN** (Scheme 1.23).[77] The solid-state Th−arene$_{Ct}$ distances are 2.701(8) Å and 2.732(7) Å for **CM** and **CN**, respectively, which are shorter than in the complexes reported by Emslie and co-workers.

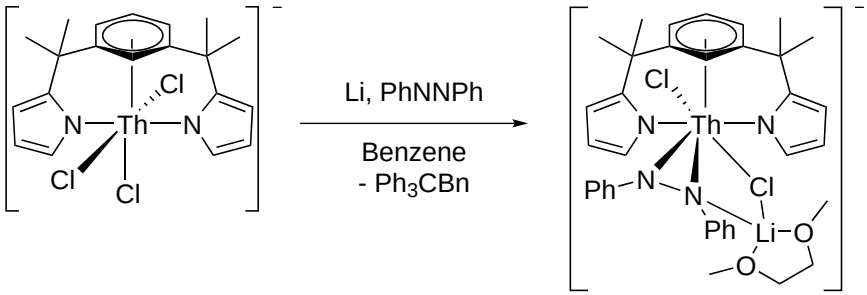

CM **CN**

Scheme 1.23 – Synthesis of compounds **CM, CN** as reported by Gambarotta and co-workers.[77]

Our group has recently reported a neutral thorium arene complex.[78] The reaction of the Lewis acid $AlMe_3$ with $[Th(OTer^{Mes})_2(BH_4)_2(dme)]$ (Ter^{Mes} = 2,6-dimesitylphenyl) resulted in the abstraction of coordinated DME to form the base-free complex $[Th(OTer^{Mes})_2(BH_4)_2]$ (**CO**, Scheme 1.24). In the solid-state structure of **CO**, the thorium centre resides between two ligand aryl groups, however they are not equidistant. One aryl group is close to the thorium centre with a Th-arene$_{ct}$ distance of 2.816(7) Å, while the other is considerably further away at 4.086(7) Å, which is likely to be a result of the large steric demand of the terphenolate ligand.[78]

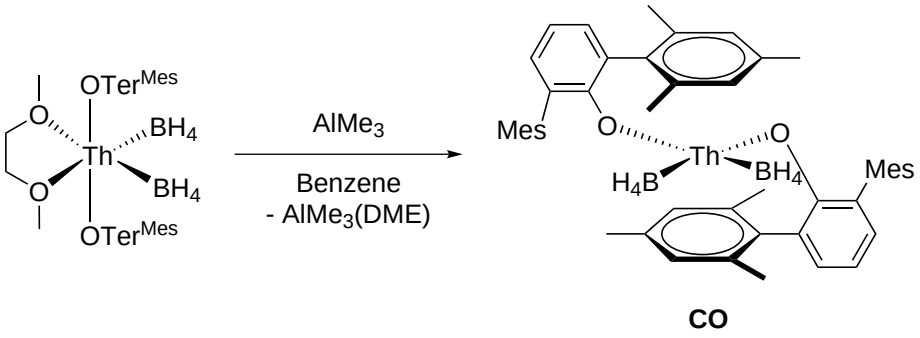

Scheme 1.24 – Synthesis of compound **CO** as reported by our group.[78]

As discussed throughout this section, actinide-arene complexes have not received much attention with sparse reports over the last 30 years and recent reports suggest that actinide arene interactions may yet have a role to play in furthering the field of actinide chemistry.[5] Uranium(IV) arenes are considerably rarer than uranium(III) arenes although the U−arene$_{Ct}$ distances are quite similar in all complexes, ranging from 2.55(1) to 2.964(3) Å. The relative prevalence of uranium(III) arenes over uranium(IV) could be explained by the more diffuse and polarisable nature of the uranium(III) ion when compared to uranium(IV). Hard-soft acid base (HSAB) theory suggests that "soft" Lewis acids which are more polarisable will tend to form adducts with Lewis bases with a matching polarisability or "softness".[79] As such, the softer uranium(III) Lewis acid will be a better match to form a soft arene complex than the relatively harder uranium(IV) ion, and therefore will have better orbital overlap and a stronger stabilising interaction. All of the thorium arene complexes reported in the literature are in the +4 oxidation state with Th−arene$_{Ct}$ distances ranging from 2.701(8) to 2.950(3) Å, remarkably similar to those of uranium. Most examples described in the literature are ionic complexes with the longest Th−arene$_{Ct}$ distances exhibited by the cationic complexes **CH** and **CI**, while the anionic complexes **CM** and **CN** have the shortest Th−arene$_{Ct}$ distances. This observation could suggest that the thorium-arene interaction is strongest when the metal centre is most electron-rich, which would be consistent with the HSAB argument. However, as the coordination environments are quite varied in these examples such comparisons may not necessarily be drawn reliably.

1.3 Actinide borohydride complexes

Borohydrides as ligands for uranium chemistry were first investigated during the Manhattan project. Schlesinger *et al*. reported the synthesis of the dark green [U(BH$_4$)$_4$] (**CP**) from UF$_4$ and [Al(BH$_4$)$_3$].[80] The uranium(IV) complex **CP** decomposes rapidly at 100 °C to give the

red brown uranium(III) borohydride $[U(BH_4)_3]$ (**CQ**, Scheme 1.25). Reactions of **CP** with BMe_3 result in the formation of the lavender complex $[U(BH_3CH_3)_4]$ (**CR**).[81] Both complexes **CP** and **CR** were shown to react with HCl to yield UCl_4, H_2 and volatile boron-containing products. In the 25 years following Schlesinger's initial investigations, many reports of X-ray and neutron diffraction measurements on the homoleptic complex **CP** and its Lewis base adducts (L = THF, dmpe, Ph_3PO) were published, with little investigation into its chemistry. The use of **CP** as a starting material in organouranium chemistry was pioneered by Ephritikhine, who demonstrated it can undergo salt metathesis chemistry to yield mixed ligand uranium(IV) borohydride complexes such as $[U(COT)(BH_4)_2]$ or $[U(C_5Me_5)_2(BH_4)_2]$.[82,83] Ephritikhine also demonstrated the contrasting reactivity of **CP** compared to other uranium(IV) starting materials such as UCl_4.

This is well exemplified by the decomposition of **CP** in various solvents. For example, the dissolution of **CP** in DME lead to quantitative formation of the uranium hydride complex $[UH(BH_4)_3(dme)]$ (**CS**, Scheme 1.25) by elimination of diborane.[84] From its crystal structure, **CS** was found to be dimeric with two bridging hydride ligands. In contrast, heating solutions of **CP** in aromatic solvents such as mesitylene resulted in the formation of the uranium arene complex $[U(\eta^6-Mes)(BH_4)_3]$ (**CT**, Scheme 1.25) by reduction of the metal centre and loss of B_2H_6 and H_2.[67] As discussed in Section 1.2.1, the formation of a uranium-arene bonding interaction was unexpected, and the spontaneous reduction to uranium(III) is in stark contrast to other common uranium(IV) reagents such as UCl_4, which requires treatment with KC_8 to reach the $+3$ oxidation state and obtain the poorly defined starting material UCl_3, which can only be prepared *in situ*.[85] As discussed in Section 1.2.1, **CT** constitutes a rare example of an arene-solvent soluble uranium arene complex (*vide supra*).

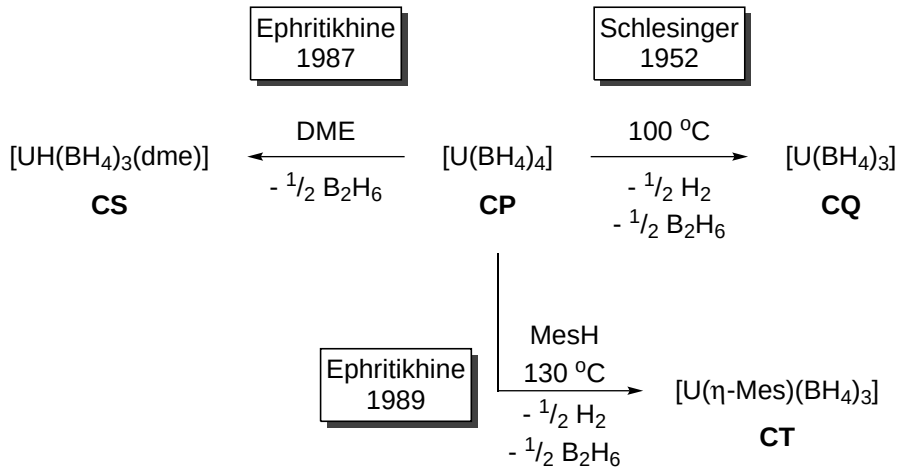

Scheme 1.25 – Synthesis and decomposition of $[U(BH_4)_4]$ under various conditions, as reported by Schlesinger and Ephritikhine.[67,80,84]

The facile access to the uranium(III) oxidation state by **CP** is remarkable, as oxidation of uranium(III) to uranium(IV) is often the major decomposition pathway in low oxidation-state organouranium chemistry. In 2010, Girolami and co-workers demonstrated that a similar process occurred when treating UCl_4 with $Na(BH_3NMe_2BH_3)$ in toluene, which provided the dark brown uranium(III) complex $[U(BH_3NMe_2BH_3)_3]$ (**CU**, Scheme 1.26) in good yields.[86] When the reaction was carried out in ethereal solvents (THF, DME), a green colour persisted in solution, that afforded dark brown solids after removal of volatiles. The authors attributed to a uranium(IV) product stable in solution but not in the solid-state. The analogous reactions carried out with $[ThCl_4(dme)_2]$ led to the isolation of the fifteen-coordinate thorium complex $[Th(BH_3NMe_2BH_3)_4]$ (**CV**, Scheme 1.26), which is highest coordination number reported to date.[3] These reactions provide evidence that the uranium(III) oxidation state may be stabilised by borates as well as borohydrides. Ligands containing borate moieties could prove useful in accessing uranium(II) organometallic complexes, an emerging area in the organometallic uranium chemistry community.

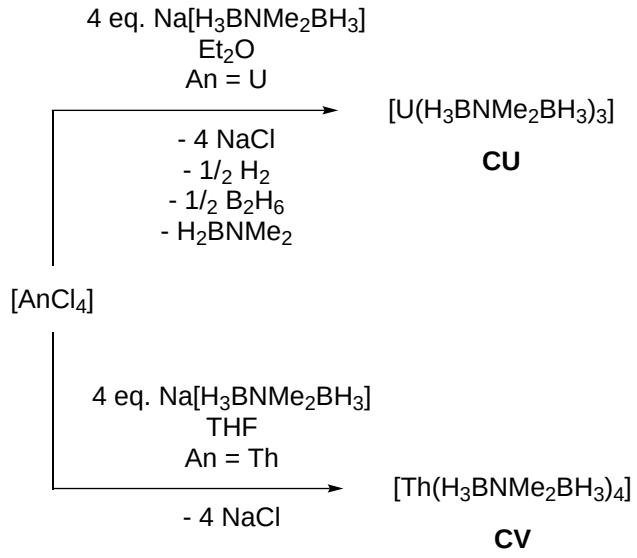

Scheme 1.26 – Spontaneous formation of the uranium(III) dimethylaminoboronate **CU** and of the fifteen coordinate thorium(IV) dimethylaminoboronate **CV** by Girolami and co-workers.[3,86]

In 1979, Moody and co-workers reported the synthesis of the poorly defined complex $[U(BH_4)_3(thf)]$ (**CW**) from UCl_3 and $NaBH_4$.[85] The authors commented that the isolated powder of **CW** from the reaction was consistent with a 1 : 1 adduct with THF but could not determine the nuclearity of the compound. Reports following this authenticated **CW** as a uranium(III) complex by XRD measurements on the DMPE (DMPE = bis(dimethylphosphino)-ethane) and diphenylphosphinopyridine adducts. The poor characterisation of **CW** rendered it an unattracive reagent in uranium(III) chemistry. This is well exemplified by the work of Ryan and co-workers in 1989, in which they report the reaction of **CW** with $[Th(C_5Me_5)_2(PPh_2)_2]$ which led to the isolation of $Na[U(C_5Me_5)(BH_4)_3]$ (**CX**), as determined by XRD measurements. The unexpected inclusion of sodium in **CX** led the authors to suggest it was carried over from the UCl_3 starting material. The authors state they were unable to synthesise the compound rationally.[85]

In comparison, Ephritikhine and co-workers were able to use their arene coordinated complex **CT** to access uranium(III) complexes.[87] They reported the reaction of **CT** with two equivalents of KC_4Me_4P (Ktmp), which yielded the potassium bisphospholide uranium-ate complex $K[U(TMP)_2(BH_4)_2]$. Redissolving the -ate complex in toluene provided the dimeric uranium(III) complex $[U(TMP)_2(BH_4)]_2$ (**CY**), which was structurally characterised. The phospholide ligand acts as the bridging ligand through the phosphorus lone pair. Complex **CY** could

also be synthesised by reduction of the uranium(IV) complex $[U(TMP)_2(BH_4)_2]$ with Na(Hg) (Scheme 1.27).[87] Ephritikhine and co-workers also investigated reactions of cyclopentadienes, finding that -ate complexes were obtained when reacting two or three equivalents of sodium cyclopentadienide with **CT**. Using three equivalents of potassium cyclopentadienide furnished the uranium(III) complex $[UCp_3(thf)]$.[67]

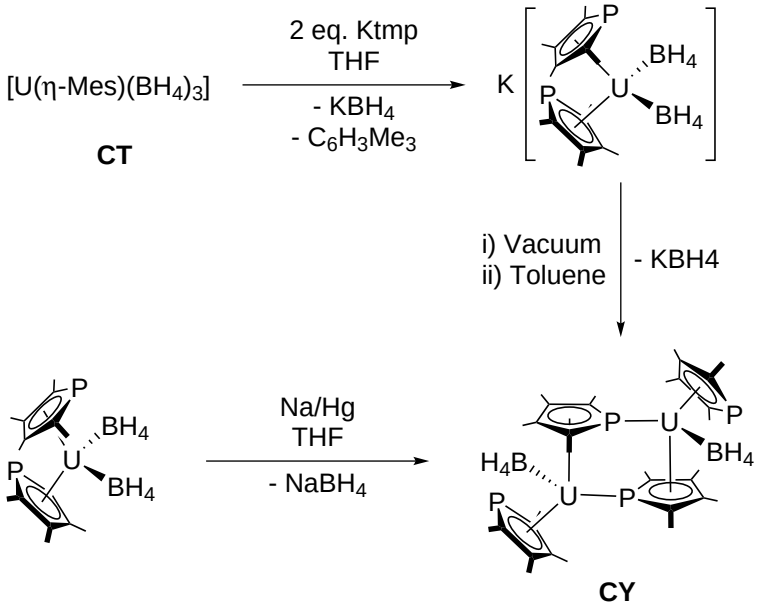

Scheme 1.27 – Synthetic routes to the dimeric uranium(III) phospholide complex **CY** from the uranium(III) arene complex **CT** and by reduction of the uranium(IV) metallocene $[U(tmp)_2(BH_4)_2]$, as reported by Ephritikhine and co-workers.[87]

As discussed in Section 1.2.1 (*vide supra*), Ephritikhine and co-workers reported the isolation of a uranium inverse-arene complex containing a triply reduced cycloheptatrienyl ring in 1994.[70] The counter-ion to the anionic complex is the uranium(III) cation $[U(BH_4)_2(THF)_5]^+$ (**CZ**). This unusual uranium(III) cation could be synthesised rationally by protonolysis of **CW** with $HNEt_3BPh_4$ to provide $[U(BH_4)_2(THF)_5][BPh_4]$ (Scheme 1.28). Ephritikhine and co-workers demonstrated that the equatorial ligands could be substituted by either 18-crown-6 or 18-thiacrown-6.[88] The protonolysis chemistry of borohydride ligands with $[HNEt_3][BPh_4]$ was expanded to uranium(IV) in the half-sandwich complexes $[U(COT)(BH_4)_2]$, to yield the mono and dicationic uranium(IV) complexes.[89]

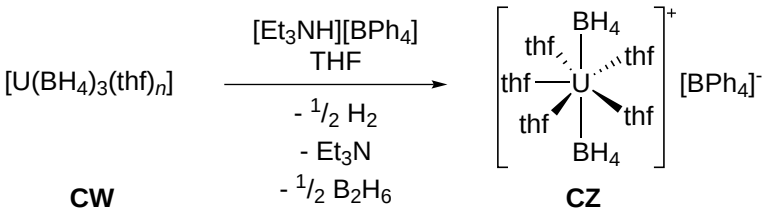

CW **CZ**

Scheme 1.28 – Synthesis of the unusual uranium(III) cation **CZ** by protonolysis of **CW** with $[Et_3NH][BPh_4]$, as reported by Ephritikhine and co-workers.[70]

The use of borohydride ligands in uranium(III) chemistry was reinvigorated with the synthesis of $[U(BH_4)_3(THF)_2]$ (**DA**) by Arnold and co-workers in 2014, obtained from the reaction of UI_3 with excess $NaBH_4$ in THF, followed by a Soxhlet extraction with Et_2O.[15] Unlike the previously reported **CW**, **DA** is a well-defined red brown solid which has been structurally characterised and does not contain incorporated alkali metal salts. Furthermore, Arnold and co-workers were able to demonstrate the advantage of **DA** over other common uranium(III) starting materials in the synthesis of mono- and bimetallic uranium(III) macrocyclic complexes. As discussed in Section 1.2.1, the monometallic uranium(III) complex **CC** could be obtained in a high yield and with greater thermal stability and solubility than its iodide analogue (Scheme 1.20, *vide supra*). When employing an anthracenyl-bridged tetrapyrrolic pacman ligand, two uranium(III) centres could be installed to give a dinuclear uranium(III) -ate complex (**DB**, Scheme 1.29) where the two metal centres are bridged by a borohydride ligand within the macrocyclic cleft. In contrast, no tractable products could be obtained in the analogous reaction with UI_3. The reaction of **DB** with two equivalents of KOttbp resulted in the formation of a bis(aryloxo) bimetallic complex (**DC**, Scheme 1.29) which retains the borohydride ligand bridging the uranium centres.[15] Complex **DC** was shown to react with CS_2 to provide sulfido- and trithiocarbonate-bridged complexes.[90]

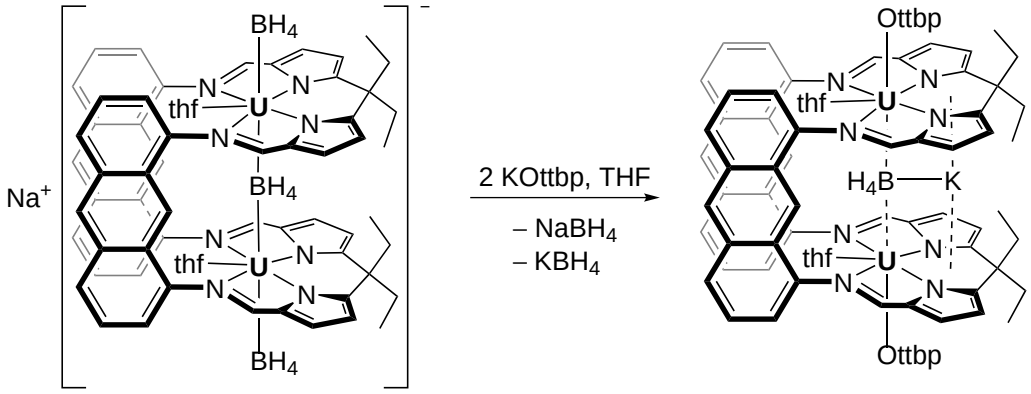

DB **DC**

Scheme 1.29 – Synthesis of bimetallic uranium(III) borohydride complexes of the anthracenyl-bridged pacman ligand by our group jointly with Prof. Love.[15]

1.4 Thesis objectives

The wealth of transformations exhibited by pairs of uranium(III) aryloxide complexes inspires the thought that research into aryloxide platform ligands that can accommodate two uranium(III) centres may result in greater control and selectivity upon reductive transformations. With the discovery of actinide-arene interactions, using a ligand frame which incorporates an arene that can be used to store electron density from the metal centre to effect a two-electron reduction of a metal coordinated substrate may give rise to new reactivity. The remarkable properties of uranium(III) borohydrides, in particular the ease of access to the $+3$ oxidation state, may be useful in small molecule activation chemistry, where the main challenge is regeneration of the reactive uranium(III) centre.

The primary objective of this project are two-fold. Firstly, the initial objective is the synthesis of heteroleptic uranium(IV) compounds of arene-tethered tetra(aryloxide) ligands. Secondly, the viability of these heteroleptic complexes as precursors for the synthesis of bimetallic uranium(III) complexes will be investigated.

The secondary objective is to synthesise uranium and thorium-arene complexes of arene-tethered tetra(aryloxide) ligands.

The final aspects of the project are to investigate the use of boroxides and borohydrides as ancillary ligands in uranium(III) chemistry and the use of those complexes in small molecule activation chemistry.

Described herein are organoactinide complexes related to the selected examples discussed

in this chapter.

1.5 Bibliography

[1] N. N. Greenwood and A. Earnshaw, *Chemistry Of The Elements*, Butterworth-Heinemann, Oxford, 2nd edn., 1997.

[2] L. Reynolds and G. Wilkinson, *J. Inorg. Nucl. Chem.*, 1956, **2**, 246–253.

[3] S. R. Daly, P. M. B. Piccoli, A. J. Schultz, T. K. Todorova, L. Gagliardi and G. S. Girolami, *Angew. Chem., Int. Ed.*, 2010, **49**, 3379–3381.

[4] M. R. MacDonald, M. E. Fieser, J. E. Bates, J. W. Ziller, F. Furche and W. J. Evans, *J. Am. Chem. Soc.*, 2013, **135**, 13310–13313.

[5] H. S. La Pierre, A. Scheurer, F. W. Heinemann, W. Hieringer and K. Meyer, *Angew. Chem., Int. Ed.*, 2014, **53**, 7158–7162.

[6] T. J. Marks, *Science*, 1982, **217**, 989–97.

[7] D. L. Clark, A. P. Sattelberger, W. G. van der Sluys and J. G. Watkin, *J. Alloys Compd.*, 1992, **180**, 303–315.

[8] M. Ephritikhine, *J. Alloys Compd.*, 1994, **213-214**, 15–19.

[9] J. Berthet and M. Ephritikhine, *Coord. Chem. Rev.*, 1998, **178-180**, 83–116.

[10] M. Ephritikhine, *Organometallics*, 2013, **32**, 2464–2488.

[11] S. T. Liddle, *Angew. Chem., Int. Ed.*, 2015, **54**, 8604–8641.

[12] D. E. Morris, R. E. Da Re, K. C. Jantunen, I. Castro-Rodriguez and J. L. Kiplinger, *Organometallics*, 2004, **23**, 5142–5153.

[13] C. D. Carmichael, N. A. Jones and P. L. Arnold, *Inorg. Chem.*, 2008, **47**, 8577–8579.

[14] M. J. Monreal, R. K. Thomson, T. Cantat, N. E. Travia, B. L. Scott and J. L. Kiplinger, *Organometallics*, 2011, **30**, 2031–2038.

[15] P. L. Arnold, C. J. Stevens, J. H. Farnaby, M. G. Gardiner, G. S. Nichol and J. B. Love, *J. Am. Chem. Soc.*, 2014, **136**, 10218–10221.

[16] O. T. Summerscales, F. G. N. Cloke, P. B. Hitchcock, J. C. Green and N. Hazari, *Science*, 2006, **311**, 829–831.

[17] O. T. Summerscales, F. G. N. Cloke, P. B. Hitchcock, J. C. Green and N. Hazari, *J. Am. Chem. Soc.*, 2006, **128**, 9602–9603.

[18] N. Tsoureas, O. T. Summerscales, F. G. N. Cloke and S. M. Roe, *Organometallics*, 2013, **32**, 1353–1362.

[19] P. L. Arnold and Z. R. Turner, *Nat. Rev. Chem.*, 2017, **1**, 1–15.

[20] A. Frey, F. Cloke and M. Coles, *Angew. Chem., Int. Ed.*, 2011, **50**, 6881–6883.

[21] N. Tsoureas, L. Castro, A. F. R. Kilpatrick, F. G. N. Cloke and L. Maron, *Chem. Sci.*, 2014, **5**, 3777–3788.

[22] P. L. Arnold, Z. R. Turner, R. M. Bellabarba and R. P. Tooze, *Chem. Sci.*, 2011, **2**, 77–79.

[23] S. M. Mansell, N. Kaltsoyannis and P. L. Arnold, *J. Am. Chem. Soc.*, 2011, **133**, 9036–9051.

[24] R. G. Jones, G. Karmas, G. A. Martin Jr. and H. Gilman, *J. Am. Chem. Soc.*, 1956, **78**, 4285–4286.

[25] R. G. Jones, E. Bindschadler, G. Karmas, F. A. Yoeman and H. Gilman, *J. Am. Chem. Soc.*, 1956, **78**, 4287–4288.

[26] D. Seyferth, *Organometallics*, 2004, **23**, 3562–3583.

[27] K. W. Bagnall, A. M. Bhandari and D. Brown, *J. Inorg. Nucl. Chem.*, 1975, **37**, 1815–1816.

[28] P. G. Edwards, R. A. Andersen and A. Zalkin, *J. Am. Chem. Soc.*, 1981, **103**, 7792–7794.

[29] A. J. Zozulin, D. C. Moody and R. R. Ryan, *Inorg. Chem.*, 1982, **21**, 3083–3086.

[30] P. B. Hitchcock, M. F. Lappert, A. Singh, R. G. Taylor and D. Brown, *J. Chem. Soc., Chem. Commun.*, 1983, 561–563.

[31] W. G. van der Sluys, C. J. Burns, J. C. Huffman and A. P. Sattelberger, *J. Am. Chem. Soc.*, 1988, **110**, 5924–5925.

[32] L. R. Avens, D. M. Barnhart, C. J. Burns, S. D. McKee and W. H. Smith, *Inorg. Chem.*, 1994, **33**, 4245–4254.

[33] P. Arnold, S. Mansell, L. Maron and D. McKay, *Nature Chem.*, 2012, **4**, 668–674.

[34] P. L. Arnold and S. M. Mansell, *Priv. Commun.*, 2016, **CCDC**, 1487672.

[35] I. Castro-Rodriguez, K. Olsen, P. Gantzel and K. Meyer, *Chem. Commun.*, 2002, 2764–2765.

[36] S. C. Bart, F. W. Heinemann, C. Anthon, C. Hauser and K. Meyer, *Inorg. Chem.*, 2009, **48**, 9419–9426.

[37] O. P. Lam, S. C. Bart, H. Kameo, F. W. Heinemann and K. Meyer, *Chem. Commun.*, 2010, **46**, 3137–3139.

[38] I. Castro-Rodriguez, H. Nakai, P. Gantzel, L. N. Zakharov, A. L. Rheingold and K. Meyer, *J. Am. Chem. Soc.*, 2003, **125**, 15734–15735.

[39] H. Nakai, X. Hu, L. N. Zakharov, A. L. Rheingold and K. Meyer, *Inorg. Chem.*, 2004, **43**, 855–857.

[40] A.-C. Schmidt, A. V. Nizovtsev, A. Scheurer, F. W. Heinemann and K. Meyer, *Chem. Commun.*, 2012, **48**, 8634–8636.

[41] A.-C. Schmidt, F. W. Heinemann, C. E. Kefalidis, L. Maron, P. W. Roesky and K. Meyer, *Chem. - A Eur. J.*, 2014, **20**, 13501–13506.

[42] I. Castro-Rodriguez, H. Nakai, L. N. Zakharov, A. L. Rheingold and K. Meyer, *Science*, 2004, **305**, 1757–1759.

[43] I. Castro-Rodriguez and K. Meyer, *J. Am. Chem. Soc.*, 2005, **127**, 11242–11243.

[44] O. P. Lam, C. Anthon, F. W. Heinemann, J. M. O'Connor and K. Meyer, *J. Am. Chem. Soc.*, 2008, **130**, 6567–6576.

[45] O. P. Lam, P. L. Feng, F. W. Heinemann, J. M. O'Connor and K. Meyer, *J. Am. Chem. Soc.*, 2008, **130**, 2806–2816.

[46] S. J. Zuend, O. P. Lam, F. W. Heinemann and K. Meyer, *Angew. Chem., Int. Ed.*, 2011, **50**, 10626–10630.

[47] O. P. Lam, F. W. Heinemann and K. Meyer, *Angew. Chem., Int. Ed.*, 2011, **50**, 5965–5968.

[48] O. P. Lam, L. Castro, B. Kosog, F. W. Heinemann, L. Maron and K. Meyer, *Inorg. Chem.*, 2012, **51**, 781–783.

[49] S. M. Franke, F. W. Heinemann and K. Meyer, *Chem. Sci.*, 2014, **5**, 942–950.

[50] O. P. Lam, S. M. Franke, F. W. Heinemann and K. Meyer, *J. Am. Chem. Soc.*, 2012, **134**, 16877–16881.

[51] I. Castro-Rodriguez, K. Olsen, P. Gantzel and K. Meyer, *J. Am. Chem. Soc.*, 2003, **125**, 4565–4571.

[52] I. Castro-Rodriguez, H. Nakai and K. Meyer, *Angew. Chem., Int. Ed.*, 2006, **45**, 2389–2392.

[53] A.-C. Schmidt, F. W. Heinemann, L. Maron and K. Meyer, *Inorg. Chem.*, 2014, **53**, 13142–13153.

[54] S. C. Bart, C. Anthon, F. W. Heinemann, E. Bill, N. M. Edelstein and K. Meyer, *J. Am. Chem. Soc.*, 2008, **130**, 12536–12546.

[55] A.-C. Schmidt, F. W. Heinemann, W. W. Lukens and K. Meyer, *J. Am. Chem. Soc.*, 2014, **136**, 11980–11993.

[56] B. Kosog, H. S. La Pierre, F. W. Heinemann, S. T. Liddle and K. Meyer, *J. Am. Chem. Soc.*, 2012, **134**, 5284–5289.

[57] H. S. La Pierre, H. Kameo, D. P. Halter, F. W. Heinemann and K. Meyer, *Angew. Chem., Int. Ed.*, 2014, **53**, 7154–7157.

[58] J. G. Brennan, F. G. N. Cloke, A. A. Sameh and A. Zalkin, *J. Chem. Soc., Chem. Commun.*, 1987, 1668–1669.

[59] P. L. Arnold, F. G. N. Cloke and P. B. Hitchcock, *Chem. Commun.*, 1997, 481–482.

[60] P. L. Arnold, M. A. Petrukhina, V. E. Bochenkov, T. I. Shabatina, V. V. Zagorskii, G. B. Sergeev and F. N. Cloke, *J. Organomet. Chem.*, 2003, **688**, 49–55.

[61] J. Li and B. E. Bursten, *J. Am. Chem. Soc.*, 1999, **121**, 10243–10244.

[62] M. Cesari, U. Pedretti, Z. Zazzetta, G. Luigi and W. Marconi, *Inorg. Chim. Acta*, 1971, **5**, 439–444.

[63] F. A. Cotton and W. Schwotzer, *Organometallics*, 1985, **4**, 942–943.

[64] G. C. Campbell, F. A. Cotton, J. F. Haw and W. Schwotzer, *Organometallics*, 1986, **5**, 274–279.

[65] F. A. Cotton, W. Schwotzer and C. Q. Simpson, *Angew. Chem., Int. Ed.*, 1986, **25**, 637–639.

[66] F. A. Cotton and W. Schwotzer, *Organometallics*, 1987, 1275–1280.

[67] D. Baudry, E. Bulot, P. Charpin, M. Ephritikhine, M. Lance, M. Nierlich and J. Vigner, *J. Organomet. Chem.*, 1989, **371**, 155–162.

[68] P. L. Diaconescu, P. L. Arnold, T. A. Baker, D. J. Mindiola and C. C. Cummins, *J. Am. Chem. Soc.*, 2000, **122**, 6108–6109.

[69] S. T. Liddle, *Coord. Chem. Rev.*, 2015, **293-294**, 211–227.

[70] T. Arliguie, M. Lance, M. Nierlich, J. Vigner and M. Ephritikhine, *J. Chem. Soc., Chem. Commun.*, 1994, 847–848.

[71] W. J. Evans, S. A. Kozimor and J. W. Ziller, *Chem. Commun.*, 2005, 4681–4683.

[72] S. M. Franke, B. L. Tran, F. W. Heinemann, W. Hieringer, D. J. Mindiola and K. Meyer, *Inorg. Chem.*, 2013, **52**, 10552–10558.

[73] P. L. Arnold, J. H. Farnaby, M. G. Gardiner and J. B. Love, *Organometallics*, 2015, **34**, 2114–2117.

[74] M. S. Dutkiewicz, J. H. Farnaby, C. Apostolidis, E. Colineau, O. Walter, N. Magnani, M. G. Gardiner, J. B. Love, N. Kaltsoyannis, R. Caciuffo and P. L. Arnold, *Nature Chem.*, 2016, **8**, 797–802.

[75] C. A. Cruz, D. J. H. Emslie, C. M. Robertson, L. E. Harrington, H. A. Jenkins and J. F. Britten, *Organometallics*, 2009, **28**, 1891–1899.

[76] C. A. Cruz, D. J. H. Emslie, L. E. Harrington and J. F. Britten, *Organometallics*, 2008, **27**, 15–17.

[77] I. Korobkov, B. Vidjayacoumar, S. I. Gorelsky, P. Billone and S. Gambarotta, *Organometallics*, 2010, **29**, 692–702.

[78] J. McKinven, G. S. Nichol and P. L. Arnold, *Dalton Trans.*, 2014, **43**, 17416–17421.

[79] R. G. Pearson, *J. Am. Chem. Soc.*, 1963, **85**, 3533–3539.

[80] H. I. Schlesinger and H. C. Brown, *J. Am. Chem. Soc.*, 1953, **75**, 219–221.

[81] H. I. Schlesinger, H. C. Brown, L. Horvitz, A. C. Bond, L. D. Tuck and A. O. Walker, *J. Am. Chem. Soc.*, 1953, **75**, 222–224.

[82] D. Baudry, E. Bulot, M. Ephritikhine, M. Nierlich, M. Lance and J. Vigner, *J. Organomet. Chem.*, 1990, **388**, 279–287.

[83] P. Gradoz, D. Baudry, M. Ephritikhine, M. Lance, M. Nierlich and J. Vigner, *J. Organomet. Chem.*, 1994, **466**, 107–118.

[84] D. Baudry, P. Charpin, M. Ephritikhine, M. Lance, M. Nierlich and J. Vigner, *J. Chem. Soc., Chem. Commun.*, 1987, 739–740.

[85] D. C. Moody and J. D. Odom, *J. Inorg. Nucl. Chem.*, 1979, **41**, 533–535.

[86] S. R. Daly and G. S. Girolami, *Inorg. Chem.*, 2010, **49**, 5157–5166.

[87] D. Baudry, M. Ephritikhine, F. Nief, L. Ricard and F. Mathey, *Angew. Chem., Int. Ed.*, 1990, **29**, 1485–1486.

[88] T. Arliguie, L. Belkhiri, S.-E. Bouaoud, P. Thuéry, C. Villiers, A. Boucekkine and M. Ephritikhine, *Inorg. Chem.*, 2009, **48**, 221–230.

[89] S. M. Cendrowski-Guillaume, G. Le Gland, M. Lance, M. Nierlich and M. Ephritikhine, *C. R. Chim.*, 2002, **5**, 73–80.

[90] P. L. Arnold, C. J. Stevens, N. L. Bell, R. M. Lord, J. M. Goldberg, G. S. Nichol and J. B. Love, *Chem. Sci.*, 2017, **8**, 3609–3617.

Chapter 2

Actinide complexes of an arene-tethered tetra-aryloxide pTP^R

Homobimetallic uranium complexes featuring uranium-arene bonds have attracted considerable interest in recent years, with increasing evidence of covalent interactions between low-oxidation uranium centres and aromatic systems. Our group has reported that electrons stored in uranium-arene bonds in the inverse-sandwich complex $[(dtbpO)_2U]_2(\mu-C_6H_6)$ can be used for reductive chemistry, resulting in arene bridge C−H activation.[1] Meyer and co-workers have shown that electrons can be stored in uranium-arene interactions in the report of the uranium(II) anion $K[(^{Ad}ArO_3)MesU]$.[2] In collaboration with Prof. J. Love, we have investigated the synthesis of bimetallic uranium(III) complexes using small and large Schiff-base macrocycles.[3–5]

This chapter describes an optimised route for the straightforward synthesis of arene-bridged tetra-phenols, and their application towards bimetallic actinide organometallic complexes. Initial investigations targeted the synthesis of halide (X = Cl, I) and silylamide complexes using ligands with different substitution. The synthesis and structural characterisation of the bimetallic actinide complexes is discussed. Also described in this chapter are reactivity studies including reduction chemistry and derivatisation reactions towards the synthesis of tethered diuranium inverse-sandwich complexes.

2.1 Synthesis of ligand precursors ($H_4(pTP^R)$)

The reported synthesis of the pro-ligand, H_4(pTP), consists of the acid-catalysed melt reaction of terephthalaldehyde in an excess of phenol ($\geq$ 10 equivalents).[6] The *p*-toluenesulfonic acid (*p*-TSA) catalysed condensation of substituted phenols ($\leq$ 5 equivalents) with a range of aldehydes inspired the application of this route for the synthesis of H_4(pTP).[7] A melt reaction of 4.4 equivalents of 2-*tert*-butyl-4-methylphenol and terephthalaldehyde with 10 mol% p-TSA provided H_4(pTP) as a colourless solid in 68 % yield. The synthesis of ligands with a durene core (1,2,4,5-tetramethylbenzene) or with methylated benzylic positions starting from

1,4-diacylbenzene were not successful under the same synthetic conditions. The general route to the proligands $H_4(pTP^R)$ and reactions that targeted ligands with a substituted arene bridge are summarised in Scheme 2.1 and Scheme 2.2, respectively.

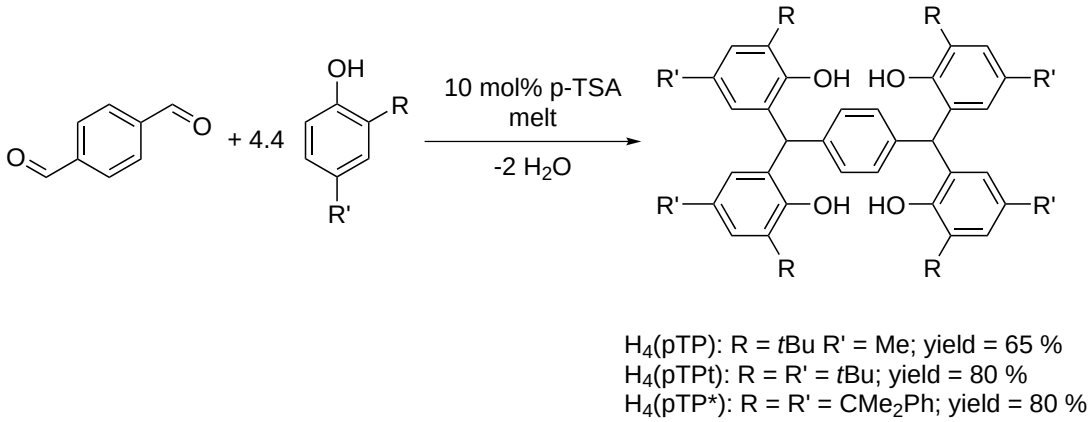

Scheme 2.1 – Synthetic route to tetra-phenol proligands.

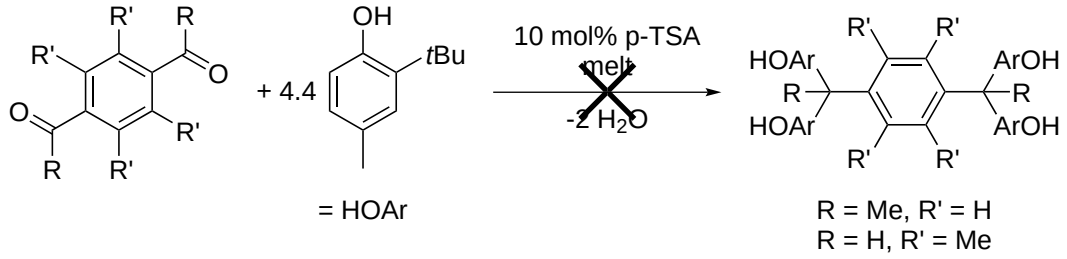

Scheme 2.2 – Unsuccessful synthetic routes to substituted arene tetra-phenol proligands.

Three ligands were successfully prepared using the improved solid melt method: the previously reported $H_4(pTP^t)$ with four pendant 2,6-di-*tert*-butylphenol group, and two new ligands with differing electronic and steric properties. The first utilising a 2-*tert*-butyl-4-methylphenol ($H_4(pTP)$) and the other with the more demanding 2,6-bis(dimethylbenzyl)phenol ($H_4(pTP^*)$). All three are colourless solids which are readily soluble in THF and sparingly in aromatic solvents with the exception of $H_4(pTP^t)$, which is appreciably soluble in aromatic solvents and sparingly in alkane solvents and diethyl ether.

2.2 Synthesis of dipotassium salts

The dipotassium salt $[K_2\{H_2(pTP^t)\}]$ has been reported by Wu *et al.* as an active catalyst in ring opening polymerisation of lactide.[8] The synthesis entails the deprotonation of the pro-ligand with KN'' in THF. In the solid-state structure, the two potassium counter ions exhibit

an arene interaction to form a dipotassium inverse-sandwich complex. The two remaining protons on the phenols bridge the O atoms of two adjacent phenols which constitute the ligand bis(aryloxide) pocket. The authors remarked that the dipotassium salt $[K_2\{H_2(pTP^t)\}]$ forms as the major product even when sub- or superstoichiometric quantities of KN″ (1 or 3-4 equivalents respectively) are used, which they attributed to the strong $p-\pi$ interactions in the dipotassium inverse-sandwich motif.[8] In order to assess the influence of varying the aryloxide substituents on the electronic and steric parameters of the ligands, the synthesis and structural characterisation of the ligand dipotassium salts were undertaken.

A colourless solution of KN″ was added to a stirred solution of $H_4(pTP^R)$ in dioxane. After 30 minutes of stirring, the colourless solution was filtered.

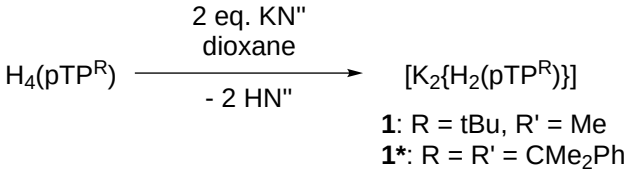

Scheme 2.3 – Synthesis of dipotassium salts **1** and **1***.

Colourless crystals of $[K_2\{H_2(pTP)\}]$ (**1**) suitable for single-crystal XRD analysis were obtained from diffusion of hexanes into the filtered reaction mixture over 18 hours. The dipotassium complex **1** contains two six-coordinate potassium centres in pseudo-octahedral geometry, which display the dipotassium inverse arene motif exhibited by the reported compound $[K_2\{H_2(pTP^t)\}]$ (Figure 2.1).[8] The axial positions are occupied by the ligand arene and a dioxane molecule, while the equatorial plane is occupied by one bis(aryloxide) pocket and two dioxane molecules. The average aryloxide K−O distance of 2.778(4) Å and the average K−arene$_{Ct}$ distance of 3.068(2) Å are comparable to those of $[K_2\{H_2(pTP^t)\}]$ at 2.73(1) and 3.068(7) Å respectively. This suggests that the steric and electronic properties of the (pTP) and (pTP^t) ligand are very similar. The O1−O2 and O3−O4 distances in **1** are 2.396(6) and 2.394(6) Å respectively, and compare well to those exhibited by $[K_2\{H_2(pTP^t)\}]$ (mean 2.38(1) Å). The short O−O distances in both **1** and $[K_2\{H_2(pTP^t)\}]$ are suggestive of a hydrogen-bonding interaction between the two adjacent phenolate oxygen atoms.

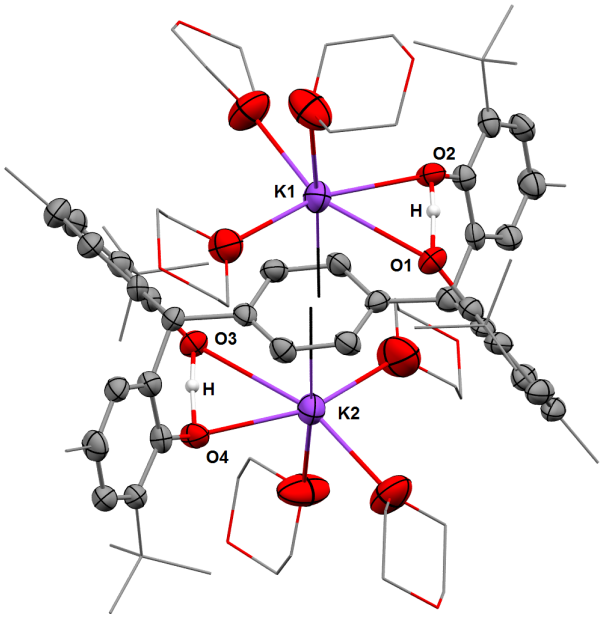

Figure 2.1 – Solid-state structure of $\mathbf{1} \cdot 2(C_4H_8O_2)$. The aryloxide methyl and *tert*-butyl group carbon atoms and non-bound dioxane carbon and oxygen atoms are depicted as wireframe for clarity. The hydrogen atoms with the exception of the bridging phenolic H-atoms, and lattice solvent molecules are omitted for clarity. The thermal ellipsoids are displayed at 50% probability.

Colourless crystals of the dipotassium complex $[K_2\{H_2(pTP^*)\}]$ ($\mathbf{1}^*$) suitable for single-crystal XRD analysis were obtained from diffusion of hexanes into the filtered reaction mixture over 18 hours. Unlike **1** and $[K_2\{H_2(pTP^t)\}]$, compound $\mathbf{1}^*$ does not exhibit the dipotassium inverse-sandwich motif, instead having two separate coordination environments for the potassium ions (Figure 2.2). The potassium ion K1 is five-coordinate and resides in a cavity formed by the ligand arene bridge and two *ortho* dimethylbenzyl groups; the K centre binds to three η^6-aryl groups and two *trans*-aryloxides. The potassium ion K2 is also five-coordinate but is located in a ligand bis(aryloxide) pocket, coordinating η^6 to an aryloxide *ortho* dimethylbenzyl group, η^2 to an aryloxide C−O bond, a phenol *O* atom and two dioxane molecules. Both of the deprotonated phenols coordinate to the *endo* potassium centre, which sits in the tris(arene) cavity, while the two protonated phenols engage in H-bonding with the proximal aryloxide *O* atoms. Both the average aryloxide K1−O and the phenol K2−O distances of 2.551(1) and of 2.680(1) Å, respectively, are shorter than in **1** and $[K_2\{H_2(pTP^t)\}]$. The discrepancy between the K−O distance of two metals in $\mathbf{1}^*$ can be explained by the fact that K1 is bound to two anionic aryloxides, while K2 is bound to a neutral phenol. The average K1−arene$_{Ct}$ and

K2−arene$_{Ct}$ distances of 2.9712(4) and 2.9622(5) Å are very similar and are comparable to the K−arene$_{Ct}$ distances in **1** and [K$_2${H$_2$(pTP^t)}]. The O1-O2 and O3-O4 distances in **1*** of 2.470(2) and 2.428(2) Å respectively. These distances are consistent with a hydrogen-bonding interaction between the two oxygen atoms, however they are longer than in **1**. The elongation of the bond length suggests a disruption in the hydrogen-bonding interaction. In the case of the H$_4$(pTP*) ligand, the increase in steric demand of the dimethylbenzyl substituent has a drastic impact on the coordination mode of the ligand, and is likely to be the cause of the disruption of the inverse-sandwich motif and hydrogen-bonding interaction. Furthermore, presence of the soft coordinating groups in the *ortho* position could be advantageous for the synthesis of low-coordinate actinide complexes.

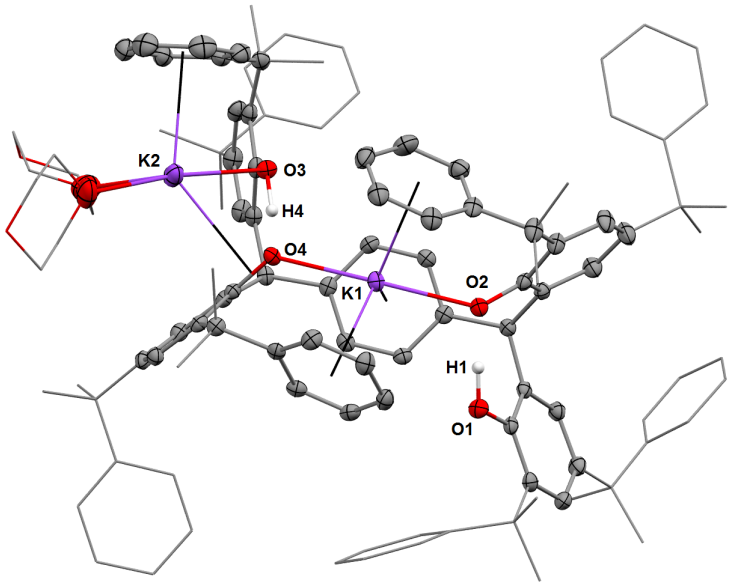

Figure 2.2 – Solid-state structure of **1**$^* \cdot 3\,(C_4H_8O_2)$.The aryloxide dimethylbenzyl group carbon atoms and non-bound dioxane carbon and oxygen atoms are depicted as wireframe for clarity. The hydrogen atoms with the exception of the bridging phenolic H-atoms, and lattice solvent molecules are omitted for clarity. The thermal ellipsoids are displayed at 50% probability.

2.3 General synthetic route to bimetallic actinide aryloxide complexes

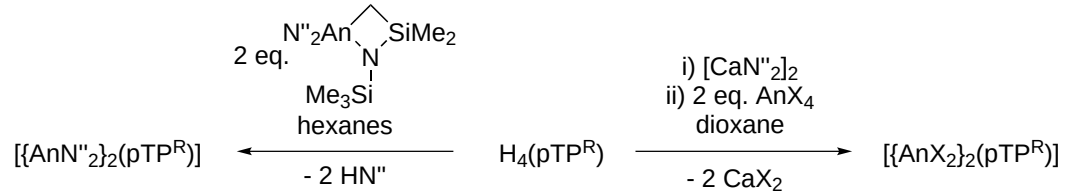

Scheme 2.4 – Synthetic route to bimetallic actinide complexes (An = U or Th; X = I or Cl).

The general synthetic routes to the bimetallic actinide complexes described in this chapter are shown in Scheme 2.4. Two are outlined; protonolysis of the pro-ligand, $H_4(pTP^R)$, with an actinide silylamide metallacycle, $[AnN''_2(\kappa^2C{:}N{-}N(SiMe_3)SiMe_2CH_2)]$, and salt metathesis reaction of actinide halides $[AnX_4]$ (X = Cl, I) with an *in situ* generated calcium salt, $[Ca_2(pTP)]$.

2.4 Synthesis of heteroleptic bimetallic actinide silylamide complexes

2.4.1 Synthesis and characterisation of $[\{UN''_2\}_2(pTP^R)]$

The bimetallic silylamide complexes $[\{UN''_2\}_2(pTP)^R)]$ were synthesised according to a modified literature procedure in yields of 75 % (Scheme 2.5).[9] A yellow-brown solution of $[UN''_2(\kappa^2C{:}N{-}N(SiMe_3)SiMe_2CH_2)]$ in hexanes was added to a colourless suspension of $H_4(pTP^R)$ in hexanes and the resulting green-brown suspension was allowed to stir for 18 hours. Complexes **2**, **2t** and **2*** were isolated as pale green solids by centrifugation from the brown supernatant and thoroughly dried under reduced pressure. The elemental analysis and spectroscopic data are in agreement with the molecular formulation. The compounds are air and moisture sensitive, but are stable at room temperature under an inert atmosphere over a period of months both in the solid state and in benzene solution.

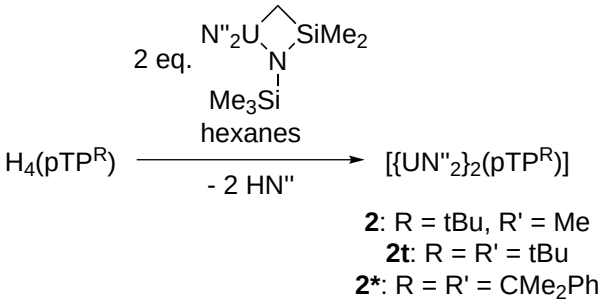

Scheme 2.5 – Synthesis of compounds $\mathbf{2^R}$.

The ^{1}H NMR spectrum of **2** is in accordance with a C_2 symmetric complex, with six ligand resonances. The chemical shift range is broad, spanning 55 ppm, as expected for paramagnetic U(IV) complexes. The ^{1}H NMR spectrum of **2*** at 345 K ranges 60 ppm with nine ligand resonances, indicating a symmetric complex. The ^{1}H NMR spectrum at room temperature contains broad resonances, which can be attributed to fluxional behaviour. In both complexes, the aryloxide H atoms resonate around 35 and 22 ppm and the silylamide methyl groups around −21 ppm. The aryloxide *tert*-butyl H atoms in **2** resonate at −10 ppm while the H atoms of the *ortho*-dimethyl groups in **2*** give rise to two singlets at −4.5 and −10 ppm. A singlet at 4.4 ppm can be attributed to the methyl H atoms in the spectrum of **2**, and two singlets at 4.4 and 3.8 arise from the *para*-dimethyl H atoms in **2***. No resonance could be observed in the ^{29}Si NMR spectra of **2** or **2*** possibly due to proximity to the paramagnetic uranium centre.

Compounds **2**, **2**^{t} and **2*** readily crystallise from saturated aromatic or ethereal solvent solutions, yielding yellow blocks suitable for single-crystal X-ray diffraction (XRD) analysis (Figures 2.3 to 2.5). The structures of **2**, **2**^{t} and **2*** are comparable; in all three cases the complexes are base free and display distorted tetrahedral geometry at the uranium centre. The U−O and U−N bond distances are similar in all three complexes **2** and **2**^{t} and comparable to distances exhibited by homoleptic U(IV) aryloxides and mixed aryloxide amide complexes.[9–12] The bond angles in **2**, **2**^{t} and **2*** are comparable with the exception of one O−U−N angle in **2*** which is more obtuse than in **2** and **2**^{t} (140.0(1)° *versus* 120.13(6) and 127.4(2)° respectively). This distortion could be due to a short U···C contact with the silylamide ligand in the solid state. Selected bond metrics for **2**, **2**^{t} and **2*** are presented in Table 2.1.

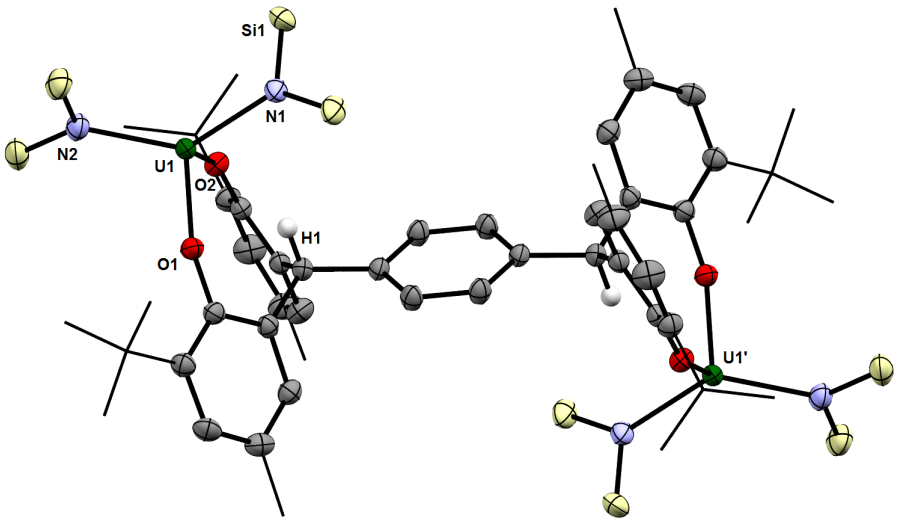

Figure 2.3 – Solid-state structure of **2** · C_6H_6. The aryloxide methyl and *tert*-butyl group carbon atoms are depicted as wireframe for clarity. The silylamide methyl groups and hydrogen atoms with the exception of the benzylic H-atoms, and lattice solvent molecules are omitted for clarity. The thermal ellipsoids are displayed at 50% probability.

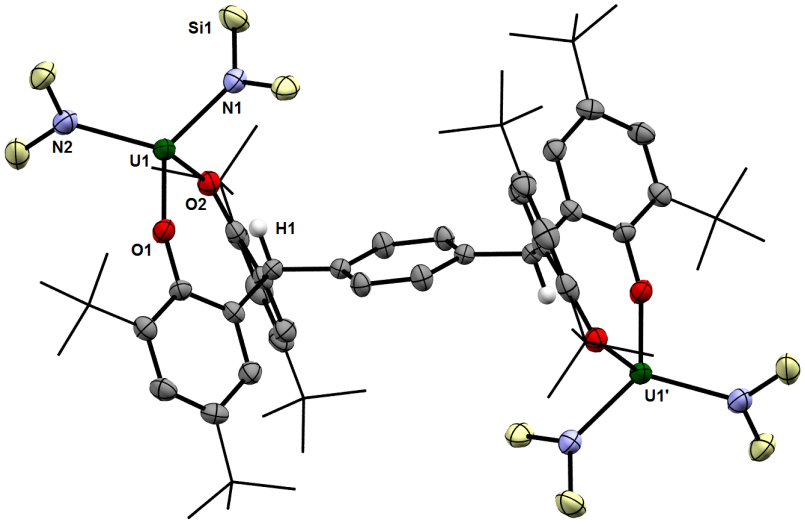

Figure 2.4 – Solid-state structure of **2^t** · C_6H_6. The aryloxide *tert*-butyl group carbon atoms are depicted as wireframe for clarity. The silylamide methyl groups and hydrogen atoms with the exception of the benzylic H-atoms, and lattice solvent molecules are omitted for clarity. The thermal ellipsoids are displayed at 50% probability.

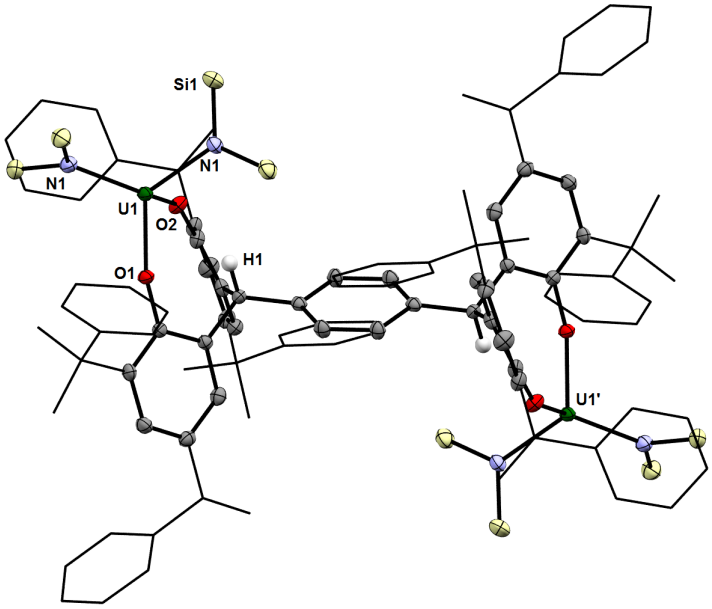

Figure 2.5 – Solid-state structure of $\mathbf{2}^{*} \cdot C_6H_6 \cdot THF$. The aryloxide methyl and phenyl group carbon atoms are depicted as wireframe for clarity. The silylamide methyl groups and hydrogen atoms with the exception of the benzylic H-atoms, and lattice solvent molecules are omitted for clarity. The thermal ellipsoids are displayed at 50% probability.

Table 2.1 – Selected bond distances (Å) and angles (°) for **2**, $\mathbf{2}^{t}$ and $\mathbf{2}^{*}$.

Parameter	**2**	$\mathbf{2}^{t}$	$\mathbf{2}^{*}$
U−O1	2.103(1)	2.137(4)	2.160(2)
U−O2	2.136(1)	2.107(4)	2.128(2)
U−N1	2.258(2)	2.249(5)	2.267(3)
U−N2	2.248(2)	2.261(5)	2.266(3)
O1−U−O2	98.49(5)	98.6(1)	96.57(8)
O1−U−N1	109.67(6)	98.4(2)	97.13(9)
O1−U−N2	99.99(6)	127.4(2)	140.0(1)
O2−U−N1	97.99(6)	114.6(2)	113.0(1)
O2−U−N2	120.13(6)	99.8(2)	101.53(9)
N1−U−N2	127.09(6)	117.2(2)	107.2(1)
U−O1−C11	152.2(1)	147.4(3)	148.4(2)
U−O2−C21	146.8(1)	152.6(3)	153.0(2)

2.4.2 Synthesis and characterisation of $[\{ThN''_2\}_2(pTP)]$

The synthesis of the thorium analogue of **2** was of interest as the limited redox chemistry and diamagnetism associated with organometallic thorium(IV) complexes simplifies the interpretation of NMR spectra, which can provide further insight into the solution behaviour of organometallic complexes. The bimetallic thorium complex $[\{ThN''_2\}_2(pTP)]$ (**3**) was synthesised according to the method described in Section 2.4.1.

Treating a stirring colourless suspension of $H_4(pTP)$ in hexanes with a pale yellow solution of $[ThN''_2(\kappa^2 C{:}N{-}N(SiMe_3)SiMe_2CH_2)]$ in hexanes provided a pale purple suspension which was allowed to stir for 18 hours. Complex **3** was isolated as a pale purple solid from a pale purple solution by centrifugation and dried under reduced pressure. The elemental analysis and spectroscopic data are in agreement with the proposed formulation. Similarly to the uranium complexes, **3** was air and moisture sensitive, and can be stored at room temperature under an inert atmosphere in the solid state and in benzene solution for a period of at least two months. Additionally, samples of **3** in benzene solution showed no sign of decomposition after three weeks at 80 °C.

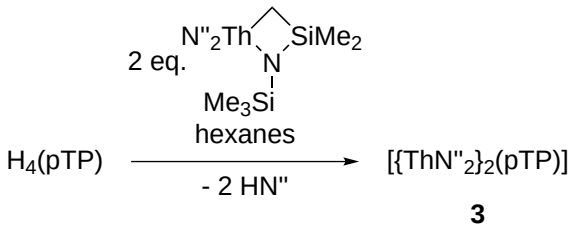

Scheme 2.6 – Synthesis of compound **3**

The ^{1}H spectrum of **3** spans 7 ppm, characteristic of a diamagnetic thorium (IV) complex, and suggests a symmetric ligand environment exhibiting six ligand resonances. However two silylamide resonances are present at 0.37 and 0.32 ppm in the ^{1}H NMR spectrum and two singlets at -11.5 and -11.8 ppm in the ^{29}Si NMR spectrum, suggesting magnetic inequivalence.

Complex **3** was recrystallised from a concentrated benzene solution as colourless blocks suitable for single-crystal XRD analysis. The four-coordinate thorium centre possesses distorted tetrahedral geometry (Figure 2.6). The Th$-$O distances are short compared to similar complexes in the literature ((2.162(5) and 2.189(5) Å *versus* mean 2.230(3) Å).[13–16] The Th-N distances of 2.328(6)4 and 2.330(6) Å are comparable to crystallographically characterised thorium silylamide complexes.[17–19] Similarly to complex **2*** (*vide supra*) there is a short Th$\cdots$C contact with a trimethylsilyl group of a silylamide ligands. The Th$\cdots$C contact *trans* to the

aryloxide ligand is significantly shorter than the next two shortest distances (3.068 Å *versus* 3.387 and 3.813 Å for C(56) and C(50) respectively).

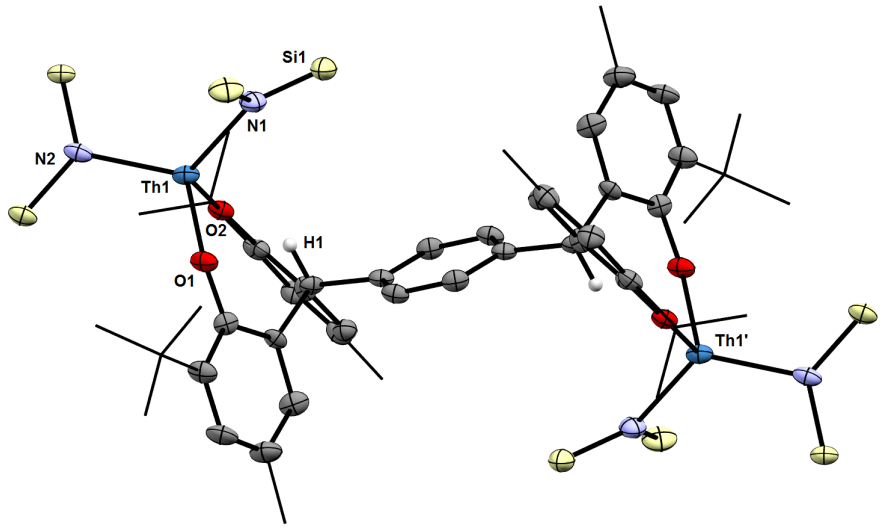

Figure 2.6 – Solid-state structure of **3** · C_6H_6. The aryloxide methyl and *tert*-butyl group carbon atoms are depicted as wireframe for clarity. The silylamide methyl groups and hydrogen atoms with the exception of the benzylic H-atoms, and lattice solvent molecules are omitted for clarity. The thermal ellipsoids are displayed at 50% probability.

2.5 Reactivity of complex [{UN″$_2$}$_2$(pTP)]

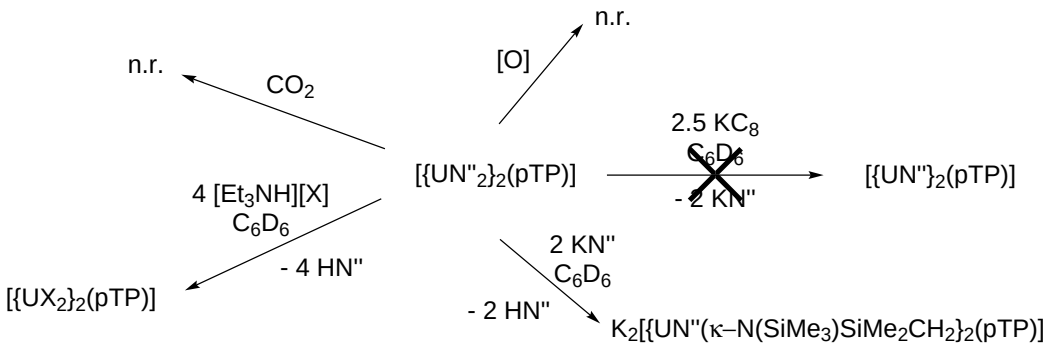

Scheme 2.7 – Reactivity of compound **2**.

Compound **2** and analogues are rare examples of well-defined bimetallic uranium complexes in

a non-macrocyclic environment, which could prove to be useful precursors to a wide range of derivatives of this class.

2.5.1 Reduction with KC_8

The reduction of U(IV) organometallic complexes has historically been the major route of entry into U(III) chemistry until the development of straightforward syntheses of U(III) starting materials, and remains an attractive route as uranium(IV) products often result from reactions of uranium(III) reagents. NMR-scale reactions of **2** with a two-fold excess of the strong reductant KC_8 in benzene provided a purple/brown suspension. After removal of graphite, a purple/black solution was obtained from which new paramagnetic resonances can be observed in the ^{1}H NMR spectrum, along with resonances corresponding to **2** (4:1 **2**:new resonances). The many new resonances present in the spectrum suggest a mixture of products. Attempts to carry out this reaction with more equivalents of KC_8 produced dark brown solutions from which only resonances for **2** could be detected in the ^{1}H NMR spectra, suggesting decomposition. No reaction was observed between **2** and $[Co(C_5Me_5)_2]$, suggesting the U(III)/U(IV) redox couple in **2** is more negative than that of the Co(II)/Co(III) couple of -1.94 V in $(C_5Me_5)_2Co$.

2.5.2 Reaction with KN″

Bond homolysis of ancillary ligands is a possible outcome of reactions with reductants. In complexes containing alkylated silyl groups, this often leads to metallacyclic, or "tuck-in", complexes.[20] To determine whether such a reaction was occurring between **2** and KC_8, reactions with bases were investigated. Reaction of **2** with KN″ produces a yellow solution. The ^{1}H NMR spectrum contains a mixture of starting material and new paramagnetically shifted resonances suggesting incomplete reaction. The resonances from this reaction do not match the new resonances which arose from the reduction of **2** with KC_8, suggesting that metal-centred reduction is occurring in the reaction of **2** with KC_8 rather than ligand C-H bond homolysis. Despite our best efforts, recrystallisation from a range of solvents did not yield crystalline material suitable for XRD analysis and full characterisation of the product was not pursued further.

2.5.3 Reactions with Brønsted acids

A halide-containing complex of the type $[\{UN''X\}_2(pTP)]$ (X = BPh_4,Cl) was targeted in order to provide a uranium(IV) precursor that would eliminate a salt by-product upon reduction as an

alternative route to bimetallic uranium(III) complexes. Protonolysis of uranium amides with Brønsted acids such as Et_3NHCl or Et_3NHBPh_4 by amine elimination is a known route for the synthesis of uranium halides or complexes with charge-separated ion pairs. The reduction of a uranium(IV) complex should be favoured with a halide co-ligand, as the elimination of a poorly soluble inorganic salt is more favourable than that of a soluble organic salt such as KN″. Reactions of **2** with PyHCl or Et_3NHCl in benzene resulted in a change from a yellow solution to a green suspension, accompanied by the formation of the by-product HN″ as evidenced by ^{1}H NMR spectroscopy. The poor solubility of the resulting complex in a range of solvents precluded its characterisation.

2.5.4 Reaction with gases

The insertion chemistry of uranium(III) silylamides with carbon dioxide has been demonstrated by Arnold and Mazzanti.[21–23] Our group reported the reaction of UN''_3 with atmospheric pressures of CO_2 to form $U(OSiMe_3)_4$ and $OCNSiMe_3$ by CO_2 insertion into the U−N bond. Exposing the U(III) potassium ate complex $K[UN''_4]$ to atmospheric pressures of CO_2, Mazzanti and co-workers showed that multiple N-Si bond cleavage was possible to yield the polymeric isocyanate bridged complex $[K(18-c-6)][UN''_3(NCO)_2]_n$. A degassed solution of **2** was exposed to 1 bar of dry CO_2, however no change was evident in the ^{1}H NMR spectrum. This could be a result of the large steric demand of the ligands, preventing small gas molecules from accessing the uranium centre.

2.5.5 Reaction with oxidants

Hayton and co-workers have demonstrated that UN''_3 can react with oxidants (2,2,6,6-tetramethylpiperidin-1-yl)oxyl (TEMPO) and trimethylamine *N*-oxide (TMANO) to yield the terminal U(V) oxo complex $[OUN''_3]$ or the oxo-bridged dimer $[N''_3UOUN''_3]$ respectively.[24] Reaction of **2** with excessive amounts of the oxidants TEMPO or TMANO produced dark brown solutions. Although a colour change was observed in both reactions, no change was evident in the ^{1}H NMR spectra.

A range of synthetic routes were investigated to target derivatives of **2**. Reduction of **2** with the strong reductant KC_8 provided a mixture containing unreacted material and a new unidentified product, while reaction of **2** with the milder reductant $[Co(C_5Me_5)_2]$ gave no reaction. Reaction with oxidants (TEMPO and TMANO) or caarbon dioxide gave no change by ^{1}H NMR spectroscopy. Reaction of **2** with the a Brønsted base (KN″) or Brønsted acids (PyHCl

or Et_3NHCl) gave new products which could not be isolated cleanly. The lack of reactivity of **2** could be explained by the large steric demand of the silylamide ancillary ligands which prevent coordination of reagents to the uranium centre. The halide analogues of **2** were targeted in the following section to facilitate the synthesis of new derivatives.

2.6 Synthesis of halide-containing complexes

2.6.1 Synthesis and characterisation of $[\{UI_2(solvent)_n\}_2(pTP^R)]$

The bimetallic halide complexes were targeted due to the broader synthetic possibilities offered by salt metathesis chemistry. As discussed in Section 2.2, Wu and co-workers commented that the dipotassium salt of the (pTP^t) ligand forms as the major product when the pro-ligand is reacted with $1-4$ equivalents of KN''. In order to avoid unwanted side-products, the dicalcium salt of the ligands, $[Ca_2(pTP^R)]$, were targeted as transfer reagents.

Treating $H_4(pTP)$ with $[CaN''_2]_2$ in 1,4-dioxane generates $[Ca_2(pTP^R)(dioxane)_n]$ as a colourless suspension. Transferring this suspension to a red $UI_4(dioxane)_2$ solution provided a bright green suspension after two days of stirring, from which $[\{UI_2(dioxane)_{1.5}\}_2(pTP)]_n$ (**4**) was isolated as a yellow-green powder in 75% yield. Elemental analysis and spectroscopic data were found to agree with the formulation for **4**. This route could be used to reproducibly provide pure material with convenient precipitation of the calcium iodide by-product in 1,4-dioxane. In contrast, reduced yield and purity was achieved from THF reactions due to concomitant precipitation of $[\{UI_2(thf)_3\}_2(pTP)]$ (**5**) and calcium iodide.

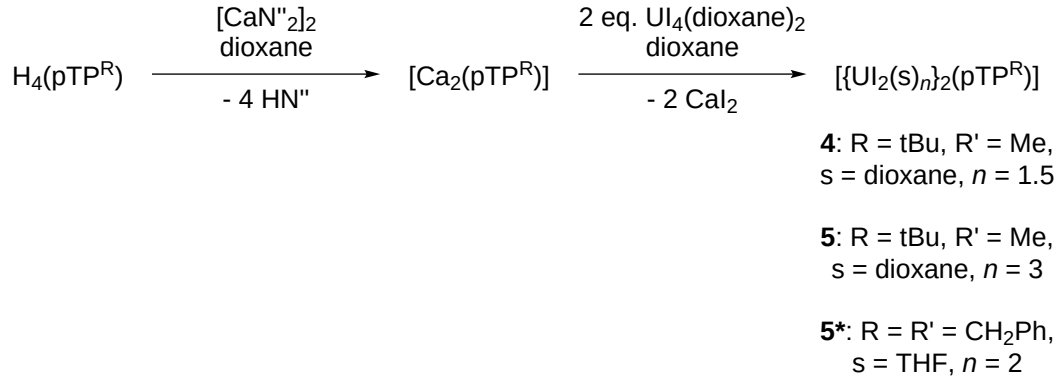

Scheme 2.8 – Synthesis of compounds **4**, **5**, **5***.

The ^1H NMR spectrum of **4** is narrow, ranging from 13 to 4 ppm, but still exhibiting paramagnetism as expected for a uranium(IV) complex. Six resonances are observed, indicative of a

C_2-symmetric product in solution. Complex **4** was further characterised by single-crystal XRD analysis. The formulation of the bulk material as $[\{UI_2(\text{dioxane})_{1.5}\}_2(\text{pTP})]_n$ was confirmed by elemental analysis. Compound **4** has appreciable solubility in aromatic and donor solvents with the exception of THF, in which it is only sparingly soluble due to rapid formation and deposition of the solvated complex **5**.

Crystals of the THF and dioxane adducts of **4** were obtained from concentrated THF or benzene solutions respectively (Figures 2.7 and 2.8). In **5**, the seven-coordinate uranium centre exhibits distorted pentagonal bipyramidal geometry. The aryloxide and iodo ligands occupying the equatorial plane alongside a THF molecule, while the axial plane is occupied by the two remaining THF molecules. In contrast, the uranium centre in **4** possesses octahedral geometry, with the equatorial plane occupied by the aryloxide and iodo ligands and the dioxane molecules in the axial positions. The *exo* dioxane ligand intermolecularly bridges two uranium centres leading to a one dimensional coordination polymer.

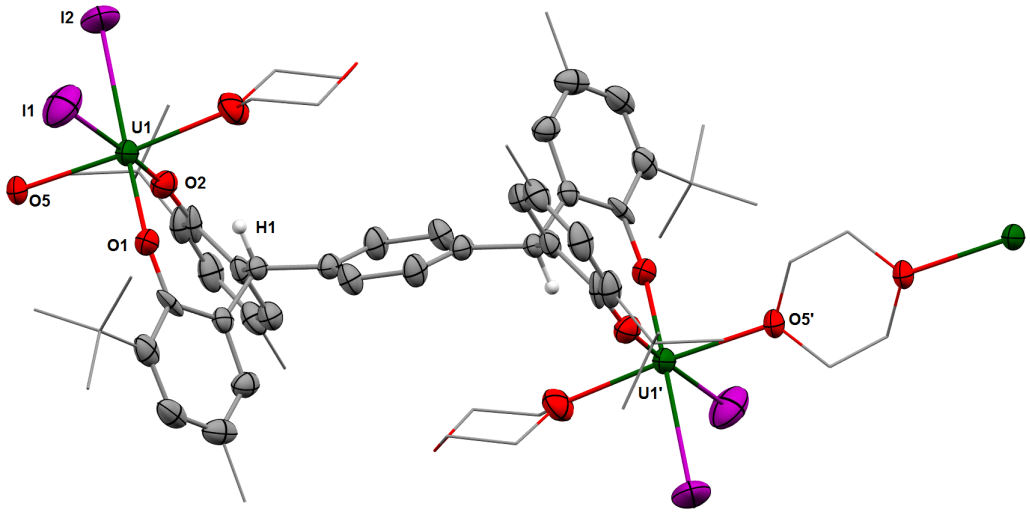

Figure 2.7 – Solid-state structure of **4** · 6(C_6D_6). The non-bound atoms of coordinated dioxane molecules, and aryloxide methyl and *tert*-butyl group carbon atoms are depicted as wireframe for clarity. The hydrogen atoms with the exception of the benzylic H-atoms, and lattice solvent are omitted for clarity. The thermal ellipsoids are displayed at 50% probability.

The pTP* analogue of **5**, $[\{UI_2(\text{thf})\}_2(\text{pTP*})]$ (**5***) could be prepared in 40% yield by treatment of $IU_4(\text{dioxane})_2$ with $[Ca_2(\text{pTP*})(\text{dioxane})_n]$ in THF. Similarly to **5**, the ^{1}H NMR spectrum of **5*** in THF-d_8 is narrow, ranging 12 ppm, with 11 ligand resonances consistent with a fully equilibrated ligand environment at room temperature in solution.

Crystalline **5*** suitable for single-crystal XRD analysis was grown from concentrated THF

solutions of **5***. The six-coordinate uranium centre in **5*** possesses distorted octahedral geometry (Figure 2.9). The iodo and aryloxide ligands occupy the equatorial plane, while the axial positions are occupied by THF ligands. The reduction in coordination number from seven in **5** to six in **5*** can be attributed to the greater steric demand of the (pTP*) ligand in **5***. Selected bond distances and angles for **4**, **5** and **5*** are displayed in Table 2.2.

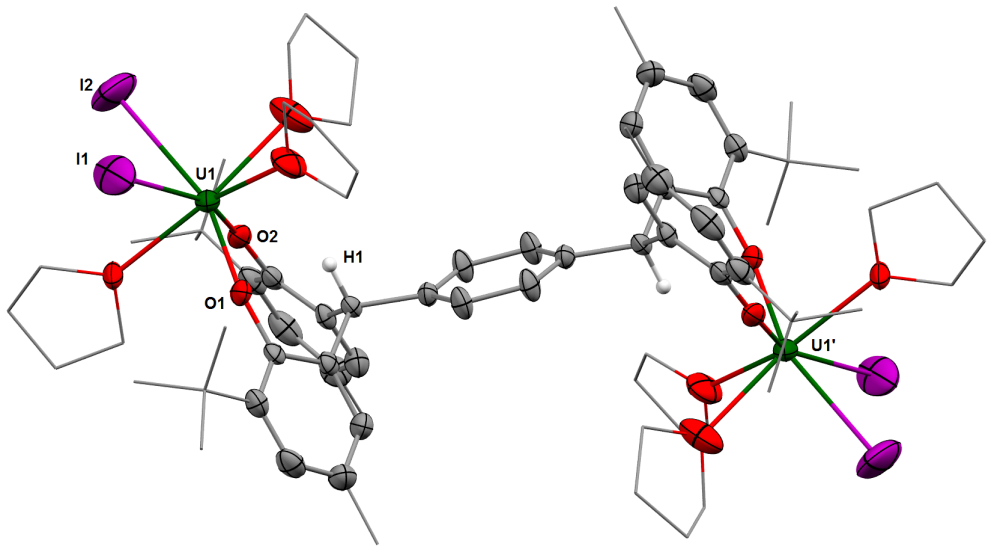

Figure 2.8 – Solid-state structure of **5** · (THF). The non-bound atoms of coordinated THF molecules, and aryloxide methyl and *tert*-butyl group carbon atoms are depicted as wireframe for clarity. The hydrogen atoms with the exception of the benzylic H-atoms, and lattice solvent are omitted for clarity. The thermal ellipsoids are displayed at 50% probability.

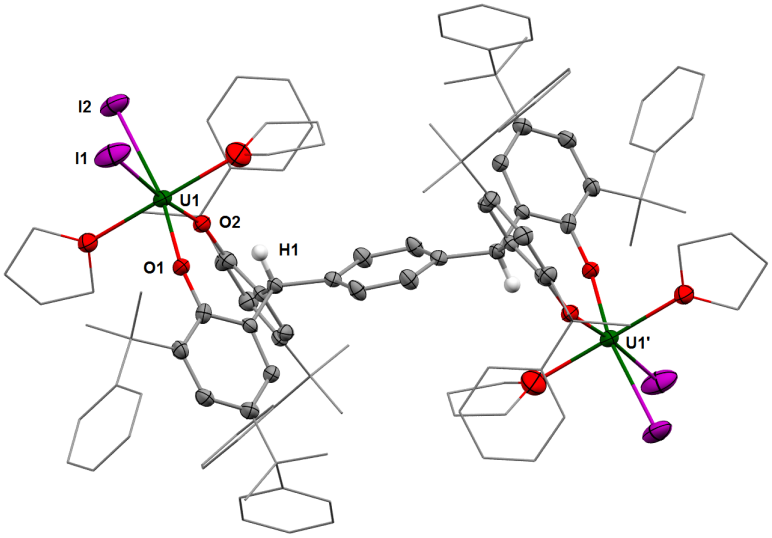

Figure 2.9 – Solid-state structure of $\mathbf{5}^{*} \cdot 2\,(\mathrm{THF})$. The non-bound atoms of coordinated THF molecules, and aryloxide methyl and phenyl group carbon atoms are depicted as wireframe for clarity. The hydrogen atoms with the exception of the benzylic H-atoms, and lattice solvent are omitted for clarity. The thermal ellipsoids are displayed at 50% probability.

Synthesis and characterisation of $[\{AnCl_2(solvent)\}_2(pTP)]$

The calcium ligand salt generated *in situ*, $[Ca_2(pTP)(solvent)_n]$, can be used as a reagent with the actinide chlorides, UCl_4 and $[ThCl_4(dme)_2]$, to furnish green $[\{UCl_2(dioxane)_2\}_2(pTP)]$ (**6**) and colourless $[\{ThCl_2(dme)(dioxane)\}_2(pTP)]$ (**7**) in yields of 70% and 90%, respectively.

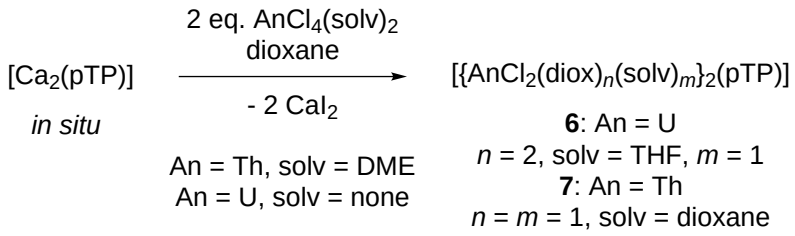

Scheme 2.9 – Synthesis of compounds **6** and **7**.

Compounds **6** and **7** crystallise from concentrated dioxane solutions as yellow-green and colourless plates, respectively. In both structures the metal centre exhibits distorted pentagonal bipyramidal geometry, similarly to that of **5**, with the aryloxide and chloro ligands occupying the equatorial plane along with one solvent molecule and the axial positions occupied by remaining solvent molecules. Complex **6** was found to crystallise as an adduct of THF and dioxane (Figure 2.10); while no THF was used during the reaction, THF vapours are likely to have

been present in the glovebox atmosphere during crystallisation. The thorium centre in **7** has bound DME and dioxane molecules (Figure 2.11). Although the reaction was carried out in dioxane, residual DME from $[ThCl_4(DME)_2]$ was present in solution, and its ability to act as a intramolecular bidentate ligand may favour its coordination to thorium over dioxane. Selected bond distances and angles can be found in Table 2.2.

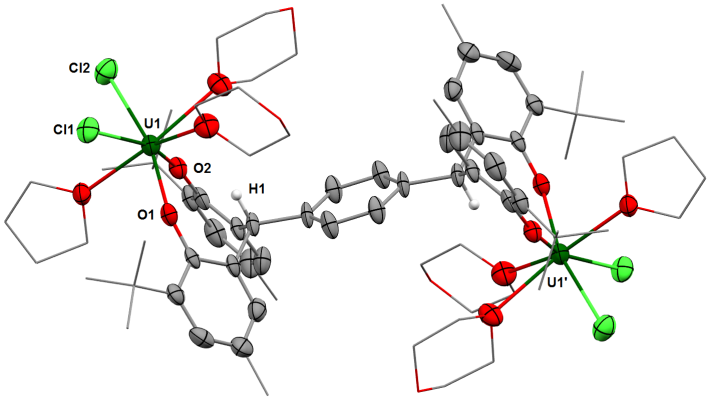

Figure 2.10 – Solid-state structure of **6** · 2 (dioxane). The non-bound atoms of coordinated dioxane and THF molecules, and aryloxide methyl and *tert*-butyl group carbon atoms are depicted as wireframe for clarity. The hydrogen atoms with the exception of the benzylic H-atoms, lattice solvent and another molecule of **6** are omitted for clarity. The thermal ellipsoids are displayed at 50% probability.

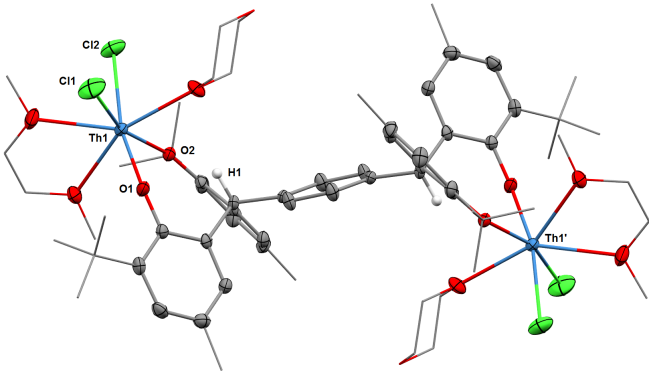

Figure 2.11 – Solid-state structure of **7** · 6 (dioxane). The non-bound atoms of coordinated dioxane and DME molecules, and aryloxide methyl and *tert*-butyl group carbon atoms are depicted as wireframe for clarity. The hydrogen atoms with the exception of the benzylic H-atoms are omitted for clarity. The thermal ellipsoids are displayed at 50% probability.

Table 2.2 – Selected bond distances (Å) and angles (°) for compounds **4**, **5**, **5***, **6** and **7**.

Parameter	**4**	**5**	**5***	**6**	**7**
U−O1	2.089(5)	2.109(5)	2.103(3)	2.133(4)	2.183(2)
U−O2	2.088(5)	2.118(5)	2.106(3)	2.131(4)	2.178(2)
U−X1	3.0368(7)	3.0973(7)	2.10551(4)	2.656(2)	86.62(6)
U−X2	3.0110(7)	3.1095(8)	2.10417(5)	2.655(2)	87.51(6)
O−U−O	92.7(2)	89.0(2)	91.2(1)	88.8(1)	88.29(8)
O−U−X	89.6(1)	91.5(1)	92.73(1)	90.5(1)	87.06(1)
U−O−C_{ipso}	156.5(1)	157.0(1)	156.2(3)	156.9(1)	156.6(1)

2.7 Reaction of [{UI_2(dioxane)$_{1.5}$}(pTP)] with reducing agents

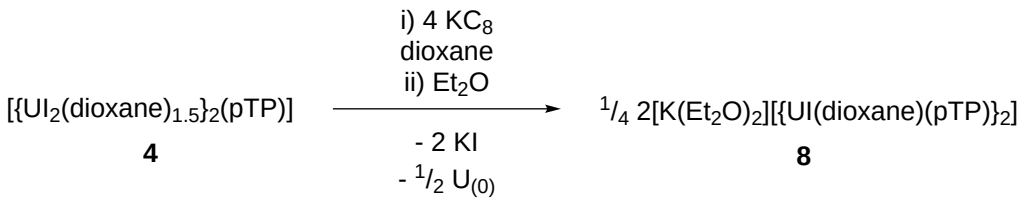

Scheme 2.10 – Synthesis of compounds **8**.

The first reported diuranium inverse-sandwich of a neutral arene by Cummins and co-workers was obtained by reduction of an iodo tris(amido)uranium(IV) complex in toluene.[25] As a bimetallic uranium(III) complex was targeted, the reduction of **4** in aromatic solvent was investigated. Addition of a yellow solution of **4** in benzene to a bronze KC_8 slurry immediately furnished a dark green suspension. The suspension was centrifuged after 15 minutes of stirring and the filtrate decanted to remove graphite. Pale blue crystals were obtained from the filtrate upon standing for 18 hours in the presence of Et_2O. The crystalline material was found to be extremely air sensitive, showing a colour change to dark brown within seconds when exposed to air, even under oil. The material was suitable for single-crystal XRD and revealed the reaction product to be a dimeric uranium(IV) complex with incorporated potassium iodide $K_2[U_2(pTP)_2I_2]$ (**8**, Figure 2.12). The two uranium centres are bridged by two tetra-aryloxide ligands. Both uranium centres are six-coordinate and have identical coordination spheres; four sites are occupied by the four aryloxide ligands and the two remaining sites are occupied by *cis* dioxane and iodide ligands. The iodide ligand bridges the uranium centre and the neighbouring

potassium cation which is incorporated in the molecular structure. The potassium ion resides within a cavity formed by a ligand bis(aryloxide) pocket coordinated η^3 to an aryloxide aryl group and η^2 to an aryloxide C−O bond, and two further coordination sites occupied by two diethyl ether molecules.

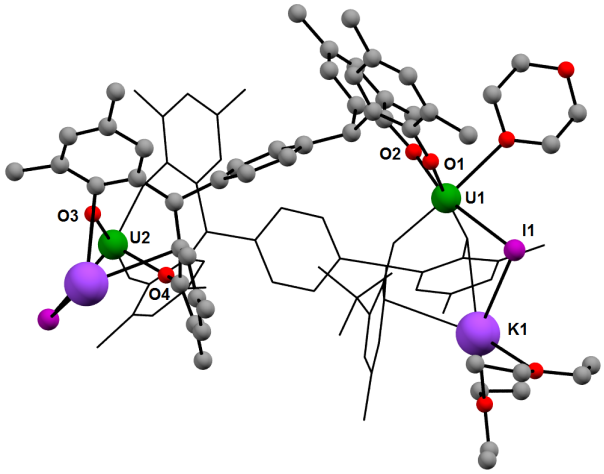

Figure 2.12 – Solid-state structure of **8**. The non-bound atoms of coordinated Et_2O molecules, and methyl and *tert*-butyl group carbon atoms are depicted as wireframe for clarity. The hydrogen atoms with the exception of the benzylic H-atoms, and lattice solvent are omitted for clarity. The thermal ellipsoids are displayed at 50% probability.

2.7.1 Synthesis and characterisation of $[U(pTP)(THF)_2]_2$

Complex **8** has an unusual structure in that it is a bimetallic complex with a protected cavity between the two metal centres and as such could exhibit interesting reduction chemistry. An analogous complex to **8** without salt incorporation was targeted. The preparation of $[Ca_2(pTP)]$ in dioxane and subsequent treatment with a single equivalent of $[UI_4(dioxane)_2]$ afforded a pale green-brown solution, after work-up from dioxane. Pale brown crystals of $[U(thf)_2(pTP)_2]_2$ (**9**) were obtained by diffusion of hexanes into a THF solution of **9**, and were collected in reasonable yields (60-75%). Spectroscopic data agree with the formulation for **9**. Carrying out the reaction of $K_4[pTP]$ prepared *in sity* with $[UI_4(dioxane)_2]$ in THF also provided **9** with minimal difference in yield. This route is preferred as KN″ is required for the synthesis of $[CaN''_2]_2$. Compound **9** is appreciably soluble in arene and ethereal solvents.

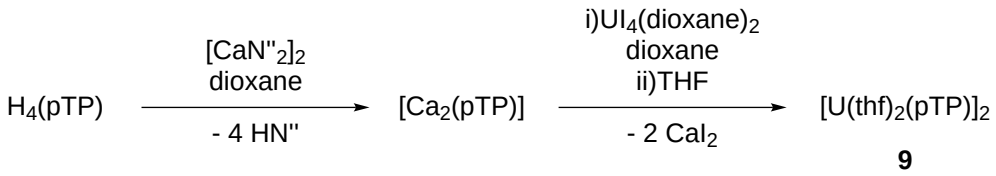

Scheme 2.11 – Synthesis of compound **9**.

The ^{1}H NMR spectrum of **9** in either d_8-THF and C_6D_6 contains ten ligand resonances, consistent with an unsymmetrical ligand environment, which range from $+34$ to -15 ppm as expected for an organometallic U(IV) complex. The *tert*-butyl resonances are at $+23.7$ and -14.6 ppm, methyl resonances at $+16.1$ and -4.4 ppm and the aromatic resonances at $+33.8$, $+25.2$, $+7.0$, -8.9 and -11.6 ppm. The resonances of the benzylic protons could not be located in the ^{1}H spectra in either solvent.

Single crystals of **9** were obtained from slow diffusion of hexanes into a THF solution of **9** or from concentrated benzene solutions of **9**. The unit cell consists of two uranium centres bridged by two staggered tetra(aryloxide) ligands, binding in a μ-κ^2 : κ^2 fashion (Figure 2.13). The two uranium centres display octahedral geometry with two *cis* equatorial positions occupied by THF molecules and the remaining coordination sites are occupied by aryloxide ligands. The inequivalent environments are retained in solution, as indicated in the ^{1}H NMR spectrum. The axial U$-$O aryloxide distances range from 2.143(6) to 2.164(6) Å (mean 2.160(8) Å) and the equatorial U$-$O aryloxide distances range from 2.143(6) to 2.164(6) Å (mean 2.152(8) Å). These are longer than those found in the silylamide complex **2** and the iodo and chloro complexes **4**, **5**, **6** (mean 2.113(8) Å), which can be ascribed to the greater steric congestion about the metal centre in **9**.

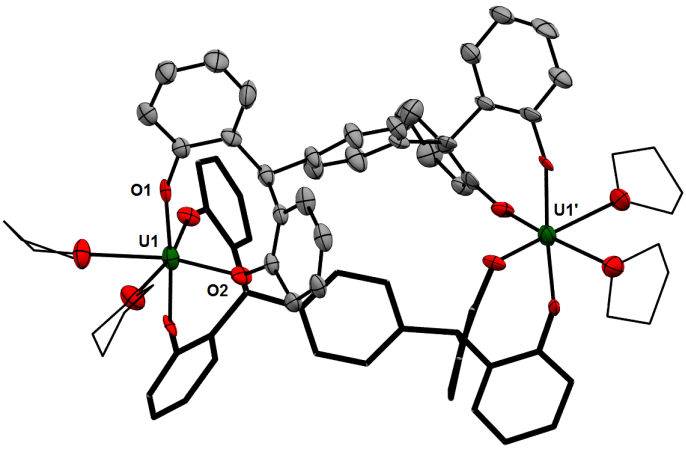

Figure 2.13 – Solid-state structure of **9**. The non-bound atoms of coordinated Et_2O molecules, and methyl and *tert*-butyl group carbon atoms are depicted as wireframe for clarity. The hydrogen atoms with the exception of the benzylic H-atoms, and lattice solvent are omitted for clarity. The thermal ellipsoids are displayed at 50% probability.

2.7.2 Synthesis and characterisation of $[U(pTP)(THF)_2]_3$

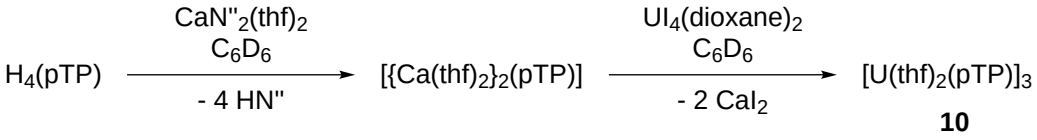

Scheme 2.12 – Synthesis of compound **10**.

Generation of $[Ca_2(pTP)]$ from $[CaN''_2]_2$ and $H_4(pTP)$ in aromatic solvent yields a bright green slurry. Addition of a single equivalent of $[UI_4(dioxane)_2]$ to this suspension results in slow discolouration to a dark brown suspension with large amounts of precipitate, from which no material could be isolated. In contrast, reaction of $[CaN''_2(thf)_2]$ with $H_4(pTP)$ yields a yellow solution, which cleanly reacts with $UI_4(dioxane)_2$ to give a brown suspension. The ^1H NMR spectrum in C_6D_6 was identical to that of **9**, however dark brown crystals suitable for single-crystal XRD analysis consistent with the trimeric product $[U(thf)_2(pTP)]_3$ (**10**, Figure 2.14) were obtained by slow evaporation of hexanes into the reaction mixture after filtration. The difference between dimeric and trimeric material may arise from the difference in crystallisation solvent, however the ^1H NMR spectra of **9** in C_6D_6 and d_8-THF are almost identical.

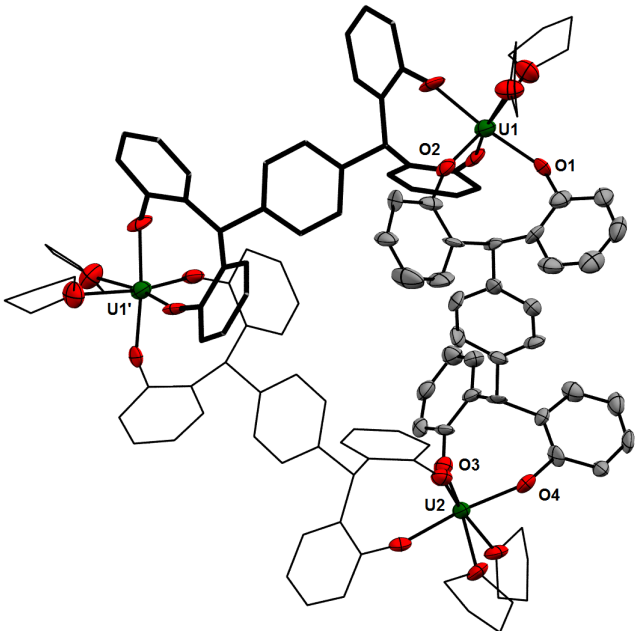

Figure 2.14 – Solid-state structure of **10**. The non-bound atoms of coordinated Et_2O molecules, and methyl and *tert*-butyl group carbon atoms are depicted as wireframe for clarity. The hydrogen atoms with the exception of the benzylic H-atoms, and lattice solvent are omitted for clarity. The thermal ellipsoids are displayed at 50% probability.

2.8 Reactions to target bimetallic uranium(III) complexes from uranium(III) starting materials

Complexes containing two uranium(III) centres within the same ligand frame to impart control or selectivity upon concerted two-electron reductive transformation effected by two uranium (III) cations are of considerable interest. Work has been undertaken in our laboratory with Prof. J. Love using a Schiff base pyrrolic macrocycle to synthesise a bis uranium(III) borohydride and aryloxide complex.[3] Protonolysis reactions of UN''_3 with H_4(pTP) and salt metathesis reactions of uranium (III) borohydride and iodide with various group 1 and 2 metal salts of the ligand invariably furnished uranium(IV) products, which could be identified from their ^{1}H NMR spectra and crystallographic cell measurements, and are summarised in Table 2.3.

Table 2.3 – Products obtained from reactions of various uranium(III) starting materials and ligand precursors.

	H_4(pTP)	Na_4(pTP)	K_4(pTP)	Ca_2(pTP)	Sr_2(pTP)
UN''_3	**2**				
UI_3		**9**	**9**	**n.r.**	**9**
$U(BH_4)_3(THF)_2$		**9**	**9**	**n.r.**	**9**

2.8.1 Reaction of $[U\{N(SiMe_3)_2\}_3]$ with H_4(pTP)

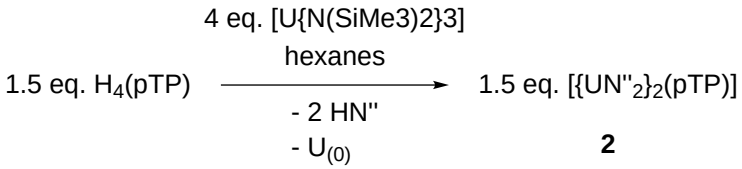

Scheme 2.13 – Alternative synthesis of compound **2**.

The reaction of two equivalents of $[U\{N(SiMe_3)_2\}_3]$ with H_4(pTP) in hexanes resulted in the isolation of **2**. This is likely to be the result of the disproportionation of uranium(III) to uranium(IV) and uranium metal, a decomposition process which is well documented in the literature.[26]

2.8.2 Salt metathesis reactions of $[U(BH_4)_3(thf)_2]$ and UI_3 with group I and group II ligand salts

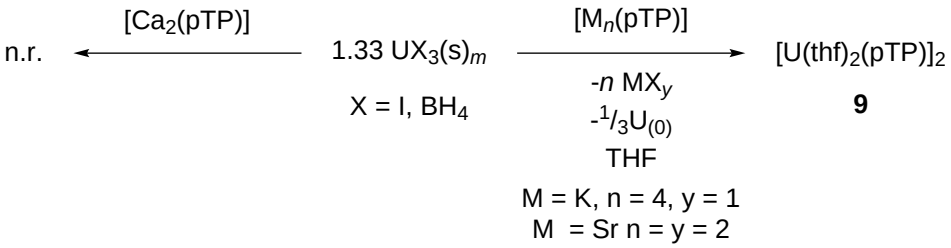

Scheme 2.14 – Alternative synthesis of compound **9**.

The reaction of two equivalents of $[U(BH_4)_3(thf)_2]$ or UI_3 with $[Ca_2(pTP)]$ generated *in situ* in THF did not results in a reaction. In contrast, using a strontium or potassium salt of the ligand resulted in the isolation of **9**, likely due the same decomposition pathway discussed

in Section 2.8.1. Unlike the reaction with UN''_3, the stoichiometry of the product is 1:1 with respect to metal and ligand. This difference could be due to the reaction conditions employed; a non donor solvent for UN''_3 and a donor solvent for UX_3. The contrasting reactivity between the calcium and strontium or potassium salts may be due to the higher oxophilicity of calcium when compared to strontium and potassium. The elimination of CaI_2 is not a sufficient driving force to break the strong Ca−O bond in Ca_2(pTP), preventing further reactivity with the soft uranium(III) salts.

2.9 Chapter summary and conclusions

The tetra-aryloxide ligand discussed in this chapter is well-suited to accommodating two actinide(IV) ions, and has been employed to synthesise ten new homobimetallic uranium and thorium, and one homotrimetallic uranium complexes. The successful synthesis of these complexes fulfil one of the primary aims of the this project. Increasing the aryloxide steric bulk from methyl to *tert*-butyl at the *para* positions results in an increase in solubility in hydrocarbon solvents with little to no effect on solid-state structures (compounds **2** and $\mathbf{2^t}$). Employing the more sterically demanding ligand with *ortho* and *para* dimethylbenzyl substituted aryloxides resulted in the distortion of the O−U−N angle in the silylamide complex $\mathbf{2^*}$, and a reduction in coordination number in the iodide complexes $\mathbf{5^*}$.

The redox properties of the new complexes were investigated chemically, satisfying the second primary aim of this project. Reduction of bimetallic silylamide complex **2** with the strong reductant KC_8 yielded a new paramagnetic species, but it could not be separated from unreacted starting materials. The new bimetallic cavitand **8** was obtained from the reduction of the iodide complex **4** with KC_8, which incorporates potassium iodide into the molecular structure. A synthetic route to the salt-free analogue, **9**, was established and the trimetallic congener, **10**, was also synthesised when the reaction was carried out in aromatic solvents with small quantities of THF present. The bimetallic complex **9** was also the major product from salt metathesis reactions using a range uranium(III) starting materials. These findings suggest that the bimetallic cavitand motif exhibited by **8** and **9** may be a thermodynamic sink in the system, rather than the targeted bimetallic uranium(III) complex [$\{UI\}_2$(pTP)], based on the motif of complexes **2**, **4** and related complexes. Additionally, the controlled formation of bi- or trimetallic cavitand complexes may be effected by careful consideration of the reaction conditions.

If **9** is a thermodynamic sink, the bimetallic uranium(IV) complexes which have been

synthesised may not be suitable precursors for the synthesis of bimetallic uranium(III) complexes, as the reducing environment required for their formation likely to favour metal results in metal disproportionation and ligand redistribution to form **9**. If **9** is a thermodynamic sink, further reduction of **9** may provide a stable bimetallic uranium(III) complex which exhibits small molecule reactivity in the intermetallic cleft. Further work would be required to investigate the redox properties of **9** and its reactivity with small molecules.

Further work could also be carried out to investigate related ligand systems with slight modifications. As discussed in Chapter 1, the thermodynamics of a system can be very dependent on the steric environment. The larger steric requirements of the (pTP*) ligand in **1*** disrupts the dipotassium inverse-sandwich motif that is present in the dipotassium salts (pTP) ligand (**1**) and $[K_2\{H_2(pTP^t)\}]$. It is possible that dimerisation to $[U(pTP^*)]_2$ would be disfavoured upon reduction of **5*** and could therefore provide the targeted bimetallic uranium(III) complex $[(UI)_2(pTP^*)]$. Additionally, the proximity of aryl groups to the uranium centre in the (pTP*) ligand could prove useful to stabilise the softer uranium(III) oxidation state.[27]

Additionally, other simple modifications to the ligand system may provide better steric stabilisation to the metal centre. Using a tetra-aryloxide based on a durene core as opposed to the xylene core in H_4(pTP) would reduce the bis(aryloxide) pocket bite angle and thus protect a larger portion of the metal centre, reducing the likelihood of disproportionation and ligand rearrangement. Recent reports by Marçalo and co-workers, and Cloke and co-workers have detailed the syntheses of uranium(III) bis(aryloxide) complexes based on 1,4,8,11-tetraazacyclotetradecane or 1,4-di-*iso*-propylbenzene bridged bis(aryloxide) ligands, respectively.[28,29] In both of these complexes, the aryloxide arms of the ligand are such that once coordinated they are *trans* to each other, so as to offer maximal steric protection to the reactive metal centre. As suggested by the high isolated yields, ligand redistribution issues are avoided in these systems.

2.10 Bibliography

[1] P. Arnold, S. Mansell, L. Maron and D. McKay, *Nature Chem.*, 2012, **4**, 668–674.

[2] H. S. La Pierre, A. Scheurer, F. W. Heinemann, W. Hieringer and K. Meyer, *Angew. Chem., Int. Ed.*, 2014, **53**, 7158–7162.

[3] P. L. Arnold, C. J. Stevens, J. H. Farnaby, M. G. Gardiner, G. S. Nichol and J. B. Love, *J. Am. Chem. Soc.*, 2014, **136**, 10218–10221.

[4] P. L. Arnold, J. H. Farnaby, R. C. White, N. Kaltsoyannis, M. G. Gardiner and J. B. Love, *Chem. Sci.*, 2014, **5**, 756–765.

[5] P. L. Arnold, J. H. Farnaby, M. G. Gardiner and J. B. Love, *Organometallics*, 2015, **34**, 2114–2117.

[6] L. Tang, E. P. Wasserman, D. R. Neithamer, R. D. Krystosek, Y. Cheng, P. C. Price, Y. He and T. J. Emge, *Macromolecules*, 2008, **41**, 7306–7315.

[7] A. Mobinikhaledi, H. Moghanian and M. Deinavizadeh, *C. R. Chim.*, 2013, **16**, 1035–1041.

[8] J. Zhang, C. Jian, Y. Gao, L. Wang, N. Tang and J. Wu, *Inorg. Chem.*, 2012, **51**, 13380–13389.

[9] W. G. van der Sluys, A. P. Sattelberger, W. E. Streib and J. C. Huffman, *Polyhedron*, 1989, **8**, 1247–1249.

[10] P. B. Hitchcock, M. F. Lappert, A. Singh, R. G. Taylor and D. Brown, *J. Chem. Soc., Chem. Commun.*, 1983, 561–563.

[11] J. M. Berg, D. L. Clark, J. C. Huffman, D. E. Morris, A. P. Sattelberger, W. E. Streib, W. G. van der Sluys and J. G. Watkin, *J. Am. Chem. Soc.*, 1992, **114**, 10811–10821.

[12] A. J. Lewis, K. C. Mullane, E. Nakamaru-Ogiso, P. J. Carroll and E. J. Schelter, *Inorg. Chem.*, 2014, **53**, 6944–6953.

[13] S. M. Beshouri, P. E. Fanwick, I. P. Rothwell and J. C. Huffman, *Organometallics*, 1987, **6**, 2498–2502.

[14] I. Korobkov, S. Gambarotta and G. Yap, *Angew. Chem., Int. Ed.*, 2003, **42**, 4958–4961.

[15] I. Korobkov, A. Arunachalampillai and S. Gambarotta, *Organometallics*, 2004, **23**, 6248–6252.

[16] J. McKinven, G. S. Nichol and P. L. Arnold, *Dalton Trans.*, 2014, **43**, 17416–17421.

[17] D. M. Barnhart, D. L. Clark, S. K. Grumbine and J. G. Watkin, *Inorg. Chem.*, 1995, **34**, 1695–1699.

[18] N. L. Bell, L. Maron and P. L. Arnold, *J. Am. Chem. Soc.*, 2015, **137**, 10492–10495.

[19] D. E. Smiles, G. Wu, N. Kaltsoyannis and T. W. Hayton, *Chem. Sci.*, 2015, **6**, 3891–3899.

[20] R. Boaretto, P. Roussel, N. W. Alcock, A. J. Kingsley, I. J. Munslow, C. J. Sanders and P. Scott, *J. Organomet. Chem.*, 1999, **591**, 174–184.

[21] S. M. Mansell, N. Kaltsoyannis and P. L. Arnold, *J. Am. Chem. Soc.*, 2011, **133**, 9036–9051.

[22] P. L. Arnold, Z. R. Turner, A. I. Germeroth, I. J. Casely, G. S. Nichol, R. Bellabarba and R. P. Tooze, *Dalton Trans.*, 2013, **42**, 1333–1337.

[23] C. Camp, L. Chatelain, C. E. Kefalidis, P. Jacques, L. Maron and M. Mazzanti, *Chem. Commun.*, 2015, **51**, 15454–15457.

[24] S. Fortier, J. L. Brown, N. Kaltsoyannis, G. Wu and T. W. Hayton, *Inorg. Chem.*, 2012, **51**, 1625–1633.

[25] P. L. Diaconescu, P. L. Arnold, T. A. Baker, D. J. Mindiola and C. C. Cummins, *J. Am. Chem. Soc.*, 2000, **122**, 6108–6109.

[26] J. Hümmer, F. W. Heinemann and K. Meyer, *Inorg. Chem.*, 2017, **56**, 3201–3206.

[27] S. M. Franke, B. L. Tran, F. W. Heinemann, W. Hieringer, D. J. Mindiola and K. Meyer, *Inorg. Chem.*, 2013, **52**, 10552–10558.

[28] L. Maria, I. C. Santos, V. R. Sousa and J. Marçalo, *Inorg. Chem.*, 2015, **54**, 9115–9126.

[29] C. J. Inman, A. S. P. Frey, A. F. R. Kilpatrick, F. G. N. Cloke and S. M. Roe, *Organometallics*, 2017, **36**, 4539–4545.

Chapter 3

Mononuclear actinide complexes of an arene-tethered tetra-aryloxide pTP

As discussed in Section 1.2, there is a paucity of *f* element complexes with neutral arenes with only three structurally characterised bis(arene) complexes reported thus far for the *f* block metals, $Ln(C_6H_3{}^tBu_3)_2$ (Ln = Y, Gd) and $Ho(C_5H_2{}^tBu_3P)_2$ by Cloke and co-workers.[1–3] Recently, Mazzanti *et al.* reported a triple-decker cerium bis(arene) complex, expanding synthetic methods to access *f* element bis(arene) complexes beyond metal vapour synthesis. Reduction of the cerium siloxide -ate complex $K[Ce\{OSi(OtBu)_3\}]$ with potassium metal in toluene provided $K_2[(Ce\{OSi(OtBu)_3\}_3\{\mu\text{-}C_6H_5Me\})_2Ce]$.[4] Since the advent of the diuranium inverse sandwich motif at the turn of the century, the interest in uranium-arene interactions has been renewed. As discussed in Section 1.1.2, Meyer and co-workers used a tridentate aryloxide ligand based on a mesitylene core to synthesise the uranium(III) monoarene complex $[\{(^{Ad}ArO)_3Mes\}U]$. Reaction of this complex with CO_2 was shown to form a carbonate bridge bis(uranium(IV)) complex, the product of the reductive disproportionation of CO_2 by two concerted uranium-mediated one-electron reductions.[5–7] It was also shown that one-electron reduction of this complex with potassium sand provided the uranium(II) anion, $K[\{(^{Ad}ArO)_3Mes\}U]$, which was suggested to be accessible due to a uranium δ-arene bond with the ligand frame by DFT calculations.[8] As discussed in Section 1.1.1, the first crystallographically characterised uranium tris(aryloxide) complex $[U(Odipp)_3]$ is dimeric in the solid state, bridged by an Odipp aryloxide ligand through a uranium-arene interaction. A collaboration from the Mindiola and Meyer groups led to the report of uranium(III) complexes bearing the sterically demanding ligand $[2,6-(CPh_2)_2-4-MeC_6H_2OH]$ (Obdpmp), $[U(Obdpmp)_3]$, which feature an intramolecular uranium-arene interaction. Unlike $[U(Odipp)_3]$ which was shown to be unreactive towards CO and CO_2, $[U(Obdpmp)_3]$ exhibits oxidation chemistry with small molecules.[9,10] Cloke and co-workers used an arene-bridged bis(aryloxide) lig-

and, [{(2,4−$Me_2C_6H_2OH$)CMe_2}$_2C_6H_4$] (Me_2BP), to prepare the mixed ligand uranium(III) complex [U(C_5Me_5)(Me_2BP)] which exhbits a uranium η^6-arene interaction in the solid state. Reaction of [U(C_5Me_5)(Me_2BP)] with stoichiometric amounts of CO_2 produces the bimetallic uranium(IV) complex, [U(C_5Me_5)(Me_2BP)]$_2$(μ-C_2O_4).[11]

This chapter describes investigations into the synthesis of a set of uranium complexes of the arene-bridged tetra-aryloxide ligand, H_4(pTP), and their Lewis base adducts and an optimised synthetic route to Lewis base adducts of the analogous thorium complexes.

3.1 General synthetic route to mononuclear actinide aryloxide complexes

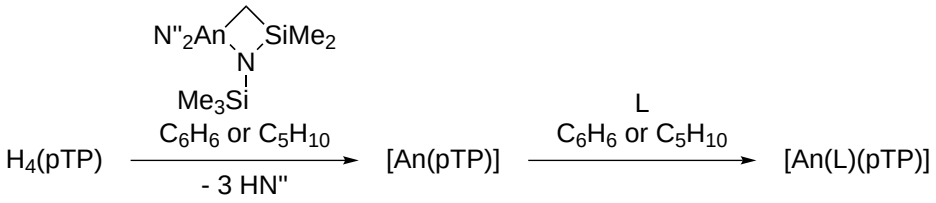

Scheme 3.1 – Synthetic route to actinide monoarene tetra-aryloxide complexes (An = U or Th; L = THF, CNXyl, Me_3SiN_3).

The general synthetic route to base-stabilised actinide monoarene tetra-aryloxide complexes is shown in Scheme 3.1. The base-free actinide monoarene is generated in non-coordinating solvent (arene, cycloalkane, alkane) by protonolysis of the proligand, H_4(pTP), with the appropriate actinide silylamide metallacycle, [AnN″$_2$(κ^2*C*:*N*−N($SiMe_3$)$SiMe_2CH_2$)], and is then exposed to one equivalent of a Lewis base. The successful synthesis and reactivity of a range of Lewis base adducts of uranium and thorium monoarene complexes and their characterisation is described, along with attempted syntheses of other adducts.

3.2 Targeted synthesis of a uranium monoarene complex, [U(pTP)]

Treating a colourless suspension of H_4(pTP) in toluene-d_8 with stoichiometric amounts of yellow-brown uranium silylamide metallacycle, [UN″$_2$(κ^2*C*:*N*−N($SiMe_3$)$SiMe_2CH_2$)], in the presence of an internal standard (C_6Me_6) provides a dark brown solution. The ^{1}H NMR spectrum of this mixture is non-trivial, displaying numerous broad and sharp resonances at room temperature. The sharp resonances are consistent with a symmetrical compound with empirical formula [U(pTP)] (**11**), with six paramagnetically shifted ligand resonances spanning 40 ppm,

and equate to 10% yield with respect to the internal standard. The remaining 90% of material may be accounted for in the broad resonances.

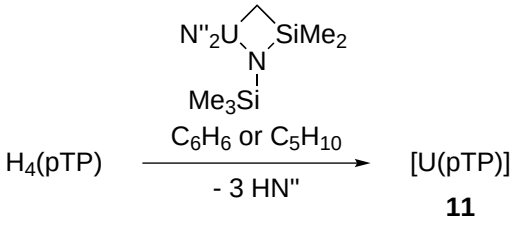

Scheme 3.2 – Synthesis of **11**.

As discussed in Chapter 2, the 1:1 complex of uranium and the tetraphenolate ligand **9** was synthesised, which was revealed to be dimeric by single-crystal XRD. With this knowledge, it was hypothesised that the broad resonances in the ^{1}H NMR spectra of **11** could be ascribed to dimeric (i.e. $[U(pTP)]_2$) or oligomeric material (i.e. $[U(pTP)]_n$), which is in equilibrium with the mmonomeric compound. The solution behaviour of this mixture was investigated by ^{1}H NMR spectroscopy at variable temperatures (310 – 380 K) in order to assess whether a thermal equilibrium could be reached. A small increase in the proportion of sharp resonances in the spectrum with temperature was observed (10% at 300 K to 12% at 380 K), along with the emergence of new resonances. Unfortunately, coalescence was not observed at elevated temperatures. It is possible that a higher temperature is required to reach coalescence, requiring a solvent with a higher boiling point. Another possibility is that the broad and sharp resonances are not in a dynamic equilibrium and are separate products. Further investigation is required to identify the components of the mixture.

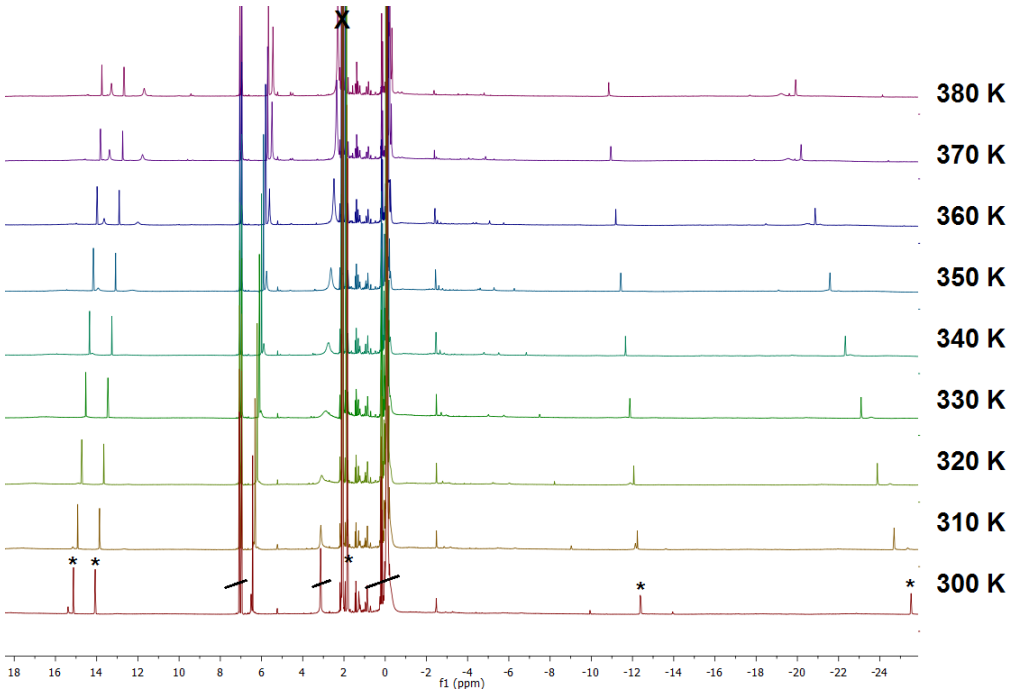

Figure 3.1 – Variable temperature ^{1}H NMR spectra of toluene solutions of **11** in the 300 − 380 K range. The resonances appertaining to compound **11** are starred and impurities and residual *protio* solvent resonances are scored through on the 300 K spectrum. The internal standard (C_6Me_6) is marked with a cross on the 380 K spectrum.

Dark red crystals suitable for single-crystal XRD analysis were obtained by storing *in situ* prepared solutions of **11** in a 3 : 1 methylcyclopentane:hexanes mixture at −30 °C for two weeks. In contrast to the bimetallic complexes, the six-coordinate uranium centre sits above the central ligand arene with the four aryloxide ligands occupying the equatorial plane and the trityl protons pointing away from the uranium centre (Figure 3.2). There is a vacant position *trans* to the arene ligand, where unaccounted electron density resides (Q1 = 20.86, Q2 = 15.33 eÅ^{-3}), suggesting the presence of an unidentified ligand and the identity of the crystallographically characterised material to be [U(L)(pTP)] (**12**). The ligand aryloxide U−O distances of 2.184(7) and 2.171(7) Å are longer than those in the bimetallic complexes **2**, **4** and **9** but are still consistent with a U(IV) centre.[12–14] The U$\cdots$arene$_{Ct}$ distance is 2.5431(5) Å.

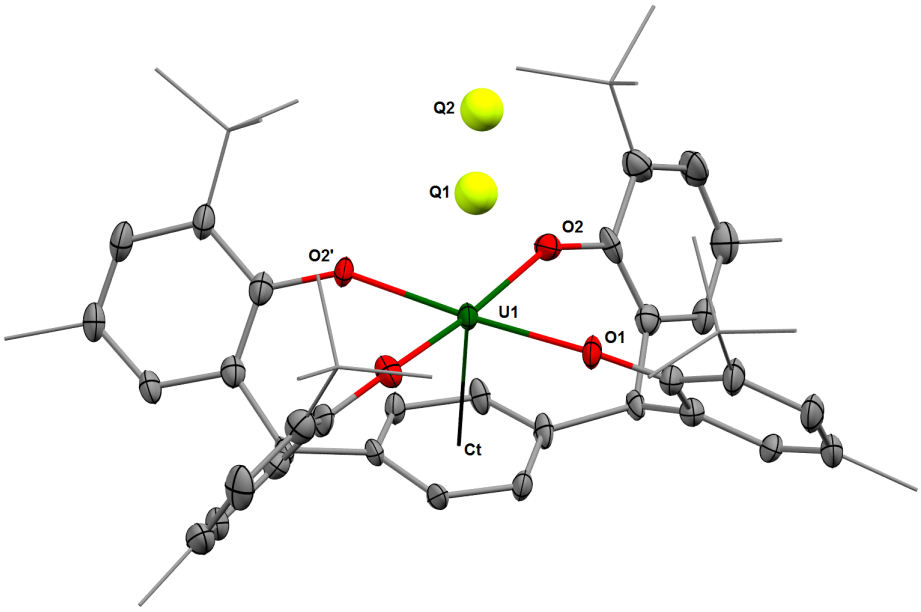

Figure 3.2 – Solid-state structure of **12** · C_6H_{14}. The aryloxide methyl and *tert*-butyl group carbon atoms are depicted as wireframe for clarity. The hydrogen atoms and lattice solvent molecules are omitted for clarity. The two largest Q peaks are depicted as yellow spheres. The thermal ellipsoids are displayed at 50% probability. Selected bond distances and angles can be found in Table 3.3.

The U−Q1 distance of 2.64369(5) Å is comparable (2.64 ± 0.01) to that of U−N bond distances to neutral donors (pyridine, pyrazole, trialkylamine or nitrile) or delocalised O donors (μ-O, carboxylate). The Q−Q distance of 1.64604(4) Å is comparable (1.65 ± 0.01) to O−E distances (E = Si, P, As, Se, V, Cr). The U−Q1−Q2 angle is 180.00(1)°. A possible ligand is the homodiatomic molecule N_2 which was plentiful during crystallisation and is known to form terminal end-on bound complexes with low-coordinate transition-metal complexes.[15] Typically, reported examples of uranium dinitrogen complexes are side-on bound bridging complexes with a [U(μ-η^1:η^2-N_2^{2-})U] core,[9,16–18] with the exception of two complexes: the monometallic complex (U(C_5Me_5)$_3$(N_2) with a labile N_2 ligand which dissociates at pressures below 80 psi reported by Evans and co-workers, and the heterobimetallic complex [{dmpN(*t*Bu)}$_3$U(μ-N_2)Mo{dmpN(R)$_3$}]) (dmp = dimethylphenyl, R = *t*Bu, Ad) reported by Cummins and co-workers.[19,20] The U−Q1 distance of 2.64369(5) Å is comparable to the U−N distance in these complexes (2.49(1) and 2.24(2) Å respectively) however, the long Q−Q distance differs significantly to the N−N distance in the complexes (1.64604(4) *versus* 1.12(1) and 1.23(2) Å respectively). Additionally, assigning the Q peaks to *N* atoms resulted in unstable

refinement. It is worth noting that speculations on the nature of the unindentified ligand based on the U−Q distances are not necessarily reliable.

3.2.1 Synthesis and characterisation of [U(OH$_2$)(pTP)]

On one occasion, the supernatant from the preparation of **11** in hexanes was isolated and redissolved in C_6D_6 after removal of volatiles under reduced pressure. The ^{1}H NMR spectrum is paramagnetic and spans 50 ppm, consistent with a uranium(IV) centre, and contains six sharp resonances corresponding to a fully symmetric ligand environment; two singlets around 15 ppm can be ascribed to the two aryloxide aromatic protons, two singlets at 6.5 and 1.9 ppm to the methyl and *tert*-butyl group *H* atoms, a singlet at −12.4 for the benzylic *H* atoms and a low frequency singlet at −27 ppm for the ligand arene bridge. No additional resonances could be detected, suggesting the compound in solution to be **11**.

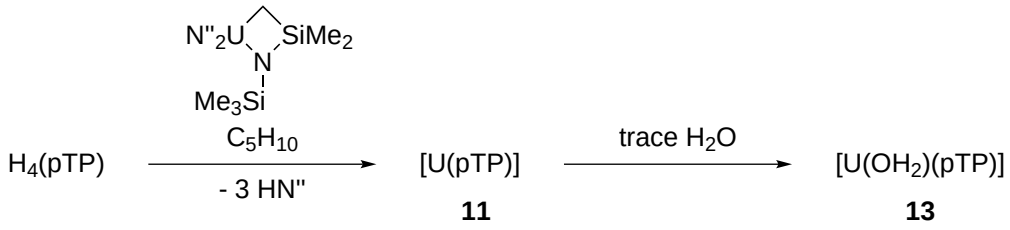

Scheme 3.3 – Synthesis of **13**.

Red crystals were obtained from C_6D_6 solution suitable for single-crystal XRD analysis, which revealed the compound to be [U(OH$_2$)(pTP)] (**13**). In the structure, the uranium centre has an arene interaction with the central ligand arene and the water ligand is *trans* to the arene (Figure 3.3). The aryloxide U−O distances which range from 2.162(2) Å to 2.192(2) Å and the U$\cdots$arene$_{Ct}$ distance of 2.5410(2) Å are comparable to those in **12**. The U−O distance of the axial ligand is longer at 2.579(3) Å, suggesting a lower U−O bond order for the axial ligand. The U−O distance is consistent with that of a U−O dative bond and is consistent with other uranium(IV) hydrates.[21,22] Furthermore, density was found in the difference Fourier map attributable to three hydrogen atoms, consistent with a rotationally disordered water ligand. The three hydrogen atom positions were refined with constraints (equal O−H and H−H distances within a standard uncertainty of 0.02 Å, and sum of occupancy of hydrogen atoms equal to two).

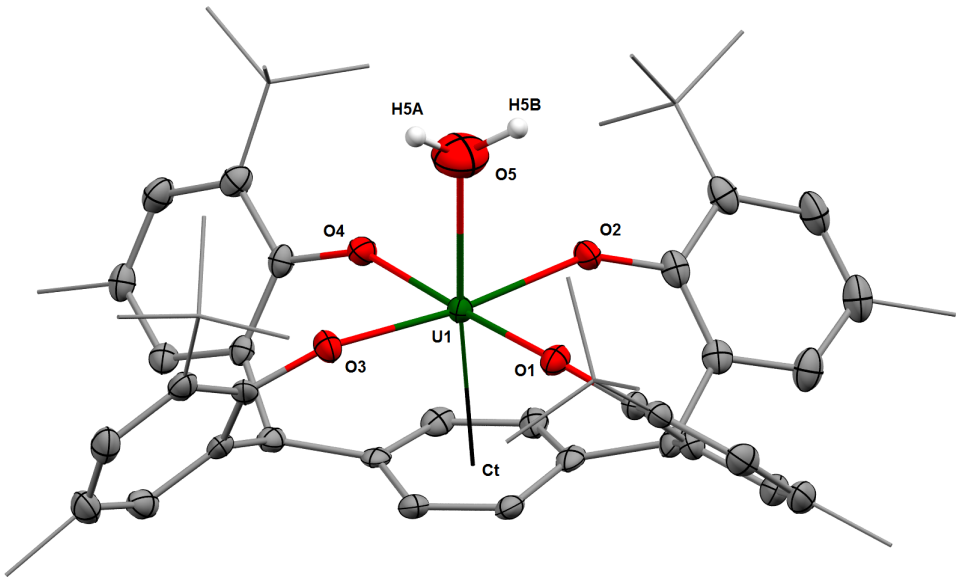

Figure 3.3 – Solid-state structure of **13** · 3(C_6H_6). The aryloxide methyl and *tert*-butyl group carbon atoms are depicted as wireframe for clarity. The hydrogen atoms, with the exception of those on the water ligand, and lattice solvent molecules are omitted for clarity. The thermal ellipsoids are displayed at 50% probability. Selected bond distances and angles can be found in Table 3.3.

Meyer and co-workers have recently reported the electrocatalytic production of H_2 from water by a uranium (III) monoarene complex, which they postulate proceeds *via* a uranium(III) water adduct.[23] During their investigations they isolated and crystallographically characterised a hydroxo uranium(IV) monoarene complex, [U(OH){(^{Ad}ArO)$_3$Mes}], which bears resemblance to **13**. The U···arene$_{Ct}$ distance is longer than in **13** at 2.703 Å compared to 2.5410(2) Å, while the U−O distance of the *trans* ligand is shorter than in **13** at 2.106(2) Å compared to 2.579(3) Å, providing further evidence for a neutral donor in **13**. The structural similarity between the complexes in Meyer's report and **13** suggest that the electrochemical properties of **13** could be of interest if a rational synthetic route to obtain preparative quantities of **13** can be found.

3.3 Synthesis of base stabilised uranium monoarene complexes, [U(L)(pTP)]

The serendipitous synthesis of compound **13** fostered the hypothesis that a mononuclear uranium complex of the arene-bridged tetra(aryloxide) ligand could be stabilised by coordination of a Lewis base to the vacant uranium coordination site *trans* to the uranium-arene interaction. To

this end, the controlled addition of a stoichiometric amount of a variety of Lewis bases to an *in situ* generated solution of **11**, as prepared in Section 3.2, was investigated.

3.3.1 Synthesis and characterisation of [U(CNXyl)(pTP)]

Isonitriles are strong σ donors that are isoelectronic with carbon monoxide and, as such, have been used to model the reactivity of organoactinide complexes with CO.[24–26] XylNC was added to a dark green-brown benzene solution of **11** prepared *in situ* in the presence of C_6Me_6 and allowed to stir at room for two hours. The ^{1}H NMR spectrum contained new resonances corresponding to a monomeric complex in agreement with the formulation [U(CNXyl)(pTP)] (**14**), which integrated to approximately 20% with respect to internal standard (C_6Me_6). The yield increase from 10% to 20% (*cf.* Section 3.2) after addition of a donor suggests that there is material in the ^{1}H NMR spectrum which is unaccounted for by the sharp resonances. This could be because the broad resonances in the ^{1}H NMR spectrum correspond to an oligomer of **11** ($[U(pTP)]_n$). Solutions of **11** prepared *in situ* may best be described a 1 : 9 [U(pTP)]:$[U(pTP)]_n$ solutions.

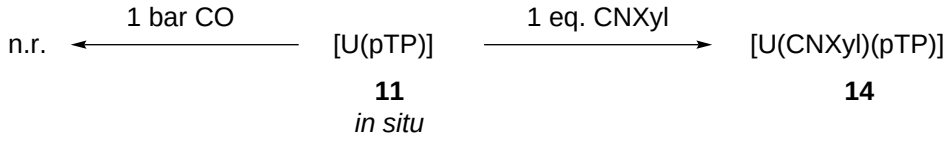

Scheme 3.4 – Synthesis of **14**.

The ^{1}H NMR spectrum possesses resonances from −30 to 16 ppm, and is in accordance with a single symmetric ligand environment with a C_2 rotational axis on the NMR timescale. The ligand *H* atoms resonate at comparable frequencies to those of **13**. The aromatic *H* atom resonances for the isocyanide ligand could not be located in the range −100 to 100 ppm, however a resonance at −11 ppm could be attributed to the xylyl group methyl group *H* atoms.

Orange crystals of **14** were obtained from slow diffusion of hexanes into a concentrated benzene solution of **14**. The uranium centre in **14** exhibits a distorted octahedral geometry in which the aryloxide ligands occupy the equatorial plane, while the ligand arene bridge and isocyanide ligand occupy the axial positions (Figure 3.4). The aryloxide U−O bond distances which range from 2.156(3) to 2.196(3) Å and the U$\cdots$arene$_{Ct}$ distance of 2.5490(2) Å compare well to those found for **12** and **13**. The isonitrile U−C distance of 2.690(4) Å is long when compared to other linear coordinated uranium(IV) isocyanides which range 2.58(1) to 2.675(3) Å.[27–29] Bond angles and distances are discussed further in Section 3.7 (*vide infra*).

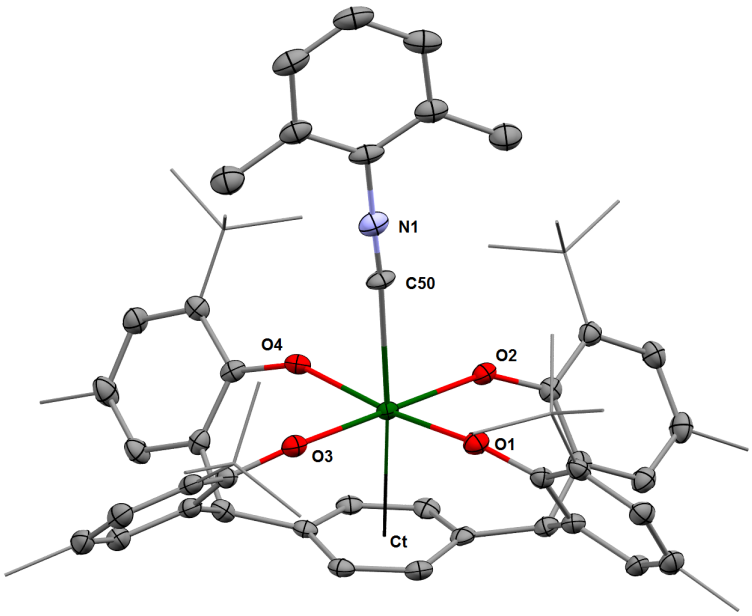

Figure 3.4 – Solid-state structure of **14** · 5(C_6H_6). The aryloxide methyl and *tert*-butyl group carbon atoms are depicted as wireframe for clarity. The hydrogen atoms and lattice solvent molecules are omitted for clarity. The thermal ellipsoids are displayed at 50% probability. Selected bond distances and angles can be found in Table 3.3.

3.3.2 Targeted synthesis of [U(CO)(pTP)]

Due to poor orbital overlap between the actinide centred orbitals and the soft π donating carbon monoxide ligand, actinide carbonyl complexes are sparse in the literature with only two structurally characterised uranium(III) molecular CO complexes so far, [U(C_5Me_5)$_3$CO] and [U(C_5Me_4H)$_3$CO]. Recently, the cationic thorium(IV) complex [Th(C_5Me_5)$_3$CO]BPh_4 was reported, which suggests that the softer trivalent oxidation state is not necessarily required to form thorium carbonyl complexes.[30–32] All three examples use extremely bulky ligands An(C_5Me_4R)$_3$ (R = Me, H) which efficiently shield the metal centre leaving a vacant coordination site accessible only to small molecules. As discussed previously, isocyanides have been used to model CO reactivity, and with a uranium isocyanide adduct in hand, the synthesis of a uranium carbonyl was investigated.

A degassed green-brown cyclopentane solution of **11** was exposed to 1 bar of CO, however no reaction was observed as suggested by ^{1}H NMR spectroscopy. Allowing the sample to reflux at 80 °C for 48 hours did not result in a change in the ^{1}H NMR spectrum.

3.3.3 Targeted synthesis of [U(pTP)(κ−OC)Cr(CO)$_2$(C$_6$H$_5$OMe)]

Arnold *et al.* have demonstrated that [U(Odtbp)$_3$] reacts with [(C$_6$H$_5$OMe)Cr(CO)$_3$] to form the adduct [U(Odtbp)$_3$(κ−OC)Cr(CO)$_2$(C$_6$H$_5$OMe)].[33] The suitability of a transition-metal carbonyl as a ligand for **11** was investigated.

A yellow-green suspension of [(C$_6$H$_5$OMe)Cr(CO)$_3$] in cyclopentane was added to a dark green-brown cyclopentane solution of **11**. THF was added to help solubilise the chromium complex. Orange plates were obtained suitable for XRD analysis, revealing the complex to be the THF adduct [U(thf)(pTP)] (**15**, Figure 3.5). The octahedral uranium centre sits atop the arene bridge with a U···arene$_{Ct}$ distance of 2.5729(3) Å. The aryloxide U−O bond distances are comparable to other complexes discussed in this chapter ranging from 2.174(6) to 2.193(6) Å, while the longer U−O distance of 2.437(8) Å for the THF ligand is consistent with U−O dative bond. The THF ligand is slightly tilted towards one of the ligand bis(aryloxide) pockets, with an U−O−arene$_{Ct}$ angle of 168.5(2)°. This is further denoted by the wide O1−U−O2 angle of 84.6(2)° for the bis(aryloxide) pocket towards which the THF tilts, compared with 78.0(2)° for the other pocket.

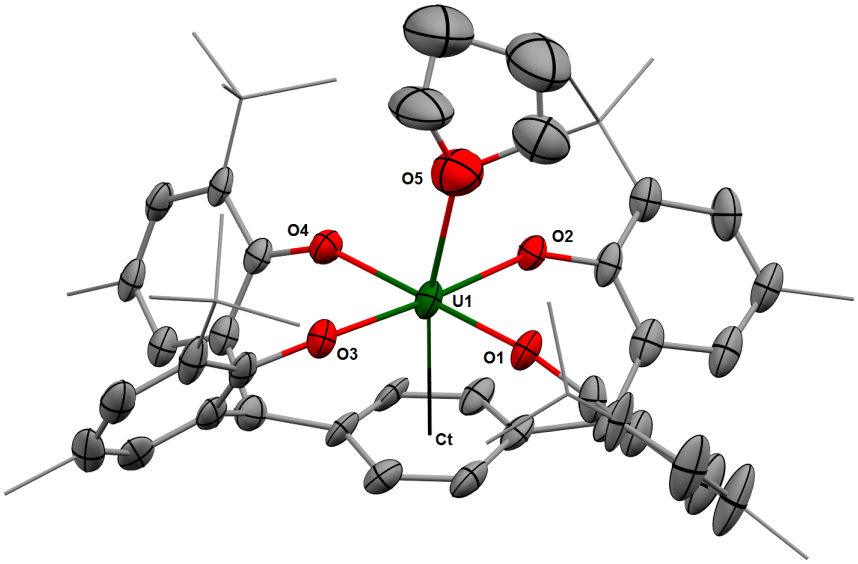

Figure 3.5 – Solid-state structure of **15**. The aryloxide methyl and *tert*-butyl group carbon atoms are depicted as wireframe for clarity. The hydrogen atoms and lattice solvent molecules are omitted for clarity. The thermal ellipsoids are displayed at 50% probability. Selected bond distances and angles can be found in Table 3.3.

The paramagnetic ^{1}H NMR spectrum of **15** in C$_6$D$_6$ spans 40 ppm with resonances com-

parable to those of **12**, **13** and **14**. The THF ligand resonances could not be detected at 300 K, possibly due to paramagnetic line broadening. Resonances corresponding to non-bound THF could not be detected, which suggests that the THF ligand remains bound to the uranium centre in benzene solution.

Insufficient material was obtained to fully characterise **15**. However, its potential as a useful starting material for the synthesis of further uranium monoarene complexes led to the investigation into a rational synthetic route to **15**. Addition of a single equivalent of THF to a cyclopentane solution of **11** provided a pale brown suspension after 18 hours of stirring. Upon crystallisation, the trimeric complex **10** was obtained rather than monomeric **15**.

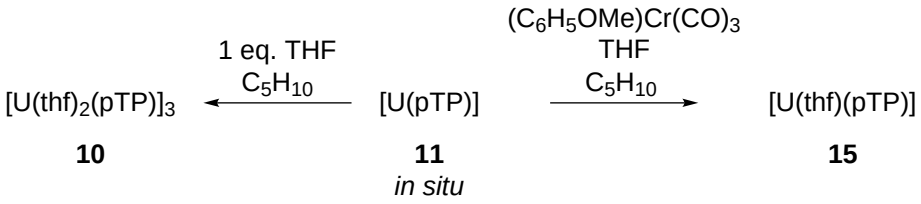

Scheme 3.5 – Synthesis of **15**.

While the targeted transition-metal carbonyl adduct [U(pTP)(κ−OC)Cr(CO)$_2$(C$_6$H$_5$OMe)] was not isolated, its synthesis may be achieved by carrying out the reaction in a non-coordinating solvent in which both reactants are soluble.

3.4 Alternative routes to uranium monoarene complexes

While HN$''$ is a volatile by-product, it can often be hard to remove completely, due to its high boiling point (127 °C) and weak donor capabilities, which can be problematic as residual amounts can react with Brønsted bases or reducing agents. Bart and co-workers have recently reported the synthesis of tetrabenzyl uranium, UBn$_4$, which can be used in protonolysis reactions *via* toluene elimination. Refluxing solutions of H$_4$(pTP) and UBn$_4$ in C$_6$D$_6$ for 18 hours provided brown solutions containing several sharp resonances. Addition of cesium to the reaction mixture followed by sonication results in consumption of the yellow metal and deposition of a dark brown powder, **16**.

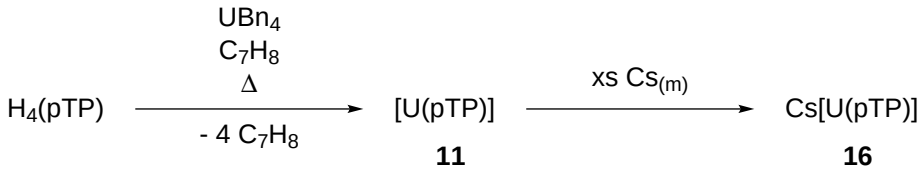

Scheme 3.6 – Synthesis of **16**.

Redissolving **16** in THF-d_8 produced a dark brown solution, the ^{1}H NMR spectrum of which spans 40 ppm and contains sharp resonances which bear resemblance to the spectra of complexes **13**, **14**, **15**; two sharp singlets at 21.7 and 13.5 ppm and a broad singlet at -18.2 ppm of equivalent integration (4H), and two larger singlets at 6.8 and -5.5 ppm (12H and 36H respectively). The uranium centre in **16** is likely to be in a similar coordination environment to those in **13**, **14**, **15**, as suggested by a spectrum containing five resonances consistent with a symmetrical ligand environment. The difference in chemical shift of the ligand $H-$atoms may indicate a different oxidation state at uranium in **16** compared to **13**, **14**, **15** but further investigations are required to validate this hypothesis. The powder **16** was tentatively assigned as the uranium(III) anion, Cs[U(pTP)]. Despite our best efforts, crystals suitable for single-crystal XRD could not be obtained to authenticate **16**.

3.5 Synthesis of thorium monoarene complexes [Th(L)(pTP)]

As previously discussed in Section 1.2.2, thorium-arene interactions are rare with a handful of reported examples from the Gambarotta and Emslie groups, and our group. The complexes reported by Gambarotta and Emslie feature a charged thorium centre, the anionic Li[(NArN)ThCl$_3$] and cationic complexes [(NON)Th(Bn)(η^6-C$_6$H$_5$Me)], [(NON)Th(CH$_2$SiMe$_3$)(η^6-C$_6$H$_6$)] and the bimetallic compex [(NNN)Th(Bn)($\mu\eta^6\kappa^1$-BnTh(Bn)(NNN)].[34,35] Neutral thorium arene complexes are rarer with two reported examples thus far, [(NON)Th(η^6-C$_6$H$_5$CH$_2$B(C$_6$F$_5$)$_3$)$_2$] synthesised by Emslie and co-workers, and Th(O$^{\text{Ter}}$Mes)$_2$(BH$_4$)$_2$ synthesised in our group which employs a bulky terphenolate ligand.[36,37]

With the ligands apparent propensity to form uranium-arene interactions under conditions put forward in Section 3.2, the use of this ligand as a platform to probe thorium-arene interactions was investigated.

3.5.1 Synthesis and characterisation of [Th(CNXyl)(pTP)]

An *in situ* generated deep purple solution of [Th(pTP)] (**17**) in cyclopentane was treated with

one equivalent of XylNC and allowed to stir for 18 hours to produce an off-white suspension. Analytically pure [Th(CNXyl)(pTP)] (**18**) was isolated as an off-white solid in 65% yield by filtration and recrystallised from slow diffusion of hexanes into a benzene solution of **18** in 35% yield . Compound **18** was characterised by XRD, NMR spectroscopy and elemental analysis.

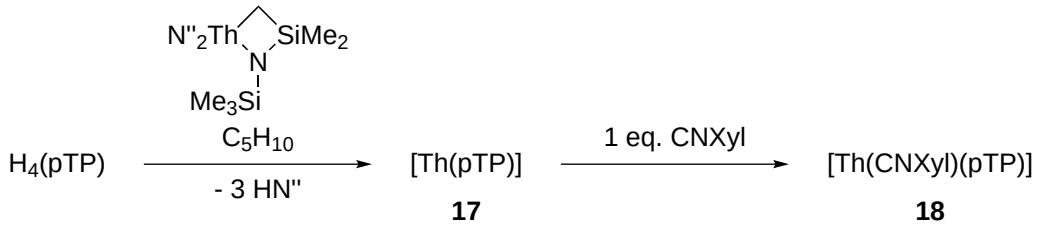

Scheme 3.7 – Synthesis of **18** by reaction of *in situ* prepared **17** with CNXyl.

The ^{1}H NMR spectrum of **18** is diamagnetic and exhibits the correct multiplicity and integrals for the tetra-aryloxide ligand, as well as resonances which can be ascribed to the isonitrile ligand: a broad singlet at 2.10 ppm integrating to six protons, which corresponds to the $o-C\mathbf{H}_3$ protons, and two resonances corresponding to the phenyl ring protons at 6.61 and 6.51 ppm (t, J = 7.7 Hz, 1H, p-$C_6H_3Me_2$; d, J = 7.7 Hz, 2H, m-$C_6H_3Me_2$). The complex is sparingly soluble in cycloalkanes and readily soluble in aromatic solvents, in which it is stable at 85 °C for 18 hours with no signs of decomposition. The compound is also soluble in THF at room temperature, only showing signs of decomposition after prolonged heating, as determined by ^{1}H NMR spectroscopy, suggesting that excessive THF does not displace the isonitrile ligand at room temperature.

Crystalline material suitable for single-crystal XRD analysis was obtained from slow diffusion of hexanes into benzene solutions of **18**. The six-coordinate thorium centre is in distorted octahedral geometry with the platform ligand aryloxides occupying the equatorial positions and the isocyanide and ligand arenes in the axial plane with a near linear C−Th−arene$_{Ct}$ angle of 175.46(6)° (Figure 3.6). The Th−O bond distances which range from 2.220(2) to 2.232(3) Å are longer than those exhibited by the bimetallic thorium complexes of the same ligand (**3** and **7**, Chapter 2) but comparable to other crystallographically characterised Th(IV) aryloxide complexes.[38–41] The Th$\cdots$arene$_{Ct}$ distance is much shorter than those in reported thorium arene complexes (2.63856(5) Å *versus* 2.701(8) − 2.95Å).[34–36,41] The isonitrile Th−C distance of 2.783(3) Å is longer than the three other examples of linear coordinated thorium isonitriles, [Th(COT)$_2$(CN^{t}Bu)] and [Th(C$_5$Me$_5$)$_2$(η^2-^{t}BuNCEtipp)(CN^{t}Bu) (E = P, As).[26,42]

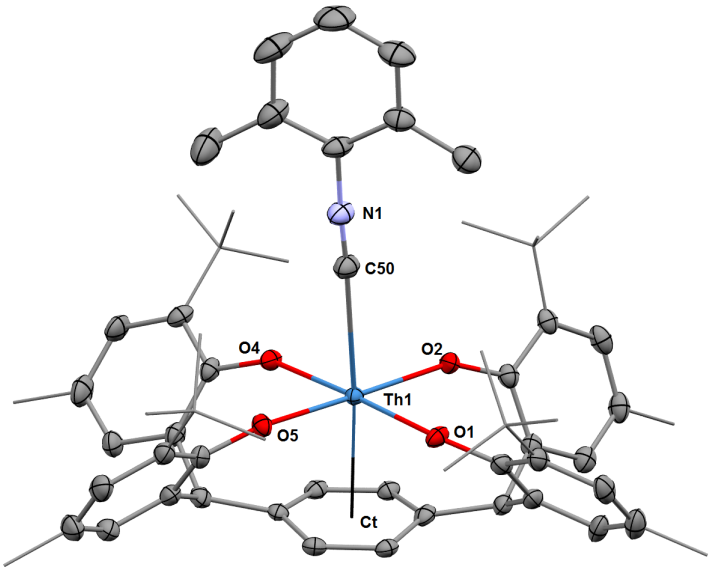

Figure 3.6 – Solid-state structure of **18** · $(2(C_6H_6)_0 \cdot 5(C_6H_{14})$. The aryloxide methyl and *tert*-butyl group carbon atoms are depicted as wireframe for clarity. The hydrogen atoms and lattice solvent molecules are omitted for clarity. The thermal ellipsoids are displayed at 50% probability. Selected bond distances and angles can be found in Table 3.3.

Reaction with excess XylNC

Exposing *in situ* generated **17** to two equivalents of XylNC in cyclopentane leads to the precipitation of **18**. When the reaction is carried out in aromatic solvent, a complex mixture of products is obtained (as determined by ^{1}H NMR spectroscopy) which includes resonances for **18** (major), free CNXyl and unidentified products (minor).

3.5.2 Synthesis of [Th(thf)(pTP)]

One equivalent of THF was added to an *in situ* generated deep purple solution of **17** in cyclopentane and allowed to stir for 18 hours, which produced a thick colourless suspension. The complex [Th(thf)(pTP)] (**19**) was isolated as an off-white solid in 70% yield by filtration and recrystallised from diffusion of hexanes into concentrated benzene or cyclopentane solutions of **19**. Compound **19** was characterised as the THF adduct by XRD, NMR spectroscopy and elemental analysis.

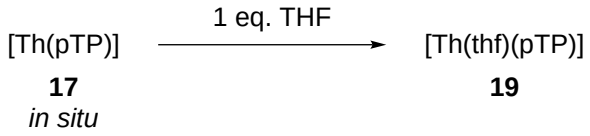

Scheme 3.8 – Synthesis of **19**.

The complex is partially soluble in cycloalkane solvent, and readily soluble in aromatic solvents and ethers. Remarkably, the complex retains its monomeric structure in neat THF solution even after reflux for 18 hours, suggesting the monomer is the thermodynamic sink for thorium. The thorium-bound THF ligand seems to exchange with the deuterated solvent, as suggested by the lack of contact-shifted THF resonances and the emergence of under-integrating *protio* THF resonances in the spectrum at 3.65 and 1.81 ppm. This could be confirmed by EXSY NMR spectroscopy. Yellow needles suitable for single-crystal XRD analysis were grown from diffusion of hexanes into a benzene or cyclopentane solution of **19**. The compound crystallises from benzene in the orthogonal space group *Ibam*, with the asymmetric unit comprising half a molecule of **19** symmetrically related by a C_2 rotation about the O5−Th−arene$_{Ct}$ axis along with two benzene solvent molecules (Figure 3.7). From cyclopentane, it crystallises in the monoclinic space group $P2_1/n$ with the asymmetric unit consisting of one molecule of **19** and two cyclopentane lattice solvent molecules (Figure 3.8). In both structures, the octahedral thorium centre is coordinated by the four aryloxides in the equatorial plane with the arene and THF molecule occupying the axial positions. The apical THF molecule in both complexes is slightly tilted towards one of the bis(aryloxide) pockets, evidenced by the the O5−Th−arene$_{Ct}$ angles of 169.2(3) and 171.2(1) for **19** $\cdot$ 2(C_6H_6) and **19** $\cdot$ 2(C_5H_{10}) respectively. The bond metrics are very similar in both complexes with the exception of the O1−Th−O2 angle which is larger in **19** $\cdot$ 2(C_6H_6) (85.2(3)° *versus* 81.9(1)°) due to inclusion of a benzene solvent molecule into the bis(aryloxide) pocket. Selected bond distances for **19** $\cdot$ 2(C_6H_6) and **19** $\cdot$ 2(C_5H_{10}) can be found in Table 3.1.

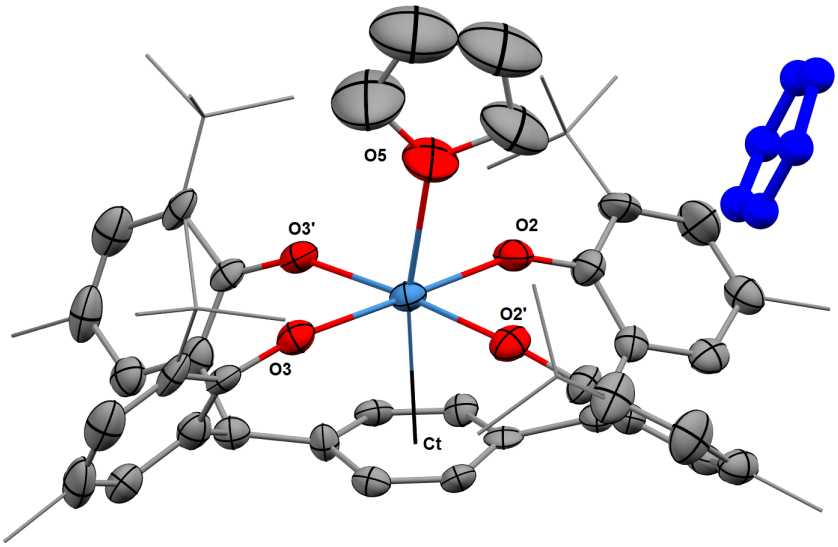

Figure 3.7 – Solid-state structure of **19** · 2(C_6H_6). The aryloxide methyl and *tert*-butyl group carbon atoms are depicted as wireframe for clarity. The hydrogen atoms and lattice solvent molecules are omitted, with the exception of one benzene molecule which is depicted in blue ball and stick model, for clarity. The thermal ellipsoids are displayed at 50% probability. Selected bond distances and angles can be found in Table 3.3.

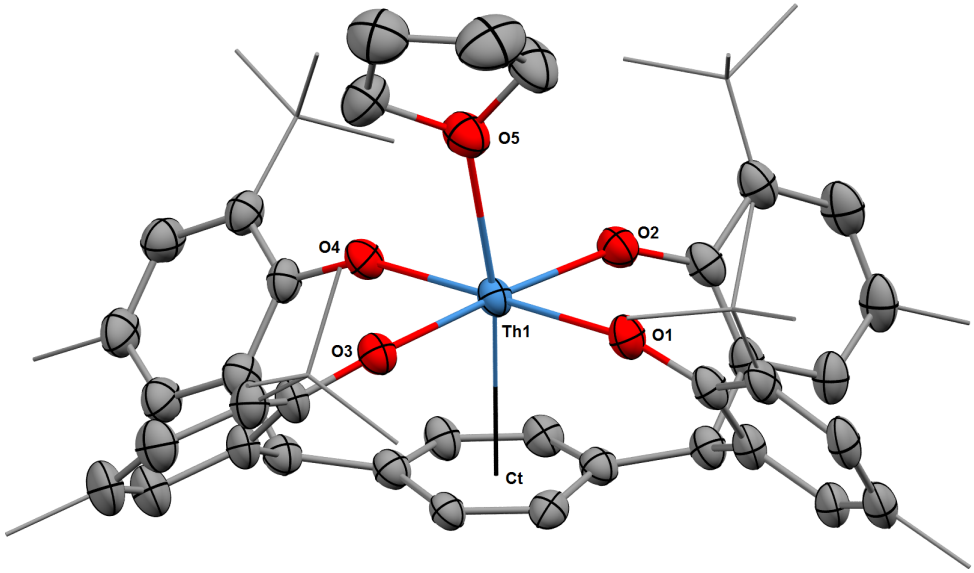

Figure 3.8 – Solid-state structure of **19** · 2(C_5H_{10}). The aryloxide methyl and *tert*-butyl group carbon atoms are depicted as wireframe for clarity. The hydrogen atoms and lattice solvent molecules are omitted for clarity. The thermal ellipsoids are displayed at 50% probability. Selected bond distances and angles can be found in Table 3.3.

Table 3.1 – Selected bond lengths (Å and angles (°) for **19** · 2(C_6H_6) and **19** · 2(C_5H_{10}).

Parameter	**19** · 2(C_6H_6)	**19** · 2(C_5H_{10})
Th−O1	-	2.235(4)
Th−O2	2.238(5)	2.236(4)
Th−O3	2.236(5)	2.248(4)
Th−O4	-	2.239(4)
Th−O5	2.470(9)	2.480(5)
Th···arene$_{Ct}$	2.6428(3)	2.6354(2)
O1−Th−O2	85.2(3)	81.9(1)
O3−Th−O4	76.4(3)	77.2(2)
O5−Th−arene$_{Ct}$	169.2(3)	171.2(1)

3.5.3 Synthesis of [Th(N_3SiMe_3)(pTP)]

Two equivalents of Me_3SiN_3 were added to an *in situ* generated deep purple solution of **17** in cyclohexane. Allowing the reaction to stir for 18 hours yielded a green-blue suspension from which colourless [Th(N_3SiMe_3)(pTP)] (**20**) was isolated in 20% yield and recrystallised from slow diffusion of hexanes into a concentrated benzene solution of **20**. The formulation of **20** as the trimethylsilyl azide adduct was determined by XRD, NMR spectroscopy and elemental analysis.

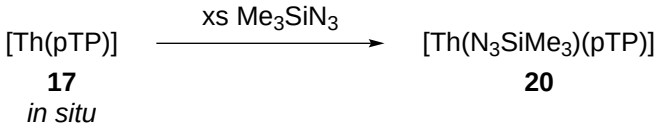

Scheme 3.9 – Synthesis of **20**.

The ^{1}H NMR spectrum of **20** contains resonances corresponding to the tetra-aryloxide ligand with the correct multiplicity and relative integrals, with chemical shifts comparable to other thorium complexes described in this chapter. In addition, a new resonance at −0.10 ppm integrating as nine protons can be ascribed as the $SiMe_3$ group of the coordinated azide. No resonance could be located in the ^{29}Si NMR spectrum within the normal spectroscopic window at room temperature. Benzene solutions of **20** were found to turn blue after two hours of reflux, however no new resonances evidencing decomposition could be detected in the ^{1}H

NMR spectrum of a sample heated to reflux for 18 hours. Additionally, solutions of **20** were observed to turn blue after a period of weeks at room temperature.

Yellow blocks suitable for single-crystal XRD were grown from slow diffusion of hexanes into a benzene solution of **20**. As seen in related compounds covered in this chapter, the six-coordinate thorium centre exhibits distorted octahedral geometry with the axial positions occupied by the trimethylsilyl azide ligand and platform ligand arene, while the aryloxide ligands occupy the equatorial plane (Figure 3.9). The aryloxide Th−O distances which range 2.210(3) to 2.241(3) Å are comparable to related complexes while the thorium$\cdots$arene$_{Ct}$ distance of 2.6198(2) Å is the shortest among related complexes in this chapter. The N−Th−arene$_{Ct}$ angle is *quasi*-linear at 178.90(8)° and the thorium-azide distance is within range of the very rare examples of metal organoazide complexes at 2.599(3) Å. The azide N_3 unit is very close to linear with an angle of 175.6(4)°, while the N−N−Si angle is 123.9(3)°. The N−N bond distances are very short at 1.190(5) and 1.151(4) Å and are, along with the linear azide unit and long Th−N distance, consistent with an electronically unperturbed azide.

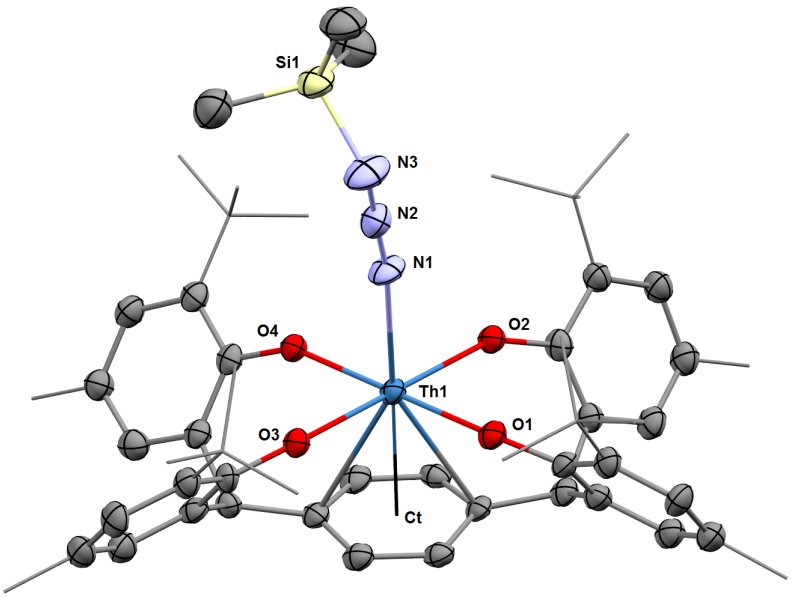

Figure 3.9 – Solid-state structure of **20** · 2(C_5H_{10}). The aryloxide methyl and *tert*-butyl group carbon atoms are depicted as wireframe for clarity. The hydrogen atoms and lattice solvent molecules are omitted for clarity. The thermal ellipsoids are displayed at 50% probability. Selected bond distances and angles can be found in Table 3.3.

Examples of metal organoazide complexes are rare throughout the periodic table. Only four examples have been structurally characterised (Figure 3.10) and they are all group V metal

complexes.[43–46] Three of the examples exhibit short M−N bonds and non-linear azide units, consistent with multiple M−N bond character. The example reported by J. Arnold (Figure 3.10, A4, bottom right) is most comparable with **20**,[46] with a linear azide unit and a comparable M−N bond accounting for the difference in covalent radii (Table 3.2).

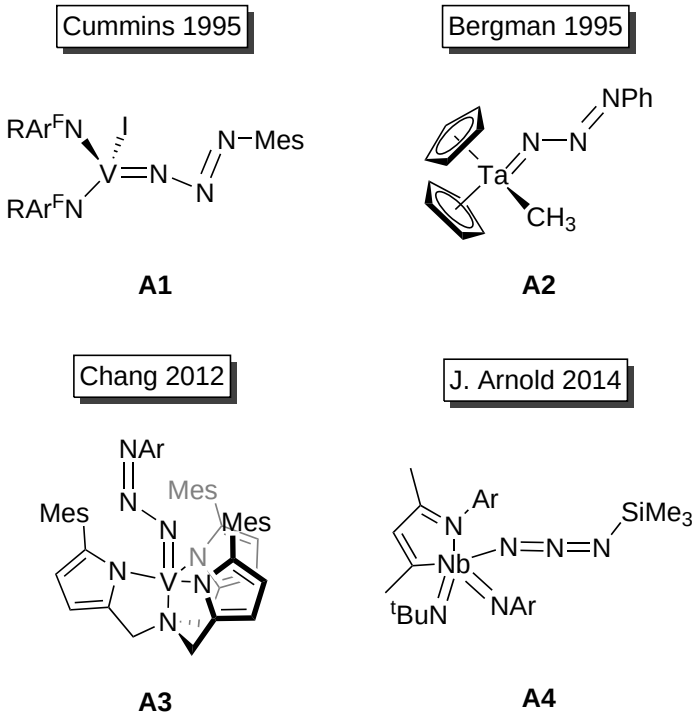

Figure 3.10 – Structurally characterised organoazide complexes as reported by the Cummins, Bergman, Chang and J. Arnold groups.[43–46]

Table 3.2 – Selected bond lengths (Å and angles (°) for reported metal organoazide complexes and **20**.[a] Bond distances were normalised with respect to the radius of vanadium.

Parameter	A1	A2	A3	A4	**20**
M−N1	1.662(4)	1.84(1)	1.707(6)	2.271(3)	2.599(3)
M−N1$_{Corr}$[a]	1.662	1.66	1.707	2.119	1.930
N1−N2	1.339(5)	1.20(2)	1.25(1)	1.131(4)	1.151(4)
N2−N3	1.198(6)	1.26(2)	1.29(1)	1.208(4)	1.190(5)
N1−N2−N3	116.6(4)	108.5(2)	114.9(1)	175.0(1)	175.6(4)
N2−N3−R	118.1	103.8(2)	113.6(1)	128.5(1)	123.9(3)
M−N1−N2	169.1(4)	166(1)	170.6(5)	167.4(1)	171.3(3)

3.5.4 Synthesis and characterisation of K[Th(O-3,5-dtbp)(pTP)]

With the knowledge that a range of neutral donors could be employed to synthesise Lewis base adducts of thorium monoarene complexes, the use of charged donors was investigated. A charged donor with similar steric parameters to the neutral ligands used previously, potassium 3,5-di-*tert*-butylphenoxide (KO-3,5-dtbp) was chosen as a target ligand. A colourless suspension of KO-3,5-dtbp in cyclopentane was added to a deep purple cyclopentane solution of **17** and allowed to stir for 18 hours. Analytically pure K[Th(O-3,5-dtbp)(pTP)] (**21**) was isolated by filtration in 90% yield, with crystalline material obtained by layering hexanes onto THF solutions of **21**. The identity of **21** was confirmed as the potassium aryloxide ate-complex by XRD and NMR spectroscopy.

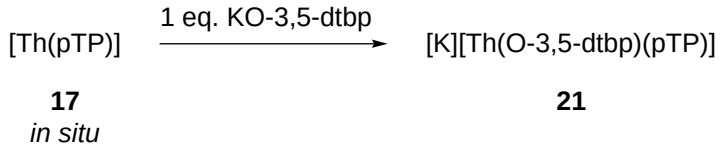

Scheme 3.10 – Synthesis of **21**.

The ^{1}H NMR spectrum of **21** in C_6D_6 spans approximately 8 ppm, which is consistent with a diamagnetic thorium(IV) complex. The spectrum contains broad resonances, from which certain characteristic peaks can be identified such as the trityl proton resonance at 5.42 ppm and the tetra-aryloxide *tert*-butyl and methyl resonances at 2.26 and 1.64 ppm respectively, in accordance with the proposed formulation. Additionally, an alkyl resonance at 1.43 ppm with a relative integration of 18 protons can be detected, suggesting that the anionic aryloxide donor is present in correct stoichiometry. Using a coordinating solvent such as THF gives rise to a sharp, well resolved spectrum in which all ligand resonances can be identified, alongside resonances which can be attributed to coordinated KO-3,5-dtbp: a singlet with an integration 18H at 1.31 ppm corresponding to the $m-C(CH_3)_3$ protons, and two resonances at 6.77 and 6.66 ppm, which can be attributed to the phenyl ring protons (d, J = 1.7 Hz, 2H, o-$C_6H_3tBu_2$; t, J = 1.7 Hz, 1H, p-$C_6H_3tBu_2$). The symmetrical ligand environment suggests that the potassium counter-ion is either fully solvated by THF and not interacting with the complex, or rapidly exchanging and the exchange cannot be detected on the NMR timescale at room temperature.

The structure of **21** was confirmed by single-crystal XRD analysis (Figure 3.11) and reveals the monodentate aryloxide to be η^1 $O-$bound to the thorium centre *trans* to the platform ligand arene in the axial plane, with the platform ligand aryloxides in the equatorial plane.

The potassium counter-ion is incorporated into a bis(aryloxide) pocket of the platform ligand, binding η^2 to both platform ligand aryloxide C−O bonds and η^1 to the axial aryloxide *O* atom, in addition to two coordinated THF molecules. This results in an unsymmetrical ligand arrangement around the thorium centre, with an elongation of the Th−O distances of the platform aryloxides which bridge the thorium and potassium centres (2.234(3) Å *versus* 2.304(3) Å). The ligand asymmetry is denoted by the ligand fold angle, measured about the carbon atom bridging the two aryloxides, which is greatly increased on the side containing the potassium counter-ion (102.2(1)° *versus* 83.4(1)°) and the non-linear O−Th−arene$_{Ct}$ angle of 172.26(8)°. The Th···arene$_{Ct}$ distance of 2.70680(4) Å is longer than in related complexes, while the axial Th−O distance of 2.214(3) Å is short when compared to related complexes with neutral donors in the axial position. The short bond length is likely to be a result of the high affinity of thorium for oxygen donors, as well as the electrostatic interaction of the charged aryloxide and the electropositive metal centre. The disruption of the thorium-arene interaction is suggestive of a *trans* influence, as a strong donor *trans* to the weak thorium-arene causes a lengthening of the bond. It is noteworthy that the XRD data were collected at 250 K, due to loss of crystallinity at lower temperature possibly due to a destructive phase transition.

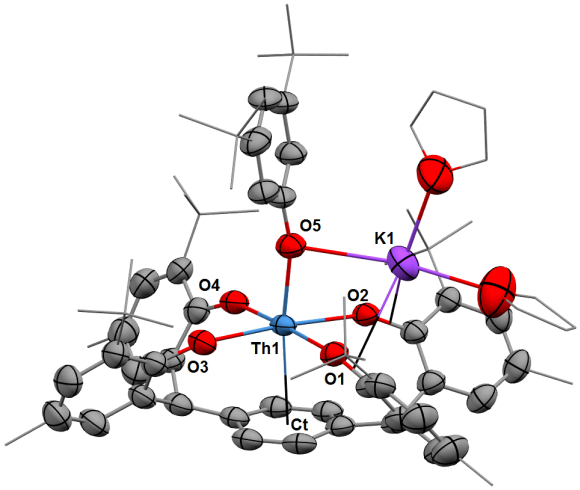

Figure 3.11 – Solid-state structure of **21**. The aryloxide methyl and *tert*-butyl group and THF carbon atoms are depicted as wireframe for clarity. The hydrogen atoms and lattice solvent molecules are omitted for clarity. The thermal ellipsoids are displayed at 50% probability. Selected bond distances and angles can be found in Table 3.3.

3.5.5 Synthesis and characterisation of K[Th(O-3,5-btfmp)(pTP)] and K_4[Th(O-3,5-btfmp)$_2$(pTP)]$_2$

With the straightforward synthesis of **21** in hand, the effect of varying the electronic properties of the donor were investigated through the use of the fluorinated analogue of KO-3,5-dtbp, potassium 3,5-bistrifluoromethylphenoxide (KO-3,5-btfmp). A purple solution of **17** in cyclopentane prepared *in situ* was treated with a cyclopentane suspension containing one equivalent of KO-3,5-btfmp and allowed to stir for 18 hours. A colourless powder was isolated by filtration from the resulting colourless suspension, which was determined to be the potassium aryloxide ate-complex K[Th(O-3,5-btfmp)(pTP)] (**22**), as confirmed by ^{1}H NMR spectroscopy and XRD.

On one occasion, a slight excess of KO-3,5-btfmp was used, which gave rise to a more complex ^{1}H NMR spectrum, consisting of a mixture of products. Upon crystallisation, it was determined that the dimeric complex K_4[Th(O-3,5-btfmp)$_2$(pTP)]$_2$ (**23**) had been synthesised. The identity of this complex was further characterised by ^{1}H NMR spectroscopy. **23** is partially soluble in arene solvents and readily soluble in THF.

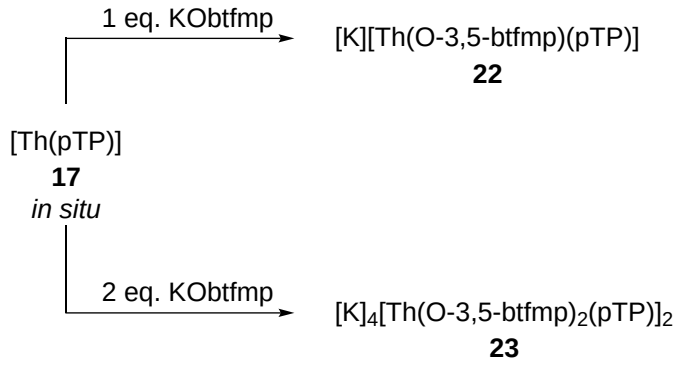

Scheme 3.11 – Synthesis of **22** and **23**.

The ^{1}H NMR spectrum of **22** in THF-d_8 spans approximately 7 ppm and possesses six resonances consistent with a single ligand environment, with the addition of two aromatic resonances corresponding to a bound KO-3,5-btfmp ligand: two singlets of integration 2H and 1H at 7.27 and 7.14 ppm. Similarly to the ^{1}H NMR spectrum of **21**, the potassium counter-ion is likely to be fully solvated by THF in solution.

The ^{1}H NMR spectrum of **23** in THF-d_8 ranges from 7.1 to 1.1 ppm and is consistent with two inequivalent ligand environments. Seven aromatic resonances corresponding to the tetra-aryloxide ligand and the fluorinated aryloxide ligands range between 7.1 to 6.7 ppm. Two singlets at 2.16 and 2.11 ppm can be attributed to the tetra-aryloxide methyl groups, while two

doublets at 1.38 and 1.15 ppm correspond to the *tert*-butyl groups.

No resonances could be detected in the ^{19}F NMR spectrum of either **22** or **23** other than free KO-3,5-btfmp.

Colourless blocks suitable for single-crystal XRD analysis were grown from diffusion of hexanes into THF solutions of **22**. The compound crystallises in the tetragonal space group $P4/nmm$ with the asymmetric unit comprising of a quarter of the molecule of **22**. The unit cell consists of a rotationally disordered molecule of **22** along the O5−Th−arene$_{Ct}$ axis, with two orthogonal molecules of **22** overlapping. Due to the challenges involved in modelling the extensive disorder in this structure, bond metrics cannot be reliably extracted. The thorium centre in the solid-state structure is six-coordinate with distorted octahedral geometry Figure 3.12. Similarly to other complexes, the thorium centre is above the ligand arene with fluorinated aryloxide in the axial position and the platform ligand aryloxides occupying the equatorial plane. The potassium counter-ion sits in a bis(aryloxide) cavity, with the same coordination motif as that of **21**.

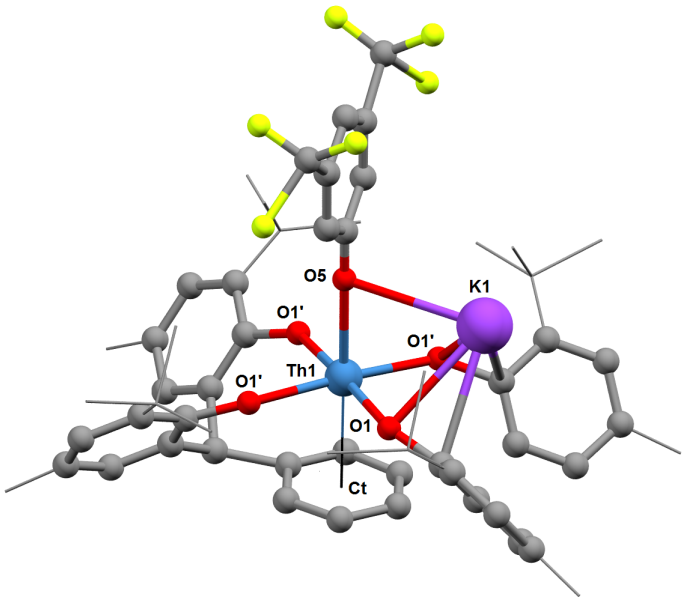

Figure 3.12 – Solid-state structure of **22**. The aryloxide methyl and *tert*-butyl group carbon atoms are depicted as wireframe for clarity. The hydrogen atoms and lattice solvent molecules are omitted for clarity.

Crystalline material suitable for single-crystal XRD analysis was obtained from diffusion of hexanes into THF solutions of **23**. The six-coordinate thorium centres in this dimeric complex have distorted octahedral geometry and are bridged by two tetra(aryloxide) ligands,

as exhibited previously by complexes **8** and **9**. Each thorium centre is coordinated to two *cis* fluorinated phenols on the equatorial plane and the platform ligand aryloxides occupy the remaining positions. The four potassium counter-ions occupy each of the platform ligand bis(aryloxide) pockets, reminiscent to the structures of **8** and **21**, by coordinating η^5 to one aryloxide aryl moiety, η^2 to an aryloxide C−O bond and two THF molecules. Each of the fluorinated aryloxides bridge an η^2 C−O coordinated potassium atom to the η^1 *O*−bound thorium centre. Unfortunately, only connectivity information can be extracted due to a technical fault during the data collection.

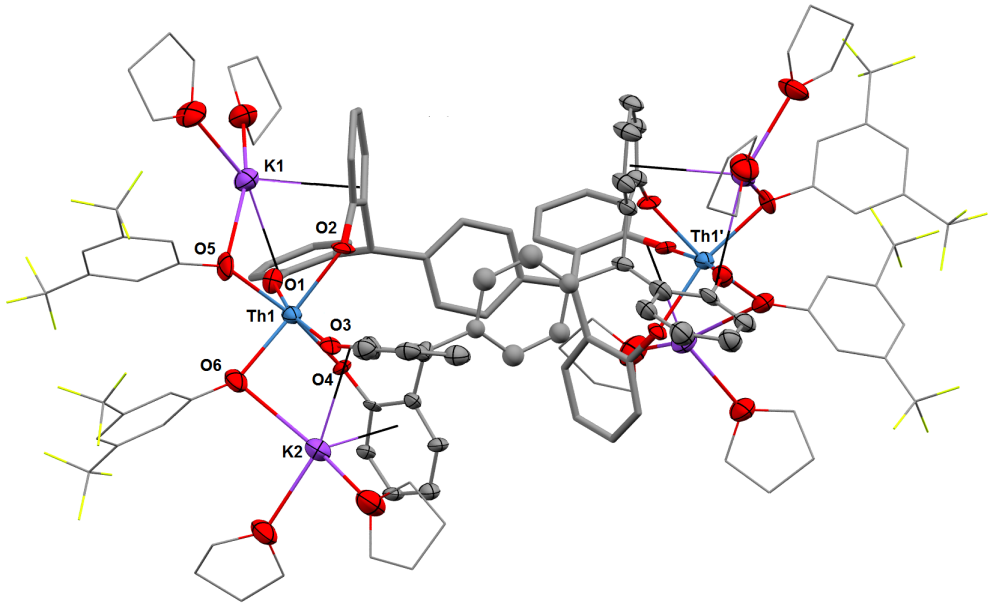

Figure 3.13 – Solid-state structure of **23** · 3 (THF). The aryloxide methyl and *tert*-butyl group and THF carbon atoms are depicted as wireframe for clarity. One of the two ligand frames is depicted as capped sticks for clarity. The hydrogen atoms and lattice solvent molecules are omitted for clarity. The thermal ellipsoids are displayed at 50% probability.

3.5.6 Targeted synthesis of K[Th(NHAr)(pTP)]

As potassium aryloxide adducts of [Th(pTP)] could be straightforwardly accessed, the viability of a potassium anilide as a Lewis base was investigated.

A suspension of KNHttbp in cyclopentane was added to a deep purple cyclopentane solution of **17** prepared *in situ* and allowed to stir for 18 hours. The light yellow suspension obtained was centrifuged and the solids redissolved in THF-d_8. The ^{1}H NMR spectrum of the solids were consistent with KNttbp, with no tetra(aryloxide) ligand resonances. Similarly, no tractable products were obtained in the reaction of **17** with 3,5-dimethylaniline.

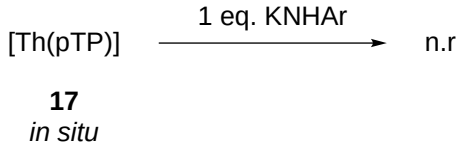

Scheme 3.12 – Targeted synthesis of a thorium anilide potassium-ate complex.

The inability of the potassium anilides to coordinate to the thorium centre may be due to the non-linearity of the anilide which has an sp^2-hybridised N donor, as opposed to the *sp* hybridised donor atoms of the other Lewis bases.

3.6 Reactions targeting monoarene complexes with other pTP ligands

3.6.1 Synthesis and characterisation of $[U(CNXyl)_2(pTP^t)]_3$

The low isolated yield of the uranium isonitrile complex **14** and the difficulty in reproducibly obtaining uranium monoarene adducts of other Lewis bases lead us to investigate whether the electronic properties of the ligand had an influence on the yield in the synthesis of uranium monoarene complexes.

The monoarene complex $[U(pTP^t)]$ (**11^t**) was prepared in a Young's NMR tube as in Section 3.2 with $H_4(pTP^t)$, and a solution of CNXyl in C_6D_6 was added. The resulting dark green solution was heated at 80 °C for 12 hours, during which time a few dark red-brown crystals were deposited on the walls of the reaction vessel. The crystalline material was suitable for single-crystal XRD analysis and was found to be consistent with the trimeric complex, $[U(CNXyl)_2(pTP^t)]_3$ (**24**).

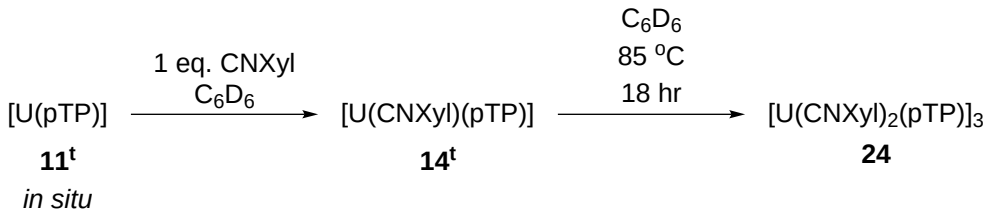

Scheme 3.13 – Synthesis of the trimeric complex **24**.

Each six-coordinate uranium centre is bound to two tetra(aryloxide) ligands, which bridge to the next uranium centre to give rise to a triangular trimeric structure (Figure 3.14). Two *cis* isonitrile ligands occupy the *exo* positions on each uranium centre, pointing away from the triangular core. There is a cavity formed within the trimer, which is inhabited by a benzene

solvent molecule. Due to poor data, the bond distances and angles cannot be discussed.

Insufficient material was obtained for full characterisation of trimeric **24**. The ^{1}H NMR spectrum of the reaction mixture before heating shows resonances corresponding to the monomeric complex [U(CNXyl)(pTP^{t})], with comparable resonances to those of **14**: two singlets corresponding to the aryloxide H atoms at 16.1 and 14.6 ppm, two singlets for the *tert*-butyl groups at 4.6 and 3.0 ppm and two singlets at −16.8 and −26.8 ppm corresponding to the benzylic and bridging arene proton resonances. Additionally, the resonnance corresponding to the xylyl methyl group $\mathbf{Me}_2C_6H_3$ *H*−atoms could be located at −10.2 ppm. After 18 hours of heating, the resonances which could be ascribed to [U(CNXyl)(pTP^{t})] are still present, along with new sharp resonances, suggesting a mixture of compounds. This mixture is likely to contain both [U(CNXyl)(pTP^{t})] and **24**.

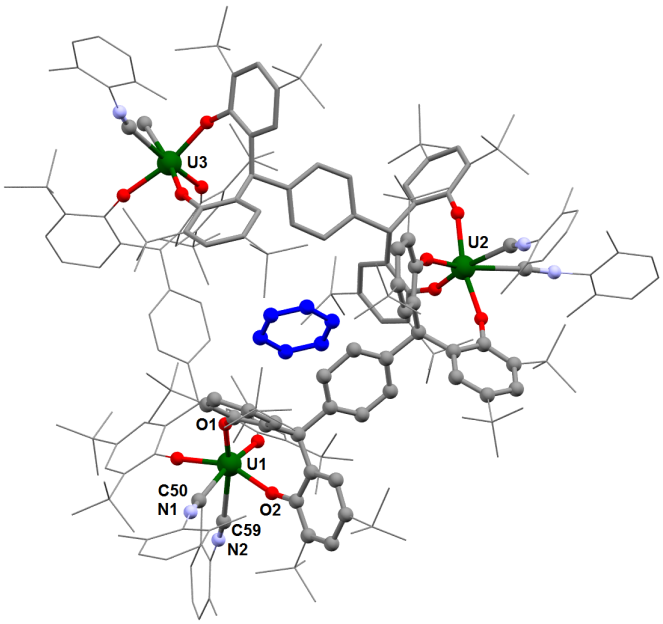

Figure 3.14 – Solid-state structure of **24** · 5 (C_6H_6). The aryloxide methyl and *tert*-butyl group and the isonitrile xylyl group carbon atoms are depicted as wireframe for clarity. Of the three ligand frames, one is depicted as capped sticks and another as wireframe for clarity. The hydrogen atoms and lattice solvent molecules are omitted, with the exception of one benzene molecule which is depicted in blue ball and stick model, for clarity. The thermal ellipsoids are displayed at 50% probability. Selected bond distances and angles can be found in Table 3.3.

3.6.2 Synthesis and characterisation of [Th(OH_2)(pTP*)]

With a straightforward and high yielding route to thorium monoarene Lewis base adducts

established, the synthesis of a base-free monoarene thorium complex of the more sterically demanding ligand H_4(pTP*) was investigated.

An off-white suspension of [Th(pTP*)] (**17***) was prepared analogously to **17** (Section 3.5.1). The colourless solid was isolated by centrifugation and redissolved in C_6H_6. A small amount of pale yellow crystals suitable for single-crystal XRD analysis consistent with [Th(OH_2)(pTP*)] (**25**) were obtained by slow diffusion of hexanes into benzene solutions of **17***.

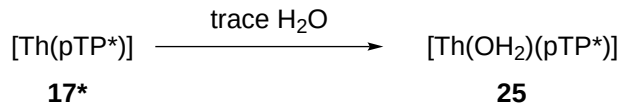

Scheme 3.14 – Synthesis of thorium hydrate complex **25**.

The six-coordinate thorium centre is in octahedral geometry, with the aryloxide ligands occupying the equatorial positions and the axial plane occupied by the ligand arene and a water ligand. Electron density was found in the difference Fourier map which was attributed to the two hydrogen atoms on the water ligand. The aryloxide Th−O distances which range 2.228(3) to 2.236(3) Å are comparably to those of related complexes described in this chapter. The long axial ligand Th−O distance of 2.594(5) Å falls within range for thorium monohydrate complexes and is consistent with a dative Th−O bond and is very similar to the U−O distance in the related uranium(IV) hydrate **13**.[47–55] The Th$\cdots$arene$_{Ct}$ distance is 2.6360(2) Å and linear O−Th−arene$_{Ct}$ of 179.4(1)° are comparable to those of other complexes discussed in this chapter. Insufficient material was obtained to fully characterise the complex.

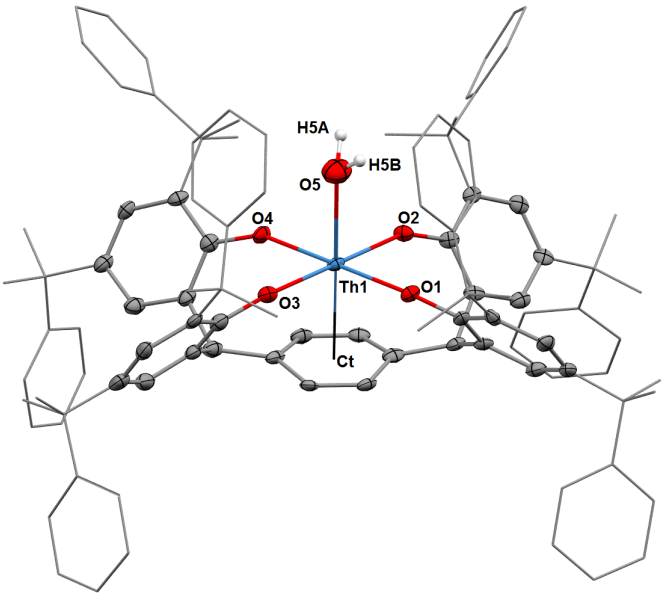

Figure 3.15 – Solid-state structure of **25** · C_6H_6. The aryloxide methyl and phenyl group carbon atoms are depicted as wireframe for clarity. The hydrogen atoms and lattice solvent molecules are omitted for clarity. The thermal ellipsoids are displayed at 50% probability. Selected bond distances and angles can be found in Table 3.3.

3.7 Structural comparison of actinide monoarene complexes, [An(L)(pTP)]

The uranium monoarene complexes **12**, **13**, **15** and **14** all feature a pseudo octahedral uranium centre in the same coordination environment. The U−O bond lengths are comparable in all four complexes ranging 2.178 – 2.184 Å, and are longer than in the complexes discussed in Chapter 2 (mean U−O 2.122(12) Å). The uranium···arene$_{Ct}$ distances are similar for all three complexes ranging 2.5410 – 2.5729 Å, and are short compared to crystallographically characterised uranium(IV) arene complexes (range 2.517 – 2.828 Å, mean 2.64(2) Å).[5,11,23,56–58] The U−L distance between the uranium centre and ligand *trans* to the arene varies between ligands in the order CNXyl > H_2O > THF at 2.690(4), 2.579(3) and 2.43466(6) Å respectively. The L−U−arene$_{Ct}$ angles are similar for the hydrate complex **13** and isonitrile **14** at 175.55(7)° and 175.82(9)° and differs for the THF adduct **15** at 168.5(2)°.This is most likely due to the strong bond between the uranium centre and the THF ligand and the steric demand of the THF ligand compared to the H_2O ligand.

Table 3.3 – Selected bond distances (Å) and angles (°) for compounds **12**, **13**, **14**, **15**, **18**, **19**, **20**, **21** and **25**.

Parameter	**12**	**13**	**14**	**15**	**18**	**19**	**20**	**21**	**25**
	U,	U, OH_2	U, CNXyl	U, THF	Th, CNXyl	Th, THF	Th, N_3SiMe_3	Th, KO-3,5-dtbp	Th, OH_2
An-O1	2.184(7)	2.173(2)	2.156(3)	2.193(6)	2.224(2)	2.239(4)	2.221(3)	2.317(3)	2.228(3)
An-O2	2.171(7)	2.194(2)	2.196(3)	2.188(6)	2.232(2)	2.248(4)	2.210(3)	2.292(3)	2.228(3)
An-O3	-	2.183(2)	2.174(3)	2.174(6)	2.220(2)	2.236(4)	2.220(3)	2.28(3)	2.234(3)
An-O4	-	2.160(2)	2.183(3)	2.182(6)	2.232(2)	2.235(4)	2.241(3)	2.241(3)	2.236(3)
An-O_{av}	2.178(6)	2.178(2)	2.177(4)	2.184(8)	2.227(2)	2.239(5)	2.223(4)	2.270(4)	2.232(4)
An-L	2.64369(5)	2.579(3)	2.690(4)	2.437(8)	2.783(3)	2.480(5)	2.599(3)	2.214(3)	2.594(5)
An-Ct	2.5431(5)	2.5410(2)	2.5490(2)	2.5729(3)	2.63852(5)	2.6354(2)	2.6198(2)	2.70680(4)	2.6360(2)
Ct-An-L	180.00(0)	175.55(7)	175.82(9)	168.5(2)	175.45(6)	171.2(1)	178.90(8)	172.26(8)	179.4(1)
O1-An-O2	79.2(3)	84.29(7)	80.2(1)	84.6(2)	78.69(7)	81.9(1)	78.4(1)	78.6(1)	80.0(1)
O3-An-O4	-	78.95(7)	82.0(1)	78.0(2)	80.59(7)	77.2(1)	80.9(1)	78.2(1)	80.6(1)
O-An-O_{av}	79.2(3)	82.62(1)	81.1(1)	81.3(1)	79.64(1)	79.6(1)	79.6(1)	78.40	80.3(1)

The THF adduct, **15**, has both the shortest U−L distance and longest U$\cdots$arene$_{Ct}$ distance. The similarities between **12** and the authenticated uranium(IV) complexes **13**, **15** and **14** strongly suggest that it is indeed as uranium(IV) monoarene complex and the *trans* axial ligand to be a neutral donor.

The thorium monoarene complexes **18**, **19**, **20**, **21** and **25** all exhibit the same coordination motif as the uranium complexes. Like the uranium congeners, the Th−O distances are very similar ranging $2.223-2.270$ Å and are longer than those in the bimetallic complexes described in Chapter 2. The thorium$\cdots$arene$_{Ct}$ distances are comparable and range $2.6198-2.70680$ Å, which is significantly shorter than crystallographically characterised reported examples (range $2.701(8)-2.95$ Å).[34–36,41]

The Th−L distance axial ligand and the thorium centre varies between ligands in the order CNXyl $>$ N_3SiMe_3 $>$ OH_2 $>$ THF $>$ KO-3,5-dtbp at $2.783(3)$, $2.599(3)$, $2.594(5)$, $2.480(5)$ and $2.214(3)$ Å, respectively. The L−Th−arene$_{Ct}$ angle deviates from linear with increasing steric bulk at the metal centre, following the trend OH_2 $>$ N_3SiMe_3 $>$ CNXyl $>$ KO-3,5-dtbp $>$ THF, ranging $179.4(1)^\circ$ to $171.2(1)^\circ$.

The potassium aryloxide adduct **21** has the longest Th−Ct distance and shortest Th−L distance, while the trimethylsilyl azide adduct **20** has the shortest Th−Ct distance and second longest Th−L distance. However, the C−C bond distances of the ligand arene bridge in **20** and **21** are identical at 1.40(1) Å, and compare well to those of the bimetallic silylamido (**3**: 1.40(1)) and chloro (**7**: 1.392(6)) which do not feature arene coordination. This suggests that, despite the short distances, there is no orbital interaction between the thorium centre and ligand arene.

3.8 Conclusion and chapter summary

Four new uranium and six new thorium monometallic complexes of arene-tethered tetra-aryloxide ligands have been synthesised and characterised, meeting the secondary aim of this thesis. These complexes feature some of the shortest actinide−arene distances in the literature. Also synthesised and crystallographically characterised are a trimetallic uranium complex and a bimetallic thorium complex which exhibit similar structural motifs to compounds **10** and **9** which were described in Chapter 2.

Contrasting reactivity can be observed between uranium and thorium in this system. The uranium complexes can be prepared in solution in low yields (10 to 25%) and crystallised in very poor yields ($>$ 10%). The thorium analogues can be obtained quantitatively in solution and obtained in high crystalline yields (65 to 95%). The straightforward synthesis of the

monometallic thorium complexes allowed the exploration of the system with a range of Lewis bases, both neutral and ionic. In most cases, a monoarene complex was obtained with the exception of the reaction of **17** with excessive quantities of the fluorinated potassium aryloxide KO-3,5-btfmp which produced the bimetallic dimeric complex **23** in which the thorium-arene interaction has been disrupted. As this coordination motif has not been observed with thorium in reactions with excessive amounts of other Lewis bases, this is likely to be due to the strongly electron withdrawing properties of the fluorinated potassium aryloxide ligand. The lack of adduct formation with the potassium anilide KNHttbp suggests that non-linear Lewis bases or Lewis bases with sterically demanding groups close to the basic atom cannot access the Lewis acidic metal centre.

In contrast, employing the slightly more electron rich and sterically demanding ligand $H_4(pTP^t)$ for the synthesis of a uranium isocyanide complex gave rise to the trimeric complex **24**. Additionally, the trimeric complex **10** previously described in Chapter 2 was obtained when the synthesis of the uranium monoarene THF adduct **15** was attempted. These observations suggest that the monoarene complex for uranium, while kinetically accessible, is not necessarily thermodynamically favoured, resulting in poor isolated yields or ligand redistribution.

Employing the more sterically demanding ligand $H_4(pTP^*)$ allowed the isolation of a crystal of the thorium hydrate complex **25**. The large substituents on the aryloxides in this ligand are likely to prevent the coordination of more sterically demanding substrates and may prove useful to isolate a base-free complex by arene coordination at the unsaturated actinide centre.

3.9 Bibliography

[1] J. G. Brennan, F. G. N. Cloke, A. A. Sameh and A. Zalkin, *J. Chem. Soc., Chem. Commun.*, 1987, 1668–1669.

[2] P. L. Arnold, F. G. N. Cloke and P. B. Hitchcock, *Chem. Commun.*, 1997, 481–482.

[3] P. L. Arnold, M. A. Petrukhina, V. E. Bochenkov, T. I. Shabatina, V. V. Zagorskii, G. B. Sergeev and F. N. Cloke, *J. Organomet. Chem.*, 2003, **688**, 49–55.

[4] R. P. Kelly, L. Maron, R. Scopelliti and M. Mazzanti, *Angew. Chem., Int. Ed.*, 2017, 1–5.

[5] S. C. Bart, F. W. Heinemann, C. Anthon, C. Hauser and K. Meyer, *Inorg. Chem.*, 2009, **48**, 9419–9426.

[6] L. Castro, O. P. Lam, S. C. Bart, K. Meyer and L. Maron, *Organometallics*, 2010, **29**, 5504–5510.

[7] H. S. La Pierre, H. Kameo, D. P. Halter, F. W. Heinemann and K. Meyer, *Angew. Chem., Int. Ed.*, 2014, **53**, 7154–7157.

[8] H. S. La Pierre, A. Scheurer, F. W. Heinemann, W. Hieringer and K. Meyer, *Angew. Chem., Int. Ed.*, 2014, **53**, 7158–7162.

[9] S. M. Mansell, N. Kaltsoyannis and P. L. Arnold, *J. Am. Chem. Soc.*, 2011, **133**, 9036–9051.

[10] S. M. Franke, B. L. Tran, F. W. Heinemann, W. Hieringer, D. J. Mindiola and K. Meyer, *Inorg. Chem.*, 2013, **52**, 10552–10558.

[11] C. J. Inman, A. S. P. Frey, A. F. R. Kilpatrick, F. G. N. Cloke and S. M. Roe, *Organometallics*, 2017, **36**, 4539–4545.

[12] W. G. van der Sluys, A. P. Sattelberger, W. E. Streib and J. C. Huffman, *Polyhedron*, 1989, **8**, 1247–1249.

[13] I. Castro-Rodriguez, K. Olsen, P. Gantzel and K. Meyer, *Chem. Commun.*, 2002, 2764–2765.

[14] J. Hümmer, F. W. Heinemann and K. Meyer, *Inorg. Chem.*, 2017, **56**, 3201–3206.

[15] M. D. Fryzuk and S. A. Johnson, *Coord. Chem. Rev.*, 2000, **200-202**, 379–409.

[16] P. Roussel and P. Scott, *J. Am. Chem. Soc.*, 1992, **120**, 1070–1071.

[17] F. G. N. Cloke and P. B. Hitchcock, *J. Am. Chem. Soc.*, 2002, **124**, 9352–3.

[18] S. M. Mansell, J. H. Farnaby, A. I. Germeroth and P. L. Arnold, *Organometallics*, 2013, **32**, 4214–4222.

[19] W. J. Evans, S. A. Kozimor and J. W. Ziller, *J. Am. Chem. Soc.*, 2003, **125**, 14264–14265.

[20] A. L. Odom, P. L. Arnold and C. C. Cummins, *J. Am. Chem. Soc.*, 1998, **120**, 5836–5837.

[21] J. C. Berthet, M. Ephritikhine, J. C. Berthet, M. Lance and M. Nierlich, *Chem. Commun.*, 1998, **36**, 1373–1374.

[22] J. Felder, J. Yeon, M. Smith and H.-C. zur Loye, *Inorg. Chem. Front.*, 2017, **4**, 368–377.

[23] D. P. Halter, F. W. Heinemann, J. Bachmann and K. Meyer, *Nature*, 2016, **530**, 317–321.

[24] A. Dormond, A. El Bouadili, A. Aaliti and C. Moise, *J. Organomet. Chem.*, 1985, **288**, 1–5.

[25] M. Ephritikhine, *Organometallics*, 2013, **32**, 2464–2488.

[26] A. C. Behrle and J. R. Walensky, *Dalton Trans.*, 2016, **45**, 10042–10049.

[27] C. Boisson, J. C. Berthet, M. Ephritikhine, M. Lance and M. Nierlich, *J. Organomet. Chem.*, 1997, **533**, 7–11.

[28] J. Berthet and M. Ephritikhine, *Coord. Chem. Rev.*, 1998, **178-180**, 83–116.

[29] J. H. Farnaby, F. G. N. Cloke, M. P. Coles, J. C. Green and G. Aitken, *C. R. Chim.*, 2010, **13**, 812–820.

[30] R. R. Langeslay, G. P. Chen, C. J. Windorff, A. K. Chan, J. W. Ziller, F. Furche and W. J. Evans, *J. Am. Chem. Soc.*, 2017, **139**, 3387–3398.

[31] W. J. Evans, S. A. Kozimor, G. W. Nyce and J. W. Ziller, *J. Am. Chem. Soc.*, 2003, **125**, 13831–13835.

[32] J. Parry, E. Carmona, S. Coles and M. Hursthouse, *J. Am. Chem. Soc.*, 1995, **117**, 2649–2650.

[33] P. Arnold, S. Mansell, L. Maron and D. McKay, *Nature Chem.*, 2012, **4**, 668–674.

[34] I. Korobkov, B. Vidjayacoumar, S. I. Gorelsky, P. Billone and S. Gambarotta, *Organometallics*, 2010, **29**, 692–702.

[35] C. A. Cruz, D. J. H. Emslie, C. M. Robertson, L. E. Harrington, H. A. Jenkins and J. F. Britten, *Organometallics*, 2009, **28**, 1891–1899.

[36] C. A. Cruz, D. J. H. Emslie, L. E. Harrington and J. F. Britten, *Organometallics*, 2008, **27**, 15–17.

[37] J. McKinven, *Ph.D. thesis*, University of Edinburgh, 2016.

[38] S. M. Beshouri, P. E. Fanwick, I. P. Rothwell and J. C. Huffman, *Organometallics*, 1987, **6**, 2498–2502.

[39] I. Korobkov, S. Gambarotta and G. Yap, *Angew. Chem., Int. Ed.*, 2003, **42**, 4958–4961.

[40] I. Korobkov, A. Arunachalampillai and S. Gambarotta, *Organometallics*, 2004, **23**, 6248–6252.

[41] J. McKinven, G. S. Nichol and P. L. Arnold, *Dalton Trans.*, 2014, **43**, 17416–17421.

[42] J.-C. Berthet, P. Thuéry, N. Garin, J.-P. Dognon, T. Cantat and M. Ephritikhine, *J. Am. Chem. Soc.*, 2013, **135**, 10003–10006.

[43] G. Proulx and R. G. Bergman, *J. Am. Chem. Soc.*, 1995, **117**, 6382–6383.

[44] M. G. Fickes, W. M. Davis and C. C. Cummins, *J. Am. Chem. Soc.*, 1995, **117**, 6384–6385.

[45] W. H. Harman, M. F. Lichterman, N. A. Piro and C. J. Chang, *Inorg. Chem.*, 2012, **51**, 10037–10042.

[46] A. H. Obenhuber, T. L. Gianetti, X. Berrebi, R. G. Bergman and J. Arnold, *J. Am. Chem. Soc.*, 2014, **136**, 2994–2997.

[47] J. Habash, R. L. Beddoes and A. J. Smith, *Acta Crystallogr. Sect. C Cryst. Struct. Commun.*, 1991, **47**, 1595–1597.

[48] M. P. Spry, W. Errington and G. R. Willey, *Acta Crystallogr. Sect. C Cryst. Struct. Commun.*, 1997, **53**, 1388–1390.

[49] J.-Y. Kim, A. J. Norquist and D. O'Hare, *J. Am. Chem. Soc.*, 2003, **125**, 12688–12689.

[50] D. F. Back, É. Bonfada, G. M. de Oliveira and E. S. Lang, *J. Inorg. Biochem.*, 2007, **101**, 709–714.

[51] K. E. Knope, R. E. Wilson, M. Vasiliu, D. A. Dixon and L. Soderholm, *Inorg. Chem.*, 2011, **50**, 9696–9704.

[52] P. Thuery, *Inorg. Chem.*, 2011, **50**, 1898–1904.

[53] M. Fairley, D. K. Unruh, S. Abeysinghe and T. Z. Forbes, *Inorg. Chem.*, 2012, **51**, 9491–9498.

[54] D. K. Unruh, J. de Groot, M. Fairley, A. Libo, S. Miller and T. Z. Forbes, *Inorg. Chem.*, 2015, **54**, 1395–1404.

[55] P. T. Morse, R. J. Staples and S. M. Biros, *Polyhedron*, 2016, **114**, 2–12.

[56] F. A. Cotton and W. Schwotzer, *Organometallics*, 1985, **4**, 942–943.

[57] G. C. Campbell, F. A. Cotton, J. F. Haw and W. Schwotzer, *Organometallics*, 1986, **5**, 274–279.

[58] D. P. Halter, H. S. La Pierre, F. W. Heinemann and K. Meyer, *Inorg. Chem.*, 2014, **53**, 8418–8424.

Chapter 4

Uranium (III) boroxide and borohydride complexes

This chapter describes the synthesis of a uranium(III) diarylboroxide complex and its reactivity towards unsaturated small molecules. Also described in this chapter are the syntheses of heteroleptic uranium(III) borohydride complexes, their reactivity and their potential as starting materials in the synthesis of reactive uranium complexes.

4.1 Uranium boroxide complexes

Our group has carried out investigations into the functionalisation of substrates trapped between uranium centres issued from small molecule activation.[1] To this end, we have investigated ligands containing Lewis acidic groups to offer a potential secondary reaction site for chemical derivatisation of substrates.

4.1.1 Synthesis and characterisation of a uranium(III) boroxide complex

A hexane solution of $HOBtrip_2$ was slowly added to a deep purple solution of UN''_3 at room temperature. The resulting purple-brown solution was stirred for 2 hours at room temperature after which the volatiles were removed under reduced pressure. Compound $[U(OBtrip_2)_3]$ (**26**) was obtained as a dark purple-brown solid, and characterised by ^1H and ^{11}B NMR spectroscopy and single-crystal XRD analysis.

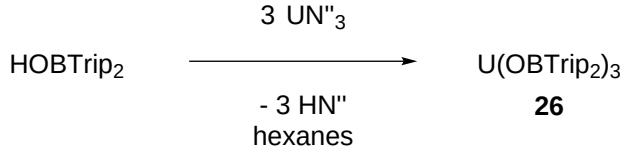

Scheme 4.1 – Synthesis of compound **26**.

The ^1H NMR spectrum of **26** contains many paramagnetically shifted resonances ranging

from 75 to −50 ppm. In comparison, the ^{11}B NMR spectrum contains a single resonance at 121 ppm.

Dark red single crystals of **26** suitable for single-crystal XRD analysis were obtained from concentrated Et_2O solutions of **26** cooled to −30 °C. The solid-state structure confirms the presence of a uranium(III) centre with three bound boroxide ligands (Figure 4.1). The average boroxide U−O distance is 2.183(7) Å, which is slightly longer than in the uranium tris(aryloxide) complex [U(Odtbp)$_3$] (2.159 Å). The longer U−O bond coupled with the near linear UOB angle (mean 171.0(8)°) is consistent with a lower degree of π donation from the boroxide ligand to the uranium centre and metal backbonding to the ligand compared to [U(Odtbp)$_3$]. This is likely to be the result of the proximal B atom drawing π density from the oxygen donor. The U−O distance of the ether ligand is 2.530(7) Å and is much shorter than in the seven-coordinate complex [{(^{Neop}ArO)$_3$tacn}U(OEt$_2$)] (2.669(2) Å) reported by Meyer and co-workers, which constitutes the only other crystallographically characterised uranium(III) diethyletherate.[2] This could be the result of a more electron-deficient uranium centre engendered by the poor π donor properties of the boroxide ligand or due to the lower coordination number in **26**.

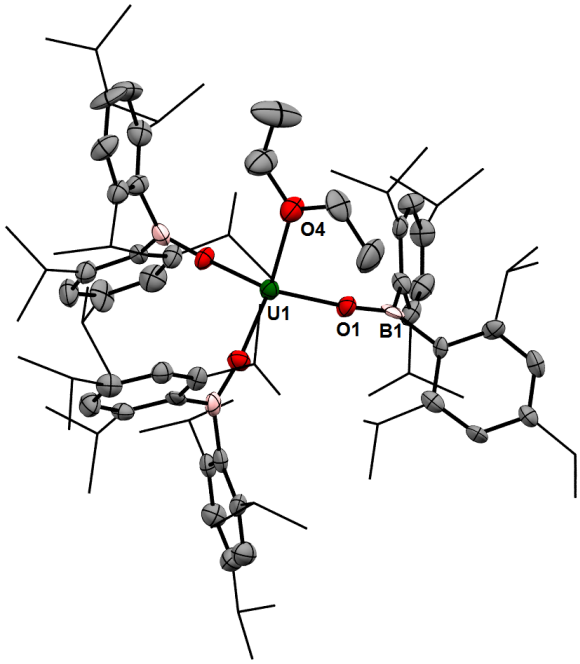

Figure 4.1 – Solid-state structure of **26**. The hydrogen atoms are omitted and the *iso*-propyl group carbon atoms are depicted in wireframe for clarity. The thermal ellipsoids are displayed at 50% probability.

4.1.2 Reactions of $[U(OBtrip_2)_3]$ with CO_2 and CO

Organometallic uranium(III) complexes have been shown to effect reductive transformations to small unsaturated gaseous molecules such as CO, CO_2, N_2O and even N_2.[3–9]

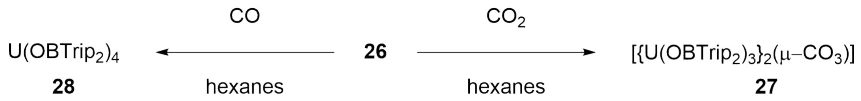

Scheme 4.2 – Synthesis of compounds **27** and **28**.

Synthesis of $[\{U(OBtrip_2)_3\}_2(\mu\text{-}CO_3)]$

Exposure of a purple-brown cyclopentane solution of **26** to one atmosphere of CO_2 results in a rapid colour change to a green solution from which crystals of $[\{U(OBtrip_2)_3\}_2(\mu{-}CO_3)]$ (**27**) were obtained. Complex **27** was confirmed as the carbonate-bridged diuranium(IV) complex by ^1H and ^{11}B NMR and IR spectroscopies, single-crystal XRD and elemental analysis.

Pale green crystals suitable for XRD analysis were obtained by slow diffusion of hexanes into the cyclopentane reaction mixture. The data were of sufficient quality to discuss connectivity information, but not bond metrics (low resolution data cut at 1.00 Å without anisotropic refinement). The solid-state structure reveals a bimetallic carbonate-bridged complex (Figure 4.2). The uranium centres are five-coordinate in distorted trigonal bipyramidal geometry, comparable to that exhibited by the uranium centres in the nitrogen-bridged complex $[\{(ttbpO)_3U\}_2(\mu\text{-}\eta^2\text{:}\eta^2\text{-}N_2)]$.[6] The carbonate bridge is disordered over two sites, resulting in the superposition of $\eta^1 : \eta^2$ and $\eta^2 : \eta^1$ binding modes with 50:50 occupancy, a common feature in bimetallic uranium carbonate complexes.[10,11] The boroxide ligands are staggered along the U−C−U axis to minimise steric interactions between ligands.

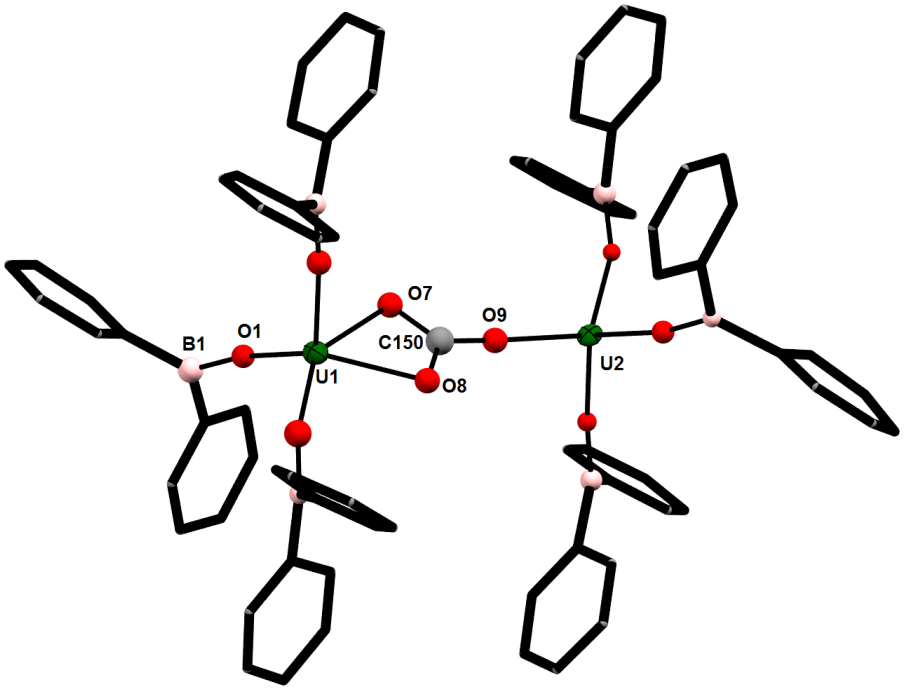

Figure 4.2 – Solid-state structure of **27**.The hydrogen atoms and *iso*-propyl group carbon atoms are omitted, and the boroxide ligand phenyl group carbon atoms are depicted as capped sticks for clarity. The thermal ellipsoids of the uranium centres are displayed at 50% probability.

Unlike the uranium tris(aryloxide) complex $U(Ottbp)_3$, no insertion occurs at the ligand U−O bond. Most uranium(III) organometallic complexes which react with CO_2 form carbonate products when reacted with an excess of CO_2. A few examples of oxalate formation have been reported under stoichiometric conditions or with the presence of an external reducing agent such as KC_8.[11–13] The lowest energy pathway for carbonate formation was calculated to comprise of the two-electron oxidative cleavage of CO_2 to form an oxo-bridged bimetallic complex, which further reacts with CO_2 to give the carbonate by insertion into a U−O bond.[12,14]

Synthesis of $U(OBtrip_2)_4$

Exposing cyclopentane solutions of **26** to atmospheric pressures of CO results in a slight colour change from purple-brown to purple-red, from which pale purple crystals of $U(OBtrip_2)_4$ (**28**) were obtained. The identity of **28** as the homoleptic uranium(IV) boroxide complex was confirmed by single-crystal XRD analysis.

Pale purple crystals of **28** were grown from concentrated benzene solution. The solid-state structure shows an unsolvated four-coordinate uranium centre in tetrahedral geometry

(Figure 4.3). The mean boroxide ligand U−O distance of 2.159(5) Å is shorter than in the uranium(III) complex **26**, consistent with a uranium(IV) centre. The U−O bond lengths in **28** are longer than those in homoleptic uranium(IV) aryloxide [U(Odtbp)$_4$] (2.135(4) Å), due to the greater steric demand of the boroxide ligand and poorer metal to ligand backbonding.[15] The B−O−U angles are comparable to those in **26** (mean 171.0(5)°), despite the considerable bulk about the uranium centre. The disproportionation of uranium(III) to uranium(IV) and uranium metal is a known oxidative pathway.

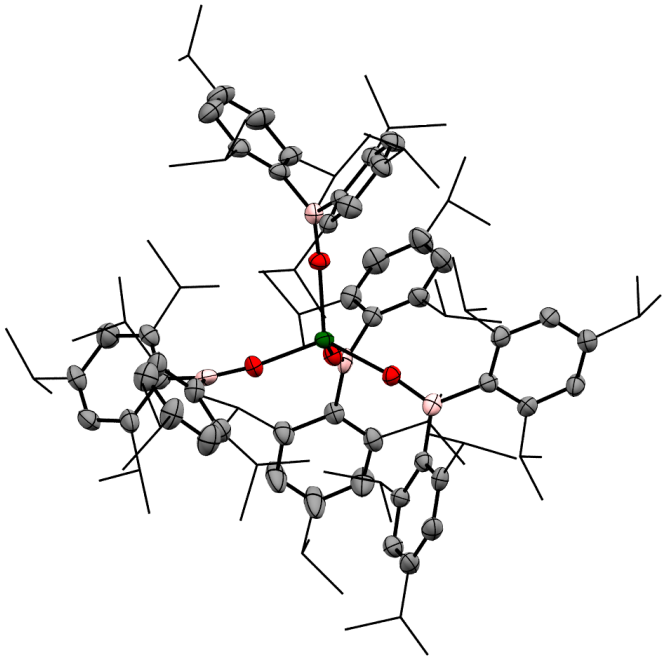

Figure 4.3 – Solid-state structure of **28**. The hydrogen atoms are omitted and *iso*-propyl group carbon atoms are depicted as wireframe for clarity. The thermal ellipsoids are displayed at 50% probability.

4.2 Heteroleptic uranium(III) borohydride complexes

Burns, Clark and co-workers reported the synthesis of mono and bis cyclopentadienyl uranium(III) iodides in 2000, which have proven to be useful starting materials in uranium(III) organometallic chemistry.[16] As discussed in Section 1.3, although synthetic routes to uranium(III) trisborohydrides have been described in the literature since 1953,[17] they have rarely been employed to access uranium(III) organometallic chemistry due to the challenges associated with the synthesis of its precursor, [U(BH$_4$)$_4$]. The development of a straightforward synthesis of the well-defined uranium(III) borohydride [U(BH$_4$)$_3$(thf)$_2$] by our group has allowed the synthesis of rare bi-

metallic uranium(III) complexes in macrocyclic environments.[18] Alkali metal borohydrides are commonly used reducing agents in organic chemistry, and it has also been shown that CO_2 can be reduced by $NaBH_4$ to form sodium hydrotris(formyl)borate, $Na[HB(OOCH)_3]$.[19] The reduction of transition metal carbonyls with $NaBH_4$ has also been reported in cationic iron half-sandwich complexes.[20] Recent investigations in our group demonstrated that a thorium borohydride complex reacted with CE_2 (E = O, S) to yield trimethylborane, a product from the reduction and chalcogen extrusion of CE_2.[21]

Combining the strong reducing power of a uranium(III) centre with a reducing ligand in an organometallic complex could lead to new or different reactivity. Investigations into the synthesis of heteroleptic uranium(III) borohydrides were carried out towards this end.

4.2.1 Synthesis and characterisation of pentamethylcyclopentadienyl uranium borohydrides

Synthesis of $[U(C_5Me_5)(\mu\text{-}BH_4)_2]_6$

Toluene was added to a mixture of KC_5Me_5 and $[U(BH_4)_3(thf)_2]$ to yield a purple-red suspension which was allowed to stir for 18 hours at ambient temperature. Filtration of the insoluble salt by-products provided $[U(C_5Me_5)(\mu\text{-}BH_4)_2]_6$ (**29**) as a purple-brown solid after removal of the volatiles under reduced pressure. The complex was characterised by ^1H and ^{11}B NMR spectroscopy, elemental analysis, IR spectroscopy and single-crystal XRD analysis. Complex **29** is readily soluble in THF and arene solvents, and sparingly soluble in alkane solvents. Cloke and co-workers have reported that carrying out the synthesis of $[(C_5Me_5)UI_2]$ in Et_2O leads to the reductive activation of the solvent, forming an oxo-bridged trimeric complex $[U(C_5Me_5)(\mu\text{-}I)_2]_3(\mu^3\text{-}O)$.[22] Using diethyl ether as the reaction solvent for the synthesis of **29** does not result in reductive activation of the solvent in this case. The difference in reactivity is likely to be due to the increased Lewis acidity of the uranium centre in the iodide complex. Compared to the borohydride ligand, the U−I bond is weaker and thus provides less electron density to the metal centre.

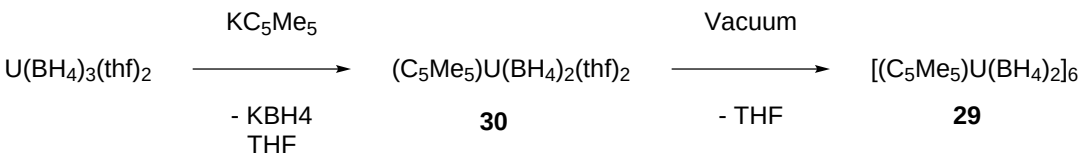

Scheme 4.3 – Synthesis of compounds **29** and **30**.

The ^{1}H and ^{11}B NMR spectra of **29** in C_6D_6 contain broad resonances. The ^{1}H spectrum in THF-d_8, in contrast, contains a broad resonance at 98.8 ppm, ascribed to the borohydride ligand resonances and a sharp resonance at −6.80 ppm corresponding to the C_5Me_5 ligand. Similarly, the ^{11}B spectrum in THF-d_8 contains a single broad resonance at 148 ppm, which is comparable to that of other uranium(III) tetrahydroborate complexes.[18] The differences in spectroscopic behaviour in donor and non-donor solvents is well explained by the solid-state structures.

Large purple-red blocks suitable for XRD analysis can be obtained from concentrated benzene solutions of **29**. Compound **29** crystallises as a donor-free hexanuclear cluster, in which each uranium centre is bridged by four borohydride ligands (Figure 4.4). Similar clusters have been reported for the related samarium and neodymium half sandwich borohydride complexes bearing the $C_5Me_4{}^{n}Pr$ ligand.[23] The borohydride ligand H-atoms could not be located crystallographically, however the U···B distances range from 2.67(1) to 3.02(1) Å (average 2.80(2) Å) and are consistent with both bridging $(\mu\text{-H})_3B(\mu\text{-H})_1$ bound and bridging $(\mu\text{-H})_2B(\mu\text{-H})_2$ bound borohydride ligands.[24]

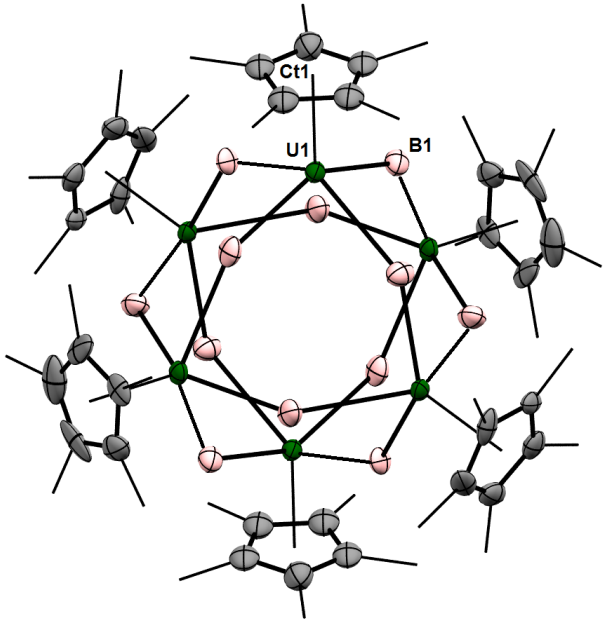

Figure 4.4 – Solid-state structure of **29**. The hydrogen atoms are omitted and the carbocyclic ligand methyl groups are depicted as wireframe for clarity. The thermal ellipsoids are displayed at 50% probability.

In comparison, crystallisation by diffusion of hexanes into concentrated THF solutions of **29** at −30 °C yield dark red blocks of $[U(C_5Me_5)(BH_4)_2(thf)_2]$ (**30**) suitable for single-crystal

XRD analysis, revealing a monometallic complex (Figure 4.5). The five-coordinate uranium centre is in distorted square pyramidal geometry, with two bound THF molecules in addition to the carbocyclic and borohydride ligands. The apical position is occupied by the C_5Me_5 ligand with the square base formed by the THF and borohydride ligands. The borohydride ligands are in a *trans*-arrangement presumably to minimise electrostatic interactions between the two anionic ligands. In comparison, the uranium centre in the iodide analogue $[(C_5Me_5)UI_2(thf)_3]$ is six coordinate with an additional THF ligand *trans* to the carbocyclic ligand. The lower coordination number in **30** can be attributed to the greater affinity of the metal centre towards the borohydride ligands, resulting in a more electron-rich uranium centre. The U$\cdots$ring$_{Ct}$ (ring$_{Ct}$ = carbocyclic ligand ring centroid) distance is considerably shorter in **29** at 2.4654(1) compared to 2.512(6) Å $[(C_5Me_5)UI_2(thf)_3]$. The borohydride H-atoms were located from the difference Fourier map and their positions refined. The borohydride ligands are bound in a $(\mu\text{-H})_3BH$ fashion, consistent with the U$\cdots$B separation of 2.670(5) Å and 2.748(4) Å.[24]

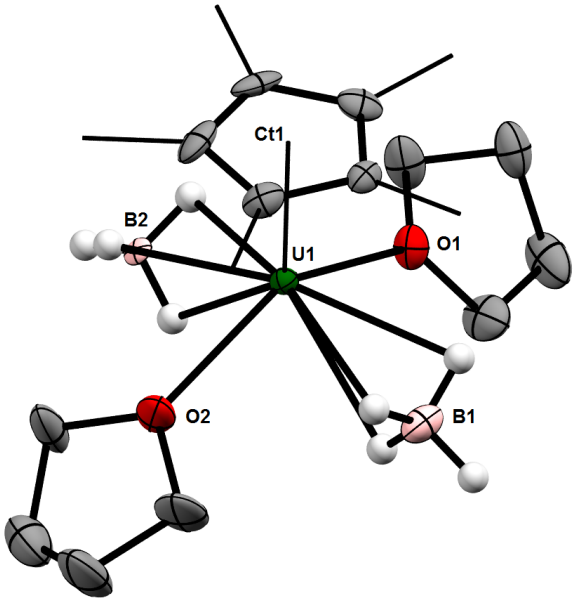

Figure 4.5 – Solid-state structure of **30**. The hydrogen atoms with the exception of those of the borohydride ligand are omitted, and the carbocyclic ligand methyl groups are depicted as wireframe for clarity. The thermal ellipsoids are displayed at 50% probability.

The clustering behaviour of **29** is comparable to that of the related lanthanide complexes $[Ln(C_5Me_4{}^nPr)(BH_4)_2]$ (Ln = Sm, Nd), where solvated monomeric complexes were observed by ^1H and ^{11}B NMR spectroscopy in THF solution and hexanuclear clusters were obtained upon crystallisation.[23] Other known crystallographically characterised uranium(III) multimetallic

clusters include the trinuclear $[U(C_5Me_5)_2Cl]_3$ reported by Marks and co-workers, which was prepared from the reduction of $U(C_5Me_5)_2(R)Cl$ with H_2 in toluene.[25] The authors commented on the stability of the adduct $U(C_5Me_5)_2Cl(thf)$ to vacuum, suggesting that formation of the trimer by removal of the THF ligand is not spontaneous upon exposure to vacuum. Another notable example is the uranium metallocene hydride $[U(C_5Me_5)_2H]_2$ as reported by Marks *et al.* and, more recently, Evans and co-workers.[26,27] The synthesis described by Evans involves the reduction of $U(C_5Me_5)_2Me_2$ with H_2 in benzene, followed by successive removal of solvent under reduced pressure and redissolution in toluene. While there are a few examples of clusters in uranium(III) chemistry, the spontaneous formation of hexameric **29** upon removal of solvent is remarkable as the strongly Lewis acidic nature of low coordinate uranium(III) centres renders them unlikely to dissociate from Lewis bases once an adduct is formed. This can in part be ascribed to the range of coordination modes available to the borohydride ligand, which has previously been shown by our group to bridge two uranium(III) centres in a macrocyclic environment in a $U-(\mu\text{-}BH_4)-U$ fashion.[18]

Synthesis of $[U(C_5Me_5)_2(BH_4)(thf)]$

Addition of toluene to a stirred mixture of KC_5Me_5 and $[U(BH_4)_3(thf)_2]$ provided a dark green suspension from which $[(C_5Me_5)_2U(BH_4)(thf)]$ (**31**) was isolated as a dark green solid after filtration and removal of the solvent under reduced pressure. The identity of **31** as the uranium(III) borohydride metallocene was confirmed by ^1H and ^{11}B NMR and IR spectroscopy, single-crystal XRD and elemental analysis. Compound **31** is readily soluble in ethereal solvents and sparingly soluble in aromatic and alkane solvents.

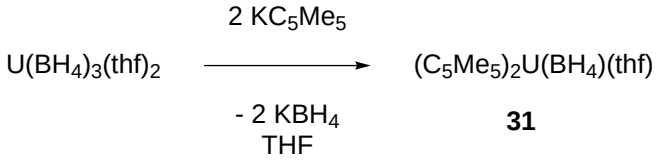

Scheme 4.4 – Synthesis of compound **31**.

The ^1H NMR spectrum of **31** in C_6D_6 contains four resonances: a broad singlet at 58.5 ppm corresponding to the borohydride ligand, a sharp singlet at -2.5 ppm assignable to the C_5Me_5 ligand and two broad singlets at -14.8 and -42.5 ppm, which can be ascribed to a coordinated THF molecule. The ^{11}B NMR spectrum displays a broad singlet at 55 ppm. While the 1 H and ^{11}B NMR spectroscopy resonances for **29** and **29** differ significantly, they remain

comparable to those observed in other uranium(III) tetrahydroborate complexes synthesised by our group.[18] The IR spectrum of **31** displays strong stretching bands in the $2500-2000$ cm^{-1} region consistent with $(\mu\text{-H})_3$BH binding: ν(B$-$H$_t$) 2476 cm^{-1} and ν(B$-$H$_\mu$) 2236 and 2103 cm^{-1}.[28]

Dark green plates suitable for single-crystal XRD analysis were obtained from slow evaporation of a concentrated pentane solution of **31**. Complex **31** crystallises with two independent molecules in the asymmetric unit and exhibits the expected bent metallocene structure with a THF solvent molecule occupying the vacant site on the uranium centre (Figure 4.6). The average U$-$ring$_{Ct}$ distance (2.5066(4) Å), THF ligand U$-$O distance (2.552(6) Å) and average ring$_{Ct}-$U$-$ring$_{Ct}$ angle (133.39(2)°) are typical of the limited examples of crystallographically characterised uranium(III) metallocene complexes.[29–31] The borohydride H-atoms were located from the difference Fourier map and their positions refined. The borohydride ligands were found to be bound in a $(\mu\text{-H})_3$BH fashion, consistent with the average U$\cdots$B distance of 2.64(1) Å.[24]

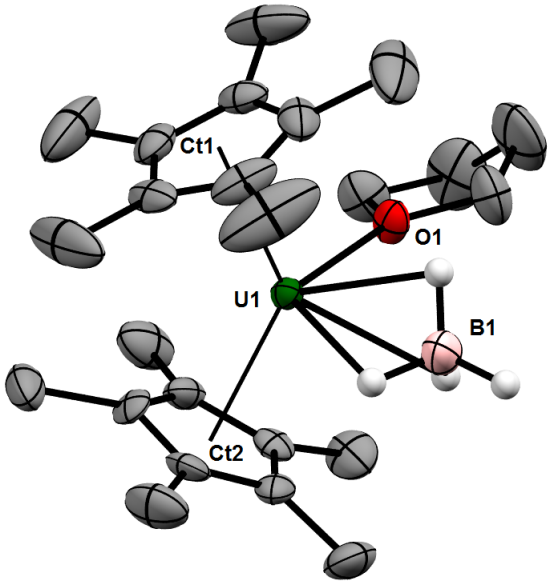

Figure 4.6 – Solid-state structure of **31**. The hydrogen atoms with the exception of those of the borohydride ligand and a second molecule of **31** within the asymmetric unit are omitted for clarity. Thermal ellipsoids displayed 50% probability.

Synthesis of U(C$_5$Me$_5$)$_2$(BH$_4$)$_2$

Oxidation of **29** and **31** with trace O_2 resulted in the formation of the previously reported

uranium(IV) metallocene $[(C_5Me_5)_2U(BH_4)_2]$ (**32**) as confirmed by ^{1}H NMR spectroscopy and single-crystal XRD cell check.[32]

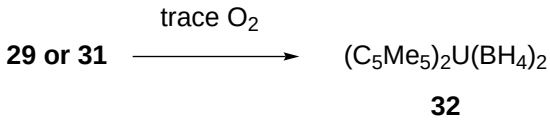

Scheme 4.5 – Synthesis of compound **32**.

The previously unreported ^{11}B NMR spectrum of **32** contains a singlet at 39 ppm and was found to be useful to identify the formation of **32** during reactivity studies of **29** and **31** (*vide infra*).

4.2.2 Reactivity studies of $[U(C_5Me_5)(BH_4)_2]_6$ and $[U(C_5Me_5)_2(BH_4)(thf)]$

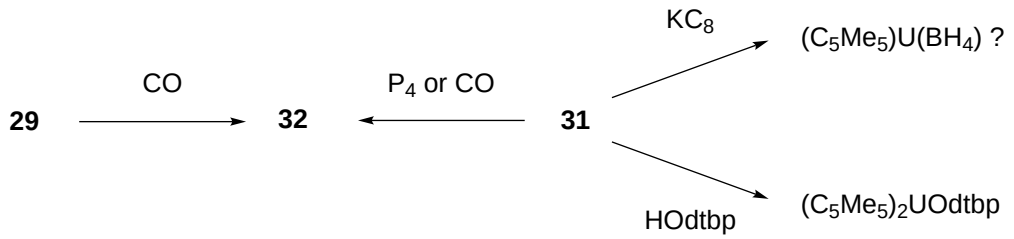

Scheme 4.6 – Reactivity of complexes **29** and **31**.

As discussed in Chapter 1, organometallic uranium(III) complexes can effect one- or two electron small molecule reduction. However, regeneration of the reactive uranium(III) centre is a major challenge in small molecule activation chemistry often requiring harsh conditions.[33] Complexes **29** and **31** contain both a reducing metal centre and a ligand capable of reductive chemistry. Additionally, the tendency of uranium borohydride complexes to favour the uranium(III) oxidation state over uranium(IV), as discussed in Section 1.3, may provide a reactive metal centre which can be regenerated more straightforwardly.[17,34,35] As a result, the reactivity of **29** and **31** with small molecules was investigated.

Addition of a colourless P_4 solution in benzene to a dark green benzene solution of **31** in a Young's tap NMR tube immediately produced a red solution. The ^{1}H and ^{11}B NMR spectra revealed the major product to be the uranium(IV) metallocene **32** along with unidentified minor products. No resonances could be located in the ^{31}P{^{1}H} NMR spectrum. Exposing degassed benzene solutions of **31** to atmospheric pressures of CO resulted in slow decomposition to **32**.

In comparison, degassed solutions of **29** exposed to atmospheric pressures of CO resulted in rapid decomposition to **32**, along with unidentified minor resonances.

The reduction of uranium(III) or uranium(IV) complexes with strong reducing agents in aromatic solvents has been shown to provide a route to diuranium complexes in which a reduced arene solvent molecule is the bridging ligand (Scheme 1.18m *cf.* Chapter 1).[36–41]

The addition of KC_8 to a stirred dark green benzene solution of **31** resulted in a slight darkening in colour. After 30 minutes, the reaction was monitored by ^{1}H and ^{11}B NMR spectroscopy. Two new resonances consistent with a single ligand set were observed in the spectra along with resonances corresponding to the starting material **31** (3:2; compound **31**:new resonances). Two new resonances in the ^{1}H NMR spectrum at 13.66 and -1.61 ppm with relative integrals of 4:15 suggest equal numbers of borohydride and C_5Me_5 ligands. The ^{11}B NMR spectrum shows a new singlet at 66 ppm. These new resonances do not match the ^{1}H NMR spectrum of the uranium(IV) metallocene **32**, suggesting a new species. Refluxing the reaction mixture for 48 hours led to decomposition, as evidenced by NMR spectroscopy.

A preliminary reaction of **31** with HOdtbp in benzene in a Young's NMR tube did not result in a change at room temperature. Heating the reaction mixture to reflux for two days produced a dark red solution with new paramagnetic resonances. Due to the acidity of the phenolic proton and the reducing nature of the borohydride ligand, a likely product of this reaction is the uranium(III) metallocene aryloxide $[U(Odtbp)(C_5Me_5)_2]$ accompanied by the elimination of hydrogen gas and diborane. Despite our best efforts, single crystals for XRD characterisation could not be obtained and this compound was not pursued further.

4.2.3 Synthesis and characterisation of uranium(III) borohydride complexes using non-carbocyclic ligands

The uranium(III) borohydride starting material $[U(BH_4)_3(thf)_2]$ was shown in Section 4.2 to be a useful precursor to the uranium(III) borohydride half sandwich complex **29** and uranium(III) metallocene borohydride complex **31** in a similar fashion to the iodide complexes reported by Burns and Clark.[16] Due to the good solubility of $[U(BH_4)_3(thf)_2]$ in aromatic solvents, the syntheses could be carried out in benzene or toluene to yield the desired products cleanly in good yields and with no signs of oxidation, precluding salt incorporation. Another notable difference is the formation of the donor-free hexameric **29**. Coordinative unsaturation is often key to reactivity in actinide chemistry, and facile access to donor-solvent free starting materials is synthetically advantageous. With the knowledge that $[U(BH_4)_3(thf)_2]$ could form uranium(III) complexes

of carbocyclic ligands straightforwardly, the viability of $[U(BH_4)_3(thf)_2]$ as a precursor to complexes with non-carbocyclic ligands and monodentate ligands was investigated.

Synthesis of $[U(Tp^*)(BH_4)_2(thf)]$

Hydrotrispyrazolylborate ligands have found wide application in transition-metal chemistry and have recently been reported to support uranium(III) alkyl complexes.[42] The electronic properties of the Tp* (Tp* = hydrotris(3,5-dimethylpyrazol-1-yl)borate) ligand are similar to those of the C_5Me_5 ligand, although the bulkier steric properties of the Tp* ligand can impart a greater degree of solubility and handling to the resulting complexes. The Tp* ligand has been employed by the Edelmann and Cloke groups independently to synthesise half sandwich complexes with the general formula $M(\eta-C_8H_6R_2)(Tp^*)$ (M = Ce, Pr, Nd, Sm, R = H; M = U, R = $Si^iPr_3-1,4$) and $U(\eta-C_8H_4\{Si^iPr_3-1,4\}_2)(Tp^*)$.[43–45]

Dropwise addition of KTp* THF solution to a red-brown solution of $[U(BH_4)_3(thf)_2]$ in THF produces a purple solution which was stirred for 18 hours. A purple powder characterised as $[U(Tp^*)(BH_4)_2(thf)]$ (**33**) could be isolated after filtration and removal of volatiles under reduced pressure. Complex **33** was characterised by ^1H NMR spectroscopy and single-crystal XRD analysis.

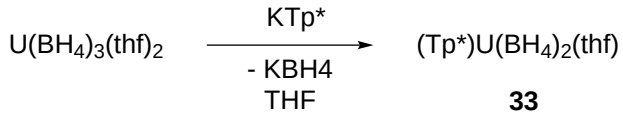

Scheme 4.7 – Synthesis of compound **33**.

The ^1H NMR spectrum of **33** in C_6D_6 contains seven resonances; a broad resonance at 145 ppm corresponding to the borohydride ligand, two broad resonances at 0.68 and −4.46 corresponding to the bound THF ligand and four resonances for the Tp* ligand at 12.33, 7.32, −2.84 and −13.16. The high resonance frequency of the BH_4 ligand H atoms still remains comparable to that observed for U(III) tetrahydroborate complexes.[18] Purple-red crystals of **33** were obtained from slow diffusion of hexanes into concentrated benzene solutions of **33**.

Complex **33** crystallises with no lattice solvent (Figure 4.7). The uranium centre is eight-coordinate, displaying distorted octahedral geometry. The tridentate Tp* ligand occupies one face of the octahedron, while the remaining three positions are occupied by two borohydride ligands and a THF molecule. The Tp* ligand average U−N distance of 2.556(6) Å is within the normal range of uranium(III) pyrazolate complexes.[42,45,46] The borate and borohydride

H-atoms were located in the difference Fourier map. The borohydride ligands are $(\mu\text{-H})_3\text{BH}$ bound, consistent with the U···B separation of 2.655(9) Å.[24]

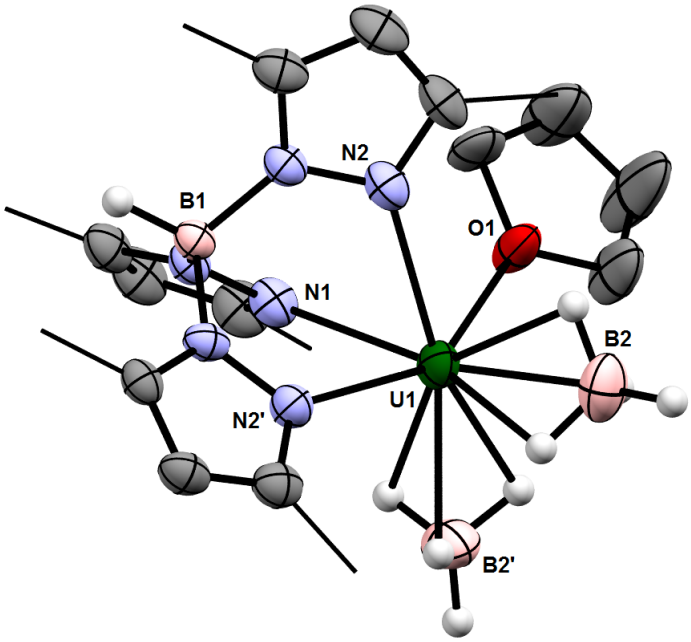

Figure 4.7 – Solid-state structure of **33**. The hydrogen atoms are omitted with the exception of the borate and borohydride H-atoms and the pyrazolate methyl group carbon atoms are depicted as wireframe for clarity. The thermal ellipsoids are displayed at 50% probability.

The structure of the pyridine adduct of the related complex $[\text{U}(\text{Tp}^\dagger)\text{I}_2(\text{Py})_2]$ ($\text{Tp}^\dagger$ = hydrotris (3,5-di-*iso*-propylpyrazol-1-yl)borate) reported by Santos and co-workers shows a similar co-ordination geometry with two bound pyridine molecules.[47] Despite the greater steric demand of the *iso*-propyl substituted $\text{Tp}^\dagger$ ligand, the coordination number is lower in **33** (six *versus* seven), which can be attributed to the shorter U−X bond between the metal centre and borohydride ligand.

Synthesis of $[\text{U}(\text{Odtbp})(\text{BH}_4)_2(\text{thf})_2]$

The widespead use of aryloxides in low-coordinate uranium(III) small molecule activation chemistry make uranium(III) starting materials containing aryloxide ligands attractive targets for the development of new reactive uranium complexes.[6,11,48–51]

Addition of a colourless solution of KOdtbp to a stirring red-brown solution of $\text{U}(\text{BH}_4)_3(\text{thf})_2$ produced an orange-brown suspension which was allowed to stir for 18 hours. After this time, the solvent was removed under reduced pressure and the red-brown solids extracted in toluene.

The mono(aryloxide) complex [U(Odtbp)$(BH_4)_2(thf)_2$] (**34**) was isolated as a dark red powder and characterised by ^{1}H and ^{11}B NMR and IR spectroscopies and single-crystal XRD analysis.

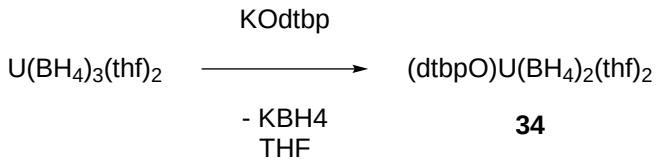

Scheme 4.8 – Synthesis of compound **34**.

The ^{1}H NMR spectrum of **34** in C_6D_6 exhibits a broad singlet at 121 ppm corresponding to the borohydride ligand and three resonances for the aryloxide ligand; two resonances corresponding to the aryl protons at 15.28 and 12.46 ppm and a singlet at 0.64 ppm corresponding to the *tert*-butyl protons. A single broad resonance is observed in the ^{11}B NMR spectrum at 146 ppm. The ^{1}H and ^{11}B NMR spectroscopy resonances for **34** are comparable to those of **29**. The IR spectrum of **34** displays strong stretching bands in the 2500-2000 cm^{-1} region consistent with (μ-H)$_3$BH binding: ν(B$-$H$_t$) 2453 cm^{-1} and ν(B$-$H$_\mu$) 2203 and 2142 cm^{-1}.[28]

Crystals of **34** were grown from concentrated pentane solutions of **34** stored at -30 °C. The five-coordinate uranium centre displays trigonal bipyramidal geometry (Figure 4.8). The axial positions are occupied by two coordinated THF solvent molecules and the equatorial plane by the aryloxide and two borohydride ligands. The aryloxide ligand *tert*-butyl groups are aligned with the equatorial plane, most likely to minimise steric interactions with the axial THF ligands. This results in a reduction of the B$-$U$-$B angle to 112.3(7)° compared with the average aryloxide O$-$U$-$B angle of 123.8(1)°. The borohydride ligand H-atoms were located in the difference Fourier map and suggest a (μ-H)$_3$BH binding mode for borohydride ligand, which is consistent with the mean U$\cdots$B distance of 2.64(2) Å.[24] The U$-$O distance of 2.167(9) Å is slightly longer to the U$-$O distance in the homoleptic complex [U(Odtbp)$_3$] (2.160(2) Å). Unlike **29**, the uranium centre in **34** retains two THF molecules in the solid-state possibly due to the lower steric demand of the aryloxide ligand.

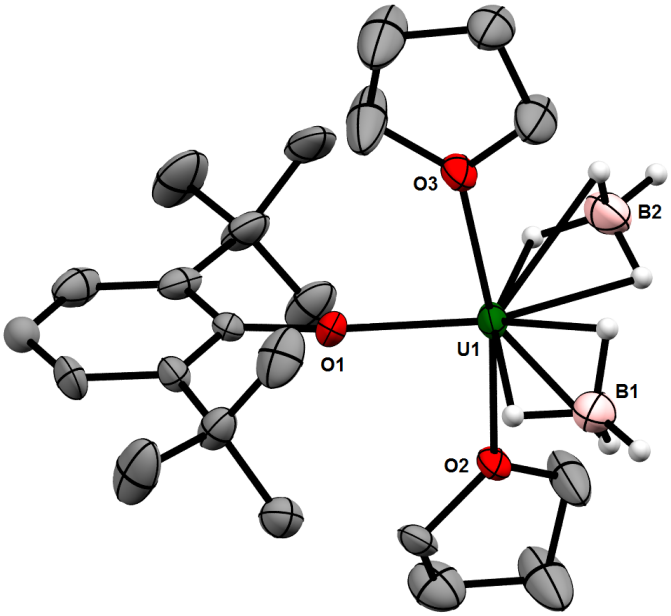

Figure 4.8 – Solid-state structure of **34**. The hydrogen atoms are omitted for clarity with the exception of the borohydride H-atoms. Thermal ellipsoids displayed at 50% probability.

Targetted synthesis of $U(OAr)_2(BH_4)$

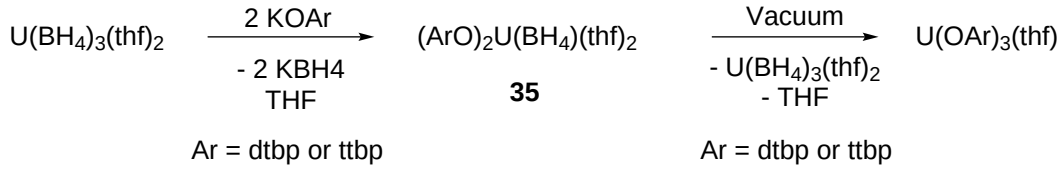

Scheme 4.9 – Synthesis of compound **35**

As $[U(BH_4)_3(thf)_2]$ was a suitable precursor for the synthesis of the uranium(III) mono(aryloxide) complex **34**, the synthesis of a uranium(III) bis(aryloxide) complex was targetted.

A colourless solution of KOttbp in THF was added dropwise to a red-brown THF solution of $[U(BH_4)_3(thf)_2]$. ^1H and ^{11}B NMR spectra of the deep red reaction mixture in THF-d_8 contained new paramagnetic resonances attributable to the desired bis(aryloxide) borohydride compound $U(Ottbp)_2(BH_4)$ (**35**): a broad singlet at 93.4 ppm corresponding to the borohydride ligand and four broad singlets ascribed to the aryloxide ligand in the ^1H NMR spectrum and a singlet at 23 ppm in the ^{11}B NMR spectrum. Upon removal of the reaction solvent and crystallisation in pentane, however, large crystals identified as $[U(Ottbp)_3(thf)]$ were obtained, suggesting ligand redistribution had occurred.[6] Analogous reactivity was observed using the less electron

donating Odtbp ligand.

On one occasion, deep red crystals were obtained from concentrated hexane solution at −30 °C. Structural elucidation revealed a structure consistent with **35** (Figure 4.9). The data were of sufficient quality to obtain connectivity information and qualitative bond metrics. The compound crystallises in P1 and consists of two symmetrically inequivalent molecules of **35** in the asymmetric unit. The five-coordinate uranium centre exhibits trigonal bipyramidal geometry. Similarly to **34**, the axial positions are occupied by two THF ligands and the equatorial plane is occupied by the borohydride and aryloxide ligands. The two aryloxide ligands are staggered such that the *tert*-butyl groups of one ligand line up with the axial plane, and those of the other line up with the equatorial plane to minimise steric hindrance. The average aryloxide O−U−O angle is 120.1(2)°. While the borohydride H-atoms could not be located, the mean U···B distance of 2.60(6) Å is comparable to the (μ-H)$_3$BH-bound borohydride ligands in **34** (2.64(2) Å).[24] The mean U−O bond distance of 2.18(6) Å is comparable to the U−O bond distance in **34** (2.167(9) Å).

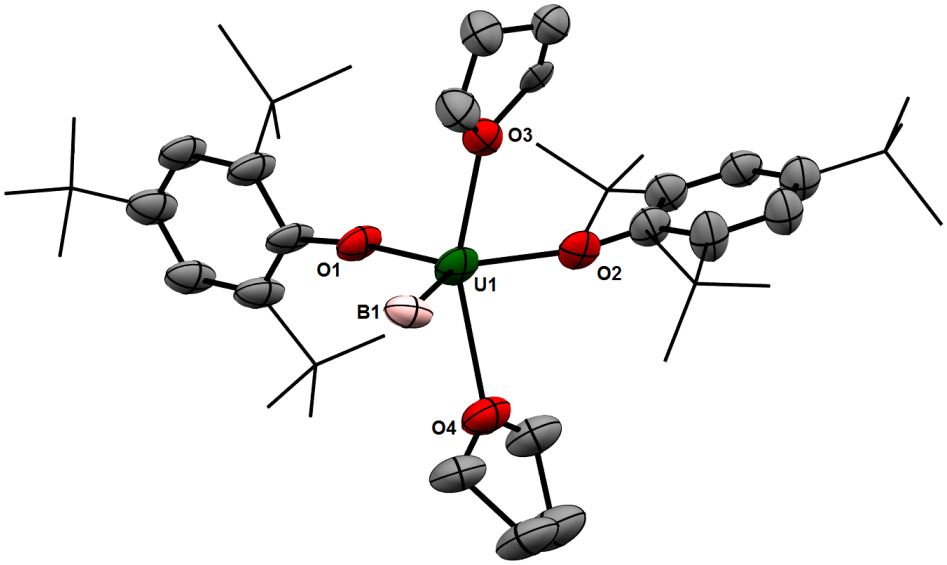

Figure 4.9 – Solid-state structure of **35**. The hydrogen atoms except those of the BH_4 ligand and another molecule of **31** are omitted, and the peripheral carbons are depicted in wireframe for clarity. Thermal ellipsoids displayed at 50% probability.

4.3 Chapter summary and conclusions

The uranium(III) boroxide complex **26** was synthesised and its reactivity towards CO and CO_2 investigated. It was found to reductively disproportionate CO_2 to the carbonate dianion CO_3^{2-}

and the bimetallic uranium(IV) carbonate-bridged complex **27** was isolated and structurally characterised. No reductive coupling of CO was observed with **26**, instead the homoleptic uranium(IV) boroxide complex **28** was obtained. The ligand environment is well suited to the formation of a mononuclear uranium(III) complex, however this complex is not suitable for the activation and reduction of carbon monoxide under reaction conditions employed in this chapter. Further work should include investigations of the reactivity of the carbonate product **27** to determine whether the reactive complex **26** can be regenerated.

A series of heteroleptic uranium(III) borohydride complexes have been synthesised containing carbocyclic (half-sandwich complex **29** and metallocene complex **31**), multidentate (pyrazolylborate complex **33**) and monodentate (aryloxide complex **34**) ligands. Attempted syntheses of bis(aryloxide) complexes **35** led to the isolation the tris(aryloxide) complexes $[U(OAr)_3(thf)]$ (Ar = ttbp, dtbp). The metallocene complex **31** was shown to react with the strong reductant KC_8 to produce an unidentified compound, and the phenol HOdtbp to yield a mixture of products. The stronger interaction between the uranium centre and the borohydride ligand compared to a halide ligand results in a more electron-rich metal centre with a tighter coordination sphere with lower coordination numbers when compared to iodide analogues. This is advantageous as vacant coordination sites are instrumental in uranium small molecule activation chemistry.

While the borohydride ligand was suitable in accommodating a range of ligands of varying hapticities and denticities, the bis(aryloxide) complex **35** was found to be prone to ligand rearrangement upon exposure to vacuum. The low-coordinate metal centre engendered upon removal of coordinated THF solvent is likely to be electronically deficient and oligomerise in the solid state. This suggests that while the range of coordination modes available to the borohydride ligand make it better suited to prevent ligand rearrangement of uranium(III) heteroleptic complexes than halides, it cannot stablise extremely low coordination numbers. Complexes **34** and **35** are rare examples of uranium(III) mono- and bis(aryloxide) complexes with *pseudo*-halide ligands. While prone to ligand rearrangement upon exposure to vacuum, the solution reactivity of **35** with unsaturated small molecules could be investigated. Furthermore, employing aryloxides ligands with larger substituents, such as the adamantyl-substituted ligand reported by Meyer and co-workers, could prevent ligand rearrangement to give the desired bis(aryloxide) complex.[51]

4.4 Bibliography

[1] P. L. Arnold, Z. R. Turner, R. M. Bellabarba and R. P. Tooze, *Chem. Sci.*, 2011, **2**, 77–79.

[2] A.-C. Schmidt, F. W. Heinemann, W. W. Lukens and K. Meyer, *J. Am. Chem. Soc.*, 2014, **136**, 11980–11993.

[3] F. G. N. Cloke and P. B. Hitchcock, *J. Am. Chem. Soc.*, 2002, **124**, 9352–3.

[4] O. T. Summerscales, F. G. N. Cloke, P. B. Hitchcock, J. C. Green and N. Hazari, *Science*, 2006, **311**, 829–831.

[5] O. T. Summerscales, F. G. N. Cloke, P. B. Hitchcock, J. C. Green and N. Hazari, *J. Am. Chem. Soc.*, 2006, **128**, 9602–9603.

[6] S. M. Mansell, N. Kaltsoyannis and P. L. Arnold, *J. Am. Chem. Soc.*, 2011, **133**, 9036–9051.

[7] A.-C. Schmidt, A. V. Nizovtsev, A. Scheurer, F. W. Heinemann and K. Meyer, *Chem. Commun.*, 2012, **48**, 8634–8636.

[8] S. M. Mansell, J. H. Farnaby, A. I. Germeroth and P. L. Arnold, *Organometallics*, 2013, **32**, 4214–4222.

[9] P. L. Arnold and Z. R. Turner, *Nat. Rev. Chem.*, 2017, **1**, 1–15.

[10] O. T. Summerscales, A. S. P. Frey, F. G. N. Cloke and P. B. Hitchcock, *Chem. Commun.*, 2008, 198–200.

[11] C. J. Inman, A. S. P. Frey, A. F. R. Kilpatrick, F. G. N. Cloke and S. M. Roe, *Organometallics*, 2017, **36**, 4539–4545.

[12] N. Tsoureas, L. Castro, A. F. R. Kilpatrick, F. G. N. Cloke and L. Maron, *Chem. Sci.*, 2014, **5**, 3777–3788.

[13] A.-C. Schmidt, F. W. Heinemann, C. E. Kefalidis, L. Maron, P. W. Roesky and K. Meyer, *Chem. - A Eur. J.*, 2014, **20**, 13501–13506.

[14] L. Castro, O. P. Lam, S. C. Bart, K. Meyer and L. Maron, *Organometallics*, 2010, **29**, 5504–5510.

[15] W. G. van der Sluys, A. P. Sattelberger, W. E. Streib and J. C. Huffman, *Polyhedron*, 1989, **8**, 1247–1249.

[16] L. R. Avens, C. J. Burns, R. J. Butcher, D. L. Clark, J. C. Gordon, A. R. Schake, B. L. Scott, J. G. Watkin and B. D. Zwick, *Organometallics*, 2000, **19**, 451–457.

[17] H. I. Schlesinger and H. C. Brown, *J. Am. Chem. Soc.*, 1953, **75**, 219–221.

[18] P. L. Arnold, C. J. Stevens, J. H. Farnaby, M. G. Gardiner, G. S. Nichol and J. B. Love, *J. Am. Chem. Soc.*, 2014, **136**, 10218–10221.

[19] I. Knopf and C. C. Cummins, *Organometallics*, 2015, **34**, 1601–1603.

[20] C. Lapinte, D. Catheline and D. Astruc, *Organometallics*, 1988, **7**, 1683–1691.

[21] J. McKinven, *Ph.D. thesis*, University of Edinburgh, 2016.

[22] C. P. Larch, F. G. N. Cloke and P. B. Hitchcock, *Chem. Commun.*, 2008, 82–84.

[23] F. Bonnet, M. Visseaux, D. Barbier-Baudry, A. Hafid, E. Vigier and M. M. Kubicki, *Inorg. Chem.*, 2004, **43**, 3682–3690.

[24] N. Edelstein, *Inorg. Chem.*, 1981, **20**, 297–299.

[25] J. M. Manriquez, P. J. Fagan, T. J. Marks, S. H. Vollmer, C. S. Day and V. W. Day, *J. Am. Chem. Soc.*, 1979, **101**, 5075–5078.

[26] P. J. Fagan, J. M. Manriquez, E. a. Maatta, A. M. Seyam and T. J. Marks, *J. Am. Chem. Soc.*, 1981, **103**, 6650–6667.

[27] W. J. Evans, K. A. Miller, S. A. Kozimor, J. W. Ziller, A. G. DiPasquale and A. L. Rheingold, *Organometallics*, 2007, **26**, 3568–3576.

[28] T. J. Marks and J. R. Kolb, *Chem. Rev.*, 1977, **77**, 263–293.

[29] E. J. Schelter, R. Wu, B. L. Scott, J. D. Thompson, D. E. Morris and J. L. Kiplinger, *Angew. Chem., Int. Ed.*, 2008, **47**, 2993–2996.

[30] C. R. Graves, B. L. Scott, D. E. Morris and J. L. Kiplinger, *Organometallics*, 2008, **27**, 3335–3337.

[31] C. Boisson, J. C. Berthet, M. Ephritikhine, M. Lance and M. Nierlich, *J. Organomet. Chem.*, 1997, **533**, 7–11.

[32] P. Gradoz, D. Baudry, M. Ephritikhine, M. Lance, M. Nierlich and J. Vigner, *J. Organomet. Chem.*, 1994, **466**, 107–118.

[33] A. Frey, F. Cloke and M. Coles, *Angew. Chem., Int. Ed.*, 2011, **50**, 6881–6883.

[34] D. Baudry, M. Ephritikhine, F. Nief, L. Ricard and F. Mathey, *Angew. Chem., Int. Ed.*, 1990, **29**, 1485–1486.

[35] S. R. Daly, P. M. B. Piccoli, A. J. Schultz, T. K. Todorova, L. Gagliardi and G. S. Girolami, *Angew. Chem., Int. Ed.*, 2010, **49**, 3379–3381.

[36] P. L. Diaconescu, P. L. Arnold, T. A. Baker, D. J. Mindiola and C. C. Cummins, *J. Am. Chem. Soc.*, 2000, **122**, 6108–6109.

[37] P. L. Diaconescu and C. C. Cummins, *J. Am. Chem. Soc.*, 2002, **124**, 7660–7661.

[38] W. J. Evans, S. A. Kozimor, J. W. Ziller and N. Kaltsoyannis, *J. Am. Chem. Soc.*, 2004, **126**, 14533–14547.

[39] M. J. Monreal, S. I. Khan, J. L. Kiplinger and P. L. Diaconescu, *Chem. Commun.*, 2011, **47**, 9119.

[40] D. Patel, F. Moro, J. McMaster, W. Lewis, A. J. Blake and S. T. Liddle, *Angew. Chem., Int. Ed.*, 2011, **50**, 10388–10392.

[41] P. L. Diaconescu and C. C. Cummins, *Inorg. Chem.*, 2012, **51**, 2902–2916.

[42] E. M. Matson, J. J. Kiernicki, P. E. Fanwick and S. C. Bart, *Eur. J. Inorg. Chem.*, 2016, **2016**, 2527–2533.

[43] U. Kilimann and F. T. Edelmann, *J. Organomet. Chem.*, 1993, **444**, C15–C17.

[44] H.-D. Amberger, F. T. Edelmann, J. Gottfriedsen, R. Herbst-Irmer, S. Jank, U. Kilimann, M. Noltemeyer, H. Reddmann and M. SchaÌĹfer, *Inorg. Chem.*, 2009, **48**, 760–772.

[45] J. H. Farnaby, F. G. N. Cloke, M. P. Coles, J. C. Green and G. Aitken, *C. R. Chim.*, 2010, **13**, 812–820.

[46] M. A. Antunes, G. M. Ferrence, Â. Domingos, R. McDonald, C. J. Burns, J. Takats and N. Marques, *Inorg. Chem.*, 2004, **43**, 6640–6643.

[47] L. Maria, Â. Domingos, A. Galvão, J. Ascenso and I. Santos, *Inorg. Chem.*, 2004, **43**, 6426–6434.

[48] I. Castro-Rodriguez and K. Meyer, *J. Am. Chem. Soc.*, 2005, **127**, 11242–11243.

[49] S. C. Bart, C. Anthon, F. W. Heinemann, E. Bill, N. M. Edelstein and K. Meyer, *J. Am. Chem. Soc.*, 2008, **130**, 12536–12546.

[50] S. M. Franke, B. L. Tran, F. W. Heinemann, W. Hieringer, D. J. Mindiola and K. Meyer, *Inorg. Chem.*, 2013, **52**, 10552–10558.

[51] C. J. Hoerger, H. S. La Pierre, L. Maron, A. Scheurer, F. W. Heinemann and K. Meyer, *Chem. Commun.*, 2016, **52**, 10854–10857.

Chapter 5

Uranium complexes of a diphenylphosphinoaryloxide ligand

5.1 Introduction

In contrast to transition metals, metallic bonds between two (or more) actinide centres have not been observed experimentally and metallic bonds with actinides and metals from other blocks of the periodic table are rare. A considerable amount of attention has been given to transition metal heterobimetallic complexes due to their potential in catalysis and small molecule activation chemistry.[1,2] The general understanding of metallic bonding between *f* elements and other metal cations increases as more examples are reported, facilitating the development of computational methods to model these unusual compounds.[3–5] The synthetic challenges associated with uranium heterobimetallic complexes had precluded a systematic study until our group reported the investigation of a family of uranium-group 10 complexes supported by a diphenylphosphinoaryloxide ligand (OAr^P).[6] The heterobimetallic complexes could be obtained conveniently by treatment of $IU(OAr^P)_3$ (**36**) with a group 10 metal tetra(phosphine) or bis(cyclooctadiene) complex. The robust complexes feature the shortest uranium-metal bonds reported to date and electrochemical investigations suggested that the uranium-metal bond is strongest for Ni and decreases down the group, which is supported by theoretical calculations.

This chapter describes the extension of the heterobimetallic chemistry to group 9 and the use of **36** and its cerium analogue in lactide ring opening polymerisation (ROP). The work presented in this chapter was carried out with Dr. Johann A. Hlina (synthesis and characterisation, Sections 5.2 and 5.3), Dr. James R. Pankhurst and Prof. Jason B. Love (electrochemistry, Section 5.2), and Prof. Michael P. Shaver and Dr. Fern Sinclair (polymerisation and kinetics, Section 5.3).

5.2 Uranium-rhodium bimetallic complexes

5.2.1 Synthesis and characterisation of $[I_2U(OAr^P)RhO]_2$

As for the uranium group 10 bimetallic complexes, the synthesis of a uranium rhodium bimetallic complex was envisaged by ligand displacement of a rhodium-centered labile ligand. In this case, the displacement of a labile olefin by the phosphine was investigated.

Addition of a toluene solution of **36** to a stirred toluene solution of $[(cod)RhI]_2$ provided an orange solution, which produced green crystals of $[I_2U(OAr^P)RhO]_2$ (**37**) upon standing for 18 hours. The crystalline material was isolated in 18% yield after decantation of the mother solution. Complex **37** was characterised by ^{1}H and ^{31}P NMR and UV/vis-NIR spectroscopies, single-crystal XRD and elemental analysis. Complex **37** is insoluble in benzene or THF and only sparingly soluble in dichloromethane, in which it shows significant decomposition within hours. Analysis of the supernatant by ^{31}P NMR spectroscopy indicated the presence of two other products with ^{31}P-^{103}Rh coupling, providing a reason for the low isolated yield of **37**.

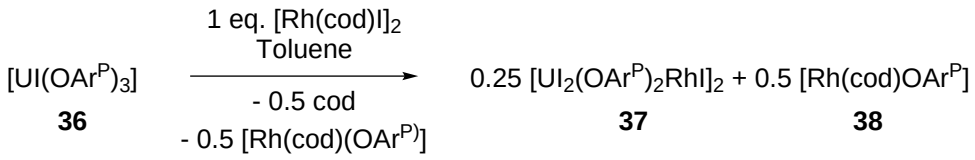

Scheme 5.1 – Synthesis of compounds **37** and the monometallic rhodium(I) by-product, **38**.

The ^{1}H NMR spectrum of **37** in CD_2Cl_2 consists of seven resonances spanning 65 ppm. The phenolate resonances range 26.78 to 53.40 ppm and the phenyl proton resonances range -12.84 to -8.83 ppm. The phenyl resonances of the diphenylphosphine group under-integrate, which has previously been noted for the uranium-group 10 analogues.[6] The ^{31}P NMR spectrum consists of a broad doublet centered at 111.6 ppm with a $^1J_{P-Rh}$ coupling constant of 145 Hz, comparable to other rhodium triarylphosphine complexes.[7]

The UV-Vis/NIR spectrum of **37** in pyridine shows a broad absorption at 312 nm with an extinction coefficient $\varepsilon = 2.8 \times 10^4$ M^{-1}cm^{-1} which can be attributed to the aromatic ligand system.[8] Additionally, a broad shoulder at 510 nm can be seen with extinction coefficient $\varepsilon = 1.2 \times 10^4$ M^{-1}cm^{-1}, reminiscent of the heterobimetallic uranium-group 10 complexes.[6] The NIR region shows weak features suggestive of U(IV) f-f transitions, however these cannot be unambiguously assigned as metal-to-metal charge transfer bands.

Crystalline **37** suitable for single-crystal XRD analysis was obtained from the reaction

mixture upon standing for 18 hours. The complex is dimeric in the solid state, and shows each trigonal-bipyramidal uranium centre to be coordinated to two iodo ligands, two aryloxide ligands and the rhodium centre (Figure 5.1). The rhodium centre is bound to two aryloxides by the phosphine group and two iodo ligands which bridge to another rhodium centre. The U−O and U−I bond distances of 2.127(2) and 2.9899(4) respectively are within range of those observed for uranium-group 10 metal complexes featuring the same ligand.[6] The Rh−I and Rh−P bond distances of 2.7036(4) and 2.2883(8)Å are comparable to those of the limited examples of iodo bis(triorganophosphine)rhodium(I) dimers.[9,10] The uranium(IV)-rhodium(I) intermetallic distance is 2.7601(5) Å, which is significantly longer than that of the palladium(0) analogue (U-Pd: 2.686(2) – 2.694(1)).[6]

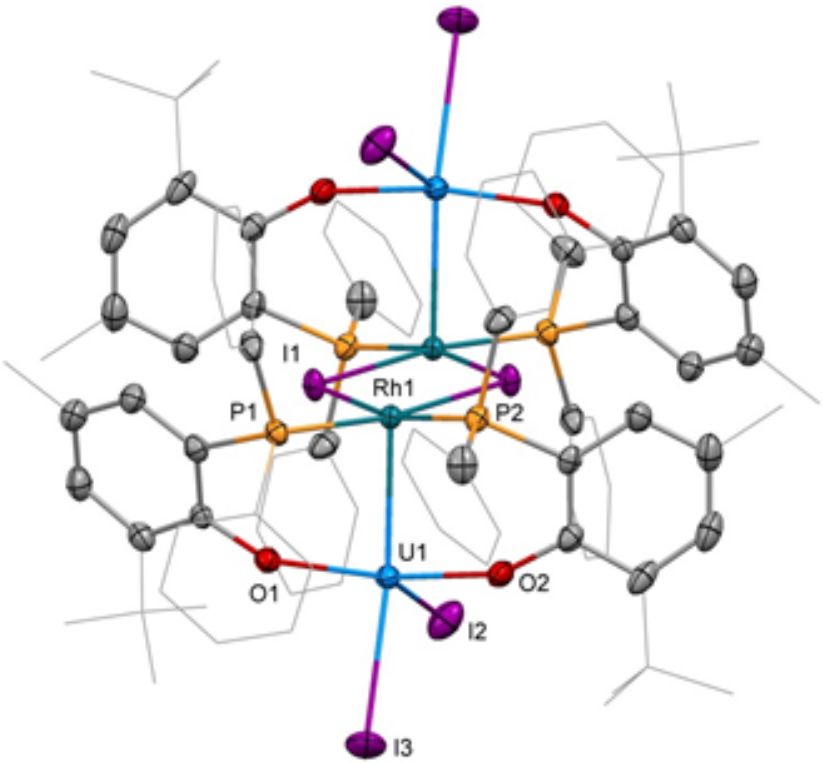

Figure 5.1 – Molecular structure of **37**. Solvent molecules and hydrogen atoms are omitted, and peripheral carbon atoms are depicted as wireframe for clarity. Thermal ellipsoids drawn at 50% probability.

Synthesis of (cod)RhOAr^{P}

The formation of **37** rather than the expected complex [IU(OAr^{P})$_3$RhI] must occur by metathesis of a uranium-centered aryloxide ligand for a rhodium-based iodo ligand, suggesting the reaction byproduct to be the rhodium(I) phosphino aryloxide, [Rh(cod)(OAr^{P})] (**38**). The synthesis of

38 was undertaken to prove its formation during the synthesis of **37**. A reaction between $KOAr^P$ and $[(cod)RhCl]_2$ in toluene furnished an orange solution from which **38** was obtained as an orange powder from work-up in hexanes in 86% yield. Compound **38** was characterised by ^1H, ^{31}P NMR and UV-vis/NIR spectroscopies, and single-crystal XRD and elemental analysis.

The diamagnetic ^1H NMR spectrum of **38** contains the expected resonances and multiplicity for a cyclooctadiene ligand and a phosphino aryloxide ligand. The ^{31}P NMR spectrum contains a doublet at 33.5 ppm with $^1J_{P-Rh}$ = 164 Hz, which is comparable to that of **37** and other rhodium triarylphosphine complexes.[7]

Crystals of **38** suitable for single-crystal XRD analysis were grown from Et_2O solutions of **38**. The rhodium centre in **38** exhibits square planar geometry (Figure 5.2). The Rh−O and Rh−P distances are 2.037(1) and 2.2676(5) Å respectively, and the cod ligand Rh−C distances range 2.105(2)2.216(2) Å, all of which are comparable to related complexes.[7,11,12]

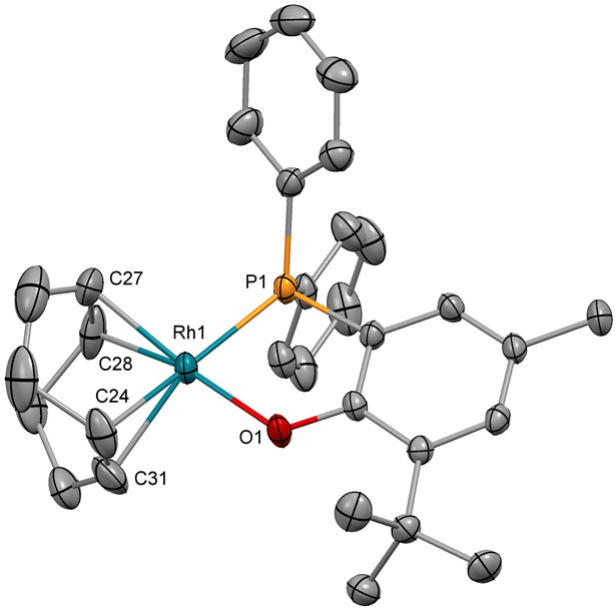

Figure 5.2 – Solid-state structure of **38**. Hydrogen atoms are omitted for clarity and thermal ellipsoids drawn at 50% probability.

5.2.2 Synthesis and characterisation of $[IU(OAr^P)_3RhI$

Due to the formation of the tetrametallic complex **37** when $[(cod)RhI]_2$ was used as a starting material, the use of weakly coordinating cyclooctene as a labile olefin ligand to install the rhodium centre was investigated.

The iodo rhodium(I) bis(cyclooctene) reagent was prepared *in situ* by reaction of $[(coe)_2RhCl]_2$ with iodotrimethylsilane in toluene, and a toluene solution of **36** was added.[13] The result-

ing green solution was heated to 80 °C for one hour to provide UI(μ-I)(OAr^P)$_3$RhI (**39**) as green crystals after workup. Complex **39** was characterised by ^{1}H, ^{31}P NMR and UV-vis/NIR spectroscopies, and single-crystal XRD and elemental analysis.

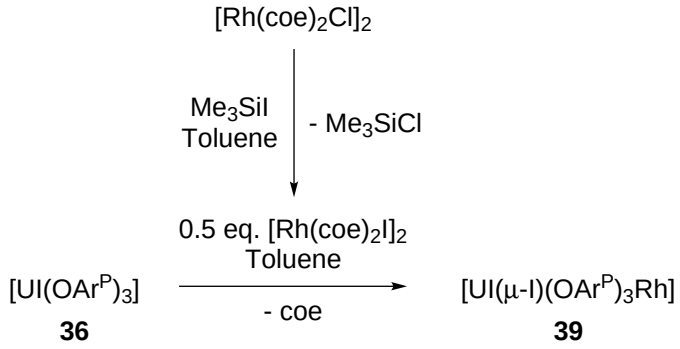

Scheme 5.2 – Synthesis of compound **39**

The ^{1}H NMR spectrum of **39** in C_6D_6 consists of eight resonances spanning 65 ppm and exhibit two resonances for the phenolate ligand in a 2:1 ratio, consistent with a square planar rhodium centre. The resonances for the two aryloxide ligands range from 18.93 to 41.97 ppm and from -19.27 to -4.94 ppm respectively. The phenyl resonances of the diphenylphosphine group could not be detected, possibly due to paramagnetic signal broadenning and possible fluxional behaviour. The ^{31}P NMR spectrum consists of a broad doublet centered at -227.4 ppm with a $^1J_{P-Rh}$ coupling constant of 160 Hz, which is comparable to that of **37**, **38** and other rhodium triarylphosphine complexes.[7] The other ^{31}P resonance could not be located at 300 K.

Crystalline material suitable for single-crystal XRD analysis was obtained from concentrated toluene solutions of **39**. The solid-state structure consists of a monomeric complex with a square planar rhodium centre and the uranium centre in a distorted octahedral geometry (Figure 5.3). The rhodium centre is coordinated to three phosphines and one iodo ligand, which bridges to the uranium centre. In addition to the bridging iodine atom, the uranium centre is coordinated to the three aryloxides on the equatorial plane, and the rhodium centre and an iodo ligand on the axial plane. The U$-$O bond distances which range 2.129(4)2.156(3) Å are comparable to those exhibited by **37** and the group 10 analogues.[6] The terminal U$-$I bond distance is also comparable to those complexes at 3.0428(5) Å, however the U$-$I distance of the bridging iodine atom is elongated, at 3.2264(2) Å. The U$-$Rh distance is 2.7630(5) Å, which is very similar to that of **37**, and longer than that of the palladium(0) analogue (UPd: 2.686(2)âĂŞ 2.694(1)).[6]

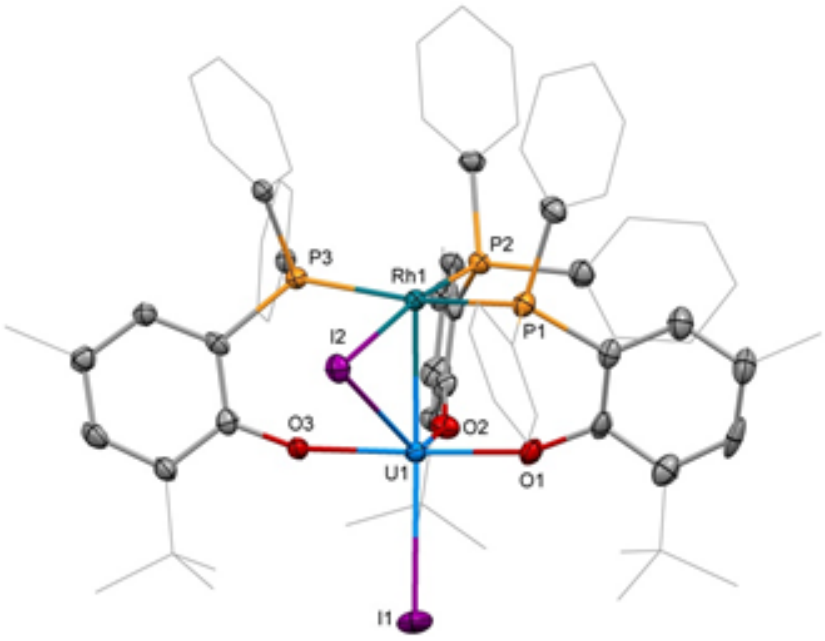

Figure 5.3 – Molecular structure of **39**. Solvent molecules and hydrogen atoms are omitted, and peripheral carbon atoms are depicted as wireframe, for clarity. Thermal ellipsoids drawn at 50% probability.

5.2.3 Electrochemsitry of $[I_2U(OAr^P)RhO]_2$, $[Rh(cod)OAr^P]$ and $IU(OAr^P)_3RhI$

The monometallic complex **36** undergoes a single irreversible reduction at $E_p^c - 2.87$ V *versus* ferrocene, assignable to the U(IV)/U(III) redox couple.[6] Investigations of the electrochemistry of monometallic complex **38** by cyclic voltammetry showed **38** to be completely inactive in the electrochemical window provided by CH_2Cl_2 / $[^nBu_4N][BPh_4]$.

The cyclic voltammogram of tetrametallic complex **37** showed an irreversible reduction at the edge of the electrochemical window at $E_p^c - 2.78$ V (Figure 5.4). The similarity in the CV of **37** and **36** indicates the reduction process to be uranium centered, suggesting that the Rh centre has no electronic influence on the proximal uranium centre. Despite the short uranium-rhodium separation of 2.7601(5) Å, the orbital interaction between the metal centres is minimal and the subtle change in U(IV)/U(III) reduction potential can be attributed to the change in coordination sphere about the uranium centre. The solution-phase behaviour of **37** suggests dissociation at room temperature, but the impact of such behaviour on the intermetallic interaction is unclear.

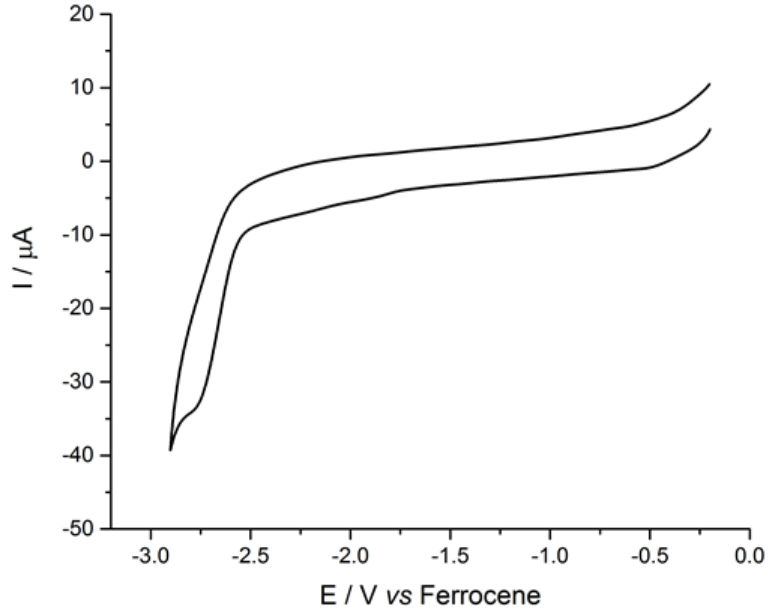

Figure 5.4 – Cyclic voltammogram of 0.1 M solution of **37**, measured at at 100 mVs^{-1} showing the full electrochemical window provided by CH_2Cl_2 / $[nBu_4N][BPh_4]$.

The CV of **39** on the other hand displays a *quasi*-reversible, one-electron oxidation process at $E_p^c - 0.37$ V and an irreversible two-electron process at $E_p^c - 2.49$ V (Figure 5.5). The concerted multielectron reduction process is likely to be transition-metal based, as actinide centres undergo single-electron redox processes. The CV of **39** is reminiscent to that of the uranium-group 10 complexes in which the reduction band was ascribed to a two-electron population of a transition-metal based orbital. This was hypothesised from calculations which suggested the LUMO to be a metal-metal antibonding orbital. This assignment suggests that orbital interactions between the metal centres exist only in **39**, depsite the shorter intermetallic separation in **37**.

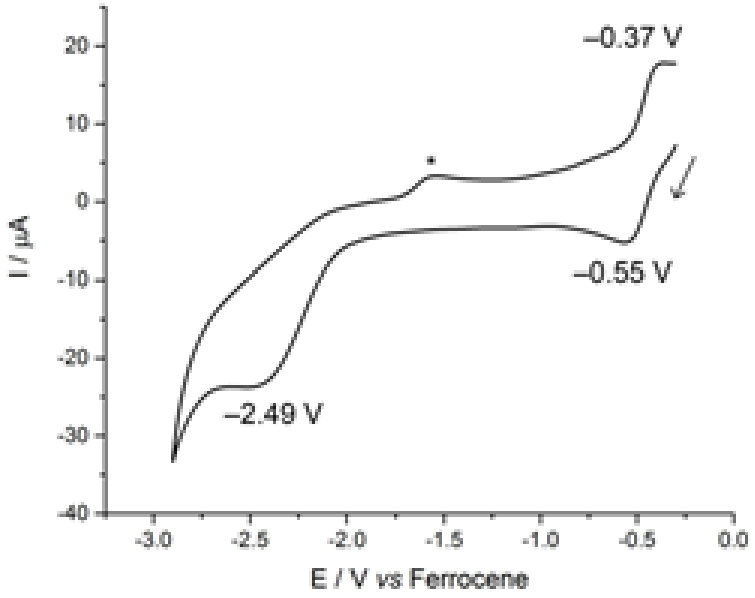

Figure 5.5 – Cyclic voltammogram of **39**, measured at 100 mVs^{-1} in 0.1 M CH_2Cl_2 / $[nBu_4N][BPh_4]$. The asterisk denotes a decomposition product that is formed only after the irreversible reduction.

5.3 Ring opening polymerisation catalysis with uranium and cerium complexes

Poly(lactic acid) (PLA) is a common biodegradable polymer which is increasingly attractive as an alternative to plastics obtained from non-renewable monomers. A range of factors affect the physical properties of PLA, but stereocontrol of monomer opening has the most drastic influence. Synthesising catalysts which impart a degree of control on the tacticity of lactide ring-opening polymerisation (ROP) is a thriving area of research, which bridges the field of inorganic and materials chemistry.

5.3.1 Synthesis and characterisation of $Me_3SiU(OAr^P)_3$

An initiator group, in the form of an alkoxide or alkyl, is necessary on the precatalyst to initiate polymerisation. To this end, the trimethylsiloxide complex $Me_3SiU(OAr^P)_3$ (**40**). Addition of THF to a Schlenk flask containing **36** and equimolar $NaOSiMe_3$ provided a green mixture which was stirred for 18 hours. The microcrystalline green $Me_3SiU(OAr^P)_3$ (**40**) was obtained from toluene workup in 63% yield. Compound **40** was characterised by ^1H NMR spectroscopy and elemental analysis.

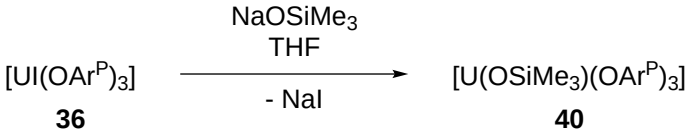

Scheme 5.3 – Synthesis of compounds **40**.

The ^{1}H, ^{29}Si and ^{31}P NMR spectra of **40** contain no observable resonances at ambient temperature, which can be attributed to highly fluxional behaviour as exhibited by the parent compound **36**.[6] Variable-temperature ^{1}H NMR experiments in the range $300-370$ K reveal broad paramagnetically shifted resonances, however their unambiguous assignment was impossible. Despite our best efforts, crystalline material suitable for single-crystal XRD analysis could not be obtained.

5.3.2 Synthesis and characterisation of U(OAr^{P})$_4$

A brown suspension of $UI_4(OEt_2)_2$ and KOArP in THF was heated to reflux for 2h to give a green suspension, from which a green solid was isolated from toluene workup. Recrystallisation from toluene furnished dark green crystals of U(OAr^{P})$_4$ (**41**) in 72% yield. The homoleptic complex **41** was characterised by ^{1}H and ^{31}P NMR spectroscopy, single-crystal XRD and elemental analysis.

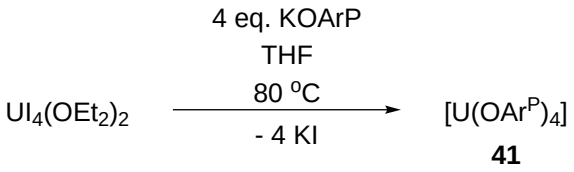

Scheme 5.4 – Synthesis of compounds **41**.

In contrast to **40**, the paramagnetic ^{1}H NMR spectrum of **41** exhibits sharp resonances which range from 1.38 to 11.73 ppm. No resonances could be detected in the ^{31}P NMR spectrum of **41**, which could be ascribed to broadening caused by an interaction between the paramagnetic uranium centre and the ligand P atom in solution.

Crystals suitable for single-crystal XRD analysis were obtained from the cooling of the reaction mixture. The four coordinate uranium centre is in tetrahedral geometry (Figure 5.6). The U−O bond distance of 2.193 Å is comparable to that of other uranium complexes of the OAr^{P} ligand reported in the literature and within this chapter.[6] The U−P distance is longer

than in the iodo tris(aryloxide) complex **36** (3.275 *versus* 3.049(1) Å) which can be ascribed to the greater steric encumbrance imposed by the additional diphenylphosphinoaryloxide ligand.

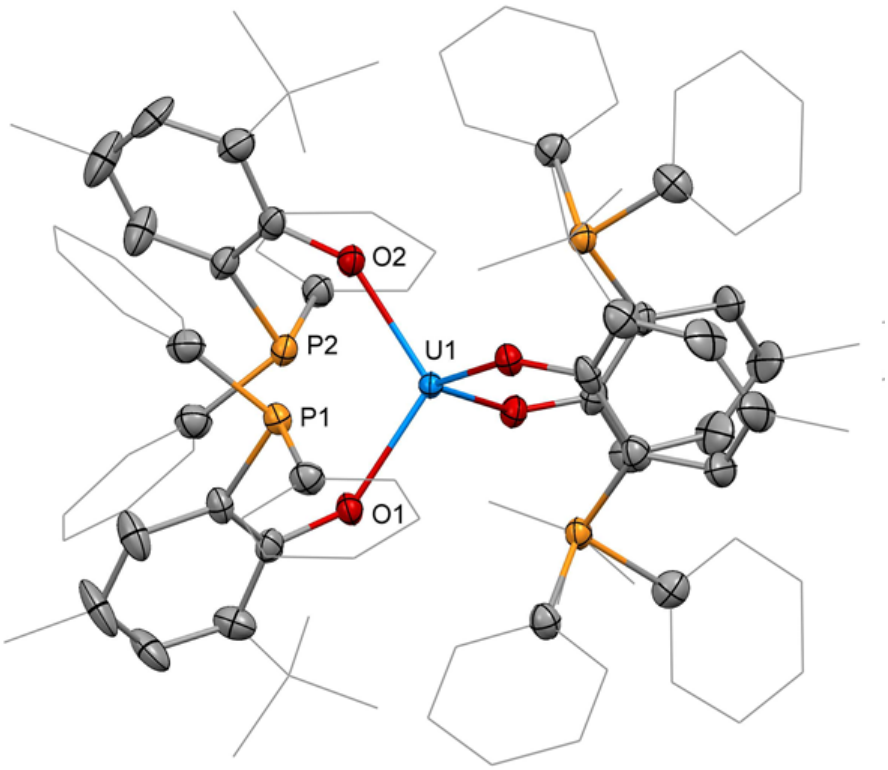

Figure 5.6 – Solid-state structure of **41**. Solvent molecules and hydrogen atoms are omitted, and peripheral carbon atoms are depicted as wireframe, for clarity. Thermal ellipsoids drawn at 50% probability.

5.3.3 Synthesis and characterisation of $Me_3SiOCe(OAr^P)_3$

Addition of toluene to a mixture of $HOAr^P$ and CeN''_3 provided a clear yellow solution which was stirred for 2 hours, after which time the volatiles were removed under reduced pressure. The resulting yellow residue was redissolved in toluene followed by the addition of a solution of $NaOSiMe_3$ in toluene and stirred for 18 hours. A toluene solution of Ph_3CCl was added to the yellow solution, resulting in an immediate change to a dark brown mixture which was allowed to stir for 5 hours. The volatiles were removed under reduced pressure and the dark brown residue extracted with hexane. Dark brown crystals of $Me_3SiCe(OAr^P)_3$ (**42**) were obtained from concentrated hexane solutions of **42** in 96% yield. Complex **42** was characterised by ^1H and ^{31}P NMR spectroscopy, single-crystal XRD and elemental analysis.

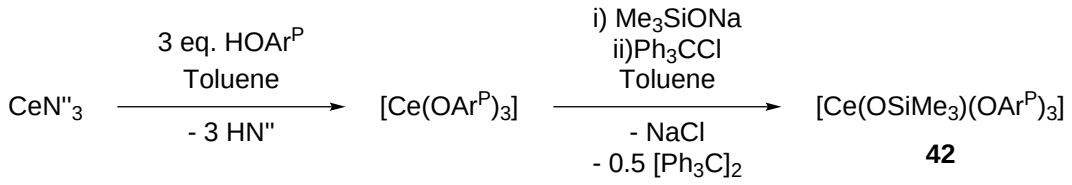

Scheme 5.5 – Synthesis of compounds **42**.

The ^{1}H NMR spectrum of **42** shows fluxional behaviour with strongly broadened resonances for the aromatic and the *tert*-butyl groups protons at 300 K, which become sharper with increase in temperature up to 370 K. The ^{31}P NMR spectrum exhibits similar behaviour, with three broad overlapping resonances at −23.6, 12.2 and 16.4 ppm at 300 K which coalesce to a single resonance at 16.23 ppm at elevated temperatures. The ^{29}Si NMR spectrum contains a single resonance for the trimethylsiloxide ligand at 6.1 ppm.

Crystalline material suitable for single-crystal XRD analysis were obtained from hexane concentrated solutions of **42** in hexanes. The seven-coordinate cerium centre is coordinated to three O- and P-bound OAr^{P} ligands and the trimethylsilanolate ligand (Figure 5.7). The aryloxide Ce−O distance of 2.175(2) Å is longer than that for the siloxide ligand at 2.067(2) Å. The broad range in the Ce−P distances, which span from 3.1575(7) to 3.307(1) Å, is likely to be a consequence of the minimisation of steric interactions between the more bulky ligands at the expense of the weak and labile Ce−P interaction.

5.3.4 Lactide polymerisation

The number of reports on actinide complexes used as initiators for lactide ROP are not extensive, with only four uranium catalysts reported thus far (Scheme 5.6).[14,15] Eisen and co-workers reported that the uranium(IV) metallocene complex $\mathbf{C_1}$ initiates polymerisation at 70 °C, whereas the tris(amido) uranium(IV) cation **C2** is active at room temperature.[14] The difference in activity is likely caused by the more accessible metal centre in **C2**, which facilitates monomer coordination. The diamidoether complexes **C3** and **C4** reported by Carpentier and Leznoff initiate the polymerisation of L-lactide at room temperature.[15] Catalyst **C3** was found to produce a heterotactic polymer with P_r of 0.73. P_r denotes the probability of racemic linkages in a polymer. A value of P_r close to 1 suggests a higher incidence of racemic linkages in the polymer.

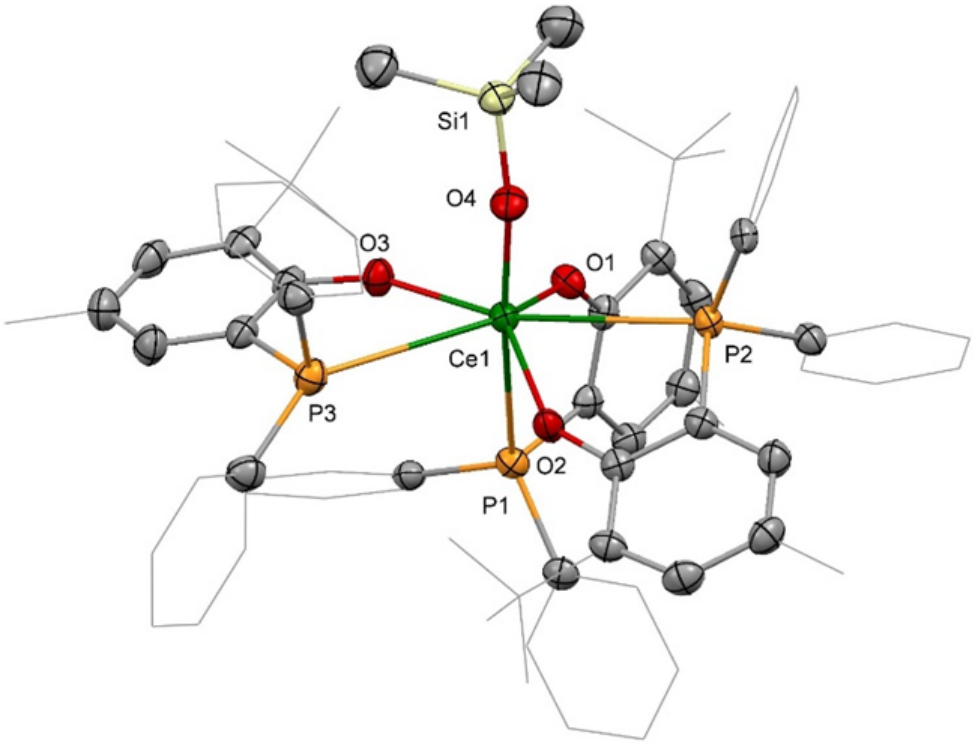

Figure 5.7 – Solid-state structure of **42**. Solvent molecules and hydrogen atoms are omitted, and peripheral carbon atoms are depicted as wireframe, for clarity. Thermal ellipsoids drawn at 50% probability.

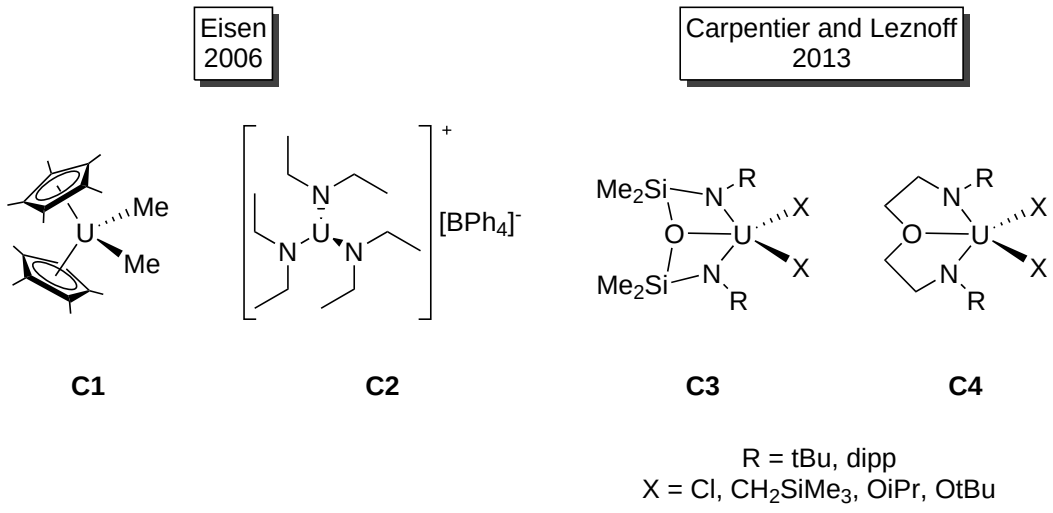

Scheme 5.6 – Reported uranium complexes shown to initiate lactide ring opening polymerisation.

The experimental conditions used to investigate the activity of **40**, **42** and **41** are summarised in Scheme 5.7 and the experimental results obtained by Dr. Fern Sinclair and Prof. Michael

Shaver are summarised in the following sections.

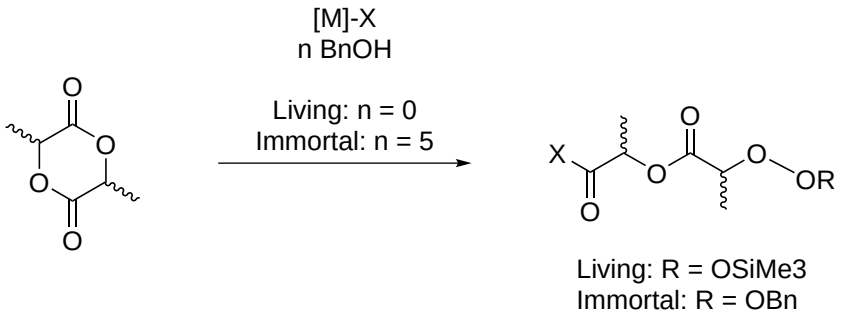

Scheme 5.7 – Conditions investigated for the polymerisation of lactide by **40**, **42** and **41**.

Living conditions

Both complexes **40** and **42** were found to be active catalyst for L-Lactide ROP, using the siloxide ligand as the polymerisation initiator group. Molecular weights obtained from GPC are in good agreement to the theoretical molecular weights, evidenced by monodisperse dispersities ($Đ$). A higher degree of control is obtained with **40** compared to **42**, as shown by narrower $Đ$s. The control is maintained for **40** in toluene, benzene and dichloroethane (DCE), but not for **42** where lower conversions are obtained and control is lost for polymerisation carried out in DCE. This could be a result of the more Lewis acidic nature of the Ce(IV) ion, which may incur solvent decomposition. Polymerisation is greatly slowed down and poorly controlled when the homoleptic compound **41** is used, giving rise to polymers with molecular weights twice as large as predicted from conversion, thus denoting the importance of the siloxide initiator group.

Installing a Ni(0) ion in the tris(phosphine) cavity of **40** dramatically alters the catalyst behaviour, shutting down all polymerisation activity. The change in activity could be ascribed to *trans* coordination of the Ni centre to the initiator group, causing a mutual strengthening of two *trans*-coordinated ligands by the Inverse *Trans* Influence (ITI) that occurs in *f*-block complexes. The strengthening of the siloxide U−O bond due to the ITI may be such that protonolysis or esterification of the activator group is no longer possible. Another possibility, is that Ni−P bonds in the heterobimetallic complex are stronger than in the parent compound **40**, and the loss of hemilability in the OAr^P ligand may hamper monomer access to the catalyst active site by rigidifying the complex. Percent buried volume calculations for **36**, the heterobimetallic complex $[UI(OAr^P)_3Ni]$ and **42** indicate little difference in accessibility of the initiator group.

Immortal conditions

Polymerisation under immortal conditions were also conducted for **40** and **42** with a ratio of monomer:catalyst:BnOH of 200:1:5, using BnOH as a chain transfer reagent to decrease catalyst loading. Both catalysts retained polymerisation control under immortal conditions and the reaction rates varied greatly. Kinetic studies were carried out by monitoring *in situ* reactions of catalysts **40** and **42** by ^{1}H NMR spectroscopy. The complete polymerisation of L-lactide occurs after 160 and 600 minutes in the absence of BnOH for **40** and **42** respectively. This difference may be explained by the relatively higher affinity of the P donor for U over Ce, which will result in a more robust coordination environment about the metal centre as the P donors are not being out competed by lactide monomers, causing non-productive coordination. Once under immortal conditions, the polymerisation rates are vastly increased and are complete in 50 and 15 minutes for **40** and CeOArP respectively. The intriguing reversal in catalytic activity suggests that the BnOH may have displaced both siloxide and phenoxide ligands, resulting in a more accessible Lewis acidic cerium(IV) centre allowing facile productive monomer coordination.

The BnOH-promoted ligand displacement is supported by ^{31}P NMR spectroscopy, with the growth of a $HOAr^{P}$ resonance upon addition of five equivalents of BnOH to a solution of **42**. The displacement of aryloxide ligands is secondary to the protonolysis of the siloxide ligand, as evidenced by the formation of $HOSiMe_3$ by ^{1}H NMR spectroscopy. Additionally, the polymerisation rates and control for catalyst **41** are also improved under immortal conditions, suggesting once again ligand displacement and the formation of a new active complex.

Oligomers of L-lactide using **42** under immortal conditions in a 300:1:5 molar ratio were prepared for end-group analysis. The PLA chain was found to be capped with a hydroxyl group at one end and a OBn group at the other by ^{1}H and 2D (COSY, HSQC, HMBC) NMR spectroscopy, which was confirmed by MALDI mass spectrometry and indicates a coordination insertion mechanism (Scheme 5.8).

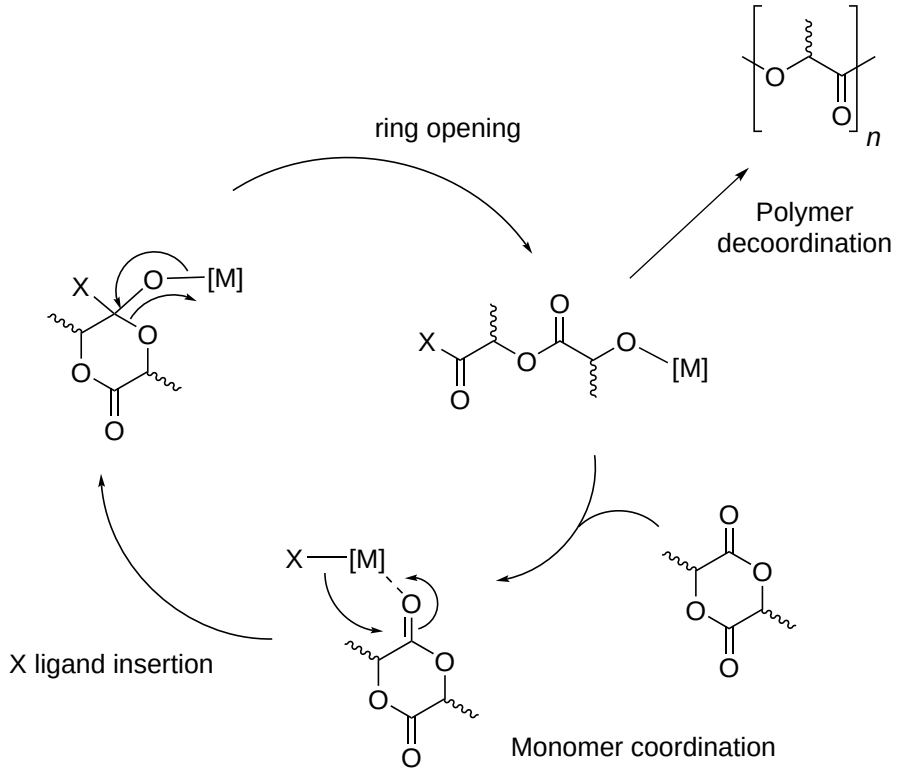

Scheme 5.8 – General coordination and insertion mechanism in lactide ring opening polymerisation.

rac-lactide polymerisation

The influence of catalysts **40** and **42** on the stereoselectivity of polymerisation was examined using *rac*-lactide. Complex **40** promotes the formation of heterotactic PLA with P_r = 0.79 whereas no stereocontrol is achieved with **42**. The rigidity of the coordination environment enforced by the relatively strong U− interaction induces chain end control stereoselectivity. For cerium, the more flexible coordination environment resulting from weaker M−P bonds causes a loss of chain end influence, producing atactic PLA. Heterotacticity is decreased for **40** under immortal conditions, which is consistent the chain exchange observed previously. The tacticity is also influenced by reaction conditions, with the best results achieved in DCE, likely due to the higher solubility of *rac*-lactide. Increase in temperature negatively impacts heterotacticity, with P_r = 0.58 at 90 °C. As discussed in Section 5.3.4, the highest P_r reported for a uranium catalyst thus far is of 0.79 achieved by **C3**,[15] making compound **40**, to the best of our knowledge, the uranium catalyst which offers the greatest control over lactide ROP stereoselectivity.

5.4 Target synthesis of $U(OAr^P)_3$

Reaction of UN''_3 with $HOAr^P$ in a range of solvents invariably leads to the formation of the uranium(IV) homoleptic complex **41**. On one occasion, reaction with UN''_3 containing a *circa* 10% NaN'' impurity, orange crystals of $Na[U(OAr^P)_2(\kappa^2O{:}P\text{-}OAr^{P-})(C_6H_5)]$ ($OArP^-$ = OC_6H_2-6-^{t}Bu-4-Me-2-PPh, **43**).

The seven-coordinate uranium centre is in distorted pentagonal bipyramidal geometry with two coordinated diphenylphosphinoaryloxide ligands. The two remaining ligands are a phenyl group and a bidentate phenylphosphidoaryloxide ligand, suggestive of a oxidative addition process. The axial plane is occupied by the phenyl ligand and a phosphine tether of the OAr^P ligand, while the remaining aryloxide group occupies the equatorial plane along with another OAr^P ligand and the dianionic OAr^{P-} ligand. The anionic charge on the uranium centre is balanced by a sodium cation which bridge to another molecule giving rise to a dimeric structure. The sodium cations are coordinating η^4 to the OCCP fragment on the OAr^{P-} ligand, η^2 to the aryl ligand and η^6 to the phenyl ring of the neighbouring molecules OAr^{P-} ligand. The U-P bond distances are 3.2717(9) and 3.1041(9) Å for the equatorial and axial phosphines which are much longer than the phosphido ligand at 2.9219(9) Å.

The neutral U−P distances are comparable to those exhibited by related uranium(IV) complexes employing the OAr^P ligand. The U−P distance of the dianionic aryloxide phosphide ligand is long when compared to reported examples of uranium phosphides, which typically range between 2.666 to 2.883 Å. The U−P distances in the uranium Zintl complex reported by Liddle and co-workers range from 2.948(2) to 3.030(2) Å which is comparable to that in exhibited by **43**. The long U−P bond distance in the Zintl complex was ascribed by the authors to the distribution of the negative charge over seven P atoms and to the considerable steric demand imposed by the supporting tris(amido) ligand. The metal centre in **43** is quite sterically encumbered which could explain the long U−P distance. The aryloxide U−O distances are unremarkable for uranium(IV) aryloxide complexes, ranging from 2.167(2) to 2.194(2) Å. The phenyl ligand U−C distance is 2.502(4) Å. Only one other uranium phenyl complex has been structurally characterised $(C_5Me_5)_2$(hpp)UPh (hpp = 1,3,4,6,7,8-hexahydro-2*H*-pyrimido[1,2-α]pyrimidinato) exhibits a comparable U−C distance of 2.513(2) Å. Liddle and co-workers have also reported uranium(III) mediated E-Ph bond cleavage resulting in the formation of an imido aryl bridged dimer. The U−C bond distance in the example reported by Liddle and co-workers is notably longer than in **43**, ranging from 2.548(8) and 2.728(8) Å.

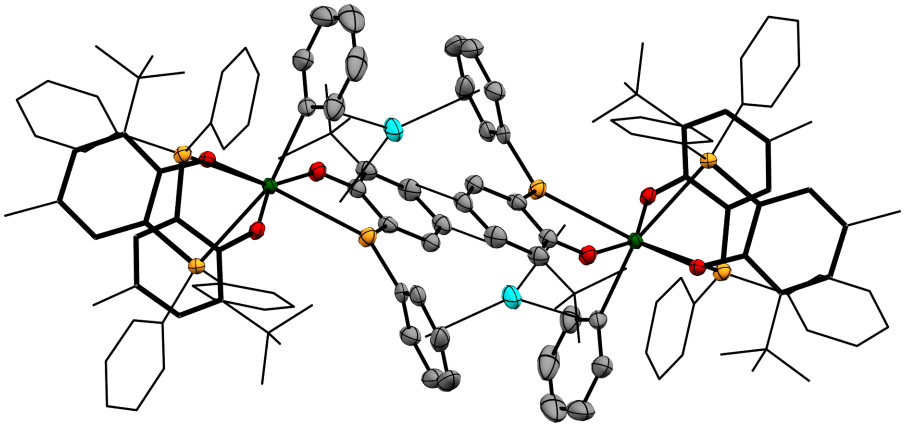

Figure 5.8 – Solid-state structure of **43** with 50% probability ellipsoids.The hydrogen atoms and lattice solvent are omitted for clarity. The ligand *tert*-butyl, methyl and diphenylphosphino groups are represented in wireframe. The OAr^P ligand frame is represented in capped sticks and the phosphidoaryloxide ligand is represented as ellipsoids for clarity.

Alkali metals have been shown to induce P−C bond cleavage in triarylphosphines by one-electron reduction to give the corresponding alkali metal phosphide and coupled diaryl.[16] A similar pathway is likely occur for the formation of **43** proceeding *via* a reactive uranium(III) complex.

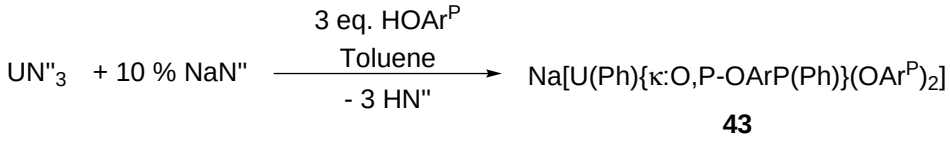

Scheme 5.9 – Synthesis of compound **43**.

5.5 Chapter summary and conclusions

Two new complexes containing a uranium-rhodium bond were synthesised. The solid state uranium-rhodium distances are comparable in both **37** and **39** and electrochemical experiments suggest that the uranium-rhodium bond is weak in **39** and possibly not retained in solution for **37**.

Two uranium complexes and one cerium complex were synthesised and their behaviour as initiators for lactide ROP catalysis was investigated under living and immortal conditions. All three complexes were found to be active, with **40** being the fastest. Under immortal conditions,

42 was the fastest catalyst. Furthermore, **40** was found to produce heterotactic PLA with *rac*-lactide with $P_r = 0.79$, suggesting **40** to be the most stereoselective lactide ROP uranium catalyst reported to date.

The synthesis of a uranium(III) tris(phosphinoaryloxide) complex was attempted, which provided **41**. On one occasion, **43** was obtained, which contains a rare unsupported uranium-phenyl, as well as a uranium-phosphide bond. These reactions suggest that the $HOAr^P$ ligand frame is not well suited to uranium(III), resulting in disproportionation to uranium(IV) and depositing uranium metal.

5.6 Bibliography

[1] B. G. Cooper, J. W. Napoline and C. M. Thomas, *Catal. Rev. - Sci. Eng.*, 2012, **54**, 1–40.

[2] P. Buchwalter, J. Rosé and P. Braunstein, *Chem. Rev.*, 2015, **115**, 28–126.

[3] S. T. Liddle and D. P. Mills, *Dalton Trans.*, 2009, **9226**, 5592.

[4] D. Patel and S. T. Liddle, *Rev. Inorg. Chem.*, 2012, **32**, 1–22.

[5] B. Oelkers, M. V. Butovskii and R. Kempe, *Chem. - A Eur. J.*, 2012, **18**, 13566–13579.

[6] J. A. Hlina, J. R. Pankhurst, N. Kaltsoyannis and P. L. Arnold, *J. Am. Chem. Soc.*, 2016, **138**, 3333–3345.

[7] Y. Nishihara, K. Nara, Y. Nishide and K. Osakada, *Dalton Trans.*, 2004, 1366.

[8] C. Janiak, A.-C. Chamayou, A. K. M. Royhan Uddin, M. Uddin, K. S. Hagen and M. Enamullah, *Dalton Trans.*, 2009, **9226**, 3698.

[9] G. L. Williams, C. M. Parks, C. R. Smith, H. Adams, A. Haynes, A. J. H. M. Meijer, G. J. Sunley and S. Gaemers, *Organometallics*, 2011, **30**, 6166–6179.

[10] L. Zámostná, S. Sander, T. Braun, R. Laubenstein, B. Braun, R. Herrmann and P. Kläring, *Dalton Trans.*, 2015, **44**, 9450–9469.

[11] D. Selent, W. Baumann, R. Kempe, A. Spannenberg, D. Röttger, K.-D. Wiese and A. Börner, *Organometallics*, 2003, **22**, 4265–4271.

[12] Y.-S. Uh, A. Boyd, V. R. Little, P. G. Jessop, K. D. Hesp, J. Cipot-Wechsler, M. Stradiotto and R. McDonald, *J. Organomet. Chem.*, 2010, **695**, 1869–1872.

[13] J. Chatt and L. M. Venanzi, *J. Chem. Soc.*, 1957, 4735.

[14] E. Barnea, D. Moradove, J.-C. Berthet, M. Ephritikhine and M. S. Eisen, *Organometallics*, 2006, **25**, 320–322.

[15] C. E. Hayes, Y. Sarazin, M. J. Katz, J.-F. Carpentier and D. B. Leznoff, *Organometallics*, 2013, **32**, 1183–1192.

[16] H.-F. Klein, M. Gaß, U. Zucha and B. Eisenmann, *Zeitschrift für Naturforsch. B*, 1988, **43**, year.

Chapter 6

Experimental Details

6.1 General Procedures and Techniques

Standard high-vacuum Schlenk-line techniques and MBraun and Vac gloveboxes were used to manipulate and store moisture- and air-sensitive compounds under an atmosphere of dried and air-free dinitrogen. All gases were supplied by BOC gases UK. All glassware was dried in a 160°C oven, cooled under vacuum and purged with nitrogen before use. All cannulae and Fisherbrand 1.2μm retention glass microfibre filters were dried in an oven for a minimum of 18 hours at 160°C.

Toluene, diethyl ether, tetrahydrofuran and hexane for use with moisture- and air-sensitive compounds were collected from a Vac Atmospheres solvent purification system and stored over activated 4Å molecular sieves in ampoules. The solvent was cycled over a drying column containing molecular sieves for 12 hours prior to collection. 1,4-Dioxane, cyclopentane and methylcyclopentane were refluxed over sodium or potassium for 3 days, distilled and collected in an ampoule containing activated 4Å molecular sieves. All solvents were degassed and stored for 2 days prior to use. C_6D_6 and THF$-d_8$ were refluxed over potassium for 24 hours, degassed and distilled by trap to trap distillation under an atmosphere of nitrogen prior to use. All solvents were purchased from Sigma-Aldrich or Fisher Scientific.

All NMR spectroscopic analyses were recorded at 298K using Bruker Avance III 500.12 MHz spectrometers with ^{1}H NMR spectra run at 500.12 MHz, ^{13}C NMR spectra run at 125.77 MHz and ^{29}Si NMR spectra at 99.37 MHz. The ^{1}H NMR and ^{13}C NMR spectra were referenced internally to residual solvent signals and are reported relative to tetramethylsilane. Chemical shifts are quoted in ppm and coupling constants in Hz.

Elemental Analyses were performed by Mr Stephen Boyer at London Metropolitan University.

6.1.1 Preparation of Reagents

All commercially available solid reagents for use in air sensitive reaction were dried under vacuum for a minimum of 18 hours or used as received for air stable reactions. Liquid reagents for use with air- and moisture-sensitive reactions were either dried with alkali metal or activated molecular sieves, as appropriate, and purified by trap to trap vacuum distillation. Reported procedures were used for the synthesis of KN″,[1] $UI_4(dioxane)_2$,[2] $UI_4(Et_2O)_2$,[3] $U(BH_4)_3(thf)_2$,[4] $AnN''_2(\kappa^2 C{:}N{-}N(SiMe_3)SiMe_2CH_2)$ (An = U or Th),[5] $[U\{N(SiMe_3)_2\}_3]$,[2] $[UI_3]$,[3] $(MgN''_2)_2$,[6] $[Ca(N'')_2]_2$[7], $CaN''_2(thf)_2$[7], $[Sr(N'')_2]_2$,[7] $[UBn_4]$[8] and KC_5Me_5[2] were synthesised according to literature procedures with slight modifications. Potassium salts of phenols and anilines were prepared by deprotonation of the appropriate conjugate acid with KN″ in diethyl ether.

6.2 Experimental Details for Chapter 2

6.2.1 Synthesis of H_4(pTP)

A two neck 250 cm^3 round bottom flask was charged with 2-*tert*-butyl-4-methylphenol (41.80 g, 250 mmol, 4.4 eq.), terephthalaldehyde (7.5 g, 56 mmol, 1 eq.) and p-toluenesulfonic acid (1.06 g, 5.6 mmol, 0.1 eq) and equipped with a stir bar and an oil bubbler. The flask was placed under nitrogen flow, stirred and heated to 110 °C. The solids melted to yield a yellow solution, which darkened with time. After *circa* 2 hours, the reaction mixture had turned to a reddish solid. The flask was allowed to cool to room temperature, at which point 50 cm^3 of 20 % H_2O in MeCN solution was added. The resulting beige suspension was filtered to provide an off-white solid which was collected and washed with boiling ethanol. The resulting colourless solid was dried under vacuum at 65 °C for 18 hours and stored in a glove box. Yield: 27.5 g, 65 %.
^{1}H NMR (500 MHz, C_6D_6): δ_H 7.12 (d, Aryloxide **H**, $^1J_{HH} = 1.9$ Hz, 4H); 7.06 (Aromatic **H**, 4H); 6.72 (d, Aryloxide **H**, $^1J_{HH} = 1.9$ Hz, 4H); 5.56 ($Ar_3C\mathbf{H}$, 2H); 4.95 (ArO**H**, 4H); 2.06 ($C\mathbf{H}_3$, 12H); 1.44 ($C(C\mathbf{H}_3)_3$, 36H).

6.2.2 Synthesis of H_4(pTP*)

In an analogous manner to that described in Section 6.2.1, H_4(pTP*) was synthesised using terephthalaldehyde (3.8 g, 28 mmol, 1 eq.), 2,4-bis(α,α-dimethylbenzyl)phenol (41.31 g, 125 mmol, 4.4 eq.), and p-toluenesulfonic acid (0.53 g, 2.6 mmol, 0.1 eq). Yield 32.9 g, 82 %.

^{1}H NMR (600 MHz, C_6D_6): δ_H 7.34 – 7.28 (Aromatic **H**, 12H); 7.20 (Aromatic **H**, 8H); 7.12 (Aromatic **H**, 8H); 7.07 (Aromatic **H**, 4H); 7.03 (Aromatic **H**, 4H); 6.99 (Aromatic **H**, 8H); 6.96 – 6.90 (Aromatic **H**, 4H); 6.89 (Aromatic **H**, 4H), 7.03 (Aromatic **H**, 4H); 5.89 (Ar_3C**H**, 2H); 4.48 (ArO**H**, 4H); 1.65 (C**H**$_3$, 24H); 1.47 (C**H**$_3$, 24H).

6.2.3 Synthesis of [{UN″$_2$}$_2$(pTP)] (2)

A schlenk flask was charged with UN″$_2$(κ^2*C*:*N*−N(SiMe$_3$)SiMe$_2$CH$_2$) (200 mg, 0.278 mmol, 2.1 eq.) and H_4(pTP) (100 mg, 0.133 mmol, 1 eq.) and equipped with a stir bar. The reaction mixture was dissolved in hexane to yield a dark brown solution, which was allowed to stir at room temperature for 18 hours. The resulting olive green suspension was allowed to settle and filtered to yield an off-white solid. Recrystallisation of the solid in benzene or toluene provided yellow blocks suitable for single-crystal X-ray crystallography. Yield: 150 mg, 60 %.
^{1}H NMR (500 MHz, C_6D_6): δ_H 35.3 (Aryloxide **H**, 4H); 20.0 (Aryloxide **H**, 4H); 5.5 (Aromatic **H**, 4H); 4.4 (C**H**$_3$, 12H); −2.9 (Ar_3C**H**, 2H); −9.6 (C(C**H**$_3$)$_3$, 36H); −18.9 (Si(C**H**$_3$)$_3$, 36H).
Elemental analysis: C 48.85 %, H 7.23 %, N 3.00 % calculated. C 48.03 %, H 7.10 %, N 2.90 % found.

6.2.4 Synthesis of [{UN″$_2$}$_2$(pTP^t)] (2^t)

In an analogous manner to that described in Section 6.2.3, [{UN″$_2$}$_2$(pTP^t)] was synthesised using H_4(pTP^t) (91 mg, 0.10 mmol, 1 eq.) and UN″$_2$(κ^2*C*:*N*−N(SiMe$_3$)SiMe$_2$CH$_2$) (150 mg, 0.21 mmol, 2.1 eq.). Recrystallisation of the solid in benzene/THF provided yellow blocks suitable for single-crystal X-ray crystallography.

6.2.5 Synthesis of [{UN″$_2$}$_2$(pTP*)] (2*)

In an analogous manner to that described in Section 6.2.3, [{UN″$_2$}$_2$(pTP*)] was synthesised using H_4(pTP*) (142 mg, 0.10 mmol, 1 eq.) and UN″$_2$(κ^2*C*:*N*−N(SiMe$_3$)SiMe$_2$CH$_2$) (150 mg, 0.21 mmol, 2.1 eq.). Yield 165 mg, 65 %. Recrystallisation of the solid in benzene/THF provided yellow blocks suitable for single-crystal X-ray crystallography. Yield: 164 mg, 65 %.
^{1}H NMR (500 MHz, 345 K, C_6D_6): δ_H 36.1 (Aryloxide **H**, 4H); 24.0 (Aryloxide **H**, 4H); 8.67 (Aromatic **H**, 8H); 7.86 (Aromatic **H**, 4H); 6.91 – 6.75 (Aromatic **H**, 4H); 4.38 (C**H**$_3$, 12H); 3.80 (C**H**$_3$, 12H); −4.55 (C**H**$_3$, 12H); −9.64 (C**H**$_3$, 12H); −24.9 (Si(C**H**$_3$)$_3$, 36H).
Elemental analysis: C 60.68 %, H 6.92 %, N 2.21 % calculated. C 60.51 %, H 6.93 %, N 1.99 % found.

6.2.6 Synthesis of [$\{ThN''_2\}_2$(pTP)] (3)

In an analogous manner to that described in Section 6.2.3, [$\{ThN''_2\}_2$(pTP)] was synthesised using H_4(pTP) (76 mg, 0.10 mmol, 1 eq.) and thorium metallacycle (144 mg, 0.21 mmol, 2.1 eq.). Yield 205 mg, 81 %. Recrystallisation of the solid in benzene/THF provided colourless blocks suitable for single-crystal X-ray crystallography. Yield: 140 mg, 75 %.

^{1}H NMR (400 MHz, C_6D_6): δ_H 7.37 (Aryloxide **H**, *J*= 2.2 Hz 4H); 6.96 (Aryl **H**, 4H); 5.65 ($Ar_3C\mathbf{H}$, 2H); 2.16 ($C\mathbf{H}_3$, 12H); 1.61 ($C(C\mathbf{H}_3)_3$, 36H); 0.37 ($Si(C\mathbf{H}_3)_3$, 36H); 0.32 ($Si(C\mathbf{H}_3)_3$, 36H).

^{29}Si NMR (79 MHz, C_6D_6): δ_{Si} −11.53 ($\mathbf{Si}(CH_3)_3$); −11.77 ($\mathbf{Si}(CH_3)_3$).

6.2.7 Reaction of 2 with KC_8

To a golden brown solution of **2** (40 mg, 0.022 mmol, 1eq.) in C_6D_6 (0.5 cm^3) was added KC_8 (5.8 mg, 0.044 mmol, 2 eq.) with stirring in a 10 cm^3 vial in an inert atmosphere glovebox. The reaction mixture was left to stir for 15 minutes, during which the solution darkened to a brown colour. The slurry was centrifuged and the supernatant was filtered into a Young's NMR tube. NMR yield 20%.

^{1}H NMR (500MHz, C_6D_6): δ 28.5 (1H); 22.6 (2H); 18.2 (3H); 15.8 (4H); 13.8 (3H); 9.2 (5H); 8.0 (3H); 4.6 (6H); 3.8 (12H); 3.2 (6H); 2.9 (7H); −4.9 (20H); −6.0 (16H); −6.6 (19H); −7.2 (16H); −10.5 (18H); −12.0 (18H).

6.2.8 Reaction of 2 with KN″

To a golden brown solution of **2** (40 mg, 0.022 mmol, 1eq.) in C_6D_6 (0.5 cm^3) was added KN″ (88 mg, 0.044 mmol, 2 eq.) in Young's NMR tube. The reaction mixture changed to yellow-green and was allowed to stand at room temperature for 18 hours. NMR yield 20%.

6.2.9 Reaction of 2 with PyHCl

A golden brown solution of **1** (20 mg, 0.011 mmol, 1eq.) in 0.5 cm^3 of C_6D_6 was added dropwise to a colourless C_6D_6 suspension of $C_5H_5N \cdot HCl$ (5 mg, 0.043 mmol, 4eq.) in a Young's NMR tube. The mixing of the two solutions resulted in the dissolution of all solids and formation of a green solution. A green precipitate dropped out of solution after leaving the reaction to stand. The solid was isolated by centrifuge and dissolved in THF to yield a green solution.

6.2.10 Reaction of 2 with CO_2

A golden brown solution of **1** (20 mg, 0.011 mmol, 1eq.) in 0.5 cm^3 of C_6D_6 in a Young's NMR tube was degassed by three freeze pump thaw cycles and exposed to a 1 bar pressure of CO_2. The resulting solution was allowed to react at room temperature for 18 hours. No change was detected in the ^{1}H NMR spectrum.

6.2.11 General reaction of 2 with oxidants

To a golden brown solution of **1** (20 mg, 0.011 mmol, 1eq.) in 0.5 cm^3 of C_6D_6 was added dropwise a C_6D_6 solution of oxidant (0.015 mmol, 1.4eq.) in a Young's NMR tube. The mixing of the two solutions resulted in the dissolution of all solids and formation of a brown solution. No change could be detected by ^{1}H NMR spectroscopy.

6.2.12 Synthesis of $[\{UI_2(dioxane)_{1.5}\}_2(pTP)]$ (4)

Two 100 cm^3 Schlenk flasks equipped with stirrer bars were respectively charged with $[CaN_2]_2$ (0.978 g, 1.36 mmol, 1 eq.) and H_4(pTP) (1.024 g, 1.36 mmol, 1 eq.). 30 cm^3 of 1,4-dioxane was added to both solids to provide off-white solutions which were combined with vigorous stirring. The resulting off-white solution was stirred for an hour at room temperature to provide an off-white suspension. To a 250 cm^3 Schlenk flask containing $UI_4(dioxane)_2$ (2.51 g, 2.72 mmol, 2 eq.) and a stirrer bar, 100 cm^3 of 1,4-dioxane was added to yield a slightly turbid red solution, to which was added the $[Ca_2(pTP)]$ suspension generated *in situ* with vigorous stirring. The brown reaction mixture was left to stir for 48 hours to yield a light green suspension. The green-brown solution was filtered and isolated from the colourless precipitate, and the solvent removed to give a yellow-brown solid (1.75 g, 65%). Crystals suitable for single crystal X-ray diffraction analysis were grown from slow evaporation of concentrated benzene, dioxane or THF solutions at room temperature.

^{1}H NMR (500 MHz, 329 K, THFd_8): δ_H 12.7 (Aryl **H**, 4H); 10.4 (Aryl **H**, 4H); 8.89 ($Ar_3C\mathbf{H}$, 2H); 6.63 ($C(C\mathbf{H}_3)_3$, 36H); 4.25 ($C\mathbf{H}_3$, 12H); 3.94 (Aryl **H**, 4H).

Elemental analysis: C 38.45 %, H 4.34 % calculated. C 38.62 %, H 4.36 % found.

6.2.13 Synthesis of $[\{UI_2(thf)_2\}_2(pTP^*)]$ (5^*)

In an analogous manner to that described in Section 6.2.12, $[\{UI_2(thf)_3\}_2(pTP^*)]$ was syn-

thesised using H_4(pTP*) (142 mg, 0.10 mmol, 1 eq.), $[CaN_2]_2$ (72 mg, 0.10 mmol, 1 eq.) and $UI_4(dioxane)_2$ (150 mg, 0.21 mmol, 2.1 eq.) in THF. Crystalline yield 81 mg, 30 %.
^{1}H NMR (500 MHz, 345 K, C_6D_6): δ_H 36.1 (Aryloxide **H**, 4H); 24.0 (Aryloxide **H**, 4H); 8.67 (Aromatic **H**, 8H); 7.86 (Aromatic **H**, 4H); 6.91 − 6.75 (Aromatic **H**, 4H); 4.38 (C**H**$_3$, 12H); 3.80 (C**H**$_3$, 12H); −4.55 (C**H**$_3$, 12H); −9.64 (C**H**$_3$, 12H); −24.9 (Si(C**H**$_3$)$_3$, 36H).
Elemental analysis: C 60.68 %, H 6.92 %, N 2.21 % calculated. C 60.51 %, H 6.93 %, N 1.99 % found.

6.2.14 Synthesis of [{UCl(thf)(dioxane)$_2$}$_2$(pTP)] (6)

In an analogous manner to that described in Section 6.2.12, [{UCl_2(thf)(dioxane)$_2$}$_2$(pTP)] was synthesised using H_4(pTP) (76 mg, 0.10 mmol, 1 eq.), $[CaN_2]_2$ (72 mg, 0.10 mmol, 1 eq.) and UCl_4 (80 mg, 0.21 mmol, 2.1 eq.). Green crystals suitable for single crystal X-ray diffraction were obtained from slow diffusion of hexanes in concentrated dioxane solutions.

6.2.15 Synthesis of [{UTh(dme)(dioxane)}$_2$(pTP)] (7)

In an analogous manner to that described in Section 6.2.12, [{UTh(dme)(dioxane)}$_2$(pTP)] was synthesised using H_4(pTP) (76 mg, 0.10 mmol, 1 eq.), $[CaN_2]_2$ (72 mg, 0.10 mmol, 1 eq.) and $ThCl_4(dme)_2$ (116 mg, 0.21 mmol, 2.1 eq.). Large colourless crystals suitable for single crystal X-ray diffraction were obtained from slow diffusion of hexanes in concentrated dioxane solutions.

6.2.16 Synthesis of 2[K(OEt$_2$)$_2$][{UI(dioxane)(pTP)}$_2$]

To a green-brown solution of **4** (40 mg, 0.022 mmol, 1eq.) in 0.5 cm^3 of C_6D_6 was added KC_8 (5.8 mg, 0.044 mmol, 4 eq.) with stirring in a 10 cm^3 vial in an inert atmosphere glovebox. The reaction mixture was left to stir for 15 minutes, during which the solution darkened to a brown colour. The slurry was centrifuged and the supernatant was filtered into a vial and layered with Et_2O. Pale blue crystals of 2[K(OEt$_2$)$_2$][$UI(dioxane)(pTP)2$] suitable for single crystal X-ray diffraction analysis were obtained upon standing for 48 hours.

6.2.17 Synthesis of [U(thf)$_2$(pTP)]$_2$

From [Ca$_2$(pTP)]

To a stirring colourless solution of H_4(pTP) (76 mg, 0.1 mmol, 1eq.) in 0.5 cm^3 of dioxane was

added $[CaN''_2]_2$ (72 mg, 0.1 mmol, 1 eq.) with stirring in a 10 cm^3 vial in an inert atmosphere glovebox. The off-white solution was allowed to stir for 15 minutes after which $UI_4(dioxane)_2$ (92 mg, 0.1 mmol. 1 eq.) in dioxane (0.5 cm^3) was added in a single portion. The resulting pale brown suspension was stirred for 12 hours, centrifuged to remove insoluble salts and the light brown supernatant stripped to dryness. Yield 80 mg, 70 %.

From $[K_4(pTP)]$

To a stirring colourless solution of $H_4(pTP)$ (76 mg, 0.1 mmol, 1eq.) in 0.5 cm^3 of THF was added KN'' (80 mg, 0.4 mmol, 4 eq.) with stirring in a 10 cm^3 vial in an inert atmosphere glovebox. The off-white solution was allowed to stir for 15 minutes after which $UI_4(dioxane)_2$ (92 mg, 0.1 mmol. 1 eq.) in THF (0.5 cm^3) was added in a single portion. The resulting pale brown suspension was stirred for 12 hours, centrifuged to remove insoluble salts and the light brown supernatant filtered into a vial. Crystalline material was obtained from slow diffusion of hexanes into the reaction mixture. Yield 35 mg, 30 %.
^{1}H NMR (400 MHz, THFd_8): δ_H 33.6 (Aryl **H**, 4H); 25.2 (Aryl **H**, 4H); 24.5 (Aryl **H**, 4H); 24.2 (C(C**H**$_3$)$_3$, 36H); 16.0 (C**H**$_3$, 12H); 6.12 (Aryl **H**, 4H); −4.65 (C**H**$_3$, 12H); −9.15 (Aryl **H**, 4H); −12.2 (Aryl **H**, 4H); −14.8 (C(C**H**$_3$)$_3$, 36H).

6.2.18 Synthesis of $[U(thf)_2(pTP)]_3$

To a stirring colourless suspension of $H_4(pTP)$ (76 mg, 0.1 mmol, 1eq.) in 1 cm^3 of C_6D_6 was added $[CaN''_2(thf)_2]$ (110 mg, 0.2 mmol, 2 eq.) with stirring in a 10 cm^3 vial in an inert atmosphere glovebox. The yellow-orange solution was allowed to stir for 15 minutes after which solid $UI_4(dioxane)_2$ (92 mg, 0.1 mmol. 1 eq.) was added in a single portion. The resulting dark brown suspension was stirred for 12 hours, centrifuged to remove insoluble salts and the brown supernatant was filtered into a vial. Dark brown crystals were obtained by slow diffusion of hexanes into the reaction mixture.

6.3 Experimental Details for Chapter 3

6.3.1 Synthesis of [U(pTP)] (11)

A Young's NMR tube was charged with and $UN''_2(\kappa^2C{:}N{-}N(SiMe_3)SiMe_2CH_2)$ (215 mg, 0.300 mmol, 1 eq.), $H_4(pTP)$ (38 mg, 0.050 mmol, 1 eq.), C_6Me_6 (8 mg, 0.050 mmol, 1eq.)

and C_6D_6 (0.5 cm^3) and sonicated for 1 hour. The mixture was allowed to stand for 18 hours, after which time the ^{1}H NMR spectrum was recorded. NMR yield = 10 %.
^{1}H NMR (500 MHz, C_6D_6): δ_H 15.13 (Aryloxide **H**, 4H); 14.09 (Aryloxide **H**, 84); 6.41 (C**H**$_3$, 12H); 1.89 (C(C**H**$_3$)$_3$, 36H); −12.36 (Ar$_3$C**H**, 2H); −25.15 (Arene-**H**, 4H).
Elemental analysis: C 48.85 %, H 7.23 %, N 3.00 % calculated. C 48.03 %, H 7.10 %, N 2.90 % found.

6.3.2 Synthesis of [U(OH$_2$)(pTP)] (13)

A Schlenk flask was charged with UN″$_2$(κ^2*C*:*N*−N(SiMe$_3$)SiMe$_2$CH$_2$) (215 mg, 0.300 mmol, 1 eq.) and H_4(pTP) (226 mg, 0.300 mmol, 1 eq.) and equipped with a stir bar. The reaction mixture was dissolved in hexane to yield a dark brown solution, which was allowed to stir at room temperature for 18 hours. The dark brown solution was isolated from the green-brown solids by cannula filtration and the volatiles removed under reduced pressure to yield a dark red-brown solid. Recrystallisation of the solid in benzene provided red blocks suitable for single-crystal X-ray crystallography. Yield: 15 mg, 5 %.
^{1}H NMR (600 MHz, C_6D_6): δ_H 15.19 (Aryloxide **H**, 4H); 14.15 (Aryloxide **H**, 84); 6.45 (C**H**$_3$, 12H); 1.89 (C(C**H**$_3$)$_3$, 36H); −12.38 (Ar$_3$C**H**, 2H); −25.34 (Arene-**H**, 4H).

6.3.3 Synthesis of [U(CNXyl)(pTP)] (14)

A yellow-brown cyclopentane solution of UN″$_2$(κ^2*C*:*N*−N(SiMe$_3$)SiMe$_2$CH$_2$) (72 mg, 0.1 mmol, 1 eq.) in a 7 cm^3 vial was added in one portion to a colourless suspension of H_4(pTP) (76 mg, 0.100 mmol, 1 eq.) in cyclopentane in a 7 cm^3 vial with stirring. The brown suspension darkened to a dark green-brown solution within 10 minutes, and was allowed to stir at room temperature for 4 hours, after which time a colourless solution of CNXyl (13 mg, 0.100 mmol, 1 eq.) in cyclopentane was added. The resulting dark green-brown solution was stirred for 18 hours to yield a bright yellow-green suspension. The orange-brown supernatant was isolated from the dark green-brown solids by decantation. Crystalline **14** was obtained by slow diffusion of hexanes into the reaction supernatant. NMR yield: 20 %. Crystalline yield: 10 mg, 9 %.
^{1}H NMR (600 MHz, C_6D_6): δ_H 15.83 (Aryloxide **H**, 4H); 14.29 (Aryloxide **H**, 84); 6.74 (C**H**$_3$, 12H); 2.86 (C(C**H**$_3$)$_3$, 36H); −10.23 (Xylene C**H**$_3$, 6H); −16.52 (Ar$_3$C**H**, 2H); −27.30 (Arene-**H**, 4H).

6.3.4 Synthesis of [U(thf)(pTP)] (15)

To a dark green-brown cyclopentane solution of [U(pTP)] as prepared in Section 6.3.3 was added a bright yellow suspension of ($\eta-C_6H_5OMe)Cr(CO)_3$ (24 mg, 0.100 mmol, 1 eq.) in cyclopentane. After *circa* 15 minutes of stirring, 0.5 cm^3 THF was added to the dark brown suspension to solubilise the chromium complex and the resulting brown reaction mixture was stirred for 18 hours. Centrifugation of the dark brown reaction mixture provided an orange solution by decantation of the supernatant. Crystalline **15** was obtained by storing the supernatant at −30 °C for 72 hours. Yield: 6 mg, 6 %.

^{1}H NMR (500 MHz, C_6D_6): δ_H 15.14 (Aryloxide **H**, 4H); 14.09 (Aryloxide **H**, 84); 6.41 (CH_3, 12H); 1.89 ($C(CH_3)_3$, 36H); −12.35 (Ar_3CH, 2H); −25.14 (Arene-**H**, 4H).

6.3.5 Synthesis of Cs[U(pTP)] (16)

A Young's NMR tube was charged with H_4(pTP) (38 mg, 0.050 mmol, 1 eq.) UBn_4 (30 mg, 0.050 mmol, 1 eq.) and C_6D_6 (0.5 cm^3. The orange brown solution was allowed to react for 18 hours at room temperature to yield a dark brown solution after which time it was heated to 95 °C for two hours. Cesium metal (10 mg, 0.075 mmol. 1.5 eq.) was added to the dark brown solution and the reaction mixture was sonicated for 10 minutes. The resulting dark orange-brown suspension was centrifuged and the solids redissolved in THF-d_8. Yield: 25 mg, 44 %.

^{1}H NMR (600 MHz, thf-D_8): δ_H δ_H 27.70 (Aryloxide **H**, 4H); 13.54 (Aryloxide **H**, 84); 6.83 (CH_3, 12H); −5.53 ($C(CH_3)_3$, 36H); −18.23 (Arene-**H**, 4H).

6.3.6 Synthesis of [Th(CNXyl)(pTP)] (18)

A pale yellow cyclopentane solution of $ThN''_2(\kappa^2C{:}N-N(SiMe_3)SiMe_2CH_2)$ (71 mg, 0.100 mmol, 1 eq.) was added with magnetic stirring to a colourless cyclopentane suspension of H_4(pTP) (76 mg, 0.100 mmol, 1 eq.) in a 7 cm^3 vial equipped with a stir bar. The off-white suspension darkened to a deep purple solution within 10 minutes and was allowed to stir for 4 hours, after which time a colourless cyclopentane solution of CNXyl (13 mg, 0.100 mmol, 1 eq.) was added. The resulting deep purple solution was stirred for 18 hours to yield an off-white suspension. The off-white solids were collected by centrifugation and redissolved in toluene, to yield a pale yellow solution. Crystalline **18** was obtained by slow diffusion of hexanes into the benzene solutions. Yield: 72 mg, 65 %.

^{1}H NMR (500 MHz, C_6D_6): δ_H 7.82 (Arene-**H**, 4H); 7.14 (Aryloxide **H**, 8H); 6.69 (t, Xylene *para*-**H**, $^1J_{HH} = 7.7$ Hz, 1H); 6.51 (d, Xylene *meta*-**H**,$^1J_{HH} = 7.7$ Hz, 2H); 5.46 (Ar_3C**H**, 2H); 2.27 (C**H**$_3$, 12H); 2.10 (Xylene C**H**$_3$, 6H); 1.61 (C(C**H**$_3$)$_3$, 36H).

6.3.7 Synthesis of [Th(THF)(pTP)] (19)

A pale yellow cyclopentane solution of $ThN''_2(\kappa^2C{:}N{-}N(SiMe_3)SiMe_2CH_2)$ (87 mg, 0.123 mmol, 1 eq.) in cyclopentane was added with magnetic stirring to a colourless cyclopentane suspension of H_4(pTP) (92 mg, 0.123 mmol, 1 eq.) in a 7 cm^3 vial equipped with a magnetic stir bar. The off-white suspension darkened to a deep purple solution within 10 minutes and was allowed to stir for 4 hours, after which time THF (10 µl, 0.112 mmol, 1 eq.) was added *via* micropipette. The resulting pale purple solution was stirred for 18 hours to yield a thick off-white suspension. The off-white solids were collected by centrifugation and redissolved in toluene, to yield a pale yellow solution. Crystalline **19** was obtained by slow diffusion of hexanes into the benzene solutions. Yield: 74 mg, 70 %.

^{1}H NMR (400 MHz, C_6D_6): δ_H 7.76 (Arene-**H**, 4H); 7.13 (Aryloxide **H**, 8H); 5.45 (Ar_3C**H**, 2H); 4.04 – 3.86 (O(C**H**$_2$CH$_2$)$_2$, 4H); 2.25 (C**H**$_3$, 12H); 1.50 (C(C**H**$_3$)$_3$, 36H); 1.24 – 1.19 (O(CH$_2$C**H**$_2$)$_2$, 4H).

^{13}C NMR (126 MHz, C_6D_6): δ_C 160.0 (Aryloxide q**C**−O); 137.2 (q**C**(C$_6$H$_4$)CH(ArO)$_2$; 133.9 (t**C**−C$_6$H$_4$) 132.6, 132.1, 131.3 (Aryloxide q**C**); 126.6, 126.4 (Aryloxdide **C**−H); 72.6 (THF O(**C**H$_2$CH$_2$)$_2$); 57.2 (Ar_3**C**); 35.1 (**C**(CH$_3$)$_3$); 31.2 (C(**C**H$_3$)$_3$); 24.52 (THF O(CH$_2$**C**H$_2$)$_2$); 20.72 (**C**H$_3$).

6.3.8 Synthesis of [Th(N_3SiMe_3)(pTP)] (20)

A pale yellow cyclopentane solution of $ThN''_2(\kappa^2C{:}N{-}N(SiMe_3)SiMe_2CH_2)$ (72 mg, 0.100 mmol, 1 eq.) was added with magnetic stirring to a colourless cyclopentane suspension of H_4(pTP) (76 mg, 0.100 mmol, 1 eq.) in a 7 cm^3 vial equipped with a magnetic stir bar. The off-white suspension darkened to a deep purple solution within 10 minutes and was allowed to stir for 4 hours, after which time Me_3SiN_3 (26.5 µl, 0.200 mmol, 2 eq.) was added *via* micropipette. The resulting dark purple solution was stirred for 18 hours to yield a pale blue suspension. The off-white solids were collected by centrifugation and redissolved in toluene, to yield a yellow solution. Crystalline **20** was obtained by slow diffusion of hexanes into the a bezene solution. Yield: 22 mg, 20 %.

^{1}H NMR (400 MHz, C_6D_6): δ_H 7.79 (Arene-**H**, 4H); 7.13 − 7.08 (m, Aryloxide **H**, 8H); 5.42 (Ar_3C**H**, 2H); 2.27 (C$\mathbf{H}_3$, 12H); 1.63 (C(C$\mathbf{H}_3$)$_3$, 36H); −0.10 (N_3Si(C$\mathbf{H}_3$)$_3$, 9H).
Elemental analysis: C 60.15 %, H 6.52 %, N 3.83 % calculated. C 60.25 %, H 6.34 %, N 3.54 % found.

6.3.9 Synthesis of K[Th(O−3,5−dtbp)(pTP)] (21)

A pale yellow cyclopentane solution of Th$N''_2(\kappa^2 C{:}N-N(SiMe_3)SiMe_2CH_2)$ (36 mg, 0.050 mmol, 1 eq.) was added with magnetic stirring to a colourless cyclopentane suspension of H_4(pTP) (38 mg, 0.050 mmol, 1 eq.) in a 7 cm^3 vial equipped with a magnetic stir bar. The off-white suspension darkened to a deep purple solution within 10 minutes and was allowed to stir for 4 hours, after which time solid KO−3,5−dtbp (12 mg, 0.050 mmol, 1 eq.) was added in one portion. The resulting pale purple suspension was stirred for 18 hours to yield an off-white suspension. The off-white solids were collected by centrifugation and redissolved in THF, to yield a colourless solution. Crystalline **21** was obtained by slow diffusion of hexanes into THF solutions. Yield: 55 mg, 90 %.
^{1}H NMR (400 MHz, THF-d_8): δ_H 7.75 (Arene-**H**, 4H); 6.96 (d, Aryloxide **H**, $^1J_{HH} = 2.3$ Hz, 4H); 6.78 (d, Aryloxide **H**, $^1J_{HH} = 2.3$ Hz, 4H); 6.96 (d, dtbp *ortho*-**H**, $^1J_{HH} = 1.8$ Hz, 2H); 6.62 (t, dtbp *para*-**H**, $^1J_{HH} = 1.8$ Hz, 1H) 5.39 (Ar_3C**H**, 2H); 2.16 (C$\mathbf{H}_3$, 12H); 1.40 (C(C$\mathbf{H}_3$)$_3$, 36H); 1.27 (dtbp C(C$\mathbf{H}_3$)$_3$, 18H).

6.3.10 Synthesis of K[Th(O−3,5−btfmp)(pTP)] (22)

A pale yellow cyclopentane solution of Th$N''_2(\kappa^2 C{:}N-N(SiMe_3)SiMe_2CH_2)$ (36 mg, 0.050 mmol, 1 eq.) was added with magnetic stirring to a colourless cyclopentane suspension of H_4(pTP) (38 mg, 0.050 mmol, 1 eq.) in a 7 cm^3 vial equipped with a magnetic stir bar. The off-white suspension darkened to a deep purple solution within 10 minutes and was allowed to stir for 4 hours, after which time solid KO−3,5−btfmp (12 mg, 0.045 mmol, 0.9 eq.) was added in one portion. The resulting pale purple suspension was stirred for 18 hours to yield an off-white suspension. The off-white solids were collected by centrifugation and redissolved in THF, to yield a colourless solution. Crystalline **22** was obtained by slow diffusion of hexanes into THF solutions. Yield: 46 mg, 75 %.
^{1}H NMR (500 MHz, THF-d_8): δ_H 7.79 (Arene-**H**, 4H); 7.27 (btfmp *ortho*-**H**, 2H); 7.14 (btfmp *para*-**H**, 1H); 6.92 (d, Aryloxide **H**, $^1J_{HH} = 2.5$ Hz, 4H); 6.75 (d, Aryloxide **H**, $^1J_{HH} = 2.5$ Hz, 4H); 5.38 (Ar_3C**H**, 2H); 2.15 (C$\mathbf{H}_3$, 12H); 1.35 (C(C$\mathbf{H}_3$)$_3$, 36H).

6.3.11 Synthesis of $K_4[Th(O-3,5-dtbp)_2(pTP)]_2$ (23)

A pale yellow cyclopentane solution of $ThN''_2(\kappa^2 C{:}N-N(SiMe_3)SiMe_2CH_2)$ (36 mg, 0.050 mmol, 1 eq.) was added with magnetic stirring to a colourless cyclopentane suspension of $H_4(pTP)$ (38 mg, 0.050 mmol, 1 eq.) in a 7 cm^3 vial equipped with a magnetic stir bar. The off-white suspension darkened to a deep purple solution within 10 minutes and was allowed to stir for 4 hours, after which time solid KO−3,5−btfmp (28 mg, 0.101 mmol, 2.0 eq.) was added in one portion. The resulting pale purple suspension was stirred for 18 hours to yield an off-white suspension. The off-white solids were collected by centrifugation and redissolved in THF, to yield a colourless solution. Crystalline **22** was obtained by slow diffusion of hexanes into THF solutions. Yield: 43 mg, 75 %.

^{1}H NMR (500 MHz, THF-d_8): δ_H 7.08 (2 × Arene-**H**, 8H); 7.04 (btfmp-**H** 4H); 6.96 (btfmp-**H** 4H); 6.92 (2× Aryloxide **H**, 8H); 6.84 (btfmp-**H** 4H); 6.79 (2× Aryloxide **H**, 8H); 6.73 (d, 2 × $Ar_3C\mathbf{H}$, 4H); 2.16 ($C\mathbf{H}_3$, 12H); 2.11 ($C\mathbf{H}_3$, 12H); 1.38 ($C(C\mathbf{H}_3)_3$, 36H); 1.15 ($C(C\mathbf{H}_3)_3$, 36H).

6.3.12 General procedure for targeted synthesis of K[Th(NHAr)(pTP)]

To a stirring deep purple cyclopentane solution of **17** (0.050 mmol, 1 eq.) prepared in situ in a 7 cm^3 vial was added KNHAr (0.050 mmol, 1 eq.). The solution rapidly discoloured to give an off-white suspension which was allowed to stir for 18 hours. The insoluble material was isolated by centrifugation and redissolved in THF, the ^{1}H NMR spectrum of which contained no resonances appropriating to the targeted compound.

6.3.13 Synthesis of $[U(CNXyl)_2(pTP^t)]_3$ (24)

A Young's NMR tube was charged with $U''_2(\kappa^2 C{:}N-N(SiMe_3)SiMe_2CH_2)$ (36 mg, 0.050 mmol, 1 eq.), $H_4(pTP^t)$ (46 mg, 0.050 mmol, 1 eq.), C_6Me_6 (8 mg, 0.050 mmol, 1eq.) and benzene (0.5 cm^3) and sonicated for 1 hour. The dark green-brown reaction mixture was allowed to react for 18 hours, after which time CNXyl (6 mg, 0.050 mmol, 1 eq.) was added and the solution heated to 80 °C for 12 hours, during which time dark brown crystals of **24** deposited on the reaction vessel walls. Yield: 8 mg, 6 %.

6.3.14 Synthesis of $[Th(OH_2)(pTP^*)]$ (25)

A pale yellow solution of $ThN''_2(\kappa^2 C{:}N-N(SiMe_3)SiMe_2CH_2)$ (72 mg, 0.100 mmol, 1 eq.) in cyclopentane was added to a colourless suspension of $H_4(pTP^t)$ (142 mg, 0.100 mmol, 1 eq.) in

a cyclopentane in a 7 cm^3 vial with stirring. The off-white suspension was allowed to stir for 18 hours, after which time it was centrifuged and the off-white solids redissolved in benzene. A few crystals of **25** were obtained by slow diffusion of hexanes into the supernatant. Yield: 4 mg, 2 %.

6.4 Experimental Details for Chapter 4

6.4.1 Synthesis of [U(OBTrip$_2$)$_3$] (26)

A colourless solution of $HOBTrip_2$ (135 mg, 0.310 mmol, 3.1 eq.) in diethyl ether 0.5 cm^3 was added dropwise to a stirring purple red diethyl ether solution (0.5 cm^3) of UN″) (72 mg, 0.100 mmol, 1 eq.) in a 7 cm^3 vial with stirring. The resulting purple red solution was stirred at room temperature for 18 hours, after which time it was placed at -30 °C. Red prisms were obtained from the store reaction mixture at -30 °C after 72 hours.

6.4.2 Synthesis of [{U(OBTrip$_2$)$_3$}$_2$(μ-CO$_3$)] (27

) A purple-brown solution of **26** (75 mg, 0.048 mmol, 1 eq.) in C_5H_{10} prepared *in situ* in a Young's NMR tube was degassed by three freeze pump thaw cycles and placed under a 1 bar pressure of CO_2 at room temperature. The mixture was agitated to give an immediate colour change to light green-brown. The reaction mixture was allowed to stand overnight at room temperature. Crystalline **27** was obtained by slow diffusion of hexanes into the reaction mixture. Yield: 4 mg, 2 %.

6.4.3 Synthesis of [U(OBTrip$_2$)$_4$] (28)

A purple-brown solution of **26** (75 mg, 0.048 mmol, 1 eq.) in C_5H_{10} prepared *in situ* in a Young's NMR tube was degassed by three freeze pump thaw cycles and placed under a 1 bar pressure of CO at room temperature. The mixture was agitated to give a slight colour change to red-brown. The reaction mixture was allowed to stand overnight at room temperature. Crystalline **28** was obtained directly from the reaction mixture. Yield: 4 mg, 2 %.

6.4.4 Synthesis of [U(C$_5$Me$_5$)(μ-BH$_4$)$_2$]$_6$ (29)

To a Schlenk flask charged with red-brown $U(BH_4)_3(thf)_2$ (210 mg, 0.49 mmol, 1 eq.), colourless KC_5Me_5 (82 mg, 0.46 mmol, 0.95 eq.) and a stir bar was added THF (20 cm^3). The resulting red suspension was stirred at room temperature for 18 hours, after which time the volatiles were

removed under reduced pressure. The purple-red solids were extracted with toluene (2×10 cm^3) to yield a purple-brown solution, from which **29** was isolated as a purple-brown powder after filtration. Yield: 128 mg, 65 %.

^{1}H NMR (500 MHz, C_6D_6): δ_H 116 (B**H**$_4$, 8H); -1.25, -3.30 (THF-**H**, 24H); -5.0 (C_5Me_5-**H**, 15H).

^{11}B NMR (128 MHz, C_6D_6): δ_B 148 (**B**H$_4$, 8H).

6.4.5 Synthesis of [U(C_5Me_5)$_2$(BH_4)(thf)] (31)

To a Schlenk flask charged with red-brown U(BH_4)$_3$(thf)$_2$ (210 mg, 0.49 mmol, 1 eq.), colourless KC_5Me_5 (177 mg, 1 mmol, 2.05 eq.) and a stir bar was added THF (20 cm^3). The resulting forest green suspension was stirred at room temperature for 18 hours, after which time the volatiles were removed under reduced pressure. The light green solids were extracted with diethyl ether (2×10 cm^3) to yield a deep green solution, from which **31** was isolated as a dark green powder after filtration. Yield: 204 mg, 70 %.

^{1}H NMR (500 MHz, C_6D_6): δ_H 58.4 (B**H**$_4$, 4H); -2.48 (C_5Me_5-**H**, 30H); -14.8, -42.4 (THF-**H**, 24H).

^{11}B NMR (128 MHz, C_6D_6): δ_B 55 (**B**H$_4$).

6.4.6 Synthesis of [U(Tp*)(BH_4)$_2$(thf)] (33)

To a Schlenk flask charged with red-brown U(BH_4)$_3$(thf)$_2$ (210 mg, 0.49 mmol, 1 eq.), colourless KTp* (159 mg, 0.47 mmol, 0.95 eq.) and a stir bar was added THF (20 cm^3). The resulting purple-red solution was stirred at room temperature for 18 hours, after which time the volatiles were removed under reduced pressure. The light purple-red solids were extracted with toluene (2×10 cm^3) to yield a deep purple-red solution, from which **33** was isolated as a purple-brown powder after filtration. Yield: 160 mg, 52 %.

^{1}H NMR (500 MHz, C_6D_6): δ_H 145 (B**H**$_4$, 8H); 12.3 (Tp*B**H**, 1H); -2.84, -13.2 (Tp*C**H**$_3$, 2×9H); -0.68, -4.46 (THF-**H**, 2×4H).

6.4.7 Synthesis of [U(Odtbp)(BH_4)$_2$(thf)$_2$] (34

To a stirring red-brown THF (1 cm^3) solution of U(BH_4)$_3$(thf)$_2$ (86 mg, 0.20 mmol, 1 eq.) in a 7 cm^3 vial was added a colourless THF solution of Kodtbp (46 mg, 0.19 mmol, 0.95 eq.) dropwise over five minutes. The resulting bright red suspension solution was stirred at room temperature for 18 hours, after which time the volatiles were removed under reduced pressure.

The light red solids were extracted with hexanes (2×10 cm^3) to yield a deep red solution, from which **34** was isolated as a red powder after filtration. Yield: 41 mg, 33 %.
^{1}H NMR (500 MHz, C_6D_6): δ_H 94 (B**H**$_4$, 8H); 15.0 (Aryloxide *meta*H, 2H); 12.7 (Aryloxide *para*H, 1H); -1.67 (Aryloxide C(C**H**$_3$)$_3$, 18H) ^{11}B NMR (128 MHz, C_6D_6): δ_B 145 (**B**H$_4$). .

6.4.8 General route to attempted synthesis of [U(OAr)$_2$(BH$_4$)]

To a stirring red-brown THF (1 cm^3) solution of U(BH$_4$)$_3$(thf)$_2$ (86 mg, 0.20 mmol, 1 eq.) in a 7 cm^3 vial was added a colourless THF solution of KOAr (0.38 mmol, 1.9 eq.) dropwise over five minutes. The resulting bright red suspension solution was stirred at room temperature for 18 hours, after which time the volatiles were removed under reduced pressure to yield brown solids.

6.5 Experimental Details for Chapter 5

Synthetic procedures for Section 5.2 and Section 5.3 were developed by Dr. J. A. Hlina and can be found within the publications in Appendix B.

6.5.1 General procedure for attempted synthesis of [U(OAr^P)$_3$]

A hexane solution of HOAr^P (97 mg, 0.280 mmol, 2.8 eq.) was added dropwise to a stirring purple-red hexane solution of UN$''_3$ (72 mg, 0.100 mmol, 1 eq.) in hexanes at room temperature. After 18 hours stirring, the solvent was removed from the green brown solution. Crystals consistent with [U(OAr^P)$_4$] were grown from benzene solutions. No other products were observed.

6.6 Bibliography

[1] S. M. Mansell, B. F. Perandones and P. L. Arnold, *J. Organomet. Chem.*, 2010, **695**, 2814–2821.

[2] M. J. Monreal, R. K. Thomson, T. Cantat, N. E. Travia, B. L. Scott and J. L. Kiplinger, *Organometallics*, 2011, **30**, 2031–2038.

[3] C. D. Carmichael, N. A. Jones and P. L. Arnold, *Inorg. Chem.*, 2008, **47**, 8577–8579.

[4] P. L. Arnold, C. J. Stevens, J. H. Farnaby, M. G. Gardiner, G. S. Nichol and J. B. Love, *J. Am. Chem. Soc.*, 2014, **136**, 10218–10221.

[5] A. Dormond, A. El Bouadili, A. Aaliti and C. Moise, *J. Organomet. Chem.*, 1985, **288**, 1–5.

[6] K. W. Henderson, J. F. Allan and A. R. Kennedy, *Chem. Commun.*, 1997, 1149–1150.

[7] M. Westerhausen, *Inorg. Chem.*, 1991, **30**, 96–101.

[8] S. J. Kraft, P. E. Fanwick and S. C. Bart, *J. Am. Chem. Soc.*, 2012, **134**, 6160–6168.

Appendix A

Crystallographic details

A.1 Experimental details

X-ray diffraction data for all complexes were recorded on an Excalibur Eos diffractometer at 170(2) or 120(2) K using a Mo Kα radiation source (λ = 0.71073 Å) or on a SuperNova dual source Atlas diffractometer, using a Cu Kα source (λ = 1.54184 Å) at 120(2) K. All structures were solved using SHELXT[1] and least-square refined using SHELXL[1] in Olex2.[2] Unless otherwise stated, all non-H atoms were refined anisotropically and all H atoms were placed in calculated positions and refined using a riding model. All BH4 protons were omitted from the crystallographic models unless they could be located in the residual electron density map.

Where structures were found to contain disordered solvent molecules that could not be successfully modelled, the SQUEEZE[3] routine of PLATON was used to remove the associated residual electron density. The use of SQUEEZE and any restraints applied to the main molecular residue during refinement are detailed below, along with selected structural parameters for each structure.

A summary of the crystal data, data collection and structure refinement for each X-ray structure are presented in Appendix A.2. The crystallographic data collection, solution and refinement for Chapter 5 was carried out in its entirety by Dr. Johann Hlina, and is thus not included in this appendix.

A.1.1 $[K_2\{H_2(pTP)\}]$, 1

Crystals of **1** were obtained by diffusion of hexanes into dioxane solutions of **1**. A potassium-bound dioxane molecule was found to be disordered over two sites in a 0.3 : 0.7 ratio. The disordered C and O atoms were refined anisotropically with no restraints using the SHELX software package PART function.

A.1.2 $[K_2\{H_2(pTP^*)\}]$, $\mathbf{1}^*$

Crystals of $\mathbf{1}^*$ were obtained by diffusion of hexanes into dioxane solutions of $\mathbf{1}^*$. A disordered dioxane lattice solvent molecule was restrained using SIMU and RIGU and the C−C and C−O bond lengths were set as equal using SADI.

A.1.3 $[\{UN''_2\}_2(pTP)]$, 2

2.(C_6H_6)

Crystals of $\mathbf{2}.(C_6H_6)$ were obtained from concentrated benzene solution of **2** stored at room temperature over 48 hours. A benzene lattice solvent molecule was found to be disordered over two sites in a 0.50 : 0.50 ratio. The disordered C atoms were refined anisotropically with no restraints using the SHELX software package PART function.

2.$(C_6H_5CH_3)$

Crystals of **2** were obtained from concentrated toluene solution of **2** stored at -30 °C over 48 hours. No restraints were required for the refinement of the crystal structure of $\mathbf{2}.(C_6H_5CH_3)$.

A.1.4 $[\{UN''_2\}_2(pTP^t)]$, $\mathbf{2}^t$

Crystals of **2** were obtained from concentrated toluene solution of **2** left to stand at room temperature over 48 hours. A disordered toluene lattice solvent molecule was modelled using the PART instruction and the SIMU, DELU and AFIX 66 restraints of the SHELX software package. The EADP constraint was used for a disordered *tertiary*-butyl group and some of the disordered toluene molecule. There is residual density close to the uranium centre, due to the large atomic number of the uranium nucleus.

A.1.5 $[\{UN''_2\}_2(pTP^t\cdot)]$, $\mathbf{2}^*$

Crystals of $\mathbf{2}^*$ were obtained from a $\mathbf{2}^*$ solution in benzene and THF left to stand at room temperature over 48 hours. A disordered THF lattice solvent molecule was restrained using the SHELX software package SIMU and RIGU restraints. The disorder of a benzene lattice solvent molecule which lied on a crystallographic symmetry plane was resolved using the SADI instruction.

A.1.6 $[\{ThN''_2\}_2(pTP)]$, 3

Crystals of **3** were obtained from a solution of **3** in benzene left to stand at room temperature over 48 hours. A disordered benzene lattice solvent molecule was restrained using the SHELX software package SIMU, RIGU and AFIX 66 restraints. There is residual density close to the thorium centre, due to the large atomic number of the thorium nucleus.

A.1.7 $[\{UI_2(dioxane)_{1.5}\}_2(pTP)]$, 4

Crystals of **4** were obtained from a solution of **4** in benzene left to stand at room temperature over 24 hours. Three disordered benzene lattice solvent molecules were restrained using the SHELX software package SIMU, DELU and AFIX 66 restraints. The DFIX restraint was used on the fragment of a benzene lattice solvent molecule which lied on a crystallographic symmetry plane.

A.1.8 $[\{UI_2(thf)3\}_2(pTP)]$, 5

Crystals of **5** were obtained from an NMR scale reaction of $[CaN''_2]_2$, H_4(pTP) in THF to which was added $UI_4(dioxane)_2$ in THF. Three disordered uranium-bound THF solvent molecules and one THF lattice solvent molecule were restrained using the SHELX software package SIMU and DELU restraints and the SADI instruction.

A.1.9 $[\{UI_2(thf)2\}_2(pTP^*)]$, 5^*

Crystals of $\mathbf{5}^*$ were obtained from an NMR scale reaction of $[CaN''_2]_2$, H_4(pTP*) in THF to which was added $UI_4(dioxane)_2$. Two disordered uranium-bound THF solvent molecules and two THF lattice solvent molecule were restrained using the SHELX software package SIMU and DELU restraints and the SADI instruction.

A.1.10 $[\{UCl_2(dioxane)2(thf)\}_2(pTP)]$, 6

Green plates of **6** were obtained by slow diffusion of hexanes into dioxane solutions of **6**. Two disordered uranium-bound dioxane solvent molecules and three dioxane lattice solvent molecule were restrained using the SHELX software package SIMU, DELU and RIGU restraints and the SADI instruction. The SQUEEZE algorithm was used to removed residual electron density of 194 electrons, equating to approximately two and a third dioxane molecules in the crystal lattice per unit cell.

A.1.11 [{$ThCl_2$(dme)(dioxane)}$_2$(pTP)], 7

Enormous colourless plates of **7** were obtained by slow diffusion of hexanes into dioxane solutions of **7**. No restraints were required for the crystal structure refinement of **7**.

A.1.12 $K_2[U_2(pTP)_2I_2]$, 8

Light blue plates of **8** were obtained by diffusion of diethyl ether into an NMR scale reaction of **4** and KC_8 in benzene. Three disordered potassium-bound diethyl ether molecules were restrained with DFIX, SIMU, DELU and RIGU using the SHELX software package. Five disordered benzene lattice solvent molecules were restrained with SIMU, DELU, RIGU and AFIX 66. A ligand aryloxide aryl group was restrained with SIMU and RIGU. The terminal H atoms of a diethyl ether molecule could not be included in the crystal structure due to unstable refinement.

A.1.13 [U(thf)$_2$(pTP)$_2$], 9

Light brown crystals of **9** were obtained from an NMR scale reaction of KN'', H_4(pTP) and UI_4(dioxane)$_2$ in THF. Four disordered THF lattice solvent molecules were restrained using the SIMU, DELU and RIGU restraints and required the use of EADP constraints for satisfactory refinement.

A.1.14 [U(thf)$_2$(pTP)]$_3$, 10

Dark brown crystals of **10** were obtained from an NMR scale reaction of $CaN''_2(thf)_2$, H_4(pTP) and UI_4(dioxane)$_2$ in benzene. A disordered ligand aryloxide aryl and *tertiary*-butyl group were restrained using SIMU and RIGU. The *tertiary*-butyl group required the use of the EADP constraint for satisfactory refinement. The PLATON SQUEEZE function was employed to remove residual electron density of 1538eâĹŠ from the void, corresponding to approximately 32 molecules of lattice benzene per unit cell, or two and two thirds per asymmetric unit.

A.1.15 [U(L)(pTP)], 12

Red plates of **12** were obtained by storing solutions of **11** in a 3 : 1 hexane and methylcyclopentane at -30 °C for a period of two weeks. No restraints were necessary for the crystal structure refinement of**12**. There is significant residual electron density in the structure, the nature of which cannot be ascribed with sound chemical reasoning.

A.1.16 [U(OH_2)(pTP)], 13

Red plates of **13** were obtained from a benzene solution of **13**. A rotationally disordered bezene lattice solvent molecule was restrained using SIMU, RIGU and SADI. The three, rotationally disordered water ligand H atoms were located in the difference Fourier map and the O−H and H− bond distances were fixed to be equal with the SADI instruction.

A.1.17 [U(CNXyl)(pTP)], 14

Orange-brown crystals of **14** were obtained from diffusion of hexanes into benzene solutions of **14**. A disordered benzene fragment which lied on a crystallographic symmetry plane was restrained with SIMU and RIGU.

A.1.18 [U(THF)(pTP)], 15

Orange crystals of **15** were obtained from concentrated hexane or THF solutions left to stand at room temperature or -30 °C for 48 hours. The uranium-bound THF ligand disorder was modelled by using the SIMU, RIGU and SADI restraints.

A.1.19 [Th(CNXyl)(pTP)], 18

Yellow crystals of **18** $\cdot\, 2(C_6H_6)$ were obtained by diffusion of hexanes into solutions of **18** in benzene. A disordered hexane lattice solvent molecule lying on a crystallographic symmetry plane was restrained with SADI.

A.1.20 [Th(THF)(pTP)], 19

19 $\cdot$ **2**(C_5H_{10})

Yellow crystals of **19** $\cdot\, 2(C_5H_{10})$ were obtained by diffusion of hexanes into solutions of **18** in cyclopentane. Two cyclopentane lattice solvent molecules were restrained using SIMU, DELU and SADI.

19 $\cdot$ **2**(C_6H_6)

Yellow crystals of **19** $\cdot\, 2(C_6H_6)$ were obtained by diffusion of hexanes into solutions of **18** in cyclopentane. The thorium-bound THF ligand disorder and a disordered benzene lattice solvent molecule were restrained using SIMU, RIGU and SADI. The PLATON SQUEEZE function was employed to remove electrons from accessible voids, equating to eight and nine tenths of

a benzene lattice solvent molecule per unit cell, or one and a quarter benzene lattice solvent molecules per asymmetric unit.

A.1.21 [Th(N_3SiMe_3)(pTP)], 20

Bright yellow crystals of **20** were obtained by slow diffusion of hexanes into a benzene solution of **20** containing traces of cyclohexane. No restraints were required for the crystal structure refinement of **20**.

A.1.22 K[Th(O−3,5−dtbp)(pTP)], 21

Colourless blocks of **21** were obtained from layering of hexanes onto THF solutions of **21**. The X-ray data collection was carried out at 250 K, due to a destructive phase transition at lower temperatures. A disordered potassium-bound THF molecule was restrained using SIMU and DELU. The PLATON SQUEEZE function was used to remove 365 electrons from accessible voids, equating to approximately five THF lattice solvent molecules per unit cell, or approximately one THF lattice solvent molecule per asymmetric unit.

A.1.23 K[Th(O−3,5−btfmp)(pTP)], 22

Colourless blocks of **22** were obtained from layering of hexanes onto THF solutions of **22**. The complex crystallises in the tetragonal spacegroup $P4/nmm$, with a heavily disordered molecule **22**. Only vague connectivity information can be obtained with SIMU and RIGU restraints.

A.1.24 K_4[Th(O−3,5−btfmp)$_2$(pTP)]$_2$, 23

Colourless blocks of **23** were obtained from layering of hexanes onto THF solutions of **23**. Three disordered THF lattice solvent molecules, all four disordered ligand aryloxide aryl groups and one of the disordered fluorinated aryloxide aryl groups were restrained with SIMU and RIGU. The ligand arene bridge could not be refine anisotropically and the ISOR restraint was applied. A disordered trifluoromethyl group was constrained with EADP. The PLATON SQUEEZE function was employed to remove 259 electrons from accessible voids, approximately equating to three and a half THF lattice solvent molecules. The poor quality data is the result of the unexpected warming of the sample during data collection.

A.1.25 [U(CNXyl)$_2$(pTP^t)]$_3$, 24

Red-brown plates of **24** were obtained from an NMR scale reaction of **11^t** with CNXyl heated at 85 °C and slowly cooled to room temperature. The data is of poor quality, but satisfactory connectivity information can be inferred without the use of restraints to refine the crystal structure of **24**.

A.1.26 [Th(OH$_2$)(pTP*)], 25

A light yellow plate of **25** was obtained from the slow diffusion of hexanes into a benzene solution of **25**. A ligand dimethylbenzyl group was found to be disordered over two sites in a 0.25 : 0.75 ratio. The disorder was modelled using the SIMU and RIGU restraints, and required the use of EADP constraints for satisfactory refinement.

A.1.27 [U(OBTrip$_2$)$_3$], 26

Red plates of **26** were obtained from a reaction of [UN″$_3$] with HOBTrip$_2$ in diethyl ether stored at −30 °C for 46 hours. No restraints were necessary for the crystal structure refinement of **26**.

A.1.28 [{U(OBTrip$_2$)$_3$}(μ-CO$_3$)], 27

Green-grey plates of **27** were obtained from diffusion of hexanes into the NMR scale reaction mixture of *in situ* prepared **26** with CO_2 in benzene. The bridging carbonate ligand is disordered over two sites in a 0.5 : 0.5 ratio, and required the use of the PART and SADI SHELX software suite instructions. The data could not be refined anisotropically, requiring the use of the ISOR restraint.

A.1.29 [U(OBTrip$_2$)$_4$], 28

Light purple plates of **28** were grown from the NMR scale reaction of **26** with CO in benzene which was allowed to stand at room temperature for 48 hours. Two disordered benzene lattice solvent molecules and a disordered ligand iso-propyl group required the use of the SIMU, DELU and RIGU restraints.

A.1.30 [U(C$_5$Me$_5$)(BH$_4$)$_2$]$_6$, 29

Purple blocks of **29** were obtained from concentrated benzene solution. Two disordered C_5Me_5 ligand were restrained with AFIX 106, SIMU and RIGU. Two benzene lattice solvent molecules

were modelled with the AFIX 66, SIMU, DELU and RIGU restraints. The borohydride H atoms could not be located in the residual density map.

A.1.31 [U(C_5Me_5)(BH_4)$_2$(thf)$_2$], 30

Red plates of **30** were obtained by hexane diffusion into THF solutions of **30** stored at −30 °C. The borohydride H atoms were located in the difference Fourier map and the B−H and H−H distances set as equal using the SADI instruction. No other restraints were used for the refinement of the crystal structure of **30**.

A.1.32 [U(C_5Me_5)$_2$(BH_4)(thf)], 31

Forest green plates of **31** were obtained from slow evaporation of pentane solutions of **31** at room temperature over 72 hours. A disordered C_5Me_5 was modelled with SIMU and RIGU. The borohydride H atoms were located in the difference Fourier map and the B−H distances set as equal using the SADI instruction.

A.1.33 [U(Tp*)(BH_4)$_2$(thf)], 33

Purple-red plates of **33** were grown from hexane diffusion in THF solutions of **33**. The C−H bonds of a methyl group which lied on a crystallographic symmetry axis were set as equal using the SADI instruction. The borohydride H atoms were located in the difference Fourier map and the B−H distances set as equal using the SADI instruction.

A.1.34 [U(Odtbp)(BH_4)$_2$(thf)$_2$], 34

Red plates of **34** were grown from hexane solution of **34**. The aryloxide ligand aryl group was restrained using AFIX 66, SIMU and RIGU. The *para* C atom could not be refined anisotropically requiring the use of the ISOR restraint. A disordered uranium-bound THF group was modelled using the SIMU and RIGU restraints. The borohydride H atoms were located in the difference Fourier map and the B−H distances set as equal using the SADI instruction.

A.1.35 [U(Ottbp)$_2$(BH_4)(thf)$_2$], 35

Red plates of **35** were grown from hexane solution of **35**. The data is of sufficient quality to obtain connectivity information but required the use of SIMU, RIGU, SADI restraints and necessitated ISOR restraints in some cases to obtain satisfactory refinement.

A.2 Crystallographic tables

Compound	**1**	**1***	**2.PhH**	**2.PhMe**
Chemical formula	$C_{76}H_{108}K_2O_{16}\cdot 2(C_4H_8O_2)$	$C_{112.04}H_{120}K_2O_8\cdot 5(C_2H_4O)$	$C_{38}H_{67}N_2O_2Si_4U\cdot (C_6H_6)$	$C_{38}H_{67}N_2O_2Si_4U\cdot C_7H_8$
M_r	1532.02	1893.01	1012.43	1026.46
Crystal system, space group	Monoclinic $P2_1$	Triclinic $P\bar{1}$	Monoclinic $P2_1/n$	Monoclinic $P2_1/n$
Temperature (K)	170	120	293	293
***a*, *b*, *c* (Å)**	15.0824 (4) 15.2464 (4) 18.6292 (4)	12.9547 (3) 19.8569 (5) 21.3893(5)	13.89502 (11) 17.73106 (18) 20.67049 (18)	13.8909 (2) 17.9671 (3) 20.4658 (3)
α, β, γ (°)	- 90.244 (2) -	85.3880 (19) 81.8738 (18) 74.0264 (19)	- 94.3765 (8) -	- 93.7577 (14) -
***V* (Å^3)**	4283.79 (18)	5231.7 (2)	5077.81 (8)	5096.85 (14)
Z	2	2	4	4
Radiation type	Mo *K*α	Mo *K*α	Mo *K*α	Mo *K*α
μ (mm^{-1})	0.18	0.15	3.32	3.31
Crystal size (mm)	0.29 × 0.25 × 0.18	0.40 × 0.30 × 0.28	0.54 × 0.31 × 0.13	0.53 × 0.26 × 0.13
Diffractometer	Xcalibur, Eos	SuperNova	Xcalibur, Eos	Xcalibur, Eos
Absorption correction	Analytical	Gaussian	Multi-scan	Multi-scan
T_{min}, T_{max}	0.970, 0.981	0.942, 0.957	0.541, 1.000	0.314, 1.000
No. of measured, independent and observed [I > 2s(I)] reflections	58639 13622 8876	100545 23993 19138	114610 11616 10176	64618 11678 9521
R_{int}	0.081	0.047	0.041	0.065
(sin θ/λ)$_{max}$ (Å^{-1})	0.575	0.649	0.649	0.649
$R[F^2 > 2\sigma(F^2)]$, $wR(F^2)$, S	0.068, 0.138, 1.03	0.065, 0.175, 1.02	0.019, 0.043, 1.03	0.032, 0.104, 0.74
No. of parameters	1006	1431	558	508
No. of restraints	1	79	792	-
H-atom treatment	riding and independent	riding and independent	riding	riding
Δ⟩$_{max}$, Δ⟩$_{min}$ (e Å^{-3})	0.26, -0.21	1.01, -0.84	0.54, -0.38	1.26, -1.57
CCDC No.	-	-	1478891	-

Figure A.1 – Experimental details for complexes **1**, **1*** and **2** synthesised in Chapter 2.

Compound	**2***	**2t**	**3**	**4**
Chemical formula	$C_{64}H_{87}N_2O_2Si_4U\cdot C_3H_3\cdot C_4H_8O$	$C_{44}H_{79}N_2O_2Si_4U\cdot C_6H_6$	$C_{38}H_{67}N_2O_2Si_4Th\cdot 3(C_3H_3)$	$C_{32}H_{43}I_2O_5U\cdot 5.5\ (C_6H_6)$
M_r	1377.9	1096.58	1045.49	1429.08
Crystal system, space group	Triclinic $P\bar{1}$	Triclinic $P\bar{1}$	Triclinic $P\bar{1}$	Triclinic $P\bar{1}$
Temperature (K)	293	293	120	293
***a*, *b*, *c* (Å)**	13.1696 (3) 13.7113 (3) 20.4909 (4)	12.0140 (4) 13.7429 (5) 18.7726 (7)	12.6019 (3) 14.5612 (6) 15.6649 (5)	13.8429 (3) 15.6696 (4) 15.8357 (5)
α, β, γ (°)	105.6517 (16) 103.7133 (17) 95.6555 (16)	69.175 (3) 81.525 (3) 89.718 (3)	108.175 (3) 93.419 (2) 100.094 (3)	69.881 (2) 89.136 (2) 76.262 (2)
***V* (Å^3)**	3408.69 (12)	2861.60 (19)	2668.65 (16)	3124.73 (15)
Z	2	2	2	2
Radiation type	Mo *K*α	Mo *K*α	Mo *K*α	Mo *K*α
μ (mm^{-1})	2.5	2.95	2.92	3.63
Crystal size (mm)	0.57 × 0.17 × 0.08	0.31 × 0.28 × 0.03	0.43 × 0.15 × 0.09	0.51 × 0.32 × 0.13
Diffractometer	Xcalibur, Eos	Xcalibur, Eos	SuperNova	Xcalibur, Eos
Absorption correction	Analytical	Analytical	Gaussian	Analytical
T_{min}, T_{max}	0.227, 0.724	0.911, 0.991	0.468, 1.000	0.991, 0.997
No. of measured, independent and observed [I > 2s(I)] reflections	70327 13932 12437	66226 13107 11059	58986 13478 11608	58171 14313 10213
R_{int}	0.045	0.069	0.062	0.079
(sin θ/λ)$_{max}$ (Å^{-1})	0.625	0.649	0.695	0.649
$R[F^2 > 2\sigma(F^2)]$, $wR(F^2)$, S	0.029, 0.092, 0.74	0.055, 0.147, 1.14	0.067, 0.153, 1.13	0.061, 0.171, 0.96
No. of parameters	786	563	513	630
No. of restraints	135	48	72	152
H-atom treatment	riding	riding	riding	riding
Δ⟩$_{max}$, Δ⟩$_{min}$ (e Å^{-3})	0.96, -0.88	4.45, -2.23	6.06, -2.90	1.83, -0.70
CCDC No.	1478892	-	-	1478888

Figure A.2 – Experimental details for complexes **2***, **2**^{t}, **3** and **4** synthesised in Chapter 2.

Compound	**5**	**5***	**6**	**7**
Chemical formula	$C_{38}H_{55}I_2O_5U\cdot C_4H_8O$	$C_{60}H_{67}I_2O_4U\cdot 2(C_4H_8O)$	$0.5(C_{76}H_{110}Cl_4O_{14}U_2)\cdot C_4H_8O_2$	$C_{34}H_{49}Cl_2O_6Th\cdot 4.5(C_4H_8O_2)$
M_r	1155.75	1488.17	1020.85	1253.14
Crystal system, space group	Monoclinic $P2_1/n$	Triclinic $P\bar{1}$	Triclinic $P\bar{1}$	Triclinic $P\bar{1}$
Temperature (K)	170	293	293	293
***a*, *b*, *c* (Å)**	13.1203 (2) 15.46388 (16) 22.0950 (3)	14.4316 (3) 15.1187 (3) 16.3119 (3)	12.9449 (2) 14.7909 (2) 26.6783 (5)	11.4973 (2) 14.1150 (3) 18.6186 (3)
α, β, γ (°)	- 94.6475 (13) -	90.4479 (17) 92.5407 (16) 118.010 (2)	82.9690 (13) 79.2579 (14) 73.9534 (13)	74.0065 (16) 89.2493 (15) 80.3506 (18)
***V* (Å^3)**	4468.12 (10)	3137.41 (12)	4809.36 (14)	2861.71 (10)
Z	4	2	4	2
Radiation type	Mo *K*α	Mo *K*α	Mo *K*α	Mo *K*α
μ (mm^{-1})	5.06	3.62	3.53	2.76
Crystal size (mm)	0.29 × 0.15 × 0.13	0.33 × 0.17 × 0.09	0.22 × 0.16 × 0.07	0.87 × 0.64 × 0.45
Diffractometer	Xcalibur, Eos	Xcalibur, Eos	Xcalibur, Eos	Xcalibur, Eos
Absorption correction	Multi-scan	Analytical	Analytical	Analytical
T_{min}, T_{max}	0.577, 1.000	0.525, 0.783	0.942, 0.976	0.223, 0.401
No. of measured, independent and observed [I > 2s(I)] reflections	72103 9141 7365	57292 14372 12061	111954 22049 15638	66487 13114 11932
R_{int}	0.056	0.043	0.078	0.043
(sin θ/λ)$_{max}$ (Å^{-1})	0.625	0.649	0.649	0.649
$R[F^2 > 2\sigma(F^2)]$, $wR(F^2)$, S	0.053, 0.131, 1.10	0.045, 0.144, 1.04	0.058, 0.125, 1.06	0.028, 0.093, 0.77
No. of parameters	468	702	1016	641
No. of restraints	184	182	198	-
H-atom treatment	riding	riding	riding	riding
Δ⟩$_{max}$, Δ⟩$_{min}$ (e Å^{-3})	2.03, -1.80	3.55, -1.84	2.29, -2.08	1.67, -1.11
CCDC No.	1478887	1478889	-	-

Figure A.3 – Experimental details for complexes **5**, **5***, **6** and **7** synthesised in Chapter 2.

Compound	**8**	**9**	**10**
Chemical formula	$C_{128}H_{175}I_2K_2O_{16}U_2 \cdot 10(C_3H_3) \cdot C_4H_{10}O$	$C_{120}H_{156}O_{12}U_2 \cdot C_4H_6O \cdot 4(C_4H_8O)$	$C_{180}H_{230}O_{18}U_3$
M_r	3242.39	2625	3395.72
Crystal system, space group	Triclinic $P\bar{1}$	Monoclinic $P2_1/n$	Monoclinic $C2/c$
Temperature (K)	170	170	170
***a*, *b*, *c* (Å)**	14.9886 (3) 22.8715 (7) 26.6939 (7)	23.5900 (8) 20.9266 (5) 28.2386 (9)	28.1311 (7) 22.9086 (4) 34.3732 (11)
α, β, γ (°)	113.720 (3) 93.571 (2) 105.145 (2)	- 111.567 (4) -	- 105.738 (3) -
***V* (Å^3)**	7940.5 (4)	12964.3 (8)	21321.2 (10)
Z	2	4	4
Radiation type	Mo *K*α	Mo *K*α	Mo *K*α
μ (mm^{-1})	2.54	2.56	2.32
Crystal size (mm)	0.53 × 0.19 × 0.06	0.27 × 0.08 × 0.04	0.47 × 0.38 × 0.18
Diffractometer	Xcalibur, Eos	Xcalibur, Eos	Xcalibur, Eos
Absorption correction	Analytical	Analytical	Analytical
T_{min}, T_{max}	0.681, 0.934	0.944, 0.990	0.750, 0.872
No. of measured, independent and observed [I > 2s(I)] reflections	161549 28014 16706	230084 20577 12728	132976 11079 8627
R_{int}	0.168	0.26	0.123
(sin θ/λ)$_{max}$ (Å^{-1})	0.595	0.575	0.5
$R[F^2 > 2\sigma(F^2)]$, $wR(F^2)$, S	0.073, 0.182, 1.02	0.076, 0.144, 1.02	0.081, 0.183, 1.16
No. of parameters	1683	1443	924
No. of restraints	476	224	108
H-atom treatment	riding	riding	riding
Δ⟩$_{max}$, Δ⟩$_{min}$ (e Å^{-3})	2.33, -1.13	1.12, -0.72	3.59, -4.95
CCDC No.	-	-	-

Figure A.4 – Experimental details for complexes **8**, **9** and **10** synthesised in Chapter 2.

Compound	**12**	**13**	**14**	**15**
Chemical formula	$C_{26}H_{31}O_2U_{0.5}\cdot C_6H_{14}$	$C_{52}H_{64}O_5U\cdot 3(C_6H_6)$	$C_{61}H_{71}NO_4U\cdot 4.5(C_6H_6)$	$C_{56}H_{70}O_5U$
M_r	580.69	1241.38	1471.7	1061.15
Crystal system, space group	Monoclinic *C 2/c*	Triclinic $P\bar{1}$	Monoclinic *I 2/a*	Monoclinic $P2_1/c$
Temperature (K)	170	120	120	170
***a, b, c* (Å)**	29.1846 (15) 8.2467 (2) 26.3595 (8)	10.56442(15) 15.7197 (3) 19.2754 (3)	21.5161 (3) 22.3523 (3) 30.4044 (4)	13.4262 (5) 28.4334 (7) 15.1096 (5)
α, β, γ (°)	112.288 (5)	76.6753 (13) 85.0101 (13) 73.4331 (14)	93.782 (1)	114.315 (4)
***V* (Å^3)**	5870.1 (4)	2984.80 (9)	14590.7 (3)	5256.5 (3)
Z	8	2	8	4
Radiation type	Mo *K*α	Mo *K*α	Cu *K*α	Mo *K*α
μ (mm^{-1})	2.81	2.77	6.65	3.13
Crystal size (mm)	0.25 × 0.19 × 0.05	0.63 × 0.39 × 0.10	0.33 × 0.26 × 0.11	0.34 × 0.12 × 0.05
Diffractometer	Xcalibur, Eos	Xcalibur, Eos	SuperNova	Xcalibur, Eos
Absorption correction	Multi-scan	Gaussian	Multi-scan	Analytical
T_{min}, T_{max}	0.688, 1.000	0.945, 0.988	0.400, 1.000	0.498, 0.874
No. of measured, independent and observed [I > 2s(I)] reflections	52650 3764 5841	52236 9465 8447	145398 14924 14117	111538 10733 8747
R_{int}	0.118	0.043	0.09	0.12
(sin θ/λ)$_{max}$ (Å^{-1})	0.649	0.575	0.625	0.625
$R[F^2 > 2\sigma(F^2)]$, $wR(F^2)$, S	0.108, 0.625, 1.12	0.022, 0.049, 0.97	0.047, 0.121, 1.09	0.089, 0.146, 1.28
No. of parameters	322	768	865	575
No. of restraints	-	129	21	62
H-atom treatment	riding	riding and independent	riding	riding
Δ⟩$_{max}$, Δ⟩$_{min}$ (e Å^{-3})	20.95, -2.63	0.53, -0.35	1.62, -2.48	1.37, -2.06
CCDC No.	-	-	-	-

Figure A.5 – Experimental details for complexes **12**, **13**, **14** and **15** synthesised in Chapter 3.

Compound	**18**	**19.PhH**	**19.C5H10**	**20**	**21**
Chemical formula	$C_{61}H_{71}NO_4Th \cdot 2(C_6H_6) \cdot C_3H_5$	$C_{56}H_{70}O_5Th \cdot 2(C_5H_{10})$	$C_{56}H_{70}O_5Th \cdot 1.5(C_6H_6)$	$C_{55}H_{71}N_3O_4SiTh \cdot 2(C_6H_6)$	$C_{74}H_{99}KO_7Th$
M_r	1311.51	1311.51	1172.32	1254.49	1371.67
Crystal system, space group	Monoclinic $P2_1/n$	Monoclinic $P2_1/n$	Othorhombic *Ibam*	Triclinic $P\bar{1}$	Monoclinic $I2/a$
Temperature (K)	150	120	120	120	250
a, b, c (Å)	15.2421 (3) 17.7579 (3) 24.5084 (4)	16.7529 (2) 14.9351 (1) 23.4582 (3)	17.0734 (7) 32.3176 (9) 22.7717 (5)	14.3472 (2) 14.4501 (3) 15.3372 (3)	22.9187 (2) 23.1723 (2) 30.8068 (3)
α, β, γ (°)	- 96.154 (1) -	- 90.118 (1) -	- - -	76.326 (2) 88.133 (1) 89.062 (2)	- 108.957 (1) -
V (Å^3)	6595.4 (2)	5869.38 (11)	12564.8 (7)	3087.8 (10)	15473.5 (3)
Z	4	4	8	2	8
Radiation type	Mo $K\alpha$	Cu $K\alpha$	Mo $K\alpha$	Mo $K\alpha$	Cu $K\alpha$
μ (mm^{-1})	2.31	8.55	4.24	2.48	7.04
Crystal size (mm)	0.51 × 0.38 × 0.34	0.23 × 0.11 × 0.04	0.19 × 0.13 × 0.06	0.49 × 0.38 × 0.21	0.167 × 0.29 × 0.369
Diffractometer	Bruker *APEX*-II CCD	SuperNova	Xcalibur, Eos	SuperNova	SuperNova
Absorption correction	SADABS	Gaussian	Analytical	Gaussian	Gaussian
T_{min}, T_{max}	0.357, 0.431	0.613, 1.000	0.957, 0.983	0.018, 0.251	0.350, 1.000
No. of measured, independent and observed [I > 2s(I)] reflections	224824 16339 14022	93273 12003 10012	79172 5311 3750	69234 14164 13169	159556 15830 13954
R_{int}	0.046	0.098	0.218	0.078	0.081
(sin θ/λ)$_{max}$ (Å^{-1})	0.669	0.625	0.581	0.649	0.625
$R[F^2 > 2\sigma(F^2)]$, $wR(F^2)$, S	0.025, 0.115, 0.96	0.053, 0.150, 1.17	0.061, 0.145, 0.96	0.042, 0.123, 0.95	0.042, 0.119, 1.16
No. of parameters	768	665	347	704	809
No. of restraints	3	50	97	-	40
H-atom treatment	riding	riding	riding	riding	riding
Δ⟩$_{max}$, Δ⟩$_{min}$ (e Å^{-3})	0.93, -134	1.51, -2.68	2.67, -1.11	3.79, -1.73	0.95, -2.87
CCDC No.	-	-	-	-	-

Figure A.6 – Experimental details for complexes **18**, **19**, **20** and **21** synthesised in Chapter 3.

Compound	**22**	**23**	**24**	**25**
Chemical formula	$C_{62}F_8K_2O_3Th$	$C_{84}H_{100}F_{12}K_2O_{10}Th \cdot 3(C_4H_8O)$	$2(C_{235}N_5O_{12}U_3) \cdot 10(C_6)$	$C_{104}H_{104}O_5Th \cdot C_6H_6$
M_r	1495.41	2024.18	8317.58	1744.01
Crystal system, space group	Tetragonal *P*4/*nmm*	Monoclinic *C*2/*c*	Triclinic $P\bar{1}$	Triclinic $P\bar{1}$
Temperature (K)	120	120	120	120
***a*, *b*, *c* (Å)**	15.7559 (3) - 12.9176 (4)	44.0341 (15) 14.8570 (8) 31.8206 (11)	19.2911 (5) 22.7577 (5) 36.0434 (9)	13.1836 (3) 15.7901 (4) 22.8396 (6)
α, β, γ (°)	- - -	- 106.917 (4) -	76.905 (2) 85.268 (2) 66.731 (2)	100.679 (2) 104.615 (2) 100.925 (2)
***V* (Å^3)**	3206.77 (16)	19916.7 (15)	15336.7 (7)	4380.1 (2)
Z	2	8	1	2
Radiation type	Mo *K*α	Mo *K*α	Mo *K*α	Mo *K*α
μ (mm^{-1})	3.71	1.66	1.62	1.76
Crystal size (mm)	0.26 × 0.23 × 0.06	0.37 × 0.26 × 0.07	0.42 × 0.30 × 0.07	0.23 × 0.11 × 0.04
Diffractometer	Xcalibur, Eos	Xcalibur, Eos	Xcalibur, Eos	Xcalibur, Eos
Absorption correction	Analytical	Multi-scan	Analytical	Analytical
T_{min}, T_{max}	0.951, 0.986	0.765, 1.000	0.921, 0.983	0.917, 0.979
No. of measured, independent and observed [I > 2s(I)] reflections	86510 2077 1989	16258 7903 5839	160451 32024 21959	76213 13900 11860
R_{int}	0.111	0.066	0.123	0.085
(sin θ/λ)$_{max}$ (Å^{-1})	0.649	0.5	0.5	0.575
R*[*F*^{2} > 2σ(*F*^{2})], *wR*(*F*^{2}), *S	0.104, 0.327, 3.00	0.068, 0.165, 1.06	0.146, 0.386, 2.11	0.043, 0.118, 0.82
No. of parameters	73	1079	1105	1083
No. of restraints	7	607	2	222
H-atom treatment	-	riding	-	riding and independent
Δ⟩$_{max}$, Δ⟩$_{min}$ (e Å^{-3})	7.67, -4.42	1.50, -0.85	5.80, -4.28	0.92, -0.97
CCDC No.	-	-	-	-

Figure A.7 – Experimental details for complexes **22**, **23**, **24** and **25** synthesised in Chapter 3.

Compound	**26**	**27**	**28**	**29**
Chemical formula	$C_{94}H_{148}B_3O_4U$	$B_6C_{181}O_9U_2$	$C_{120}H_{184}B_4O_4U\cdot 2(C_6H_6)$	$C_{18}H_{39}B_2O_2U$
M_r	1611.57	2858.73	2128.15	547.14
Crystal system, space group	Monoclinic $P2_1/n$	Triclinic $P\bar{1}$	Monoclinic $P2_1/c$	Monoclinic $P2_1/n$
Temperature (K)	170	170	170	170
***a*, *b*, *c* (Å)**	16.5344 (7) 27.8539 (8) 20.2709 (7)	15.9113(3) 16.1748 (7) 36.3982 (10)	22.0131 (4) 19.4020 (3) 30.6714 (6)	8.6178 (1) 17.4195 (2) 14.9624 (2)
α, β, γ (°)	97.880 (4)	89.191 (3) 89.908 (2) 66.724 (3)	108.923 (2)	105.116 (1)
***V* (Å^3)**	9247.6 (6)	8604.2 (5)	12391.7(4)	2168.67 (5)
Z	4	2	4	4
Radiation type	Mo *K*α	Mo *K*α	Cu *K*α	Mo *K*α
μ (mm^{-1})	1.8	1.93	1.36	7.49
Crystal size (mm)	0.18 × 0.05 × 0.04	0.34 × 0.13 × 0.21	0.19 × 0.13 × 0.1	0.44 × 0.15 × 0.08
Diffractometer	Xcalibur, Eos	Xcalibur, Eos	SuperNova	Xcalibur, Eos
Absorption correction	Analytical	Multi-scan	Analytical	Analytical
T_{min}, T_{max}	0.976, 0.994	0.584, 1.00	0.955, 0.972	0.772, 0.956
No. of measured, independent and observed [I > 2s(I)] reflections	131293 14677 8855	151109 27315 14908	218483 19685 12561	49633 4974 4484
R_{int}	0.267	0.126	0.106	0.043
(sin θ/λ)$_{max}$ (Å^{-1})	0.575	0.579	0.575	0.649
R*[F^2 > 2σ(F^2)], *wR*(F^2), *S	0.080, 0192, 0.93	0.116, 0.319, 1.06	0.055, 0.182, 1.15	0.023, 0.090, 0.75
No. of parameters	961	809	1294	264
No. of restraints	-	3	156	58
H-atom treatment	riding	-	riding	riding and independent
Δ⟩$_{max}$, Δ⟩$_{min}$ (e Å^{-3})	0.78, -0.53	6.52, -6.77	2.66, -0.94	1.01, -1.52
CCDC No.	-	-	-	-

Figure A.8 – Experimental details for complexes **26**, **27**, **28** and **29** synthesised in Chapter 4.

Compound	**30**	**31**	**33**	**34**	**35**
Chemical formula	$2(C_{30}H_{45}B_6U_3) \cdot 2(C_6H_6)$	$C_{24}H_{42}BOU$	$C_{19}H_{38}B_3N_6OU$	$C_{22}H_{45}B_2O_3U$	$C_{44}H_{74}BO_4U$
M_r	2525.43	595.41	637.01	617.23	915.87
Crystal system, space group	Triclinic $P\bar{1}$	Triclinic $P\bar{1}$	Othorhombic *Pnma*	Monoclinic $P2_1/n$	Triclinic $P\bar{1}$
Temperature (K)	170	170	120	120	170
***a*, *b*, *c* (Å)**	16.0634 (3) 16.4583 (5) 21.8348 (5)	8.5762 (2) 17.3707 (5) 18.5475 (6)	22.4884 (5) 13.4297 (3) 8.4852 (2)	9.5699 (2) 28.0882 (3) 10.6351 (2)	10.5724 (17) 11.4907 (18) 19.884 (3)
α, β, γ (°)	90.268 (2) 109.416 (2) 118.633 (3)	63.012 (3) 88.745 (2) 86.723 (2)	- - -	- 113.394 (2) -	80.722 (14) 82.223 (14) 77.538 (14)
***V* (Å^3)**	4683.8 (2)	2458.16 (13)	2562.64 (10)	2623.73 (9)	2315.1 (7)
Z	2	4	4	4	2
Radiation type	Mo *K*α	Mo *K*α	Cu *K*α	Mo *K*α	Mo *K*α
μ (mm^{-1})	10.37	6.61	17.98	6.2	3.54
Crystal size (mm)	0.39 × 0.18 × 0.07	0.36 × 0.12 × 0.04	0.37 × 0.05 × 0.02	0.48 × 0.34 × 0.09	0.33 × 0.14 × 0.04
Diffractometer	Xcalibur, Eos	Xcalibur, Eos	SuperNova	Xcalibur, Eos	Xcalibur, Eos
Absorption correction	Analytical	Multi-scan	Guassian	Multi-scan	Analytical
T_{min}, T_{max}	0.992, 0.998	0.441, 1.000	0.375, 1.00	0.253, 1.00	0.807, 0.967
No. of measured, independent and observed [I > 2s(I)] reflections	86128 21485 16088	41660 10056 8668	49474 2734 2557	153420 5350 5159	29115 13928 6681
R_{int}	0.063	0.036	0.116	0.082	0.159
(sin θ/λ)$_{max}$ (Å^{-1})	0.649	0.631	0.625	0.625	0.575
R*[F^2 > 2σ(F^2)], *wR*(F^2), *S	0.042, 0.136, 0.86	0.048, 0.122, 1.18	0.047, 0.124, 1.11	0.086, 0.194, 1.59	0.116, 0.276, 1.00
No. of parameters	984	539	186	274	864
No. of restraints	967	147	7	129	1374
H-atom treatment	riding	riding and independent	riding and independent	riding and independent	riding
Δ⟩$_{max}$, Δ⟩$_{min}$ (e Å^{-3})	1.60, -1.07	4.40, -1.94	4.81, -1.85	3.10, -4.99	3.16, -1.84
CCDC No.	-	-	-	-	-

Figure A.9 – Experimental details for complexes **30**, **31**, **33**, **34** and **35** synthesised in Chapter 4.

Appendix B

Publications based on the work presented in this thesis

Dinuclear uranium complexation and manipulation using robust tetraaryloxides

Jordann A. L. Wells, Megan L. Seymour, Markéta Suvova and Polly L. Arnold

Dalton Transactions, 2016, **45**, 16026 – 16032

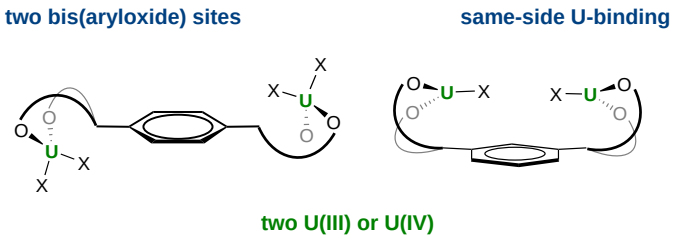

Uranium rhodium bonding in heterometallic complexes

Johann A. Hlina, Jordann A. L. Wells, James R. Pankhurst, Jason B. Love and Polly L. Arnold

Dalton Transactions, 2017, **46**, 5540 – 5545

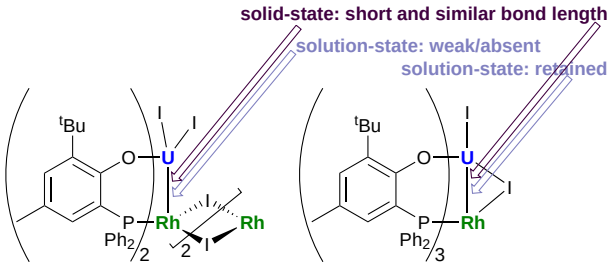

Ring opening polymerisation of lactide with uranium(IV) and cerium(IV) phosphinoaryloxide complexes

Fern Sinclair, Johann A. Hlina, Jordann A. L. Wells, Michael P. Shaver and Polly L. Arnold

Dalton Transactions, 2017, **46**, 10786 – 10790

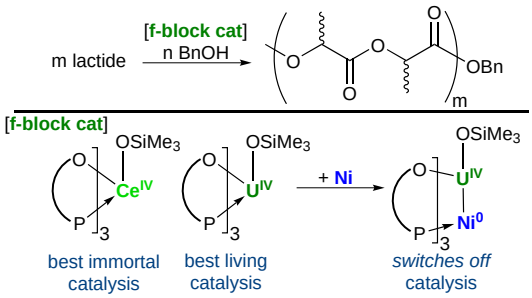

B.1 Bibliography

[1] G. M. Sheldrick, *Acta Crystallogr. Sect. A Found. Adv.*, 2015, **71**, 3–8.

[2] O. V. Dolomanov, L. J. Bourhis, R. J. Gildea, J. A. K. Howard and H. Puschmann, *J. Appl. Crystallogr.*, 2009, **42**, 339–341.

[3] A. L. Spek, *Acta Crystallogr. Sect. C Struct. Chem.*, 2015, **71**, 9–18.